Topics in Heterocyclic Chemistry 51
Series Editors: Bert Maes · Janine Cossy · Slovenko Polanc

Philipp Selig *Editor*

Guanidines as Reagents and Catalysts II

Springer

51
Topics in Heterocyclic Chemistry

Aims and Scope

The series Topics in Heterocyclic Chemistry presents critical reviews on present and future trends in the research of heterocyclic compounds. Overall the scope is to cover topics dealing with all areas within heterocyclic chemistry, both experimental and theoretical, of interest to the general heterocyclic chemistry community.

The series consists of topic related volumes edited by renowned editors with contributions of experts in the field.

More information about this series at http://www.springer.com/series/7081

Philipp Selig
Editor

Guanidines as Reagents and Catalysts II

With contributions by

V. del Amo · R.M. Capitão · C. Concellón · C. von Eßen · C.R. Göb · E.R.P. González · S. Herres-Pawlis · H.-J. Himmel · A. Hoffmann · J. Mannsperger · A. Metz · I.M. Oppel · T. Rösener · R.D.E. Santo · J. Stanek

Springer

Editor
Philipp Selig
Patheon Inc.
Linz, Austria

ISSN 1861-9282 ISSN 1861-9290 (electronic)
Topics in Heterocyclic Chemistry
ISBN 978-3-319-53012-3 ISBN 978-3-319-53013-0 (eBook)
DOI 10.1007/978-3-319-53013-0

Library of Congress Control Number: 2017936046

Printed on acid-free paper

This Springer imprint is published by Springer Nature
The registered company is Springer International Publishing AG
The registered company address is: Gewerbestrasse 11, 6330 Cham, Switzerland

Preface

Guanidines, the all-aza analogues of carbonic acids, represent a fascinating group of molecules with unique chemical and physical properties. Just as the well-known amidines, guanidines are exceedingly strong Brønsted bases and are therefore even referred to as "superbases." Moreover, guanidines can exhibit strong Lewis-basic properties and thus serve as electron-pair donors and ligands. After protonation, the highly stabilized guanidinium cation is often used as a powerful, bidentate H-bond donor, capable of tight binding and activation of a variety of H-bond acceptors such as carbonyl groups. Finally, guanidinium cations can also be regarded as Lewis-acidic species which can act as π-Lewis acids.

Guanidines and their corresponding protonated species are thus capable of exhibiting all four basic chemical functionalities: free bases are Lewis and Brønsted basic, while cations are Lewis and Brønsted acidic, all connected by a simple proton transfer.

Besides this obvious potential for synthetic applications, guanidines are also a challenging target for synthetic endeavors, mainly due to their highly basic character. In the first volume of *Guanidines as Reagents and Catalysts*, we thus wanted to open with an overview of *Prof. Rozas*, which introduces the reader to principal techniques for guanidine synthesis and offers a first glimpse on the potential of guanidines in biological applications.

A main topic of Vol. I concerns the use of guanidines as synthetic reagents or, more specifically, as organocatalysts. We are introduced into this topic with a chapter by *Prof. Ishikawa,* a pioneer of guanidine organocatalysis and also the inventor of one of the very rare examples of a commercially available guanidine catalyst, "Ciba-G." Ciba-G is also already highlighting the importance of multi-functional activations in guanidine organocatalysis, a most important concept, which is further illustrated by the works of *Prof. Takemoto* in the following chapter.

Turning the focus from catalyst structures to synthetic applications, *Prof. Najera* will elaborate on a pivotal guanidine-catalyzed reaction, i.e., the Michael addition, which makes formidable use of both the Brønsted basic and the H-bond donating properties of the guanidine and guanidinium cation. In the following chapter, structures of guanidine organocatalysts are taken to the next level by *Prof. Tan* and his introduction of bicyclic guanidine organocatalysts. These synthetically useful, as well as aesthetically pleasing structures show us that highly efficient catalysis may not be strictly contingent upon multifunctional activation, and steric effects around an isolated guanidine moiety can be sufficient to achieve excellent results. While Prof. Tan's work focuses on sterically rigid, mono-functional catalysts, a quite antipodal approach, using highly flexible guanidines with multiple functional groups attached, is shown to succeed just as well in the final chapter of Vol. I by *Prof. Nagasawa*.

While the majority of Vol. I deals with guanidines as reagents and catalysts in the field of organic synthesis, the potential uses of guanidines certainly go far beyond that. In the second of these two volumes a focus is placed on the specialized applications of guanidines. In the first chapter *Prof. Concellón* and *Prof. del Amo* show us their works on structurally simple guanidinium salts to effectively modify reactions catalyzed by the classic organocatalyst L-proline, demonstrating the design of elaborate new catalyst structures is not necessarily mandatory to benefit from guanidine catalysis. Guanidine organocatalysis is also involved in an industrially useful field, namely the nucleophilic activation of CO_2 as a sustainable C1-building block. *Prof. Pérez González* presents this "green" use of guanidine catalysis in the following chapter.

Further highlighting the potential uses of guanidines outside traditional organic synthesis *Prof. Oppel* presents guanidines as ligands for super-molecular metal-based frameworks, and the synthetic potential of such guanidinium-metal complexes is explored by *Prof. Herres-Pawlis*, exemplified in their use as highly active polymerization catalysts. Finally, at the end of this volume, *Prof. Himmel* takes us far beyond our focus on synthetic organic chemistry with his chapter on the unique electronic properties of anionic guanidinates and their complexes.

In summary, it was our goal to show that guanidines, guanidinium salts, and guanidinates offer a very diverse range of reactivity and thus great potential for a wide variety of uses. While still being regarded as a rather exotic class of molecules in the field of organocatalysis, especially in comparison to the prominent field of proline-induced imine/enamine activation or H-bond catalysis enabled by thioureas, the potential of guanidines as reagents and catalysts as well as the door to novel applications is certainly wide open. Currently, in the mid-2010s, guanidine chemistry is a highly dynamic and rapidly developing field of research, and we can expect exciting new developments in the future. Guanidines as reagents and catalysts are here to stay and will continue to show up as versatile and valuable tools both in and beyond organic chemistry.

Linz, Austria Philipp Selig
November 2016

Contents

Top Heterocycl Chem (2017) 51: 1–26
DOI: 10.1007/7081_2015_158

Published online: 2 August 2015

Cooperative Guanidinium/Proline Organocatalytic Systems

Carmen Concellón and Vicente del Amo

Abstract Organocatalysis is nowadays recognized as the third pillar of asymmetric synthesis, standing next to metal catalysis and enzymatic transformations. Proline has shown up as an ideal organocatalyst, being inexpensive and readily available. However, this amino acid has also manifested its limitations. Compared to the chemical modification of proline, the approach through adding small hydrogen-bond-donating cocatalysts to interact with proline is particularly attractive. Various additives have been investigated to date. This chapter discloses the use of guanidinium salts as additives for proline, investigated in the course of proline-catalyzed aldol reactions.

Keywords Guanidinium salts • Organocatalysis • Proline • Supramolecular chemistry

Contents

C. Concellón (✉) and V. del Amo (✉)
Departamento de Química Orgánica e Inorgánica, Universidad de Oviedo, C/Julián Clavería 8, 33006 Oviedo, Spain
e-mail: carmen.concellon@gmail.com; vdelamo@uniovi.es

1 Brief Introduction to Organocatalysis and Its Limitations

During the last decades, the demand of enantiomerically pure synthetic products has grown exponentially. This request has made asymmetric catalysis the most active area of research in contemporary organic chemistry. Illustratively, 81 of the 200 blockbuster drugs by worldwide sales are enantiopure substances.

Traditional asymmetric catalysis relies on the use of transition metal complexes (organometallic chemistry), or enzymes (biocatalysis). However, recently, a third type of catalysts has appeared: the organocatalysts, with its associated discipline asymmetric organocatalysis. This consists in the use of catalytic or substoichiometric amounts of simple organic molecules to carry out highly enantioselective processes that take place in the absence of metallic elements. The use of organocatalysts shows a number of advantages over the utilization of transition metal complexes: lower toxicity, low environmental impact, and absence of metallic elements which present potential contaminants in final products, many of them synthesized for human or animal intake. Similarly, organocatalysts display advantages over the use of enzymes, which come at a significantly higher prize and scarce availability.

Projects dealing with organocatalysis can be framed inside Green Chemistry and Sustainable Chemistry schemes. The concept of Sustainable Chemistry (in many occasions synonymous with Green Chemistry) refers to actions aiming to improve the efficiency in the use of natural resources. Consequently, it comprises the design and implementation of new chemical processes and transformations operating in a more efficient, safer, and more environmentally friendly way. Having the intention of pursuing those goals, Sustainable Chemistry has been formulated in 12 universally accepted principles, put forward by Anastas and Warner [1, 2]. Organocatalytic processes satisfy several of them: high atomic efficiency, the use of reagents of low or nontoxicity, little generation of residues, and the use of reagents in catalytic amounts. Moreover, the E-factor values of these processes are remarkably low, which is of interest for industry. The E-factor quantifies how toxic/benign a particular chemical process is and is expressed as the ratio of generated waster per kilogram of product produced.

The use of small organic molecules as catalysts in chemical transformations can be tracked back as far as the nineteenth century, to the pioneering works of Emil Knoevenagel [3–6]. It wasn't however until the year 2000, with the findings of List, Lerner, and Barbas on the potential of proline as a catalyst for the intermolecular aldol reaction [7] and those of MacMillan [8], when the research in organocatalysis commenced as a separate and well-defined field. Since then, the interest of the scientific community over this discipline has been phenomenal. Nowadays, the number of publications and literature reviews dealing with different aspects of asymmetric organocatalysis is extraordinarily large. It is far from the objectives of this monograph to cover the multiple and colored possibilities of this field. Nonetheless, the following selected citations (literature reviews) can summarize the state of the art of the discipline [9–23].

Considering their low price and ready availability and based on the study of List [7], proline, or other natural amino acids, would be the first-choice organocatalysts. These naturally occurring compounds are cheap, are readily available in both enantiomeric forms, and can be used for a wide range of synthetic transformations. However, amino acids also present some major drawbacks as organocatalysts, namely, rather limited solubility and reactivity in nonpolar organic solvents, and parasitic side reactions that make using high catalyst loadings necessary to achieve acceptable conversions. To avoid these undesired issues, large efforts have been devoted to the careful design (assisted by molecular modeling) and synthesis of novel tailor-made catalysts. In this sense, the structures shown in Fig. 1, collected from the references cited above, represent some of the thousands of different catalysts that have recently been used in organocatalytic processes. Such processes make use of a classical approach to the phenomenon of catalysis, where a certain novel asymmetric organocatalyst is designed, synthesized, and applied to a particular transformation. The efficiency of the catalyst in question is evaluated in terms of chemical yield, diastereoselection, and/or enantioselection for the product obtained. If the results are unsatisfactory, a second-generation organocatalyst (typically based on the original motif) is redesigned and resynthesized, for being once again evaluated. This type of iterative approach is unattractive for industry, which cannot afford testing every single catalyst on a particular reaction, and also constrained by both economic and time limitations. It has to be noted that the preparation of structures like those represented in Fig. 1 is not trivial and normally encompasses considerable synthetic efforts. Moreover, before having found a good catalyst, many analogues of a proposed design are normally prepared and evaluated.

2 Additives Used for Proline in Organocatalyzed Reactions

An alternative to the classical approach discussed above consists of adding simple, readily available additives to reactions containing known catalysts, ideally proline, whose behavior is thus reevaluated under the new reaction conditions. This late strategy is significantly beneficial in evading tedious chemical syntheses and would ultimately allow the construction of libraries of catalytic systems by simply changing the additives of choice. Moreover, the possibility of testing various additives in parallel with the aid of high-throughput screening methods is particularly appealing (for high-throughput screening methodologies of additives in organocatalyzed reactions, see [24–26]).

With the aim of avoiding the use of synthetically elaborated organocatalysts, various researches have recently embraced the look for rational additives capable of enhancing the reactivity and selectivity of off-the-bench catalysts, particularly (*S*)-proline, in different organic transformations. The classical proline-catalyzed cross-aldol reaction between cyclic ketones and aromatic aldehydes (Scheme 1) [7] and to

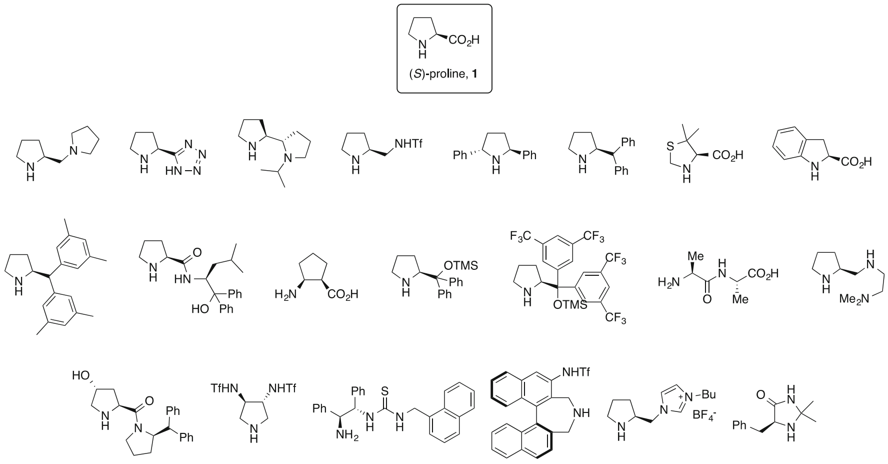

Fig. 1 Structure of (*S*)-proline (**1**) and examples of other structures used as organocatalysts

a lesser extent the proline-catalyzed addition of ketones to β-nitro-styrene (Scheme 2) [27] have been adopted as paradigms for testing multiple additives.

So far, it has been demonstrated how the addition of catalytic or substoichiometric amounts of inorganic Lewis acidic salts [28–35], Brønsted acids [36], water [37–40], chiral alcohols (BINOL or tartrates) [41, 42], achiral alcohols [43], ureas [44], thioureas [45–52], thiouronium salts [53], and imidazolium salts [54] increase the reactivity, efficiency, and selectivity of proline in cross-aldol reactions in comparison to the seminal report of List [7]. Additionally, ureas and thioureas have also been investigated to partner (*S*)-proline in the catalytic addition of ketones to β-nitro-styrene [49, 55, 56]. Although a full-bodied picture of the role played by these additives in the mechanisms of the reactions shown in Scheme 1 has not been disclosed, it seems clear that in nonpolar solvents, a network of hydrogen-bonding interactions between the carboxylate function of proline, the corresponding additive, and the reaction substrates in the transition state is established. Based on this hypothesis, Demir and co-workers proposed a transition state characterized by the formation of a doubly hydrogen-bonded complex [Schreiner's thiourea **2** [57] · proline **1**], for the thiourea **2**/proline-catalyzed aldol reaction between cyclohexanone and aromatic aldehydes (Scheme 3) [45]. The establishment of such a complex would be ultimately responsible of the high selectivity observed for the process.

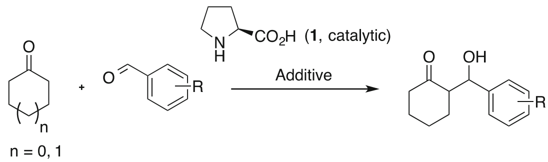

Scheme 1 Proline-catalyzed cross-aldol reaction, commonly used as a model to evaluate different additives

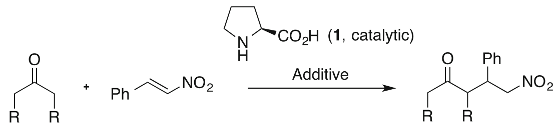

Scheme 2 Proline-catalyzed addition of ketones to β-nitro-styrene, commonly used as a model to evaluate different additives

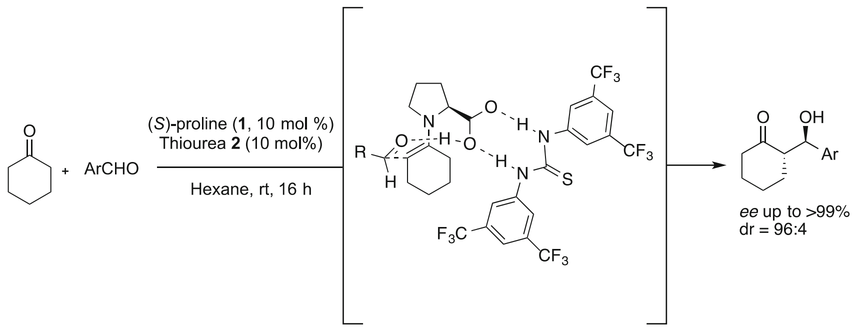

Scheme 3 Demir's (*S*)-proline/thiourea **2**-catalyzed aldol reaction between cyclohexanone and aromatic aldehydes. The proposed reaction intermediate is represented

3 Guanidinium Salts as Additives for Proline in Organocatalyzed Reactions

3.1 Cross-Aldol Reaction Between Cyclic Ketones and Aromatic Aldehydes

Inspired by the aforementioned contributions [28–52, 54] and particularly by the work of Demir [45], back in 2010, our group started to explore the feasibility of using guanidinium salts as novel additives for proline in classical organocatalyzed reactions. In order to compare our results with those reported by other methodologies, we also adopted the direct cross-aldol reaction between cyclic ketones and aromatic aldehydes as a model (Scheme 1). We founded our work on the probed ability of guanidinium salts in binding carboxylic acids and carboxylates, amply documented in the literature [58–61]. Also, backing up this idea, ionic liquids based on guanidinium cores, although not used in a catalytic manner, were demonstrated to be superb solvents for proline-promoted aldol reactions [62].

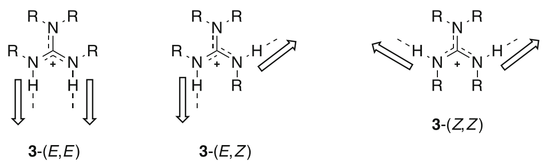

Fig. 2 Conformations of a general tetrasubstituted guanidinium cation **3**. *Bold arrows* indicate the direction in which H-bonds could be formed

Tetrasubstituted guanidinium cations can form H-bonds with appropriate partners. The conformation of the guanidinium motif, thus the directionality of the H-bonds, is ultimately determined by steric and stereoelectronic factors imposed by its substituents. Figure 2 shows the three possible conformations (named after (*E*,*E*), (*E*,*Z*), and (*Z*,*Z*)) of a general tetrasubstituted guanidinium cation **3** and the directions amenable to H-bond formation.

In acyclic guanidinium salts, the three conformers represented in Fig. 2 can interconvert into each other by the successive rotation of C–N bonds. However, only the (*E*,*E*)-conformer is capable of forming well-defined complexes with carboxylates or other oxoanions. Bearing this in mind, we judiciously choose for our study guanidinium salts derived from the bicyclic guanidine TBD (triazabicyclo [4.4.0]dec-5-ene, **4**, Fig. 3), which are conformationally restricted and have a suitable geometry for hydrogen bonding.

TBD is readily available from commercial suppliers and is a reasonably inexpensive base,[1] intensively investigated as catalyst for various transformations [63–72]. This guanidine, in which the nitrogen atoms are embedded within a decaline core, shows high rigidity and conformational restriction. When TBD **4** is protonated, its corresponding guanidinium cation **5** (Fig. 3) presents a single (*E*,*E*)-conformation, with a pair of acidic hydrogen atoms preorganized according to a donor–donor (DD) pattern, which can form doubly H-bonded arrays with an appropriate acceptor–acceptor (AA) partner (i.e., a carboxylate anion) (Fig. 3). Such motifs are stabilized not only by primary and secondary H-bonding interactions but also through coulombic forces, as a consequence of the formation of an electroneutral ionic pair. This results in supramolecular complexes [guanidinium · carboxylate] typically displaying high association constants [73] even in competitive polar media, which are generally larger than those measured for structurally related complexes [urea · carboxylate] or [thiourea · carboxylate].

We started off preparing a battery of guanidinium salts **5a**–**5g**, with anions featuring different geometries, bulkiness, and electronic properties (Fig. 4). Utilizing salts **5** as additives for proline in the direct cross-aldol reaction represented in Scheme 1, we postulated that the guanidinium cation of **5** could form doubly H-bonded motifs with the carboxylate function of proline (Fig. 4, model A), as well as with the carbonyl moieties of the ketone (Fig. 4, model B), and the

[1] 5g, 36 € (Sigma–Aldrich catalogue; April 2015).

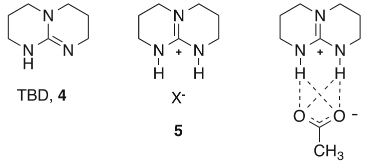

Fig. 3 Structure of guanidine TBD **4** (*left*), its corresponding guanidinium cation **5** (*center*), and the supramolecular complex [guanidinium · acetate] (*right*) with indication of its H-bond interactions

aromatic aldehyde (Fig. 4, model C), thus enhancing their electrophilicity. Moreover, the participation of the anion counterpart X^- of salt **5** could be also presumed. In fact, our studies have demonstrated that the anion accompanying the guanidinium core of salt **5** was indeed crucial in the reaction outcome of the guanidinium salt/proline-catalyzed aldol reaction.

3.1.1 Studies on the Tetrafluoroborate Guanidinium Salt 5a (5, X = BF_4^-)

From the compounds **5a**–**5i** represented in Fig. 4, the tetrafluoroborate guanidinium salt **5a** denoted being an outstanding additive for (*S*)-proline in the direct proline-catalyzed cross-aldol reaction [74]. Experimental conditions were optimized for the reaction occurring between cyclohexanone and 4-chlorobenzaldehyde **6a** to render the aldol adduct **7a** (Table 1). Looking for an inexpensive and green process, it was decided to avoid the use of any organic solvent apart from a moderate excess of cyclohexanone (tenfold excess), which acted as both reagent and reaction media. Organocatalyzed aldol reactions operating under solvent-free conditions are particularly interesting and therefore sought after (for recent examples of organocatalyzed aldol reactions carried out under solvent-free conditions, see [75–85]).

The best reaction conditions implied utilizing 15 mol% of proline **1** and 10 mol % of tetrafluoroborate guanidinium salt **5a**. The aldol reaction proceeded better at 0°C than at room temperature, although it required longer times (Table 1, entries 1 and 2). Interestingly, when a suspension of aldehyde **6a**, (*S*)-proline (15 mol%), and additive **5a** (10 mol%) in cyclohexanone was left to stand for 96 h inside a standard laboratory fridge (temperature ranging 0–3°C) without stirring or mechanical agitation, aldol **7a** was rendered in 96% conversion, with a relation of diastereoisomers 96:4 (*anti*/*syn*) peaking at 98% enantiomeric excess (Table 1, entry 3). Small differences were appreciated in terms of diastereo- and enantioselectivity of product **7a** when reaction mixtures were stirred at 0°C (Table 1, entry 2), or alternatively when they were left to stand inside the fridge at 0–3°C without any sort of agitation. However, the later protocol was favored, being significantly straightforward and avoiding the use of cryogenic baths for prolonged times. Moreover, there was no indication of any irreproducibility of results. Blank

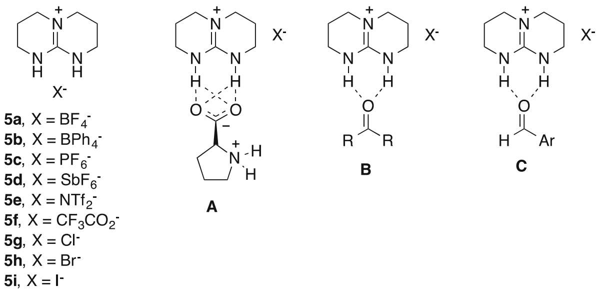

Fig. 4 TBD-derived guanidinium salts **5a–i** studied as additives for proline. Possible doubly H-bonded motifs formed by interaction of the TBD-derived guanidinium core with the carboxylate function of (*S*)-proline (model **A**), or the carbonyl moiety of a ketone (model **B**), or an aromatic aldehyde (model **C**)

Table 1 Initial screening of conditions for the guanidinium salt **5a**/proline system in the formation of aldol **7a**

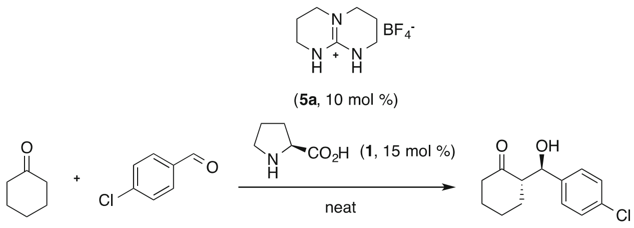

Entry	Temp. (°C)	Time (h)	Conv. (%)[a]	*anti*:*syn*	*ee* (%)[b]
1	20	48	99	76:24	82
2	0	96	98	93:7	96
3[c]	0–3	96	96	94:6	98
4[c,d]	0–3	96	81	69:31	54

Reaction conditions: cyclohexanone (10 equiv.), **6a** (1 equiv.), (*S*)-proline (**1**, 15 mol%), **5a** (10 mol%), and no solvent (neat); reaction mixture was stirred unless otherwise stated. Table figures represent an average of two experiments

[a]Conversion of aldehyde **6a** (limiting reagent) into aldol adduct **7a**

[b]Enantiomeric excess of the major (*anti*) diastereoisomer

[c]The reaction mixture was left to stand inside a fridge (0–3°C) without stirring

[d]Guanidinium salt **5a** was not added

experiments, without the participation of additive **5a**, presented modest figures of chemical conversion, diastereo- and enantioselectivity of adduct **7a** (Table 1, entry 5), hence confirming the advantageous effect of the guanidinium salt under such rather mild reaction conditions.

The scope of this aldol protocol was established by reacting a collection of aldehydes **6b–h** bearing diverse functional groups and substitution patterns with cyclohexane, or other ketones, under the ideal reaction conditions presented in Table 1, entry 3. Table 2 gathers the results obtained. Aldols **7b–f**, derived from

Table 2 Scope of the (*S*)-proline/guanidinium salt **5a** co-catalyzed synthesis of aldols

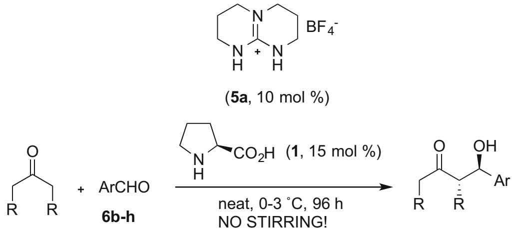

Entry	ArCHO	Product	Yield (%)[a]	*anti*:*syn*	*ee* (%)[b]
1[c]	**6b** 4-NO_2–C_6H_4	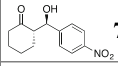 **7b**	92	92:8	99
2[c]	**6c** 4-CO_2Me–C_6H_4	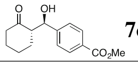 **7c**	86	92:8	99
3[c]	**6d** 4-Br–C_6H_4	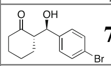 **7d**	94	97:3	99
4[c]	**6e** 2-OMe–C_6H_4	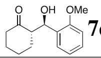 **7e**	87	95:5	98
5[c]	**6f** 3-Cl–C_6H_4	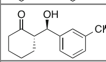 **7f**	94	96:4	98
6[c]	**6g** 2-furyl	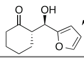 **7g**	73	86:14	91
7[c]	**6h** 2-Thiophenyl	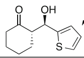 **7h**	70	93:7	90
8[d]	**6b** 4-NO_2–C_6H_4	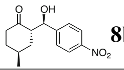 **8b**	81	86:14:0:0	97
9[e]	**6b** 4-NO_2–C_6H_4	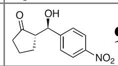 **9b**	84	74:26	98
10[f]	**6b** 4-NO_2–C_6H_4	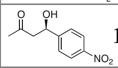 **10b**	88	–	74

Reaction conditions: ketone (10 equiv.), aldehyde (1 equiv.), (*S*)-proline (**1**, 15 mol%), **5a** (10 mol %), and no solvent (neat); reaction mixture was left to stand inside a fridge (0–3°C) for 96 h without stirring

[a]Isolated yield of analytically pure products

[b]Enantiomeric excess of the major (*anti*) diastereoisomer

[c]Cyclohexanone was used as ketone

[d]4-Methylcyclohexanone was used as ketone

[e]Cyclopentanone was used as ketone

[f]Acetone was used as ketone

cyclohexanone (Table 2, entries 1–5), were isolated in good or very good yields, and with very high diastereo- and enantioselectivity. Particularly relevant are aldols **7g** and **7h**, prepared from 2-furfural and 2-thiophenecarboxaldehyde, respectively, which are challenging substrates for the direct aldol reaction (Table 2, entries 6 and 7). 4-Methylcyclohexanone was successfully desymmetrized by means of this methodology, affording aldol **8b** with high diastereo- and enantioselectivity, in a

Table 3 Direct aldol reaction without the addition of guanidinium salt **5a**

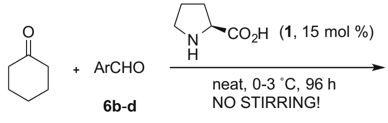

Entry	ArCHO	Product	Conv.(%)[a]	*anti*:*syn*	*ee* (%)[b]
1	**6b** 4-NO_2–C_6H_4	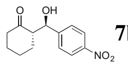 **7b**	>99	85:15	n.d.[c]
2	**6c** 4-CO_2Me–C_6H_4	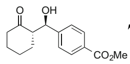 **7c**	56	76:24	95
3	**6d** 4-Br–C_6H_4	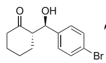 **7d**	26	69:31	94
4[d]	**6b** 4-NO_2–C_6H_4	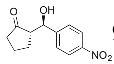 **9b**	93	38:62	92

Reaction conditions: ketone (10 equiv.), aldehyde (1 equiv.), (*S*)-proline (15 mol%), and no solvent (neat); reaction mixture was left to stand inside a fridge (0–3°C) for 96 h without stirring
[a]Conversion of aldehyde **6** (limiting reagent) into aldol adduct
[b]Enantiomeric excess of the major (*anti*) diastereoisomer
[c]Enantiomeric excess was not determined, hampered by impurities
[d]Cyclopentanone was used as ketone

process where the absolute configuration of three stereogenic centers is fixed (Table 2, entry 8). Reactions carried out with cyclopentanone or acetone were also successful.

To further confirm the positive effect of the tetrafluoroborate guanidinium salt **5a** on the course of the reactions outlined in Table 2, some were repeated under strictly analogous conditions using only (*S*)-proline as a single catalyst (Table 3). As it was anticipated, all aldol reactions performed without additive **5a** showed lower conversion as well as poorer diastereoisomeric ratios and enantiomeric excesses.

It is important to mention that, as we have observed, all transformations implying the proline/guanidinium salt **5a** methodology are heterogenous, some (*S*)-proline remaining precipitated at the bottom of the reaction vessels along the reaction course. Literature reports have presented the behavior of proline as organocatalyst under heterogenous conditions ([86], and reference therein), and it is accepted that a saturated solution of the amino acid is equilibrated with a crystalline phase. Accordingly, we considered in our system the presence of some (*S*)-proline dissolved in cyclohexanone (or either of the other ketones employed), ultimately responsible of controlling the reaction course. Indeed, high-field ^1H NMR experiments have confirmed that the guanidinium salt **5a** significantly favors the dissolution of proline in acetone-d_6. Figure 5a shows the spectrum of guanidinium salt **5a** in acetone-d_6 at $C = 75$ mM, a concentration close to that featured in the experiments of Table 2. When equimolar amounts of (*S*)-proline were added to the former solution and the corresponding ^1H NMR spectrum was recorded, a deshielding of

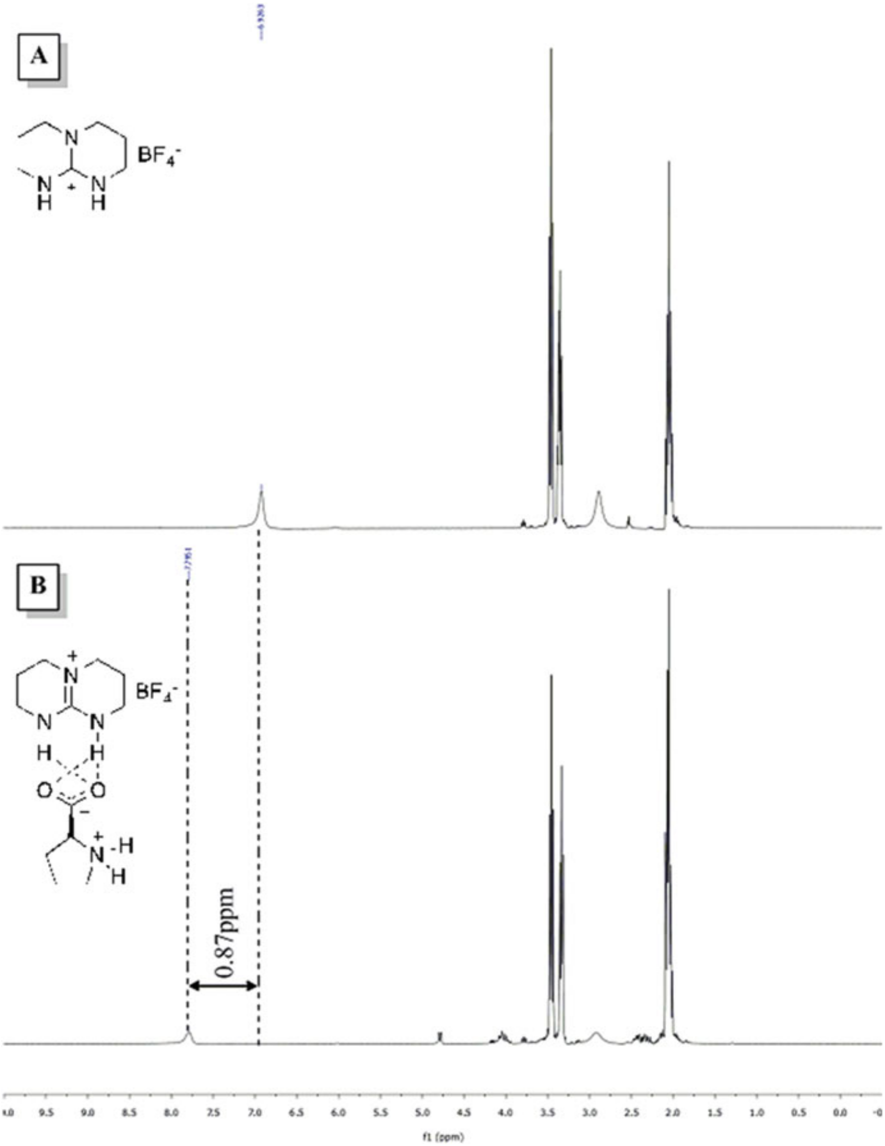

Fig. 5 (**a**) ^{1}H NMR spectrum (300 MHz, acetone-d_6) of guanidinium salt **5a** ($c = 75$ mM). (**b**) ^{1}H NMR spectrum (300 MHz, acetone-d_6) of guanidinium salt **5a** ($c = 75$ mM) and (*S*)-proline ($c = 75$ mM)

the resonances attributed to the N–H functions of guanidinium salt **5a** was observed, together with resonances of the amino acid showing up (Fig. 5b). It is important to note that proline itself, in absence of the guanidinium salt, is completely insoluble in acetone-d_6. These data confirmed the entity of the complex [proline · **5a**], which, in turn, served to validate the model A proposed in Fig. 4.

Granted the solubility of proline, the stereochemical outcome of the reaction was explained assuming that it operates through a Zimmerman–Traxler-type transition state. Similar reaction intermediates have been proposed by other authors. Therefore, the formation of a 1:1 complex between the guanidinium cation of additive **5a** and the solubilized proline would stabilize the chairlike transition state **11** (Fig. 6), which leads to the observed aldols and also accounts for their spatial configuration. Profound molecular mechanics calculations carried out by the group of Li and Cheng have recently given further support to the existence of the supramolecular complex [proline · guanidinium salt], both in the gas phase and in nonpolar solvents [87]. According to the authors, the calculated results predicted that the acidity of proline could be increased by no less than 9 pK_a units when it is assembled with the H-bond-donating guanidinium cation. Such an increment of acidity would rationalize the dramatically enhanced activity of proline in the presence of the additive. Notwithstanding with our mechanistic proposition and the suggestions of Li and Cheng, issues such as the role played by the tetrafluoroborate counterpart of salt **5a** in the reaction mechanism are yet unclear. In any case, further experiments carried out in our laboratory, discussed in Sect. 3.1.2, indicated that, as a matter of fact, the anion does play a central role.

Soon after the publication of this work, the group of Córdova studied the effect of adding guanidinium salt **5a**, or alternatively other additives, on the outcome of an aldol reaction between cyclohexanone and 4-nitrobenzaldehyde **6b** catalyzed by a *O*-silyl-protected threonine derivative **12** (Table 4) [88]. Reactions were carried out in toluene at room temperature. Under this set of conditions, it was evident that the concurrence of the additive did in fact not improve the performance of the primary amino acid catalyst.

3.1.2 Studies on the Tetraphenylborate Guanidinium Salt 5b (5, X = BPh_4^-)

In the reactions shown in Table 2, *syn*-aldols were preferentially formed when the TBD-derived tetraphenylborate guanidinium salt **5b** replaced the tetrafluoroborate salt **5a** as cocatalyst for proline. This intriguing observation was further examined in our laboratory [89]. The aldol reaction between cyclohexanone and 4-nitrobenzaldehyde, **6b**, was adopted as a model to gain proper experimental conditions that maximized the amount of *syn*-adduct produced. It was found that when a suspension of 4-nitrobenzaldehyde **6b** (1.0 equiv.), (*S*)-proline (**1**, 10 mol%), and TBD-derived tetraphenylborate guanidinium salt **5b** (15 mol%) in cyclohexanone (10.0 equiv.) was allowed to react for 120 h at 0–3°C inside a fridge without stirring, the corresponding aldol adduct **7b** was rendered in full conversion, with moderate *syn*-diastereoselectivity (35:65 *anti*/*syn*) and excellent enantioselectivity (93% *ee*, for *syn*-**7b**) (Table 5, entry 1). The stereochemistry of the product *syn*-**7b** was assigned as (*R*,*R*) by comparison with literature values. Other aromatic aldehydes

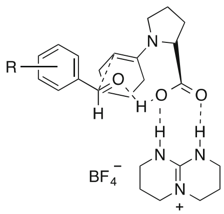

11

Fig. 6 Zimmerman–Traxler-type transition state **11** proposed to explain the observed stereochemistry of aldol **7** in the proline/tetrafluoroborate guanidinium salt **5a**-catalyzed aldol reaction

Table 4 *O*-Silylated threonine **12**/guanidinium salt **5a** co-catalyzed aldol reaction

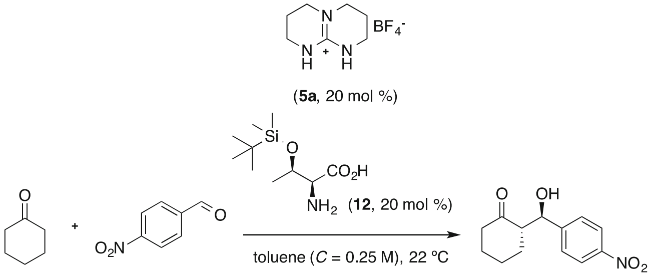

Entry	Time (h)	Conv. (%)[a]	*anti*:*syn*	*ee* (%)[b]
1	27	82 (76)	92:8	98
2[c]	24	77 (64)	91:9	99

Reaction conditions: cyclohexanone (10 equiv.), **6b** (1 equiv.), threonine derivative **12** (20 mol%), **5a** (20 mol%), in toluene ($c = 0.25$ M), 22°C

[a]Conversion of aldehyde **6b** (limiting reagent) into adduct **7b** in crude reaction mixtures. Isolated yield of analytically pure products is given in brackets

[b]Enantiomeric excess of major (*anti*) diastereoisomer

[c]Guanidinium salt **5a** was not added

6i–j decorated with nitro substituents and 4-cyanobenzaldenyde **6k** were examined as substrates for this reaction (Table 1, entries 2–4). Products **7i–k** also displayed a preferential *syn*-stereochemistry, peaking the *anti*/*syn* ratio at 25:75, and had enantiomeric excesses above 90%. It has to be highlighted that limited work had been done on the catalytic direct asymmetric aldol reaction aiming to render *syn*-adducts [90–92].

When the additive **5b** did not participate in the proline-catalyzed aldol reaction, adducts **7b**, **i–k** were rendered with poor conversion and significantly low diastereoselectivity, the *anti*-configured products being favored (Table 6, entries 1–4). In addition, the small amount of *syn*-adducts produced in the absence of guanidinium salt **5b** featured the absolute configuration (*S*,*S*), opposite to the examples shown in Table 5. These observations demonstrated how the participation of the guanidinium salt controls the stereopreference of the aldol reaction (for a general review on the stereocontrol of asymmetric reactions, including organocatalyzed transformations, see [93]). To our knowledge, only Yang and co-workers have presented another

Table 5 (*S*)-Proline/guanidinium salt **5b** co-catalyzed synthesis of *syn*-aldols derived from cyclohexanone

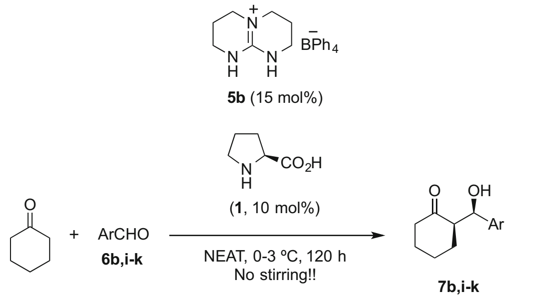

Entry	ArCHO	Conv. (%)[a]	*anti*:*syn*	*ee* (%)[b]
1	**6b** 4-NO_2–C_6H_4	>99 (86)	35:65	93
2	**6i** 3-NO_2–C_6H_4	>99 (87)	34:66	96
3	**6j** 2-NO_2–C_6H_4	>99 (92)	25:75	98
4	**6k** 4-CN–C_6H_4	>99 (98)	35:65	91

Reaction conditions: cyclohexanone (10 equiv.), aldehyde (1 equiv.), (*S*)-proline (**1**, 10 mol%), guanidinium salt **5b** (15 mol%), and no solvent. The reaction mixture was left to stand inside a fridge (0–3°C) for 120 h without stirring

[a]Conversion of aldehyde **6** (limiting reagent) into aldol **7**. Isolated yield of analytically pure products is given in brackets

[b]Enantiomeric excess of aldol adduct *syn*-**7**

organocatalytic system of this kind, where the diastereoselectivity of aldol reactions is determined by the participation of different additives [94].

Taking as an example aldol **7j** decorated with a nitro group in position 2 of the aromatic ring and making use of the methodologies represented in Tables 2 and 5, all four possible spatial configurations of this compound could be accessed with excellent enantioselectivity by choosing the appropriate combination of either (*S*)- or (*R*)-proline and either guanidinium salts **5a** or **5b** (Fig. 7). Moreover, considering that the *anti*- and *syn*-diastereoisomers of product **7j** were readily separated by standard flash chromatography on silica gel, these four products could be isolated in analytically pure form with high yield. Proline exerted the enantiocontrol on the reaction, whereas the guanidinium salt additive controlled the diastereoselection. It is worth noting that the paradigmatic organocatalyzed aldol reaction represented in Scheme 1 has been explored in depth, almost to extenuation, and consequently both *anti*- and *syn*-products have been studied and prepared independently. It was far from our interest to present a novel methodology for the proline-catalyzed aldol reaction but rather to demonstrate, as a proof of principle, how the judicious choice of an additive for the most widely known off-the-bench organocatalyst, proline, allows to gain access to either stereoisomer of a particular aldol product.

^{1}H NMR kinetic studies, DFT calculations, and further experiments were carried out in order to give an explanation for the unexpected *syn*-selectivity recorded in the case of using the tetraphenylborate guanidinium salt **5b**. In light of these experiments, the reaction mechanism shown in Fig. 8 was proposed.

Table 6 Direct aldol reaction between cyclohexanone and aromatic aldehydes **6b**,**i**–**k** catalyzed by (*S*)-proline, without the participation of tetraphenylborate guanidinium salts **5b**

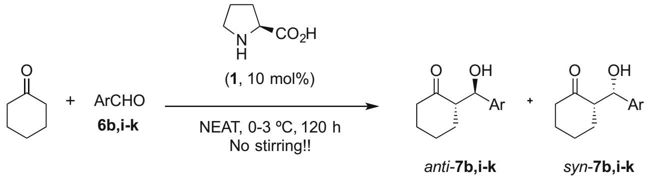

Entry	ArCHO	Conv. (%)[a]	*anti*:*syn*	*ee* (%)[b]
1	4-NO_2–C_6H_4**6b**	68	66:34	92 (95)
2	3-NO_2–C_6H_4**6i**	51	72:28	96 (89)
3	2-NO_2–C_6H_4**6j**	76	90:10	99 (80)
4	4-CN–C_6H_4**6k**	79	67:33	95 (94)

Reaction conditions: cyclohexanone (10 equiv.), aldehyde (1 equiv.), (*S*)-proline (**1**, 10 mol%), and no solvent; reaction mixtures left to stand inside a fridge (0–3°C) for 120 h without stirring or mechanical agitation

[a]Conversion of aldehyde **6** (limiting reagent) into aldol **7**

[b]Enantiomeric excess of aldol adduct *anti*-**7**. The enantiomeric excess of adduct *syn*-**7** is given in brackets (a preferred (*S*,*S*) absolute configuration is observed for these later compounds, in opposition to the (*R*,*R*) configuration of the adducts rendered according to the conditions of Table 5)

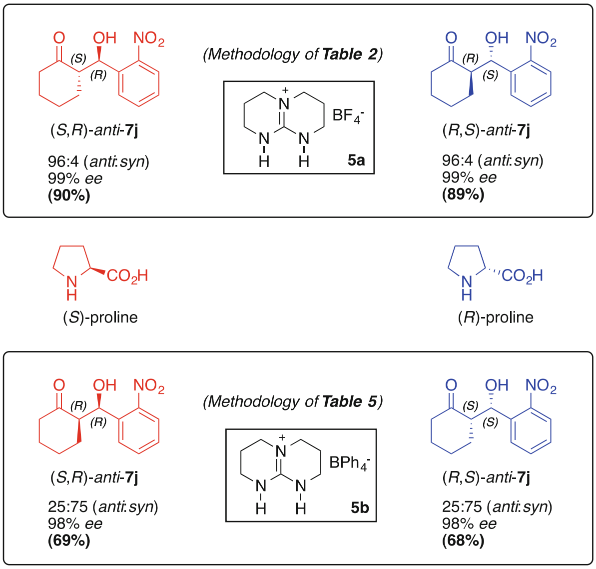

Fig. 7 Combinations of either (*S*)- or (*R*)-proline and guanidinium salt **5a** or **5b**, employed for the preparation of all possible spatial configurations of aldol product **7j** according to the methodologies shown in Tables 2 and 5. Isolated yield for each of the four stereoisomers in analytically pure form is given in *brackets*

Thus, on the one hand, *anti*-conformers would be afforded according to a Zimmerman–Traxler-type transition state **13** (similar to intermediate **11** represented in Fig. 6), stabilized by the establishment of a 1:1 complex between the guanidinium cation of additive **5b** and proline. This sort of intermediate was previously postulated

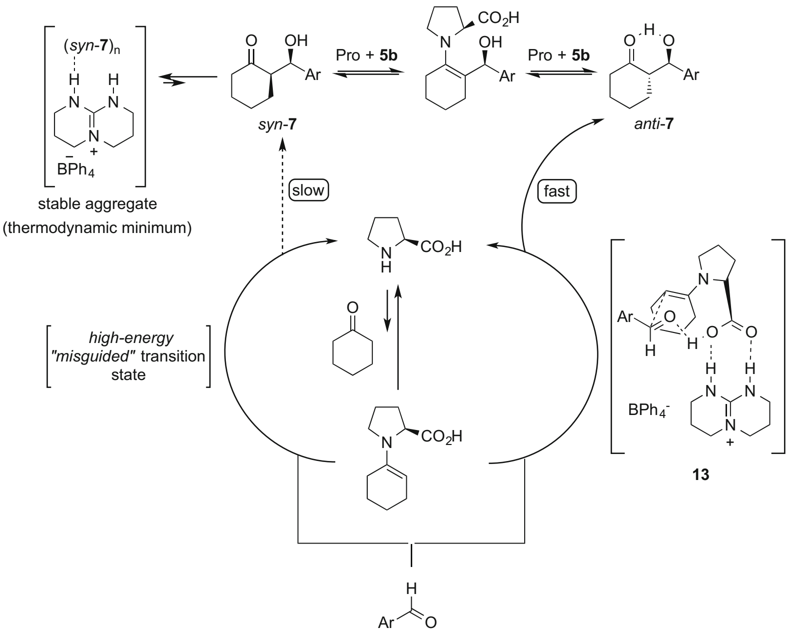

Fig. 8 Reaction mechanism proposed for the aldol reaction between cyclohexanone and aromatic aldehydes catalyzed by the system proline **1**/tetraphenylborate guanidinium salt **5b**

by others and by us to justify the high selectivity observed for *anti* products. On the other hand, *syn*-aldols would be formed slowly and in small quantity through a high-energy "misguided" transition state. While the *anti*-aldols seem to be far more stable in the gas phase (according to DFT calculations), *syn* isomers possess lower free energies under our experimental setup, being isolated as the major reaction products. Ruling out an aldol/retro-aldol sequence, the channel that connects both diastereoisomers was proposed to consist of a common proline–enamine intermediate, followed by its subsequent hydrolysis. This hypothesis served to explain the high enantiomeric excess observed for both *anti*- and *syn*-diastereoisomers. Nonetheless, it remains to be clarified why *syn*-diastereoisomers could be more stable products under the reactions conditions applied. The geometries of various adducts, optimized at the B3LYP6-31G* level of theory, showed how the *anti* adducts are stabilized by strong intramolecular hydrogen bonds, between the oxygen atom of the ketone carbonyl group and the O–*H* in β-position, accounting for 6.3–12.5 kJ/mol. The weak intramolecular interactions calculated for the *syn* compounds were suggested to be compensated with stronger intermolecular hydrogen bonds. Thus, considering the central effect played by the counter anions of our TBD-derived additives, it was reasoned that replacing the small and tightly bound tetrafluoroborate anion featured in **5a** with the bulkier tetraphenylborate of salt **5b** allows the bicyclic guanidinium core of **5b** to take part in large hydrogen-bonding networks with the *syn*-aldols. A mechanism like that depicted in

Fig. 8 offers a full account for all the experimental observations regarding this proline/guanidinium salt **5b** system.

3.2 Cross-Aldol Reaction Between Chloroacetone and Aromatic Aldehydes

The stereoselective construction of carbon stereocenters bearing halogenated substituents is a challenging synthetic task, particularly if organocatalytic methodologies are to be employed [95]. For instance, a collection of organocatalysts **14** [96], **15** [97], **16** [98, 99], and **17** [100] had been surveyed on the direct aldol reaction of chloroacetone and aromatic aldehydes, to render chlorohydrins **18** and **19** (Scheme 4). Catalysts **14–17** have to be prepared by cumbersome sequences implying various synthetic operations and manipulations. Moreover, structures such as **15** or **16** are based on expensive chiral building blocks such as (*S*)-NOBIM ((*S*)-2-amino-2′-hydroxy-1,1′-binaphthyl) and (*S*)-BINAM ((*S*)-2,2′-diamino-1,1′-binaphthyl), respectively.

2-Chloro-3-hydroxy ketones **19**, with two contiguous stereocenters, one of them halogenated, has attracted more interest than their regioisomeric analogue **18**. However, the available methodologies which employ organocatalysts **14–17** only achieved modest regioselectivities **18**:**19** and diastereoselectivities (ratio *anti*/*syn* for compounds **19**), except in the case of a few selected examples. Looking for an alternative solution to this problem, we decided to study our proline/guanidinium salt system on the reaction sketched in Scheme 4 [101]. Compared to the chemical modification of proline or the de novo synthesis of other organocatalysts, an approach employing hydrogen-bond-donating cocatalysts (guanidinium salts) to interact with proline and form a supramolecular catalyst complex is very attractive. Satisfyingly, under optimal reaction conditions, when a suspension of (*S*)-proline (**1**, 15 mol%), tetrafluoroborate guanidinium salt **5a** (10 mol%), and 4-nitrobenzaldehyde **6b** in chloroacetone (again, it was opted to work in the absence of organic solvent) was left to stand inside a standard laboratory fridge (0–3°C) for 20 days without any sort of stirring or mechanical agitation, a mixture of chlorohydrins **18b** + **19b** was produced with good regio- (96:4, **19b**:**18b**), diastereo- (*anti*:*syn*-**19b** 91:9), and enantioselectivity (98% *ee* for *anti*-**19b**) (Table 7, entry 1). Attempts to reduce the reaction time resulted in a severe decrease in selectivity for the reaction product **19b**.

A representative collection of aromatic aldehydes was reacted under analogous conditions (Table 7, entries 2–11). With no exception, all reactions proceeded smoothly with good conversion and high regio-, diastereo-, and enantioselectivity for the desired products **19**, independent of the nature of the substituents of the aldehyde. This observation highlights the robustness and reproducibility of this organocatalytic methodology. Moreover, blank experiments performed without guanidinium salt **5a** showed significantly poorer regio- and diastereoisomeric ratios

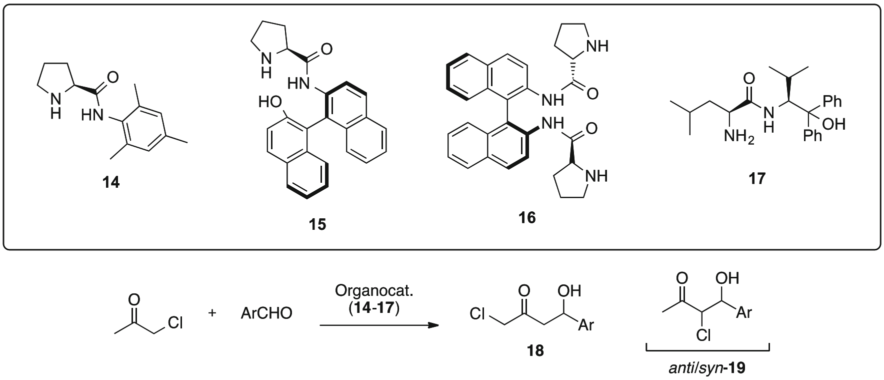

Scheme 4 Organocatalysts **14–17** previously employed for the direct aldol reaction between chloroacetone and aromatic aldehydes to afford α-chloro-β-hydroxy ketones (chlorohydrins) **18** and **19**

for chlorohydrins **19**, as well as poorer enantiomeric excesses, hence corroborating the virtues of TBD-derived guanidinium salts as additives for proline in the aldol reaction (Table 8).

Products **19**, which probed to be unstable during chromatography and when stored for prolonged times, were readily transformed into the corresponding chiral α,β-epoxy ketones *trans*-**20** according to a procedure described in the literature [98]. Interestingly, conditions were found that permitted preparing such epoxides in a one-pot procedure straight from chloroacetone and aromatic aldehydes (Table 9).

3.3 Cross-Aldol Reaction Between α-Azidoacetone and Aromatic Aldehydes

Densely functionalized α-azido-β-hydroxy ketones **21** are substances of considerable synthetic value which can be readily transformed into a broad variety of useful building blocks [102]. Access to compound **21** can be gained by a base-promoted aldol reaction of an α-azidoketone **22** and a non-enolizable aldehyde **23** (Scheme 5). There are many reports in the literature describing this type of approach [103–106], rendering the adduct **21** in optimum chemical yield, but featuring undesired mixtures of diastereoisomers. However, there were no previous works describing the synthesis of synthon **21** in a diastereo- or enantioselective manner.

Considering the efficiency of the proline/guanidinium salt organocatalytic system, it was investigated in reactions like that illustrated in Scheme 6 [107]. Azidoacetone (**24**, 1-azidopropan-2-one) was readily prepared from chloroacetone and sodium azide. In correspondence with our previous work, it was decided to evade the use of any organic solvent apart from a moderate excess of the ketone **24** acting as both reagent and reaction medium. The reaction was carefully optimized by

Table 7 (*S*)-Proline/guanidinium salt **5a** co-catalyzed synthesis of chlorohydrins **19a–d**,**f**,**i–n**

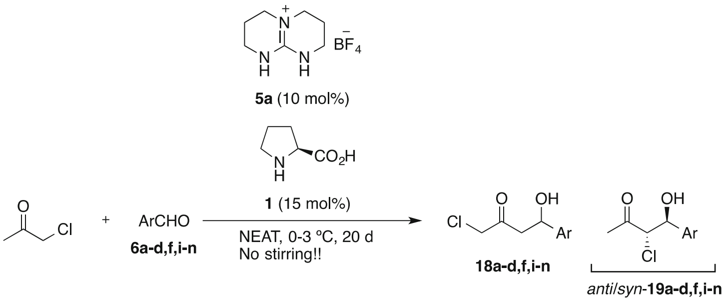

Entry	ArCHO	Conv. (%)[a]	Regioselectivity[b]	dr[c]	*ee* (%)[d]
1	**6b** 4-NO_2–C_6H_4	99	96:4	91:9	98
2	**6i** 3-NO_2–C_6H_4	97	96:4	92:8	97
3	**6j** 2-NO_2–C_6H_4	98	>99:1	93:7	97
4	**6c** 4-CO_2Me–C_6H_4	96	99:1	91:9	97
5	**6k** 4-CN–C_6H_4	>99	96:4	90:10	98
6[e]	**6l** 3-F–C_6H_4	95	92:8	94:6	94
7	**6a** 4-Cl–C_6H_4	79	95:5	94:6	95
8	**6f** 3-Cl–C_6H_4	98	96:4	93:7	96
9	**6d** 4-Br–C_6H_4	77	97:3	93:7	93
10	**6m** 2-Br–C_6H_4	90	>99:1	90:10	92
11	**6n** C_6H_5	99	98:2	93:7	94

Reaction conditions: chloroacetone (10 equiv.), aldehyde (1 equiv.), (*S*)-proline (**1**, 15 mol%), guanidinium salt **5a** (10 mol%), and no solvent. The reaction mixture was left to stand inside a fridge (0–3°C) for 20 days without stirring

[a]Conversion of aldehyde **6** (limiting reagent) into chlorohydrins **18** + **19**

[b]Ratio **19** (*anti*- + *syn*-):**18**

[c]Diastereoisomeric ratio *anti*- to *syn*-**19**

[d]Enantiomeric excess of compounds *anti*-**19**

[e]The reaction was stopped after 14 days

modifying the stoichiometry of the reagents, temperature, and reaction time. Various TBD-derived guanidinium salt **5** were also examined. Eventually, when a suspension of (*S*)-proline (**1**, 10 mol%), tetraphenylborate guanidinium salt **5b** (15 mol%), and 4-nitrobenzaldehyde **6b** was stirred in azidoacetone **24** (10 equiv. relative to the aldehyde) for 120 h at −10°C, the α-azido-β-hydroxy ketone **25b** was produced in quantitative conversion with good diastereo- (*anti*-**25b**:*syn*-**25b**, 90:10) and enantioselectivity (97% *ee* for *anti*-**25b**, Table 10, entry 1). The corresponding regioisomer **26** was not detected.

A set of aldehydes **6a**,**c**,**d**,**g**,**i**,**j**,**n**,**o**, decorated with different functional groups and substitution patterns, were reacted with azidoacetone under the best set of reaction conditions (Table 10, entries 2–7). All of these reactions proceeded with good conversion and high *anti*-diastereoselectivity and enantioselectivity (around 97% *ee* in all cases), independent of the nature of the aldehyde employed. Also, heteroaromatic aldehydes such as 2-furylcarboxaldehyde **6g** and 2-pyridylcarboxaldehyde **6o** proved

Table 8 Proline-catalyzed aldol reaction between chloroacetone and aromatic aldehydes, in the absence of guanidinium salt **5a**

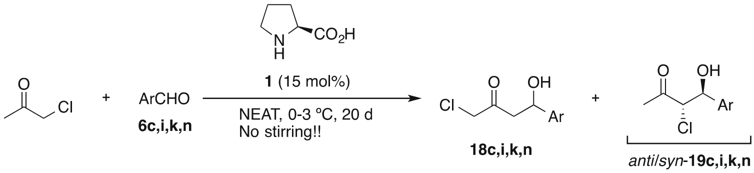

Entry	ArCHO	Conv. (%)[a]	Regioselectivity[b]	dr[c]	*ee* (%)[d]
1	**6c** 4-CO_2Me–C_6H_4	98	93:7	85:15	95
2	**6k** 4-CN–C_6H_4	99	85:15	83:17	96
3	**6n** C_6H_5	99	94:6	84:16	92
4	**6i** 3-NO_2–C_6H_4	99	80:20	78:22	97

Reaction conditions: chloroacetone (10 equiv.), aldehyde (1 equiv.), (*S*)-proline (**1**, 15 mol%), and no solvent. The reaction mixture was left to stand inside a fridge (0–3°C) for 20 days without stirring

[a]Conversion of aldehyde **6** (limiting reagent) into chlorohydrins **18** + **19**

[b]Ratio **19** (*anti-* + *syn-*):**18**

[c]Diastereoisomeric ratio *anti-* to *syn-***19**

[d]Enantiomeric excess of compounds *anti-***19**

Table 9 One-pot synthesis of representative *trans*-α,β-epoxy ketones **20j,l** from chloroacetone and aromatic aldehydes

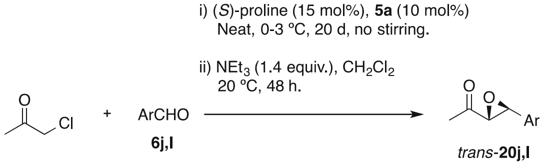

Entry	ArCHO	Product	Yield (%)[a]	*ee* (%)
1	**6j**2-NO_2–C_6H_4	**20j**	55	85
2	**6l** 3-F–C_6H_4	**20l**	33	79

Reaction conditions: chloroacetone (10 equiv.), aldehyde (1 equiv.), (*S*)-proline (**1**, 15 mol%), guanidinium salt **5a** (10 mol%), and no solvent. The reaction mixture was left to stand inside a fridge (0–3°C) for 20 days without stirring, then allowed to warm to r.t., and stirred for 48 h with NEt_3 (1.4 equiv.) and CH_2Cl_2 ($c = 0.4$ M)

[a]Isolated yield of analytically pure product

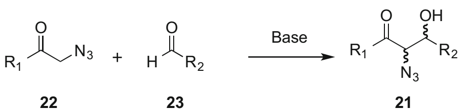

Scheme 5 Classical synthetic scheme for the preparation of α-azido-β-hydroxy ketones **21**

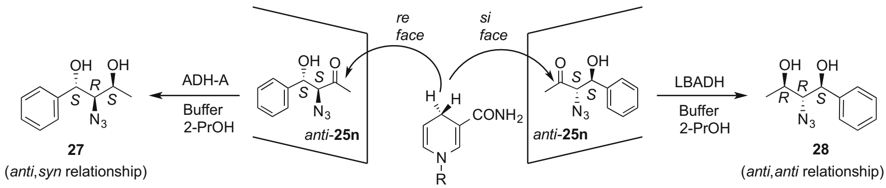

Scheme 6 Stereodivergent reduction of *anti*-**25n** with ADH-A ((*S*)-selective enzyme) affording diol **27** and LBADH ((*R*)-selective enzyme) giving access to diol **28**. In the middle, the structure of the nicotinamide cofactor present in both ADHs is drawn

Table 10 (*S*)-Proline/guanidinium salt **5b** co-catalyzed synthesis of α-azido-β-hydroxy ketones **25a–d,g,i,j,n,o**

25a-d,g,i,j,n,o.

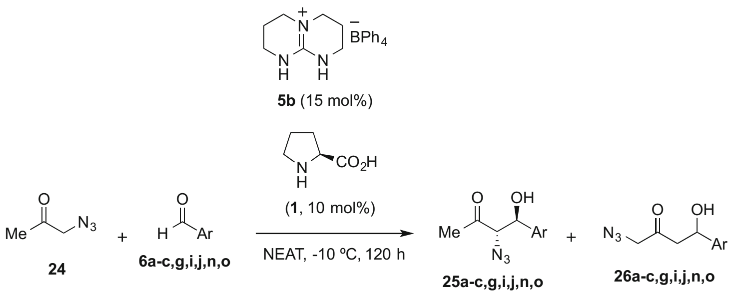

Entry	ArCHO	Conv. (%)[a]	dr[b]	*ee* (%)[c]
1	**6b** 4-NO_2–C_6H_4	>99 (90)	90:10	94
2	**6i** 3-NO_2–C_6H_4	>99 (91)	90:10	95
3	**6j** 2-NO_2–C_6H_4	99 (88)	90:10	97
4	**6n** C_6H_5	>99 (84)	90:10	95
5	**6a** 4-Cl–C_6H_4	98 (85)	90:10	94
6	**6d** 4-Br–C_6H_4	98 (84)	89:11	95
7	**6c** 4-CO_2Me–C_6H_4	99 (83)	88:12	95
8	**6g** 2–furyl	>99 (78)	85:15	93
9	**6o** 2–pyridyl	>99 (80)	87:13	88
10[d]	**6b** 4-NO_2–C_6H_4	12	82:18	n.d.

Reaction conditions: azidoacetone **24** (10 equiv.), aldehyde (1 equiv.), (*S*)-proline (**1**, 10 mol%), guanidinium salt **5b** (15 mol%), and no solvent (neat). The reaction mixtures were stirred for 120 h at −10°C

[a]Conversion of aldehyde **6** (limiting reagent) into α-azido-β-hydroxy ketone **25** (*anti*- + *syn*-). Chemical yield of analytically pure products *anti*-**25** is given in brackets

[b]Diastereoisomeric ratio *anti*- to *syn*-**25**

[c]Enantiomeric excess of analytically pure compounds *anti*-**25**

[d]Reaction carried out without the addition of guanidinium salt **5b**. The enantiomeric excess of the product **5b** was not determined as a consequence of the low conversion

to be appropriate substrates for this reaction, the corresponding products **25g** and **25o** displaying good selectivity figures (Table 10, entries 8 and 9). The tolerance of the reaction for heteroaromatic aldehydes, challenging substrates in aldol-type C–C bond-forming reactions, confirms the reproducibility and robustness of this transformation. All adducts *anti*-**25a–d**,**i**,**j**,**n**,**o** could be easily isolated by standard chromatographic techniques, affording analytically pure products in high yield and high *ee*. The presence of the corresponding regioisomers **26a–d**,**g**,**i**,**j**,**n**,**o** was not observed in any of these transformations. A blank experiment performed without additive **5b** (Table 10, entry 10) resulted in a significantly lower conversion as well as poorer diastereomeric ratio for the reaction product. Other reactions performed without additive **5b** were rather messy, rendering complex mixtures of unidentifiable products from which it was not possible to determine conversion values to aldol **25**. This demonstrates the positive effect of the guanidinium salt on the reaction course, which does not only improve the performance of the proline catalyst but even enables a transformation that is not favorable with the exclusive use of the amino acid itself. Alternatively, the sole presence of guanidinium salt **5b** was insufficient to catalyze the aldol reaction between aldehyde **6** and azidoacetone **24** to any extent.

Product **25** had not been described previously, and determining their absolute spatial configuration was a difficult exercise. After several unfruitful attempts, this was finally accomplished by the bioreduction of the ketone moiety of diastereopure α-azido-β-hydroxy ketone **25n**, used as a representative model, employing two stereocomplementary alcohol dehydrogenase enzymes (ADHs), one from *Rhodococcus ruber* (ADH-A) [108] and another from *Lactobacillus brevis* (LBADH) [109]. These enzymes have shown excellent stereoselectivities toward the reduction of α-azido ketones [110] with opposite stereopreference: ADH-A affords the corresponding (*S*)-alcohols, while LBADH gives the corresponding (*R*)-configured antipodes. So, when α-azido-β-hydroxy ketone **25n** was treated with either ADH-A or LBADH enzymes, the corresponding 2-azido-1,3-diol **27** or **28** was afforded, respectively (Scheme 6). Since the absolute configuration of the new alcohol function formed was fully predictable as a consequence of the enzyme's inherent selectivity, measuring the coupling constants between the protons at positions C2 ($CH{-}N_3$) and C3 ($CH_3CH{-}OH$) in diols **27** ($^3J_{syn}$) and **28** ($^3J_{anti}$) allowed the unambiguous assignation of the absolute stereochemical configuration of the preceding aldol adduct as *anti*-(3*S*,4*S*)-**25n**. The rest of the α-azido-β-hydroxy methyl ketones rendered from the organocatalyzed process were characterized by analogy.

4 Conclusions and Outlook

In summary, the assembly of supramolecular catalysts constructed from proline and H-bond-donating molecules has been revealed as an interesting alternative to the chemical modification of the amino acid unit. Typically, this simple and economic approach has made use of alcohols, ureas, thioureas, and other small organic molecules. Recently, conformationally restricted guanidinium salts derived from

TDB have emerged as outstanding additives for proline in organocatalyzed aldol reactions. Thus, a straightforward, green, efficient, and highly selective protocol has been developed for the direct aldol reaction between aromatic aldehydes and various ketones (cyclohexanone, cyclopentanone, or acetone) making use of a cooperative proline/guanidinium salt catalytic system. These processes operate under rather mild reaction conditions: without organic solvent, in closed-cap tubes standing inside a standard laboratory fridge, and without agitation or mechanical stirring. The participation of the guanidinium salt, forming a 1:1 supramolecular complex [guanidinium cation · proline] in the transition state, has been demonstrated to greatly enhance the reactivity and selectivity of the amino acid itself in a classical transformation such as the aldol reaction.

Besides, it has been put forward how the choice of the anion accompanying the guanidinium core of the TBD-derived salts used as cocatalysts for proline can give rise to stereodivergent pathways in the cross-aldol reaction, allowing the preparation of either *anti*- or *syn*-aldols from cyclohexanone and aromatic aldehydes. The origin of the *syn*-diastereoselectivity has been studied mechanistically and was shown to originate from an unusual equilibrium process coupled to the enamine-based catalytic cycle standard for proline. The outcome of the *syn*-selectivity reactions could not be predicted or foreseen considering the nature of the organocatalyst used (proline) and the substrates involved. It unfolds from the consideration of the whole complex network resulting from the simultaneous coexistence of *anti*-aldols, *syn*-aldols, (*S*)-proline, guanidinium and guanidine species, aromatic aldehydes, cyclohexanone, and enamines, all of which featured in the reaction media to some extent, as well as their interactions (including supramolecular contacts) and competition, their different solubility, solvation, etc. In the opinion of these authors, the study of collections/systems of compounds (i.e., catalytic systems) being considered as a whole, i.e., a System Chemistry approximation (for general comprehensive reviews on System Chemistry, see [111–115]), can lead to interesting discoveries in areas such as organocatalysis.

Relevantly, the addition of guanidinium salts does not only improve the classical aldol reaction but can also break the boundaries of proline as a catalyst. By these means, α-chloro-β-hydroxy ketones have been prepared with high enantioselectivity, employing for the first time catalytic amounts of (*S*)-proline, aided by the participation of a TBD-derived tetrafluoroborate guanidinium salt. Similarly, a cooperative proline/tetraphenylborate guanidinium salt has given rise to the pioneering synthesis of α-azido-β-hydroxy ketones. These families of compounds could be readily transformed into synthetically useful chiral α,β-epoxy ketones or different isomers of 2-azido-1,3-diols.

The construction and study of supramolecular catalytic systems involving guanidinium salts are yet in its infancy. So far, to our knowledge, only five reports have appeared in the literature about this topic [74, 88, 89, 101, 107]. Granted the success of the TBD-derived guanidinium salts, we anticipate other species of the like will be capable of displaying similar or better properties as additives for proline or other natural amino acids. The possibility of replacing the anion of these salts, possibly leading to different reactivities, is particularly appealing. Therefore, in principle, carefully designed systems could be engineered to catalyze novel transformations, even other than aldol-type reactions. Surely, the years to come will show further examples of the potential of such systems.

References

1. Anastas PT, Warner JC (1998) Green chemistry: theory and practice. Oxford University Press, New York
2. Tang SLY, Smith RL, Poliakoff M (2005) Green Chem 7:761
3. Knoevenagel E (1896) Ber Dtsch Chem Ges 29:172
4. Knoevenagel E (1898) Ber Dtsch Chem Ges 31:738
5. Knoevenagel E (1898) Ber Dtsch Chem Ges 31:2585
6. Knoevenagel E (1898) Ber Dtsch Chem Ges 31:2596
7. List B, Lerner RA, Barbas CF III (2000) J Am Chem Soc 122:2395
8. Ahrendt KA, Borths CJ, MacMillan DWC (2000) J Am Chem Soc 122:4243
9. Dalko PI, Moisan L (2001) Angew Chem Int Ed 40:3726
10. List B (2001) Synlett 1675
11. List B (2002) Tetrahedron 58:5573
12. Dalko PI, Moisan L (2004) Angew Chem Int Ed 43:5138
13. Notz W, Tanaka F, Barbas CF (2004) Acc Chem Res 37:580
14. Seayad J, List B (2005) Org Biomol Chem 3:719
15. List B (2006) Chem Commun 819
16. Lelais G, MacMillan DWC (2006) Aldrichim Acta 39:79
17. Mukherjee S, Yang JW, Hoffmann S, List B (2007) Chem Rev 107:5471
18. Dondoni A, Massi A (2008) Angew Chem Int Ed 47:4638
19. Melchiorre P, Marigo M, Carlone A, Bartoli G (2008) Angew Chem Int Ed 47:6138
20. Barbas CF (2008) Angew Chem Int Ed 47:42
21. Shao Z, Zhang H (2009) Chem Soc Rev 38:2745
22. Bertelsen S, Jørgensen KA (2009) Chem Soc Rev 38:2178
23. Liu X, Lin L, Feng X (2009) Chem Commun 6145
24. Mase N, Tanaka F, Barbas CF (2003) Org Lett 5:4369
25. Mase N, Tanaka F, Barbas CF (2004) Angew Chem Int Ed 43:2420
26. Tanaka F, Thayumanavan R, Mase N, Barbas CF (2004) Tetrahedron Lett 45:325
27. List B, Pojarliev P, Martin HJ (2001) Org Lett 3:2423
28. Darbre T, Machuqueiro M (2003) Chem Commun 1090
29. Kofoed J, Machuqueiro M, Reymond J-L, Darbre T (2004) Chem Commun 1540
30. Fernández-López R, Kofoed J, Machuqueiro M, Darbre T (2005) Eur J Org Chem 5268
31. Kofoed J, Reymond J-L, Darbre T (2005) Org Biomol Chem 3:1850
32. Kofoed J, Darbre T, Reymond J-L (2006) Chem Commun 1482
33. Majewski M, Niewczas I, Palyam N (2006) Synlett 2387
34. Penhoat M, Barbry D, Rolando C (2011) Tetrahedron Lett 52:159
35. Karmakar A, Maji T, Wittmann S, Reiser O (2011) Chem Eur J 17:11024
36. Wu YS, Chen Y, Deng DS, Cai J (2005) Synlett 1627
37. Nyberg AI, Usano A, Pikho PM (2004) Synlett 1891
38. Amedjkouh M (2005) Tetrahedron Asymmetry 16:1411
39. Pikho PM, Laurikainen KM, Usano A, Nyberg AI, Kaavi JA (2006) Tetrahedron 62:317
40. Zotova N, Franzke A, Armstrong A, Blackmond DG (2007) J Am Chem Soc 129:15100
41. Zhou Y, Shan Z (2006) J Org Chem 71:9510
42. Zhou Y, Shan Z (2006) Tetrahedron Asymmetry 17:1671
43. Jianqing L, Rong T, Yu K, Chengyong L, Donghong Y (2012) Chin J Catal 33:1133

44. Poe SL, Bogdan AR, Mason BP, Steinbacher JL, Opalka SM, McQuade DT (2009) J Org Chem 74:1574
45. Reis Ö, Eymur S, Reis B, Demir AS (2009) Chem Commun 1088
46. Companyó X, Valero G, Crovetto L, Moyano A, Rios R (2009) Chem Eur J 15:6564
47. Demir AS, Eymur S (2010) Tetrahedron Asymmetry 21:405
48. El-Hamdouni N, Companyó X, Ríos R, Moyano A (2010) Chem Eur J 16:1142
49. Wang WH, Abe T, Wang XB, Kodama K, Hirose T, Zhang GY (2010) Tetrahedron Asymmetry 21:2925
50. Opalka SM, Steinbacher JL, Lambiris BA, McQuade DT (2011) J Org Chem 76:6503
51. Demir AS, Basceken S (2013) Tetrahedron Asymmetry 24:515
52. Demircan E, Eymur S, Demir AS (2014) Tetrahedron Asymmetry 25:443
53. Cho E, Kim TH (2014) Tetrahedron Lett 55:6470
54. Porcar R, Ríos-Lombardía N, Busto E, Gotor-Fernández V, Gotor V, García-Verdugo E, Burguete MI, Luis SV (2013) Catal Sci Technol 3:2596
55. Demir AS, Eymur S (2010) Tetrahedron Asymmetry 21:112
56. Xu K, Zhang S, Hu Y, Zha Z, Wang Z (2013) Chem Eur J 19:3573
57. Well T, Kotke M, Kleiner CM, Schreiner PR (2008) Org Lett 10:1513
58. Fitzmaurice RJ, Kyne GM, Douheret, D, Kilburn JD (2002) J Chem Soc Perkin Trans I 841
59. Blondeau P, Segura M, Pérez-Fernández R, de Mendoza J (2007) Chem Soc Rev 36:198
60. Coles MP (2009) Chem Commun 3659
61. Kim SK, Sessler JL (2010) Chem Soc Rev 39:3784
62. Shah J, Blumenthal H, Yacob Z, Liesbscher J (2008) Adv Synth Catal 350:1267
63. Chinchilla R, Nájera C, Sánchez-Agulló P (1994) Tetrahedron Asymmetry 5:1393
64. Horváth A (1996) Tetrahedron Lett 37:4423
65. Simoni D, Rossi M, Rondanin R, Mazzali A, Baruchello R, Malagutti C, Roberti M, Invidiata FP (2000) Org Lett 2:3765
66. Simoni D, Rondanin R, Morini M, Baruchello R, Invidiata FP (2000) Tetrahedron Lett 41:1607
67. Ye W, Xu J, Tan C-T, Tan C-H (2005) Tetrahedron Lett 46:6875
68. Jiang Z, Zhang Y, Ye W, Tan C-H (2007) Tetrahedron Lett 48:51
69. Ghobril C, Sabot C, Mioskowski C, Baati R (2008) Eur J Org Chem 4104
70. Mahé O, Frath D, Dez I, Marsais F, Levacher V, Brière J-F (2009) Org Biomol Chem 7:3648
71. Martínez-Castañeda A, Rodríguez-Solla H, Concellón C, del Amo V (2012) Org Biomol Chem 10:1976
72. Poladura B, Martínez-Castañeda A, Rodríguez-Solla H, Concellón C, del Amo V (2012) Tetrahedron 68:6438
73. Linton B, Hamilton AD (1999) Tetrahedron 55:6027
74. Martínez-Castañeda A, Poladura B, Rodríguez-Solla H, Concellón C, del Amo V (2011) Org Lett 13:3032
75. Rodríguez B, Rantanen T, Bolm C (2006) Angew Chem Int Ed 45:6924
76. Rodríguez B, Bruckmann A, Bolm C (2007) Chem Eur J 13:4710
77. Guillena G, Hita MC, Nájera C, Viózquez SF (2007) Tetrahedron Asymmetry 18:2300
78. Guillena G, Nájera C, Viózquez SF (2008) Synlett 3031
79. Almasi D, Alonso DA, Nájera C (2008) Adv Synth Catal 350:2467
80. Worch C, Bolm C (2009) Synlett 2425
81. Almasi D, Alonso DA, Balaguer AN, Nájera C (2009) Adv Synth Catal 351:1123
82. Banon-Caballero A, Guillena G, Nájera C (2010) Green Chem 12:1599
83. Hernández JG, García-López V, Juriasti E (2012) Tetrahedron 68:92
84. Zhang F, Li C, Qi C (2013) Tetrahedron Asymmetry 24:380
85. Banon-Caballero A, Guillena G, Nájera C, Faggi E, Sebastián RM, Vallribera A (2013) Tetrahedron 69:1307
86. Kellog RM (2007) Angew Chem Int Ed 46:494
87. Xue X-S, Yang C, Li X, Cheng J-P (2014) J Org Chem 79:1166

88. Ma G, Bartoszewicz A, Ibrahem I, Córdova A (2011) Adv Synth Catal 353:3114
89. Martínez-Castañeda A, Rodríguez-Solla H, Concellón C, del Amo V (2012) J Org Chem 77:10375
90. Pousee G, Le Cavelier F, Humphreys L, Rouden J, Blanchert J (2010) Org Lett 12:3582
91. Zhou P, Luo S, Cheng JP (2011) Org Biomol Chem 9:1784
92. Kanemitsu T, Umehara A, Miyazaki M, Nagata K, Itoh T (2011) Eur J Org Chem 993
93. Escorihuela J, Burguete MI, Luis SV (2013) Chem Soc Rev 42:5595
94. Gao J, Bai S, Gao Q, Liu Y, Yang Q (2011) Chem Commun 47:6716
95. Shibatomi K (2010) Synthesis 2679
96. He L, Tang Z, Cun L-F, Mi A-Q, Jiang Y-Z, Gong L-Z (2006) Tetrahedron 62:346
97. Russo A, Botta G, Lattanzi A (2007) Tetrahedron 63:11886
98. Guillena G, Hita MC, Nájera C (2007) Tetrahedron Asymmetry 18:1272
99. Guillena G, Hita MC, Nájera C, Viózquez SF (2008) J Org Chem 73:5933
100. Xu X-Y, Wang Y-Z, Gong L-Z (2007) Org Lett 9:4247
101. Martínez-Castañeda A, Poladura B, Rodríguez-Solla H, Concellón C, del Amo V (2012) Chem Eur J 18:5188
102. Patonay T, Kónya K, Juhász-Tóth E (2011) Chem Soc Rev 40:2797
103. Patonay T, Hoffman RV (1995) J Org Chem 60:2368
104. Patonay T, Juhász-Tóth E, Bényei A (2002) Eur J Org Chem 285
105. Juhász-Tóth E, Patonay T (2002) Eur J Org Chem 3055
106. Patonay T, Jeko J, Juhász-Tóth E (2008) Eur J Org Chem 1441
107. Martínez-Castañeda A, Kędziora K, Lavandera I, Rodríguez-Solla H, Concellón C, del Amo V (2014) Chem Commun 50:2598
108. Stampfer W, Kosjek B, Moitzi C, Kroutil W, Faber K (2002) Angew Chem Int Ed 41:1014
109. Wolberg M, Hummel W, Wandrey C, Müller M (2000) Angew Chem Int Ed 39:4306
110. Cuetos A, Bisogno FR, Lavandera I, Gotor V (2013) Chem Commun 49:2625
111. Kindermann M, Stahl I, Reimold M, Pankau WM, von Kiedrowski G (2005) Angew Chem Int Ed 44:6750
112. Ludlow RF, Otto S (2008) Chem Soc Rev 37:101
113. Nitschke JR (2009) Nature 462:736
114. von Kiedrowski G, Otto S, Herdewijn P (2010) J Syst Chem 1:1
115. Hunt RAR, Otto S (2011) Chem Commun 47:847

Top Heterocycl Chem (2017) 51: 27–74
DOI: 10.1007/7081_2015_167

Published online: 29 August 2015

Guanidines as Catalysts for Direct and Indirect CO_2 Capture and Activation

Rafael Dias do Espírito Santo, Rebeca Monique Capitão, and Eduardo René Pérez González

Abstract CO_2 emissions into the atmosphere from combustion processes remain large, and minimization of this phenomenon is wanted worldwide. The control of excessive CO_2 release represents a challenge that requires new technologies. While CO_2 represents an environmental problem as a greenhouse gas, it is at the same time eco-friendly in comparison with many other gases. Therefore, the development of suitable methods for the preparation of CO_2-containing compounds like organic carbonates and urethanes could be a good alternative for recycling CO_2 and using it as a substitute for phosgene, which is a high toxic reagent. Another non-phosgene alternative for the preparation of carbonates and carbamates is the reaction of organic carbonates with alcohols or amines. One environmentally benign organic carbonate is dimethyl carbonate (DMC), and because of increasing DMC production from CO_2 reactions, using DMC can be considered as an indirect capture of CO_2. Heterocyclic guanidines, like 1,5,7-triazabicyclo[4.4.0]dec-5-ene (TBD) and *N*-methyl-1,5,7-triazabicyclo[4.4.0]dec-5-ene (MTBD), and linear guanidines like 1,1,3,3-tetramethylguanidine (TMG) are some of the most commonly used guanidines in catalysis, being strong proton acceptors, comparable in strength with aliphatic amines. This chapter summarizes a number of works on the utilization of guanidines as catalysts for the direct and indirect capture and activation of the CO_2 molecule, aiming at the insertion of this molecule into several chemical substrates to mitigate excess CO_2 release and its environmental impact.

Keywords Carbon dioxide capture and activation · DMC · Guanidines as catalysts · TBD · TMG

R.D.E. Santo, R.M. Capitão, and E.R.P. González (✉)
Faculty of Sciences and Technology, Department of Physics, Chemistry and Biology, State University of Sao Paulo – UNESP, Rua Roberto Simonsen, 305, CEP 19060-900 Presidente Prudente, Sao Paulo, Brazil
e-mail: eperez@fct.unesp.br

Contents

Abbreviations

BnTBD	*N*-Benzyl-1,5,7-triazabicyclo[4.4.0]dec-5-ene
BuTMG	*N*-Butyl-*N′*,*N′*,*N″*,*N″*-tetramethylguanidine
CCS	Carbon capture and storage
CO_2BOL	CO_2 binding organic liquids
CyTEG	*N*-Cyclohexyl-*N′*,*N′*,*N″*,*N″*-tetraethylguanidine
CyTMG	*N*-Cyclohexyl-*N′*,*N′*,*N″*,*N″*-tetramethylguanidine
DAB	1,4-Diaminobutane
DABCO	1,4-Diazabicyclo[2.2.2]octane
DBN	1,5-Diazabicyclo(4.3.0)non-5-ene
DBU	1,8-Diazabicyclo[5.4.0]undec-7-ene
DFT	Density functional theory
DMAc	Dimethylacetamide
DMAP	4-(Dimethylamino)pyridine
DMC	Dimethyl carbonate
DPC	Diphenyl carbonate
DPG	Diphenylguanidine
EtTBD	*N*-Ethyl-1,5,7-triazabicyclo[4.4.0]dec-5-ene
FAGCs	Fatty acid glycerol carbonates
FAMEs	Fatty acid methyl esters
FGBILs	Functional guanidinium-based ionic liquids
ILs	Ionic liquids
MTBD	*N*-Methyl-1,5,7-triazabicyclo[4.4.0]dec-5-ene
*n*BuTBD	*N*-Butyl-1,5,7-triazabicyclo[4.4.0]dec-5-ene
PEG	Polyethylene glycol
PhTMG	*N*-Phenyl-*N′*,*N′*,*N″*,*N″*-tetramethylguanidine
PIL	Protic ionic liquid
PMDBD	3,3,6,9,9-Pentamethyl-2,10-diazabicyclo[4.4.O]dec-1-ene
PTMG	*N*-Propyl-*N′*,*N′*,*N″*,*N″*-tetramethylguanidine

TBD 1,5,7-Triazabicyclo[4.4.0]dec-5-ene
TMG 1,1,3,3-Tetramethylguanidine

1 Introduction

Carbon dioxide emissions into the atmosphere from combustion processes remain large, and minimization of its emission is desirable [1]. The control of CO_2 emissions represents a challenging task that requires new ideas and new technologies [2].

CO_2 is an inexpensive reagent, environmentally benign, nonflammable, and ubiquitous. However, due to the inert nature of CO_2, its activation, capture, and insertion into organic molecules still remain a difficult challenge [1]. CO_2 utilization as a raw material in the synthesis of chemicals and fuels is attractive, and the implementation of such technologies on a large scale would allow for a change from a linear use of fossil carbon to its cyclic use, mimicking the natural process [2]. CO_2 can replace toxic species such as phosgene and react with dihydrogen, alcohols, epoxides, amines, olefins, dienes, and other unsaturated hydrocarbons, using various catalysts and reaction conditions to form various products such as formic acid and its esters, formamides, methanol, dimethyl carbonate, alkylene carbonates, carbamic acid esters, lactones, carboxylic acids, and polycarbonates [2].

In the field of CO_2 transformations, the CO_2 molecules are used as a starting material in chemical reactions such as photochemical, electrochemical, biological, reforming, and inorganic transformations [3]. Direct fixation of carbon dioxide into target compounds in synthetic and industrial applications is an important goal in order to decrease its release into the atmosphere [1, 4]. In 1975, CO_2 was found to be activated by transition metal complexes, and, since then, interest in the chemical conversion of carbon dioxide has shown continuous growth and development [2, 5]. A number of organic syntheses using carbon dioxide are known, but only a few were applied in industry [6–9]. The main industrial process is the syntheses of urea [3, 8–10] and its derivatives and the production of organic carbonates, where phosgene ($COCl_2$) is increasingly being replaced by CO_2 as the C1 building block [6].

Carbon Capture and Storage (CCS) technology is another vast research area [3] and one of the major options to reduce CO_2 emissions [11]. CCS has attracted much attention from the scientific community due to growing concerns about the environmental impact of this greenhouse gas [9, 12]. A key step in many CCS technologies is reversible binding of the CO_2 molecule, and therefore, it is of considerable interest to identify new mechanisms and compounds for reversible CO_2 binding [13].

Fixation of carbon dioxide can be a reversible process under mild conditions (low or moderate temperature, normal pressure, etc.), and at the same time, CO_2 release can involve a transcarboxylation process toward several nucleophiles [14, 15]. From the synthetic point of view, a CO_2 fixation release occurring as a reaction process (transcarboxylation) is more interesting because it is a kinetically reversible fixation. On the other hand, for other purposes such as industrial uses, a more thermodynamically stable fixation could be more suitable, with the CO_2 being fixed and released as the unique product [13].

1.1 Direct CO_2 Capture

While CO_2 represents an environmental issue as a greenhouse gas, it is also environmentally benign in comparison with many other chemical substances. The development of suitable methods for the preparation of interesting CO_2-containing compounds like organic carbonates and urethanes could be an alternative to recycling CO_2 and using it as a substitute for highly toxic phosgene and its derivatives [14, 16–19].

Organic carbonates are commercially produced from alcohols and phosgene [3]. Synthesis of carbamates also involves phosgene in the reaction of phosgene with alcohols, followed by aminolysis of the intermediate chloroformates ([20] and cited references), or reaction of an alcohol with isocyanates, usually obtained from phosgene ([20–22] and cited references). Both methods involve toxic and harmful compounds, and therefore, new alternatives with clean synthetic methodologies are desirable [20].

Carbon dioxide is one alternative to phosgene and isocyanates [20]. Preparation of CO_2 containing compounds like carbonates and carbamates by the respective reaction with alcohols (selected articles: [23–27]) or amines (selected articles: [25, 28–33]) is an interesting substitute to avoid the use of highly toxic phosgene and its derivatives (e.g., chloroformates) [13].

1.2 Indirect CO_2 Capture

Another non-phosgene alternative for the preparation of carbonates and carbamates is the reaction of organic carbonates with alcohols or amines [20]. Linear carbonates are important alkylating and carbonylating agents, just like alkyl halides and dialkyl sulfates, or phosgene and carbon monoxide, respectively ([2, 9]; for reviews of linear carbonates, see selected articles and cited references: [34, 35]; [36, 37]). Currently, the largest future application of organic carbonates is assumed to be as a substitute for phosgene [9] in carbonylation reactions.

One environmentally benign organic carbonate is dimethyl carbonate (DMC) that has been extensively studied due to its versatile chemical reactivity [34, 38]. DMC is used as a monomer for polymers in the chemical industry [39], in transesterification reactions (selected articles: [40–42]), as well as in the agrochemical [2] and pharmaceutical industry [43].

DMC synthesis is based on the use of phosgene or the oxidative carbonylation of methanol [38], but increasingly DMC synthesis is also starting from CO_2 (e.g., direct synthesis from CO_2 and methanol or one-pot synthesis from CO_2, methanol, and epoxides) [44–50].[1] For example, Asahi Kasei Corporation reported [36, 37] in 2003, for the first time in the world, the commercial production (50,000 ton $year^{-1}$) of a polycarbonate using carbon dioxide as a starting material. In this procedure, CO_2 is converted to DMC which is then used in the fabrication of the polymer (see Sect. 3). Because of the growing DMC production from CO_2, reactions using DMC can actually be considered as indirect CO_2 capture.

1.3 Guanidines

Amidines and guanidines are important classes of compounds that are found throughout nature and also have many uses in organic chemistry [51]. The most common use of amidines and guanidines in organic chemistry is as organic bases. They are some of the strongest neutral organic bases known, due to the ability to delocalize positive charge over their nitrogen atoms in their protonated forms (Fig. 1) [51, 52]. Traditionally, amidines and guanidines have been thought of as non-nucleophilic bases. However, with the recent increase in interest in organocatalysis [53], a number of amidines and guanidines have also been shown to act as nucleophilic catalysts in a wide range of reactions [51, 54].

Guanidinium-based molecules showed several biological activities [55, 56]. For example, several guanidines are used in the treatment of neglected tropical diseases [57]. Guanidines are also widely used in the synthesis of heterocyclic compounds [58].

Bicyclic guanidines, like TBD (**1**) (1,5,7-triazabicyclo[4.4.0]dec-5-ene) and MTBD (**2**) (*N*-methyl-1,5,7-triazabicyclo[4.4.0]dec-5-ene), and simple linear guanidines like TMG (**3**) (1,1,3,3-tetramethylguanidine) are some of the guanidines most commonly used as catalysts [51, 59]. Figure 2 shows the structures of these compounds and also other common guanidines and amidines that will be mentioned in the text (CyTMG (**4**) (*N*-cyclohexyl-*N′*,*N′*,*N″*,*N″*-tetramethylguanidine), CyTEG (**5**) (*N*-cyclohexyl-*N′*,*N′*,*N″*,*N″*-tetraethylguanidine), and DBU (**6**) (1,8-diazabicyclo[5.4.0]undec-7-ene)).

TMG and TBD are strong proton acceptors, comparable in strength with aliphatic amines [60]. TMG is regarded as a typical and fundamental guanidine compound and, in fact, has been used in many kinds of base-catalyzed reactions [52]. Barton et al. [61, 62] reported the preparation of pentaalkylguanidines and their application to organic synthesis as sterically hindered organic bases, which are called Barton’s bases. There are many reports on the synthetic uses of TMG and their analogues such as Barton’s base and TBD.[2] Among the synthetic uses of this

[1] For methods and catalysts used in DMC synthesis from CO_2, see [2, 3, 6, 9, 35, 38].

[2] For synthetic uses of TMG and their analogues, see Ishikawa [52]. For synthetic uses of TBD, see Kiesewetter et al. [54].

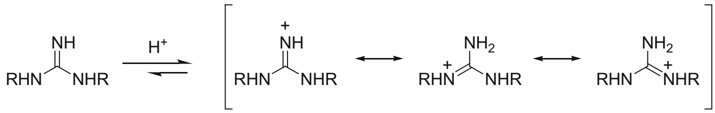

Fig. 1 Resonance of the guanidinium ion

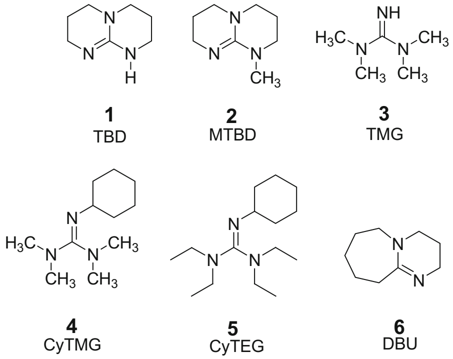

Fig. 2 Structures of the most commonly used guanidines

guanidines is the efficient catalysis in the synthesis of organic carbonates and urethanes by respective reactions of alcohols and amines with CO_2 [63–70].[3]

As a result of the crescent attention in guanidines as organocatalyst, several reviews on guanidine chemistry have appeared [52, 56, 59, 71–77]. This chapter shows literature reports of guanidines as catalysts for direct and indirect CO_2 capture and activation.

2 Direct CO_2 Capture and Activation

2.1 Synthesis of Linear Carbonates and Carbamates Catalyzed by Guanidines

Open chain organic carbonates can be divided into two groups: dialkyl (diaryl, alkyl–aryl) carbonates and polycarbonates [48, 78, 79]. Organic carbonates and carbamates are important classes of compounds and are used in a variety of industrial and synthetic applications [79] such as polymer chemistry [80], agrochemical [81] (pesticides, herbicides, insecticides, fungicides, etc.) [82], medicinal and biological fields [82, 83], solvents (electrolyte solvents for lithium–ion batteries, organic solvents for extractive separation, and fuel additives) [48, 78, 79], as

[3] Selected articles: [14, 15, 23, 24, 31].

well as intermediates in organic synthesis (selected articles: [84–87]). Carbamates are used for the protection of amino groups in peptide chemistry [88, 89] and as linkers in combinatorial chemistry [90].

Much research has been devoted to the synthesis of organic carbonates and carbamates starting from CO_2 [2, 91, 92] driven by its potential implications for climate change reduction and the associated economic benefits [50]. This chapter reviews the synthesis of linear organic carbonates and carbamates starting from CO_2 using guanidine compounds as catalysts.

In 1993, McGhee et al. [93] demonstrated the synthesis of *O*-allylic urethanes and *O*-allylic carbonates **9** from allylic chlorides **8**, CO_2, and amines or alcohols using palladium/phosphine catalysts. Syntheses were carried out by the addition of preformed carbamate/carbonate anions $RYCO_2^-$($^+$Hbase) **7**, generated from various alcohols or amines with CO_2, to THF solutions of allylic chlorides **8** under 80–100 psi of CO_2 at room temperature (or 30°C) employing a palladium/phosphine catalyst [93] (Fig. 3).

The choice of added base in the generation of carbamates/carbonates was found to be critical for high yields of *O*-allylic products. The authors used tertiary amines, guanidines, and amidines (guanidines, MTBD (**2**) and CyTMG (**4**); amidine, DBU (**6**) (Fig. 2)) and found that the use of CyTMG (**4**) or DBU (**6**) is optimal for this system [93].

Later in 1994, McGhee et al. [94] reported the synthesis of urethanes from several amines, CO_2, and alkyl chlorides by the reaction of amines with CO_2 generating the carbamate anion **10** followed by the addition of alkyl chlorides to reaction mixture to yield the respective carbamate esters **11** (Fig. 4). In this study, the guanidines MTBD (**2**), TMG (**3**), CyTMG (**4**), and CyTEG (**5**) were tested, and it was concluded that the use of pentaalkylguanidine bases increases the nucleophilicity of the oxygen center in the resulting carbamate anion and allowed for the generation of urethane materials in high yields and high selectivity [94].

The same group reported more two works [23, 95], both in 1995, dealing with the extension of the studies mentioned above. One described the synthesis of several carbamate esters from amines, CO_2, and alkyl chlorides, and the other was focused on the generation of dialkyl carbonates from alcohols/CO_2 and alkyl chlorides. In both studies, the authors used pentaalkylguanidines as catalysts, and these works resulted in a US patent to the authors in 1993 [96, 97].

In 1998, Kadokawa et al. [98] reported the direct polycondensation of CO_2 with xylylene glycols **12** using a trisubstituted phosphine/carbon tetrahalide/base system as a condensing agent, to give poly-xylylenecarbonates **13** (Fig. 5). Bases used in the reactions were CyTMG (**4**) and DBU (**6**). The screening was carried out at room temperature, and the best combination found was tributylphosphine (1.5 equiv. mol), carbon tetrabromide (2.0 equiv. mol), and CyTMG (**4**) as base (2.0 equiv. mol) for 3 h, giving 81% yield [98] (Fig. 5).

The reaction mechanism proposed by the authors is shown in Fig. 6 and involves the formation of an active intermediate ***a*** by the reaction of R_3P with CBr_4. The phosphonium species ***b*** is produced from xylylene glycols **12**, intermediate ***a***, and CO_2 in the presence of CyTMG. Then, the nucleophilic attack of the counter

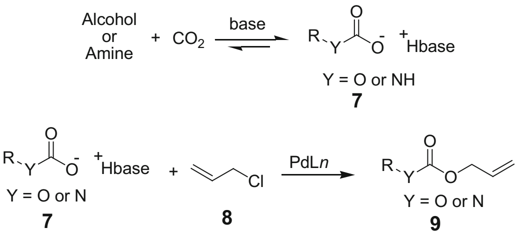

Fig. 3 *Above*: general procedure to obtain carbamate/carbonate anions **7**. *Below*: reaction between carbamate/carbonate anions **7** and allylic chlorides **8** generating *O*-allylic urethanes or *O*-allylic carbonates **9**

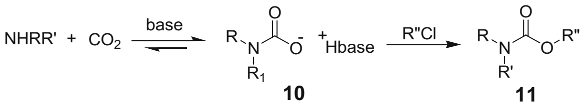

Fig. 4 General procedure for the synthesis of carbamates **11**

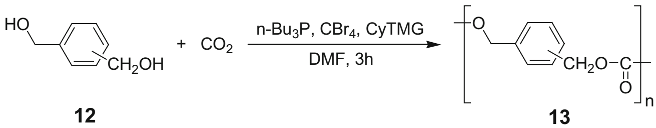

Fig. 5 General procedure of the direct polycondensation of CO_2 with xylylene glycols

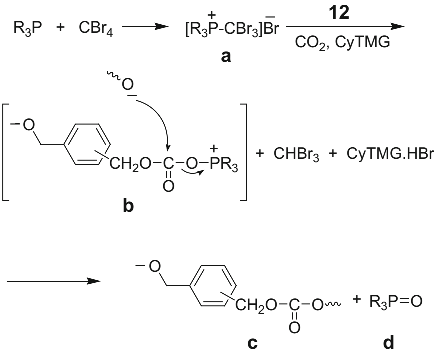

Fig. 6 Polycondensation mechanism proposed by Kadokawa et al. [98]

alcoholate anion in ***b*** at the carbonyl center of another molecule of ***b*** takes place according to an Arbuzov-type reaction, giving rise to the formation of carbonate ***c*** and phosphine oxide ***d*** [98].

One year later, the authors reported [99] the application of the same catalytic system to several primary alcohols resulting in carbonates **14** in relatively high

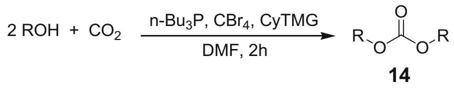

Fig. 7 General procedure for the synthesis of carbonates **14** from alcohols

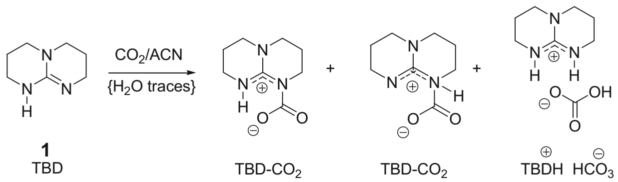

Fig. 8 Proposed structures formed by capture – activation of CO_2 by TBD (**1**)

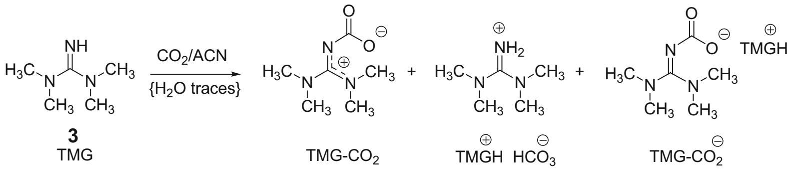

Fig. 9 Proposed structures formed by the activation of CO_2 with TMG (**3**)

yields (54.4–90.7%), whereas yields of carbonates derived from secondary alcohols were low (trace – 22.0%) (Fig. 7). The mechanism proposed by the authors is similar to the one shown in Fig. 6, involving the formation of a phosphonium intermediate and nucleophilic attack of the alcoholate to the carbonyl function followed by an Arbuzov-type reaction to yield the carbonate product and tributylphosphine oxide [99].

We have reported in 2008 [13] a study of CO_2 fixation – activation by the guanidines TBD (**1**) and TMG (**3**). In this paper, we investigated the CO_2 fixation and release by these guanidines and the nature of the guanidine-CO_2 complexes. The proposed structures for carbamate and bicarbonate products formed by the capture and activation of CO_2 with TBD (**1**) and TMG (**3**) are shown in Figs. 8 and 9, respectively.

These guanidines formed bicarbonates presumably via the preceding formation of water-solvated carbamic intermediates. CO_2 fixation with both TBD (**1**) and TMG (**3**) was a kinetically reversible process. The corresponding fixation products were shown to be useful as transcarboxylating agents, and this behavior mimics a transcarboxylase activity. TBD-CO_2 products display an interesting thermal stability with CO_2 release occurring at moderated temperatures. This could be useful for the selective separation of CO_2 from complex gas mixtures by TBD or TBD-related compounds [13].

In other works [14, 15], we suggested that CO_2 is nucleophilically activated by the amidine DBU (**6**) forming a DBU-CO_2 zwitterionic carbamate complex **15**.

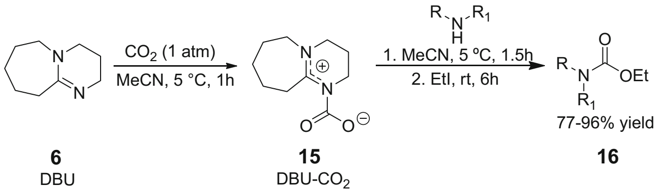

Fig. 10 Synthesis of carbamates **16** using DBU-CO_2 adduct **15** and amines

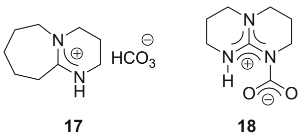

Fig. 11 Structures of DBU bicarbonate salt **17** and TBD-CO_2 adduct **18**

Transcarboxylation of amines with complex **15** followed by *O*-alkylation resulted in the *N*-alkyl carbamates **16** (Fig. 10).

However, the structure of the amidine DBU-CO_2 adduct **15** and also guanidine-CO_2 adducts was a matter of debate. Jessop et al. reported in 2005 [100] that the reaction between DBU (**6**) and CO_2 only forms the DBU bicarbonate salt [$DBUH^+$][HCO_3^-] (**17**, Fig. 11) in the presence of water, and there is no reaction in the absence of water [100].

Contradictory, Villiers et al. [67, 68] reported in 2010 the synthesis and characterization of the isolated nitrogen-base–CO_2 adduct TDB-CO_2 (**18**, Fig. 11), including its X-ray crystal structure, and suggested that this species could enable the activation of CO_2 for catalytic conversion into high value chemicals [67, 68]. The adduct was synthesized and characterized by working under strictly anhydrous conditions. It was stable at room temperature in the solid state or in solution in a polar solvent such as acetonitrile, while it is fluxional and undergoes CO_2 dissociation under vacuum. The X-ray diffraction analysis and theoretical calculations showed the zwitterionic nature of TBD-CO_2 **18**, with a N–C(CO_2) distance of 1.48 Å. The TBD-CO_2 adduct **18** was readily transformed into the bicarbonate salt [$TBDH^+$][HCO_3^-] in the presence of water, either in the solid state in air or in solution in wet solvents [67, 68].

One year later, we reported a study [101] of CO_2 capture by amidines PMDBD (**19**) and DBN (**20**) using ^{13}C solid-state NMR and thermal techniques. Solid-state ^{13}C NMR analyses showed the formation of a single PMDBD-CO_2 product which was assigned to the stable bicarbonate **21**. In the case of amidine DBN, two DBN-CO_2 products were formed which were assigned to the stable bicarbonate **22** and the unstable carbamate **23**. These results suggested that carbamate formation is favored in dry DBN but in the presence of water decomposition occurs into the bicarbonate [101]. Structures are shown in Fig. 12.

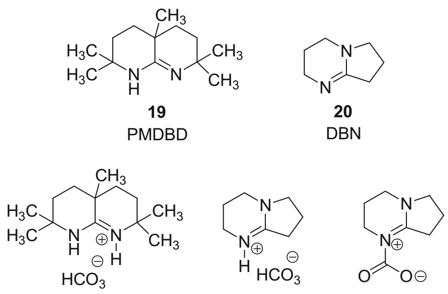

Fig. 12 Structures of PMDBD (**19**), DBN (**20**), PMDBD bicarbonate (**21**), DBN bicarbonate (**22**), and DBN carbamate (**23**)

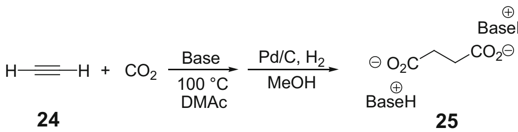

Fig. 13 General procedure for the carboxylation of acetylene with CO_2

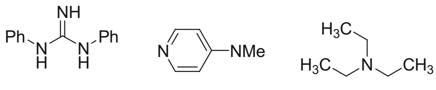

Fig. 14 Structures of DPG (**26**), DMAP (**27**), and TEA (**28**)

In 2013, Wang et al. [102] reported the TBD-mediated carboxylation of acetylene and alkynes using CO_2. First, they performed the carboxylation of acetylene **24** with CO_2, using 2 mmol of base dissolved in dimethylacetamide (DMAc) at 100°C. Following carboxylation, the crude material was exposed to a Pd/C-catalyzed hydrogenation (1 atm of H_2) to provide the succinate salt **25** (Fig. 13) (used bases: TBD (**1**), TMG (**3**), and DBU (**6**) shown in Fig. 2 and DPG (**26**), DMAP (**27**), or TEA (**28**) shown in Fig. 14). No product was observed with organic bases, except for TBD-mediated carboxylations. The reaction conditions using TBD (**1**) were optimized by varying the acetylene ratio, CO_2 pressure, and reaction time, and the best results were found by using 3 bar of acetylene, 12 bar of CO_2 and a reaction time of 42 h. Following optimization, TBD (**1**) was also applied to other alkynes with good results (41–94% yield) [102].

The authors proposed a reaction mechanism (Fig. 15) in which acetylene carboxylation was initiated by the formation of the TBD–CO_2 adduct **18**, which subsequently undergoes nucleophilic addition of acetylene to afford the propiolate-TBD salt **24a**. A second carboxylation of intermediate **24a** with adduct **18** then provides the acetylene dicarboxylate-TBD salt **24b** [102].

The TBD-CO_2 adduct releases CO_2 at moderated temperatures (80–135°C) [13], while amidine-CO_2 adducts such as DBN-CO_2 are thermally less stable, releasing CO_2 at 80–90°C [101]. Thus, a lower temperature (50°C) was applied to the corresponding DBU-mediated reaction, and with this decrease in temperature, the authors obtained propionic acid (the monocarboxylation product) in 49% yield [102].

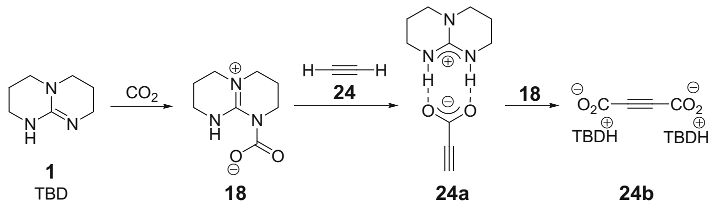

Fig. 15 Reaction mechanism proposed by Wang et al. [102]

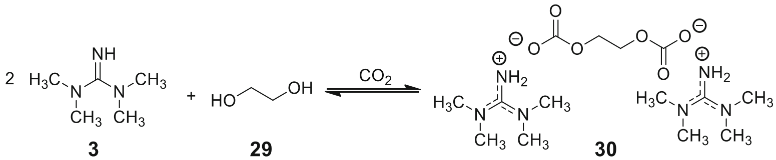

Fig. 16 Synthesis of a di-anionic ionic compound

The carboxylation of acetylene is not only controlled by basicity. Despite the comparable basicities of amidine and guanidine bases (TBD, DBU, TMG, and DPG), their reactivities with acetylene to form acetylene dicarboxylic acid are completely different. The TBD-mediated reaction provides acetylene dicarboxylation, whereas the DBU-mediated reaction forms the acetylene monocarboxylation product. Other than TBD and DBU, strongly basic guanidines (i.e., TMG and DPG) did not produce the expected results. Key factors in this reaction are the reactivities of the base-CO_2 complexes toward acetylene as well as the ease with which the base-CO_2 adduct can be formed [102].

The authors concluded that although TBD-mediated CO_2 additions to alcohols and amines have been reported previously, the TBD-mediated carboxylation of acetylene was reported for the first time under conditions that are free of transition metals, inorganic salts, and organometallic reagents. Depending on the alkyne substituent, the reactions also proceed without the use of any solvent [102].

In 2014, Xie et al. [103] reported the synthesis of TMG-based reversible mono-anionic and di-anionic ionic compounds. Di-anionic compound **30** was synthesized by a system using TMG (**3**) in conjunction with ethylene glycol (**29**) in DMSO (Fig. 16). Mono-anionic compounds were made by the use of the mono-alcohols, methanol to butanol. Compound **30** was shown to be a new solvent capable of dissolving up to 10 wt% of cellulose under mild conditions. The authors proposed that the interactions of the in situ formed carbonate anions ($2[TMGH]^+[O_2COCH_2CH_2OCO_2]^{2-}$/DMSO) with the hydroxyl groups of cellulose acted as driving force for cellulose dissolution under mild conditions. In conclusion, the authors demonstrated a facile integrated strategy for CCS together with a cellulose dissolution process [103].

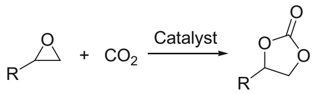

Fig. 17 Cycloaddition reaction of CO_2 with epoxides

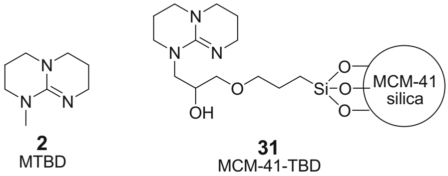

Fig. 18 Structures of MTBD (**2**) and MCM-41-TBD (**31**)

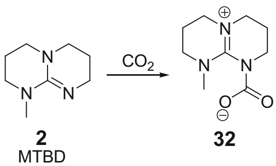

Fig. 19 MTBD-CO_2 zwitterionic compound **32**

2.2 Synthesis of Cyclic Carbonates Catalyzed by Guanidines

One of the few commercial routes using CO_2 as a raw material is the insertion of CO_2 into epoxides to afford the 5-membered cyclic carbonates (Fig. 17). Cyclic carbonates are valuable synthetic targets which can serve as electrolytes for lithium–ion batteries, valuable monomers of polycarbonates and polyurethanes,[4] aprotic polar solvents, and starting materials in a wide range of chemical reactions (see footnote 4). Cyclic carbonates are also used as constituents of oils and paints (see footnote 4).

In the past decades, numerous catalysts have been proposed for this reaction (see footnote 4) [17], and this chapter lists the guanidines used in the cycloaddition of CO_2 with epoxides.

In 2003, Barbarini et al. [1] reported a comparative study of the catalytic efficiency of homogeneous guanidine MTBD (**2**) and heterogeneous MCM-41-TBD (**31**) (Fig. 18) in the cycloaddition of CO_2 with epoxides. They concluded that reactions performed with heterogeneous catalyst **31** are slower than that with homogeneous MTBD (**2**) but show the great advantage that the catalyst can easily be recovered and reused for at least three further cycles [1].

Concerning the mechanism, they concluded that CO_2 would be activated through the formation of the MTBD-CO_2 zwitterionic compound **32** (Fig. 19).

[4] See North et al. [50] and cited references.

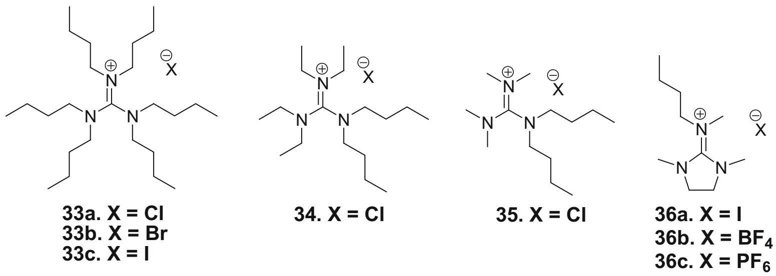

Fig. 20 Structures of hexaalkylguanidinium catalysts **33–36**

This hypothesis was elaborated by the formation of white crystals upon bubbling CO_2 into an acetonitrile solution of MTBD (**2**). This crystalline intermediate was not characterized due to its instability, but the *O*-methylated cationic derivative from the reaction with CH_3I was detected by ESI-MS. In addition, stirring the intermediate in the presence of styrene oxide led to the respective cyclic carbonate, demonstrating that it is indeed the active catalyst species [1].

In 2005, Xie et al. [104] described that both homogeneous and a silica-supported hexaalkylguanidinium chlorides were effective catalysts for CO_2 activation and fixation into carbonates without any solvent and under mild reaction conditions (4.5 MPa, 120°C, 4 h). The silica-supported hexaalkylguanidinium chlorides showed the great advantage that they could be easily recycled at least five further times using simple filtration without any obvious decrease in catalytic activity.

Initially, homogeneous guanidinium salts **33–36** (Fig. 20) were prepared, and their catalytic activities for the cycloaddition of CO_2 with propylene oxide were investigated to obtain structural information regarding the grafting of the guanidinium units. Hexabutylguanidinium chloride **33a** was found to be the best catalyst for the reaction (100% yield in 3 h) and was chosen to study the effects of reaction parameters to optimize the performance of the catalytic system. A temperature of 120°C, 1.5 mol% of catalyst, and 4.5 MPa of CO_2 pressure were the optimum experimental conditions found [104].

Subsequently, the optimum homogeneous reaction conditions were used for the cycloaddition of CO_2 with propylene oxide using silica-supported pentabutylpropylguanidinium chloride (PBGSiCl, **37**) as a catalyst (Fig. 21), and the catalytic activity remained almost unchanged. A series of epoxide substrates were examined for the synthesis of the corresponding carbonates in the presence of **37**, and the carbonates were successfully synthesized from each epoxide in good yields and with excellent selectivity [104].

The mechanism proposed by authors is shown in Fig. 22. In this proposal, the epoxide is coordinated by hexabutylguanidinium chloride **33a** to form complex **33a_1**. The chloride anion then preferentially attacks on the lesser substituted site of the coordinated epoxide followed by ring opening, producing an oxyanion species **33a_2**. A CO_2 molecule is then coordinated to the complex **33a_2** resulting

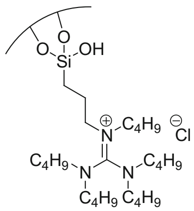

37

Fig. 21 Structure of silica-supported pentabutylpropylguanidinium chloride **37**

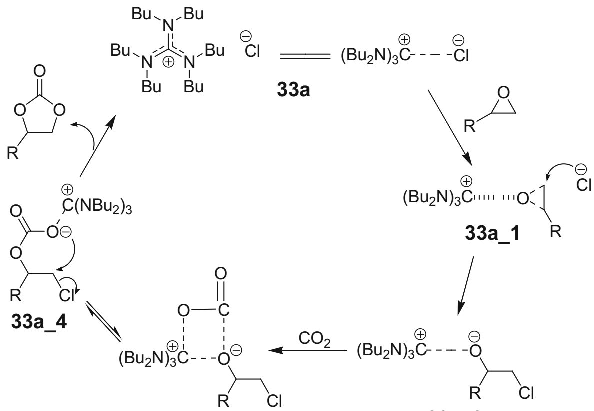

Fig. 22 Mechanism proposed by Xie et al. [104]

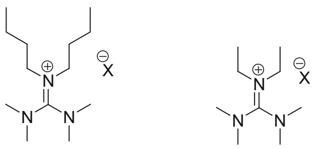

Fig. 23 Structures of hexaalkylguanidinium catalysts **38** and **39**

in the formation of **33a_3** and **33a_4** in equilibrium. Finally, the cyclic carbonate is produced by intramolecular cyclization, releasing the catalyst for recycling [104].

Later on in 2006, the researchers reported [105] a similar study using the hexaalkylguanidinium salts **33a–c** (Fig. 20), **38**, and **39** (Fig. 23), this time using a hexaalkylguanidinium salt/$ZnBr_2$ binary system. They found that the **3b**/$ZnBr_2$ system exhibited the best catalytic activity (65–95% yield) and selectivity for the synthesis of cyclic carbonates from the cycloaddition between CO_2 and epoxides [105].

In 2006, Zhang et al. [106] reported a study on the catalytic activity of amine-functionalized silica catalysts (NH_2/SiO_2, $NH(CH_2)_2NH_2/SiO_2$ and TBD/SiO_2) in cycloaddition reactions of CO_2 with propylene oxide. The reactions were carried out at 150°C and 2.0 MPa initial CO_2 pressure for 20 h. The order of catalytic activity found was $TBD/SiO_2 > NH(CH_2)_2NH_2/SiO_2 > NH_2/SiO_2$, with TBD/SiO_2 resulting in 99.5% propylene oxide conversion and 99.8% of selectivity toward the propylene carbonate [106].

To understand the role of the silanol groups, the surface of TBD/SiO_2 was modified with methyl groups to remove the surface hydroxyls, and the propylene oxide conversion (under equal conditions) decreased from 99.5% to 0.2%. This observation strongly suggests the importance of silanol groups in the reaction, and the following reaction mechanism was proposed by the authors [106] (Fig. 24).

In 2006, Lu et al. [107] reported a binary electrophile–nucleophile catalyst system for the copolymerization of CO_2 and racemic epoxides. A chiral tetradentate Schiff base cobalt complex [SalenCo^{III}X] **40** (Fig. 25) was used as the electrophile in conjunction with an ionic organic ammonium salt or a sterically hindered strong organic base (MTBD, **2**) as the nucleophile [107]. The authors concluded that an axial X group (e.g., 2,4-dinitrophenoxy) with poor leaving group ability and a bulky ionic ammonium salt (consisting of a bulky cation and a nucleophilic anion with

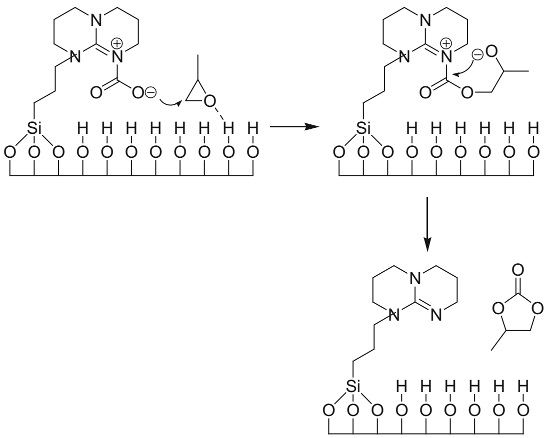

Fig. 24 Possible mechanism proposed by Zhang et al. [106] for the cycloaddition of CO_2 to an epoxide on TBD/SiO_2

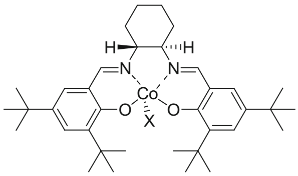

40
[SalenCo^{III}X]

Fig. 25 Chiral tetradentate Schiff base cobalt complex [SalenCo^{III}X] (**40**) used as electrophile in binary electrophile–nucleophile catalyst systems poor leaving group ability) or a sterically hindered strong organic base MTBD (**2**) with low coordination capacity was the ideal binary catalyst system [107].

Lu's group reported other similar studies making use of binary electrophile–nucleophile catalyst systems. One of them reported the copolymerization of CO_2 and propylene oxide catalyzed by SalenCr(III)X complexes **41** as electrophiles and organic bases as nucleophiles [108] (general structure of SalenCr(III) complex and organic bases utilized is presented in Fig. 26). In another work, they used a bifunctional catalyst with pyrrolidine SalenCr(III)X complexes containing an electrophilic center (Lewis acid metal ion) and a nucleophilic center (sterically hindered strong organic base, TBD (**1**)) in a single molecule [109] (**46** and **47**, Fig. 27). A nucleophilic center anchored on a ligand framework such as employed in a previous study but now using SalenCo(III) complex [110] (**48**, **49**, and **50**, Fig. 28) was also reported. All of these studies on binary catalyst systems showed high catalytic activity in the synthesis of cyclic carbonates.

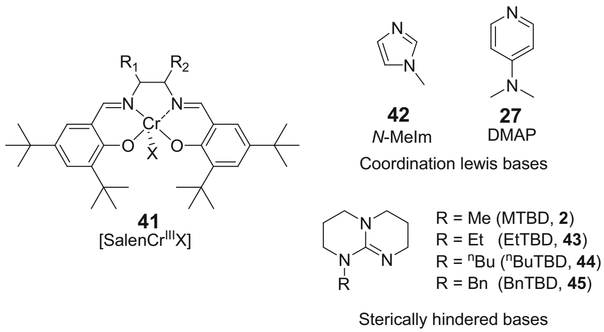

Fig. 26 General structure of SalenCr(III) complex and organic bases utilized for CO_2/propylene oxide copolymerization

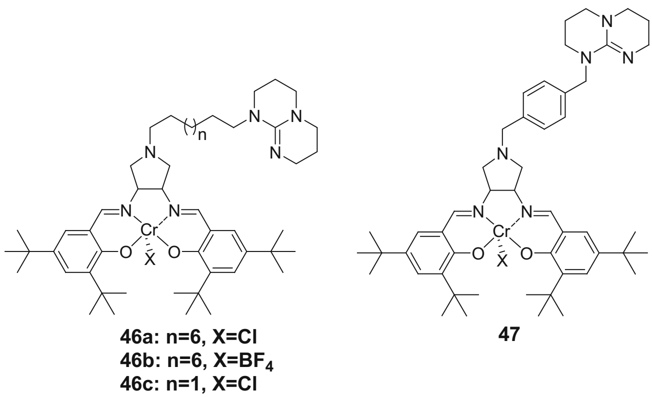

Fig. 27 General structure of pyrrolidine SalenCr(III)X complexes with anchored TBD

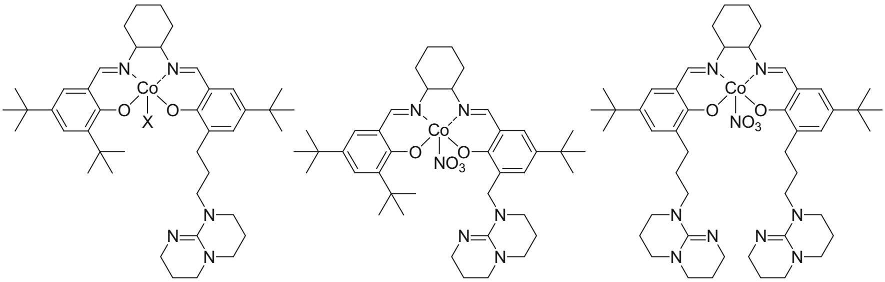

Fig. 28 SalenCo(III) complexes with anchored TBD

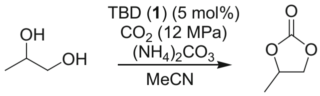

Fig. 29 Synthesis of propylene carbonate (**52**) from propylene glycol (**51**) and CO_2 using TDB (**1**) as a catalyst

In 2008, Huang et al. [111] reported the synthesis of propylene carbonate (**52**) from propylene glycol (**51**) and CO_2 in acetonitrile using organic bases as catalysts (Fig. 29). Among other catalysts used (DBU (**6**) and Et_3N (**28**)), the guanidine TBD (**1**) exhibited the highest catalytic activity with 22.5% yield and 60.3% selectivity. Ammonium carbonate was added into the reaction mixture as the coupling reagent to significantly elevate the selectivity for **52**. Under optimal conditions, the yield of **52** slightly decreased to 15.3%, but the selectivity increased to 100% [111].

In 2010, Ma et al. [69] described a theoretical study on the mechanism of the reaction of propylene glycol (**51**) with CO_2 catalyzed by TBD (**1**) by density functional theory (DFT) at the B3LYP/6-311++G(d,p) level. Through analyzing the optimized structures and energy profiles along the reaction pathways, the propylene glycol-activated route was identified as most likely (Fig. 30). The rate-determining step was the nucleophilic attack of one of the O atoms in CO_2 on the hydroxyl-linked C atom in PG with an energy barrier of 56.96 kcal/mol. The catalytic role of TBD (**1**) could be considered as a proton bridge, providing activation by the synergistic action of its two N atoms [69].

In 2010, Prasetyanto et al. [112] reported the synthesis of melamine tri-silsesquioxane (TBTS) bridged periodic mesoporous organosilica (PMO) and the investigation of this hybrid organic–inorganic material as catalyst for the CO_2 activation in the coupling of propylene oxide with CO_2. When the TBTS-PMO catalyst was employed at 100°C with 80 psi of CO_2 for 10 h in DMF as a solvent, around 40% conversion and high selectivity for the cyclic carbonate was achieved.

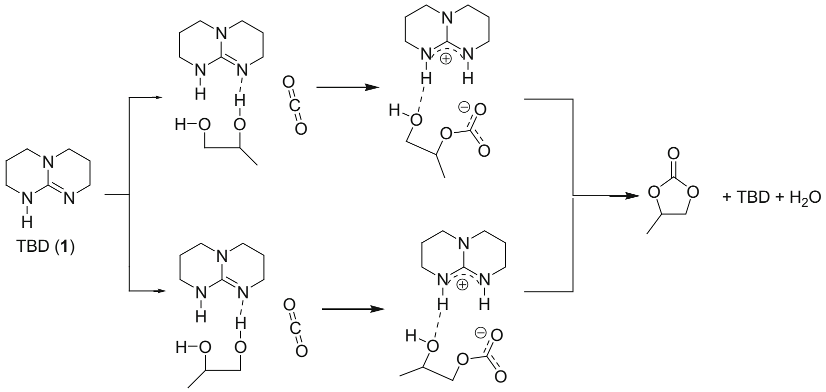

Fig. 30 Propylene glycol-activated mechanism for carboxylation with CO_2 by TBD

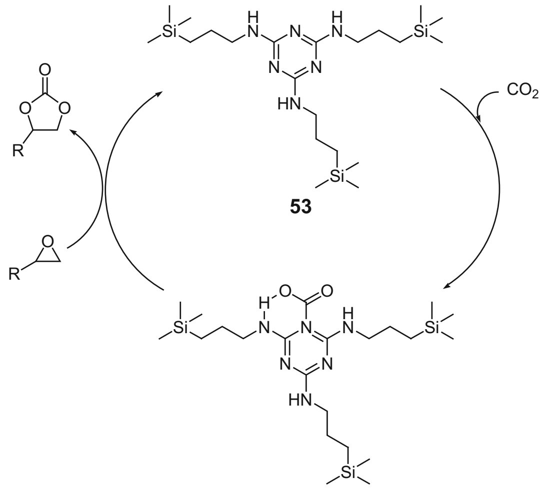

Fig. 31 Possible mechanism for the CO_2 activation via pseudo-cyclic carbamates using **53** as catalyst

The catalyst could also be recycled without any loss of activity. Compared with the previously reported catalysts, this system provided several benefits such as working at relatively low temperatures, low CO_2 pressure, no requisition of additional base, and shorter reaction time. DFT calculations were performed to support the possible mechanism for this CO_2 activation (Fig. 31). The authors used the TBTS **53** for the calculations (optimized geometry) and concluded that the mechanism involves a pseudo-cyclic carbamate. Other mechanisms are also possible, and the various different modes of activation could even give rise to synergistic effects [112].

In 2010, Yu reported [113] a study on the catalytic coupling reaction between CO_2 and propylene oxide using silica-supported and nonsupported amines **1, 54–60**

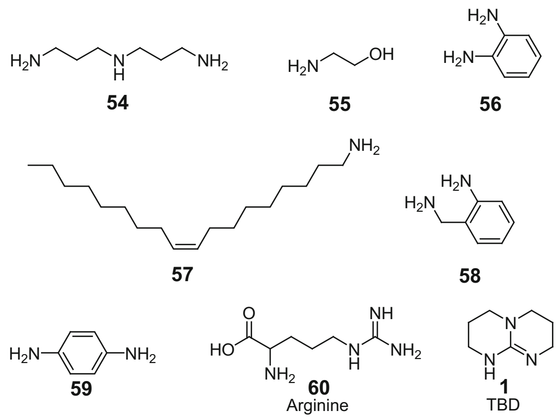

Fig. 32 Structures of compounds **54**–**60**

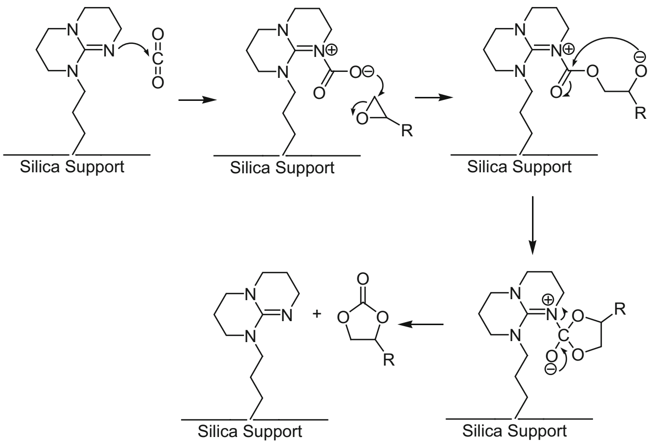

Fig. 33 Reaction mechanism proposed by Yu et al. [113]

as catalysts. Of the eight compounds tested (Fig. 32), two possess the guanidine core: arginine (**60**) and TBD (**1**). An initial screening of unsupported amines revealed that TBD (**1**) was the superior catalyst, converting propylene oxide into propylene carbonate in 100% yield after 24 h under 50 atm of CO_2 at 150°C. Arginine (**60**) also showed good catalytic activity with a conversion of 79.9% at the same conditions [113].

Moreover, TBD (**1**) covalently attached to silica also gave 100% yield under the same conditions. The amine group was suggested to have a role in activating the carbon dioxide in the form of a carbamate which could then attack and ring-open the epoxide [113] (Fig. 33).

In 2012, Yang et al. reported a process for the synthesis of cyclic carbonates by employing polyethylene glycol (PEG)-functionalized basic ionic liquids (ILs) **61**–

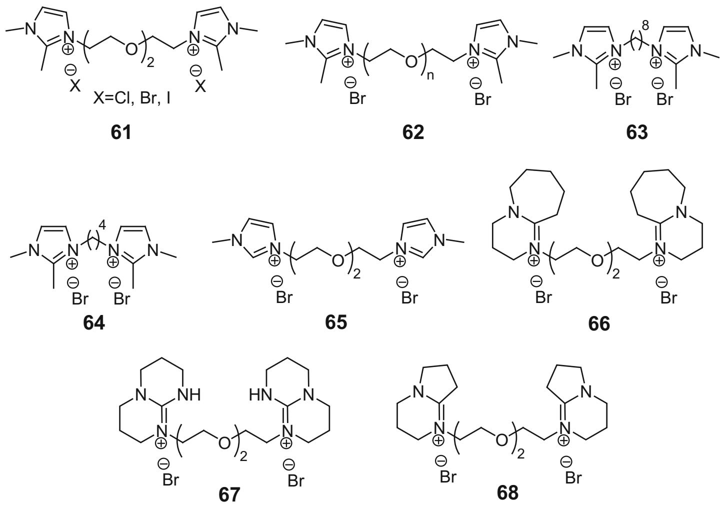

Fig. 34 PEG-functionalized ionic liquids used by Yang et al. [114]

68 as efficient and recyclable catalysts (Fig. 34) [114]. Propylene carbonate synthesis from CO_2 and propylene oxide was performed in ILs with 1 mol% catalysts, 1 MPa of CO_2 at 120°C for 3 h. Compound **67** (with a TBD core) showed the best catalytic activity with >99% yield and selectivity and was selected as the catalyst of choice for the synthesis of various carbonates using different epoxides. Compound **67** was found to be a highly efficient catalyst giving >93% yield of cyclic carbonates [114].

^{13}C NMR and in situ FT-IR spectroscopy were used to identify the possible reaction intermediates. Based on previous reports and supported by these experimental results, the authors proposed the following mechanism for the cycloaddition of CO_2 with epoxides catalyzed by **67** (Fig. 35). Initially, the secondary nitrogen of the TBD core reversibly coordinates with CO_2 to afford the carbamic acid **67a**. This activated form of CO_2 then interacts with the epoxide through hydrogen bonding, resulting in epoxide activation. The nucleophilic attack of the bromide anion on the sterically less hindered carbon atom of the epoxide then furnishes a bromoalkyl alcohol species. Nucleophilic attack of the bromoalkyl alcohol on the carbamic acid and hydrogen transfer to the nitrogen atom of TBD subsequently produces the alkyl carbonate anion **67b**. Finally, the cyclic carbonate is formed by intramolecular ring closure and the catalyst is regenerated [114].

The authors also demonstrated a two-step process for dimethyl carbonate (DMC, **69**) production utilizing CO_2 as a raw material, which included the subsequent transesterification of the intermediate cyclic carbonate (e.g., ethylene carbonate) with methanol (Fig. 36). Synthesis of DMC (**69**) was effectively catalyzed by bis-guanidine **67**, owing to the activation of methanol into the CH_3O^- anion by the secondary and tertiary nitrogen atoms in the IL. This approach realized a

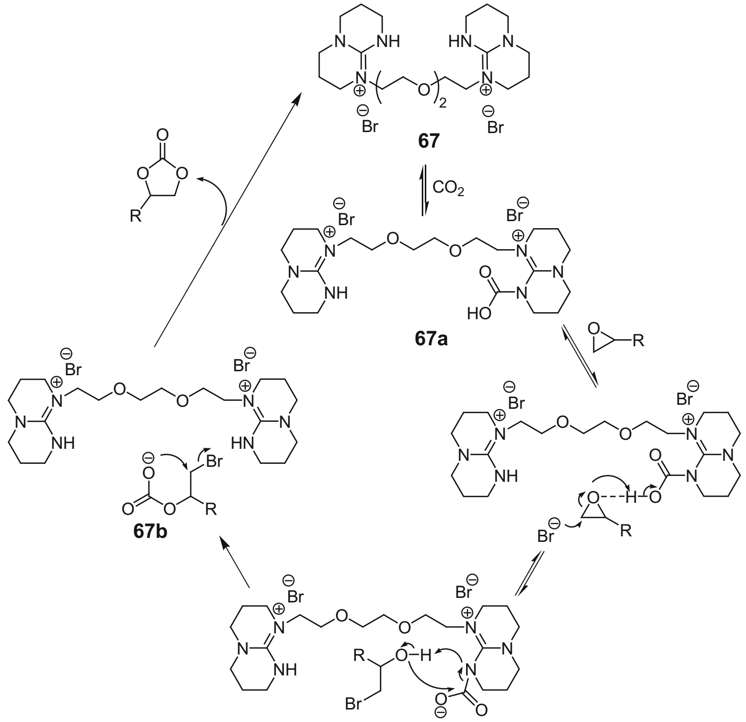

Fig. 35 Mechanism proposed by Yang et al. [114] for the cycloaddition of CO_2 with epoxides catalyzed by **67**

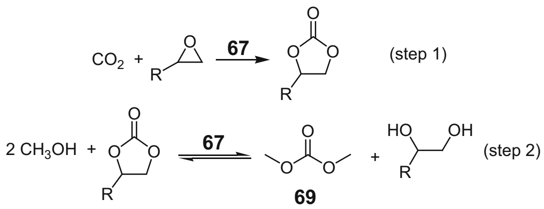

Fig. 36 Two-step process for DMC production utilizing CO_2 as a raw material

so-called one-pot two-stage access to DMC from CO_2 by using only a single type of catalyst [114].

In 2013, Adam et al. [58] reported the synthesis of cyclic propylene carbonate from CO_2 and propylene oxide using TMG covalently bound to silica (**70**) as an efficient and reusable catalyst (Fig. 37). The optimal conditions found were 200 mg of catalyst, 50 bar of CO_2 pressure, 130°C for 8 h, and giving 92% of conversion with 98% selectivity toward the product. The catalyst was easily recovered by

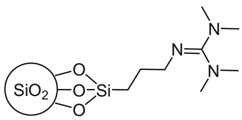

Fig. 37 Structure of TMG covalently bonded to silica

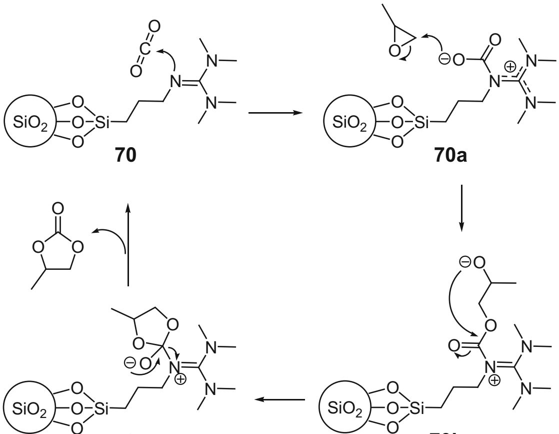

Fig. 38 Mechanism proposed by Adam et al. [58]

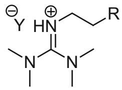

Fig. 39 Structures of FGBILs reported by Wei-Li et al. [115]

filtration and reused for at least four times without any appreciable loss of catalytic activity [58].

The authors proposed a reaction mechanism (Fig. 38) in which CO_2 is adsorbed onto the surface by the Lewis base sites. The guanidinium cation formed is stabilized by resonance about the CN_3 nucleus (**70a**), which leads to a lowering of energy in the zwitterionic system and greatly increased stability of the reaction intermediate. The carbonate anion attacks the less sterically hindered carbon atom which opens the epoxide ring, generating **70b**. The alkoxide anion in **70b** finally attacks the carbonyl carbon intramolecularly, thus forming the five-membered propylene carbonate ring (**70c**) which leaves the catalyst surface, thereby regenerating the active catalyst [58].

In 2013, Wei-Li et al. [115] reported a series of functional guanidinium-based ionic liquids (FGBILs) (**71a–g**) that contain both Lewis acid and basic sites (Fig. 39). They used these compounds as catalysts for the synthesis of cyclic carbonates through the cycloaddition of CO_2 to epoxides in the absence of any co-catalyst or solvent. The initial experiments in the synthesis of propylene carbonate used 35.7 mmol of propylene oxide, 0.5 mol% of IL, and 2.0 MPa of CO_2, at 130°C for 2 h [115].

TMG (**3**) was also tested and showed almost no activity in this reaction (1.8% yield of propylene carbonate). The FGBILs **71a**, **71b**, and **71c**, however, exhibited high catalytic activity and selectivity (yields 94.6%, 90.8%, and 88.3%, respectively; selectivity ~99.85%). On the other hand, ILs **71d** and **71e** were less efficient for the cycloaddition reaction (71.6% and 62.8% yield, respectively). These results indicate that the functional groups play an important role in the promotion of the reaction (efficiency, $NH_2 > COOH > OH$). The effect of counter anions on the catalytic performance was also evaluated. Comparing **71a** (94.6% yield) with **71f** (3.1% yield) and **71g** (2.7% yield) suggested that the nucleophilic attack of the Br^- anion to the epoxide is crucial for the successful synthesis of propylene carbonate. Comparing Br^-, BF_4^-, and PF_6^- as counter anions showed much lower activity, probably due to their poorer nucleophilicity. The FGBIL **71a** was also used as a catalyst in the cycloaddition of CO_2 with other epoxides, and it was concluded that the protocol is applicable to a variety of substrates, producing the corresponding cyclic carbonates in high yields and selectivity [115].

Using ^{1}H NMR and FT-IR analyses, the authors proposed the following mechanism for this reaction (Fig. 40). Here, the coordination of the H atom of the initially formed carbamic acid species with the O atom of the epoxide results in polarization of the epoxide C–O bond and formation of intermediate **72**. Then, nucleophilic attack of a bromide ion on the less sterically hindered carbon atom of the epoxide furnishes ring opening and formation of intermediate **73**. The oxygen of

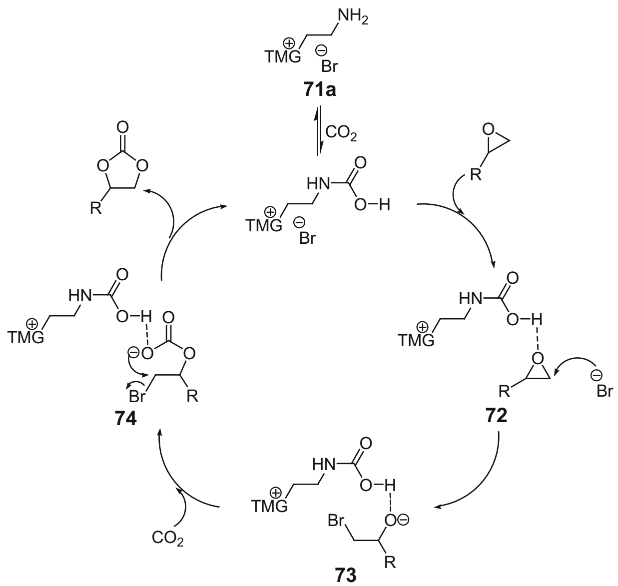

Fig. 40 Proposed mechanism by Wei-Li et al. [115] for the cycloaddition reaction

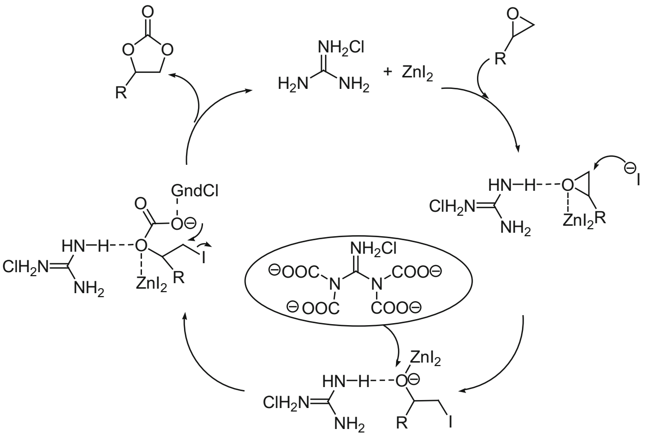

Fig. 41 Mechanism proposed by Liu et al. [116] for the guanidinium hydrochloride/ZnI_2 catalyzed cycloaddition reaction

intermediate **73** reacts with CO_2 to form halocarbonate **74** which then transforms to the cyclic carbonate through intermolecular displacement of the bromide ion [115].

In 2015, Liu et al. [116] reported the combination of guanidine hydrochloride with ZnI_2 as an efficient heterogeneous catalyst system for the environmentally benign, solvent-free synthesis of cyclic carbonates under mild reaction conditions. The effects of different Lewis acid co-catalysts as well as reaction parameters including catalyst loadings, CO_2 pressure, reaction temperature, and reaction time were investigated. With a molar ratio of guanidine hydrochloride to ZnI_2 of 5:1, excellent yield (94%) and selectivity ($\geq$99%) for propylene carbonate formation were obtained at 100°C under 1 MPa of CO_2 after 1.5 h. The catalyst system could be recycled. However, because of washing losses of guanidine hydrochloride, there was a slight decrease in the yield of propylene carbonate using the recycled system. The activity of the catalytic system was fully restored by adding an additional 20 mol% of fresh guanidine hydrochloride. Moreover, this binary catalyst was also effective for CO_2 cycloaddition when using other epoxides besides propylene oxide [116].

A possible reaction mechanism was proposed (Fig. 41) wherein guanidine hydrochloride plays a dual role in activating both CO_2 and the epoxide, and ZnI_2 activates epoxide simultaneously. It is this synergistic effect of guanidine hydrochloride and ZnI_2 which ensures that the reaction proceeds effectively [116].

2.3 *Synthesis of Oxazolidinones Catalyzed by Guanidines*

Oxazolidinones (**75**) are five-membered heterocyclic compounds which are important materials in synthetic and medicinal chemistry. Oxazolidinones are used as

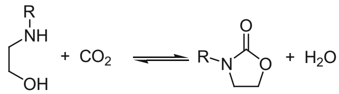

75

Fig. 42 Oxazolidinones (**75**) from amino alcohols and CO_2

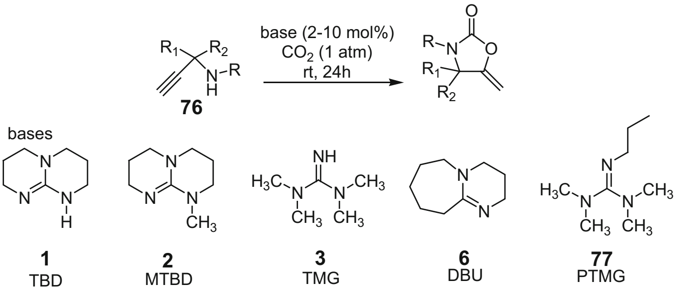

Fig. 43 Synthesis of oxazolidinones from acetylenic amines (**76**) with CO_2 and bases used as catalysts

chiral auxiliaries, intermediates in organic synthesis, and as building blocks for biologically active pharmaceuticals ([117] and cited references). However, the standard synthesis using carbonylation of amino alcohols with phosgene or CO presents some problems, such as toxicity, corrosion, and also environmental concerns as a result of commonly coproduced hydrochloric acid and alkali chloride salts [117]. Consequently, an alternative preparation process starting from CO_2 seems to be greener and more desirable [117]. Figure 42 shows an example of CO_2 utilization in the synthesis of oxazolidinones from amino alcohols. This chapter examines the literature works that used CO_2 in the synthesis of oxazolidinones in reactions catalyzed by guanidines.

Costa et al. reported two works on oxazolidinone synthesis by the reaction of acetylenic amines (**76**) with CO_2 catalyzed by various bases. In the first example in 1996 [118], guanidines TBD (**1**), MTBD (**2**), TMG (**3**), *N*-propyl-*N*′,*N*′,*N*″,*N*″-tetramethylguanidine (PTMG, **77**), and amidine DBU (**6**) were used as bases. MTBD (**2**) was the best catalyst, giving 75–93% yields at room temperature after 24 h under 1 atm of CO_2 (Fig. 43) [118].

Two years later [119], they reported an extension of this study using TBD (**1**), MTBD (**2**), TMG (**3**), CyTMG (**4**), DPG (**26**), PTMG (**77**), pentaalkylguanidines (**78**, **82**, Fig. 44), trialkylguanidines (**79**, **80**, Fig. 44), tetraalkylguanidine (**81**, Fig. 44), and the amidine DBU (**6**) as catalysts. All guanidines showed high catalytic activities with conversions ranging from 48% to >99% (8 compounds gave >95% conversion) and yields ranging from 42% to 89% [119].

In 2014, Nicholls et al. reported the observation of guanidine-CO_2 adduct complexes in solution using ATR-FTIR [120]. Solid-state NMR data for DBU-CO_2 (**15**, Fig. 10) and TBD-CO_2 (**18**, Fig. 11) complexes had previously

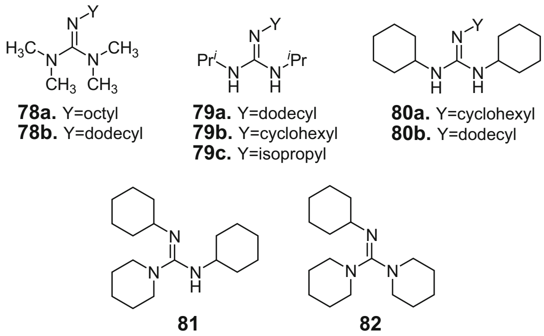

Fig. 44 Structures of guanidines **78–82**

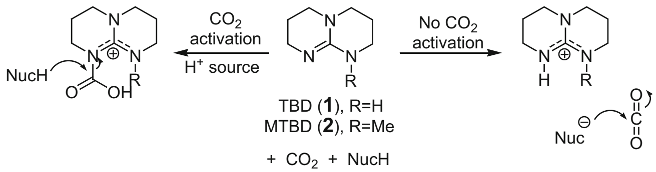

Fig. 45 Possible mechanisms with/without direct CO_2 activation

been reported [14, 15, 67, 68]. In his new work [120], Nicholls showed that while cyclic guanidines TBD (**1**) and MTBD (**2**) form stable and detectable complexes with CO_2, guanidine TMG (**3**) and tertiary amines (TEA (**28**) and DABCO) do not [120]. With this result, a reexamination of the effects of the catalyst and solvent in the reaction between CO_2 and propargylamines reported previously by Costa [118, 119] was performed (Fig. 43) to investigate the possible mechanisms with/without direct CO_2 activation (Fig. 45).

The conversion of propargylamine (**83**) to oxazolidinone (**84**) using MTBD (**2**) or TMG (**3**) as catalyst was performed in different solvents under 5 bar of CO_2 at 75°C for 18 h [120] (Table 1). From these experiments, the authors concluded that the basicity of the catalyst, rather than its ability to form complexes with CO_2, is the origin of catalytic activity, and consequently, polar solvents (e.g., DMSO) which can stabilize the guanidinium cation are beneficial to the reaction. A novel catalyst/solvent combination (TMG/DMSO/H_2O) with superior catalytic activity at low catalyst loading was reported [120].

In 2007, Maggi et al. [121] reported a study of the reaction of propargylamines with scCO_2 for the synthesis of variously substituted oxazolidinones. One of the catalysts studied was silica-supported TBD (**1**) (SiO_2-TBD). This catalyst gave 88% yield and 99% selectivity. Nevertheless, SiO_2-TBD showed a problem with deactivation on recycling, decreasing to 45% yield in the fourth cycle. Basic alumina gives similar results at first cycle (85% yield and 98% selectivity) but could be reused for at least seven runs without deactivation and was thus considered the superior catalyst for this reaction [121].

Table 1 Conversion (%) of **83** to **84**

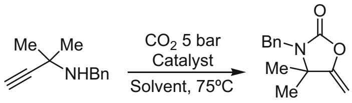

Catalyst	Loading (mol%)	Conversion (%) of **83** to **84** in solvent		
		MeCN	EtOH	DMSO
MTBD	10	100	29	54
MTBD[a]	10	99		
TMG	10	19	40	100
TMG[a]	10		39	100
MTBD	1	8		
MTBD[a]	1	8		
TMG	1		7	6
TMG[a]	1		8	61

[a]Reaction was performed in the presence of 0.1 mL of H_2O

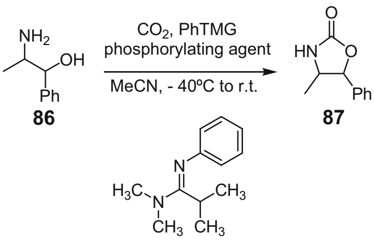

Fig. 46 General procedure for the synthesis of oxazolidinone **87** from norephedrine (**86**) and CO_2 in the presence of PhTMG (**85**) and various phosphorylating agents

In 2009, Paz et al. [122] reported the synthesis of oxazolidinones from 1,2-amino alcohols and CO_2 in the presence of tetramethyl-phenylguanidine (PhTMG, **85**) as a base and a variety of phosphorus electrophiles at room temperature. 4-methyl-5-phenyloxazolidin-2-one (**87**) was obtained from norephedrine (**86**) and CO_2 in the presence of PhTMG (**85**) and various phosphorylating agents (Fig. 46) in good yields (55–86%). The best phosphorylating agent was diphenyl chlorophosphate which was employed for other 1,2-amino alcohols giving good yields (76–90%) of the corresponding oxazolidinones [122]. One year later [123], the authors reported an extensive study of this methodology employed to several amino alcohols and also testing other sulfur and carbon electrophiles.

In 2011, Yang et al. [124] reported a study of several protic onium salts catalyzed for the synthesis of 5-aryl-2-oxazolidinones from aziridines (**88**) and CO_2 (Fig. 47). A study investigating the influence of the cation was performed at 100°C, 5 MPa of CO_2 for 1 h, and it was found that catalytic efficiency increased in

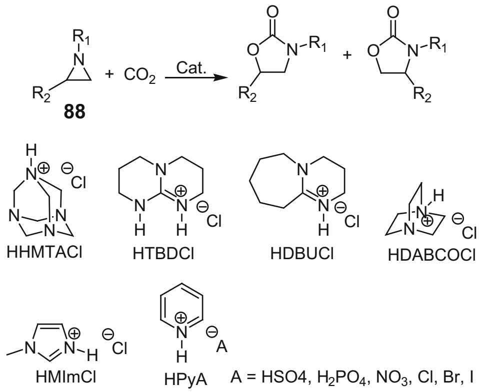

Fig. 47 Synthesis of 5-aryl-2-oxazolidinones from aziridines (**88**) and CO_2 and protic onium salts used in this study

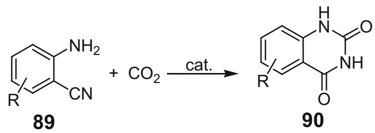

Fig. 48 Synthesis of quinazolines **90** from 2-aminobenzonitrile (**89**) and CO_2

the order $HHMTA^+ < HTBD^+ < HDBU^+ \sim HDABCO^+ < HMIm^+ < HPy^+$. $HTDB^+$ only gave 77% yield of oxazolidinone, while HPy^+ gave 97% yield and was chosen as the optimal catalyst [124].

2.4 *Synthesis of Quinazolines Catalyzed by Guanidines*

Quinazoline-2,4-(1*H*, 3*H*)-diones and their derivatives are an important class of organic compounds, and they have a wide range of biological and pharmacological activities. The traditional synthetic methods toward quinazolines involve anthranilic acid, anthranilamide, phosgene, potassium cyanate, or chlorosulfonyl isocyanate [117]. Nevertheless, highly toxic reagents or harsh conditions restrict the use of these methods [117]. In the view of greener syntheses, an effective synthetic approach for the synthesis of quinazoline-2,4-(1*H*, 3*H*)-diones **90** and their derivatives was developed from CO_2 and 2-aminobenzonitrile (**89**) using guanidine catalysis (Fig. 48). This chapter reviews the literature works that use CO_2 for the synthesis of quinazolines in reactions catalyzed by guanidines.

In 2010, Gao et al. [125] described an efficient approach for the synthesis of quinazoline-2,4(1*H*,3*H*)-diones **90** from CO_2 and 2-aminobenzonitriles **89** (Fig. 48) catalyzed by small amounts of organic guanidines without the use of any additional solvent [125]. Guanidines used in this study are presented in Fig. 49.

Exploratory experiments were made using 2-aminobenzolnitrile (R=H in Fig. 48). Non-guanidine organic bases such as hexamethylenetetramine and diethylenetriamine were inactive at 80°C. All organic guanidines, however, gave

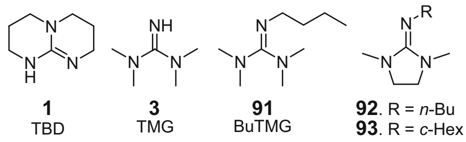

Fig. 49 Guanidines used as catalysts in the reaction of **89** and CO_2

Table 2 Conditions and yields of the guanidine-catalyzed reaction of 2-aminobenzonitrile (**89**, R=H) and CO_2 (reaction time, 4 h; CO_2 pressure, 10 MPa)

Catalyst	Amount of cat. (equiv.)	*T* (°C)	Isolated yield (%)
TBD (**1**)	0.1	120	81
TMG (**3**)	0.1	120	87
BuTMG (**91**)	0.1	120	86
92	0.1	80	25
92	0.1	100	32
92	0.1	120	88
93	0.1	120	89
TBD (**1**)	0.02	120	26
TMG (**3**)	0.02	120	82
BuTMG (**91**)	0.02	120	27
92	0.02	120	34
93	0.02	120	36

good yields with 0.1 equiv. of catalyst at 120°C (Table 2). TMG (**3**) showed the highest catalytic performance with a catalyst amount as low as 2 mol%, which was attributed to the influence of basicity and steric effects. Further reactions with several 2-aminobenzonitriles containing both electron-withdrawing and electron-donating substituents were performed under identical conditions and afforded good yields of 60–95% [125].

In 2014, Lu et al. [126] reported the synthesis of quinazoline-2,4(1*H*,3*H*)-diones **90** from CO_2 and 2-aminobenzonitriles **89** in a series of ionic liquids (ILs) as both catalysts and solvents. Seven ILs (imidazolium-based ILs) failed to produce the target product. Of the other ILs tested, the only guanidine-based IL was tetramethylguanidine acetate ([TMG]Ac, **94**), but it gave only 23% yield, while 1-butyl-3-methylimidazolium acetate ([Bmim]Ac, **95**) gave 92% yield. Therefore, [Bmim]Ac (**95**) was chosen as the optimal IL for this reaction [126].

In 2014, Zhao et al. described two works [127, 128] on the synthesis of quinazoline-2,4(1*H*,3*H*)-diones **90** from CO_2 and 2-aminobenzonitriles **89**. First, they reported [127] the reaction using a CO_2-reactive protic ionic liquid (PIL) as both catalyst and solvent at atmospheric pressure and room temperature [127]. The only guanidine-based IL tested ([$HTMG^+$][TFE^-], **96**) gave only 67% yield, while amidine-based IL ([$HDBU^+$][TFE^-], **97**) gave 97% yield. Then, a bifunctional IL catalyst, [$HDBU^+$][TFE^-] (**97**), was found to activate CO_2 and 2-aminobenzonitriles **89** simultaneously to produce quinazoline-2,4(1*H*,3*H*)-

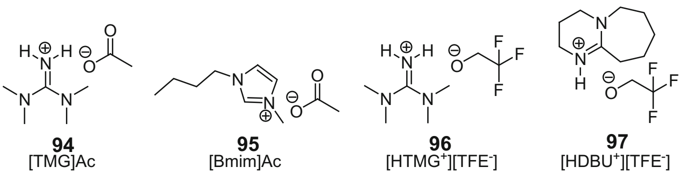

Fig. 50 Structure of ILs **94–97**

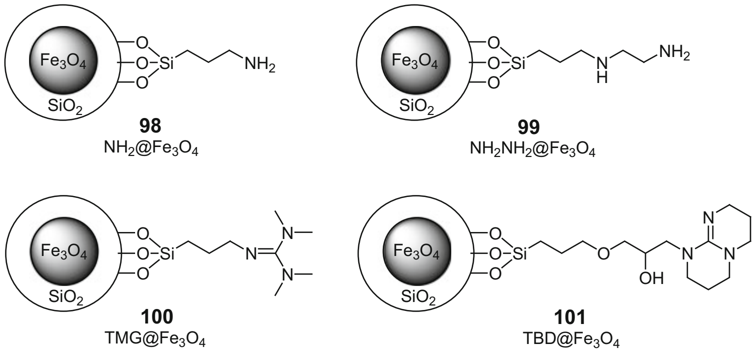

Fig. 51 Structures of magnetic catalysts (**98–101**) reported by Zhao et al. [128]

diones **90** in excellent yields under atmospheric pressure at room temperature [127]. Structures of ILs **94–97** are shown in Fig. 50.

Later on, the authors reported [128] organic superbase-functionalized magnetic Fe_3O_4 particles as catalysts for the synthesis of quinazoline-2,4(1*H*,3*H*)-diones **90**. The magnetic catalysts used in this study [128] are shown in Fig. 51 and included two guanidine-functionalized catalysts: TMG@F_3O_4 (**100**) and TBD@Fe_3O_4 (**101**). The catalytic efficiency showed the following trend: **101** > **100** > **99** > **98** with TBD@Fe_3O_4 (**101**) yielding 63% and TMG@Fe_3O_4 (**100**) yielding 35% of product [128].

TBD@Fe_3O_4 (**101**) was chosen as the optimal catalyst, and the optimal reaction conditions were 10 mol% of catalyst, 4 MPa of CO_2, 1 mL of toluene as solvent, and 120°C reaction temperature. TBD-functionalized Fe_3O_4 was proven to be an efficient and recyclable magnetic heterogeneous catalyst for the synthesis of various quinazoline-2,4(1*H*,3*H*)-diones **90** in reasonable yields (66–93%), and it could be recovered using an external magnetic field [128].

In 2015, Lang et al. [129] reported that the amino acid ionic liquid tetrabutylphosphonium arginine ([TBP][Arg], **102**, Fig. 52) was found to be an efficient and recyclable catalyst for the synthesis of quinazoline-2,4(1*H*,3*H*)-diones **90** from 2-aminobenzonitriles **89** and CO_2 under solvent-free conditions. Other arginine-based ILs such as tetrabutylammonium and 1-butyl-3-methylimidazolium arginine and non-arginine-based ILs were also examined for the reaction and were inactive or gave only moderate yields. The high efficiency of [TBP][Arg] (**102**) even in the

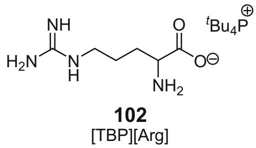

Fig. 52 Structure of [TBP][Arg] (**102**)

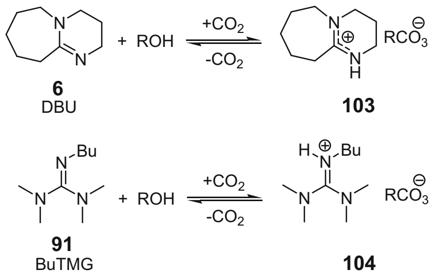

Fig. 53 Two-component reversible amidinium (**103**) or guanidinium (**104**) alkyl carbonate salt ionic liquids

presence of only 5 mol% of catalyst is presumably due to the synergistic effect of dual activation exhibited by the two functional sites, i.e., the carboxylic acid and the guanidine group [129].

2.5 Other Reactions

Jessop (2005) [130] and Phan (2008) [131] reported the first examples of two-component reversible ionic liquids based upon DBU (**6**) or BuTMG (**91**) and an alcohol. The preparation of amidinium (**103**) or guanidinium (**104**) alkyl carbonate salts as viscous liquids at room temperature was achieved by bubbling CO_2 through equimolar solutions of BuTMG (**91**) or DBU(**6**) and alcohols (methanol, 1-butanol, 1-hexanol, 1-octanol, or 1-dodecanol) (Fig. 53). These switchable solvents were readily convertible, under an atmosphere of CO_2, to ionic liquids and were returned to their original neutral states by the application of N_2 gas and/or mild heat (50–60°C) [130, 131].

In 2008, Heldebrant et al. [132] reported a new class of CO_2-binding organic liquids (CO_2BOL) that chemically capture and release CO_2 more efficiently than aqueous alkanolamine systems. These organic liquids are mixtures of organic alcohols and amidine/guanidine bases that reversibly bind CO_2 chemically as liquid amidinium/guanidinium alkyl carbonates. Among the investigated bases were the guanidines TMG (**3**) and Barton's base (**105**). Figure 54 represents the proposed hydrogen bonding between cation and anion in salts made from these guanidines. These CO_2 capturing agents do not require an added solvent and therefore have high CO_2 capacities of up to 19% by weight for neat systems and slightly less when dissolved in acetonitrile. These organic systems have been shown to bind and release CO_2 for five cycles without losing activity or selectivity [132].

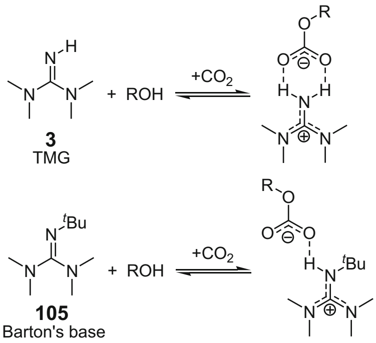

Fig. 54 Proposed hydrogen bonding between cation and anion in salts made from guanidines TMG (**3**) and Barton's base (**105**)

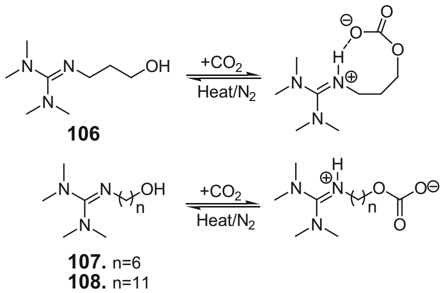

Fig. 55 Alkanolguanidines used by Heldebrant et al. [19] and their zwitterionic products

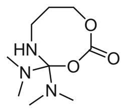
109

Fig. 56 Structure of the cyclic carbonate product of **106** proposed by Heldebrant et al. [19]

Later in 2010, Heldebrant et al. [19] reported the use of alkanolamidines, alkanolguanidines, and diamines to form single-component reversible zwitterionic liquids by the reaction with CO_2. The guanidines used in this study were TMG derivatives **106**, **107**, and **108** (Fig. 55) prepared by the reaction of TMG (**3**) with bromoalkanols [19]. They found that the chain length of the alkyl group between the alcohol and guanidine has a pronounced effect on the physical properties and CO_2 regeneration behavior of the alkanolguanidines. Short alkyl chains (as in **106**) do not release CO_2 thermally because an addition of the carboxylate to imine carbon occurs. This cyclization to form the cyclic carbonate (**109**, Fig. 56) prevents this compound from releasing CO_2, and consequently, **106** is not a useful reversible zwitterionic liquid. Longer alkyl chains (as in **107**) produced a reversible zwitterionic liquid, while very long alkyl chains (as in **108**) produced reversible zwitterionic waxlike materials [19]. Another work with low viscosity alkanolguanidine and alkanolamidine liquids for CO_2 capture was reported by Heldebrant's group in

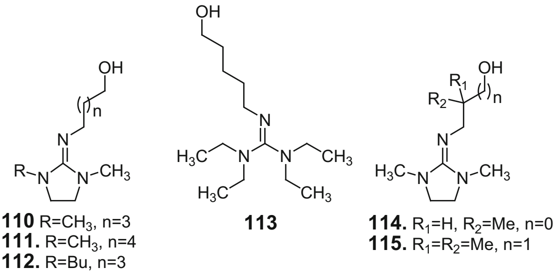

Fig. 57 Structures of alkanolguanidines **110–115**

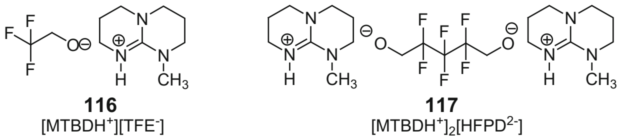

Fig. 58 Structures of ionic liquids **116** and **117**

2013 [133]. The structures of alkanolguanidines **110–115** used in this work [133] are presented in Fig. 57.

In 2010, Wang et al. [134] reported the preparation of superbase-derived protic ionic liquids (PILs), which were prepared by the proton-transfer reaction between the organic superbase MTBD (**2**) and an alcohol, imidazole, or pyrrolidone. The effect of different superbase-derived PILs on the CO_2 capture was investigated. The best CO_2 capture was observed for [$MTBDH^+$][TFE^-] (**116**, Fig. 58) with a molar ratio of CO_2 to **116** of 1.13 and [$MTBDH^+$]$_2$[$HFPD^{2-}$] (**117**, Fig. 58) with a molar ratio of 2.04 mol of CO_2 per mol of **117**. This high molar ratio achieved in **117** is due to the presence of two CO_2-reactive groups. In summary, these superbase-derived PILs with low melting points were capable of reversibly capturing CO_2 with a high capacity (more than 1 mol per mol IL), and a gravimetric capacity of more than 16% was achieved [134].

Kikuchi et al. reported two works [135, 136] on the incorporation of CO_2 into alkyne compounds mediated by silver catalysts in the presence of bases as an efficient system for utilization of CO_2 in organic synthesis. A catalytic C–C bond-forming reaction was achieved by the carboxylative cyclization of alkynyl ketones **118** with 1.0 MPa of CO_2 to afford lactone derivatives **121** in good yields under mild conditions (Fig. 59). The authors employed silver benzoate (20 mol%) in the presence of MTBD (**2**, 4 equiv.). Other metal salts and bases (TBD (**1**), DMAP (**27**) and *i*Pr_2NEt) were examined, and MTBD (**2**) showed the best catalytic activity. The authors postulated that the in situ formed enolate **119** is expected to capture CO_2 generating the β-ketocarboxylate intermediate **120** that would then be trapped by the silver-activated C–C triple bond resulting in the intramolecular cyclization to the corresponding lactone **121** (Fig. 59). This catalytic system was

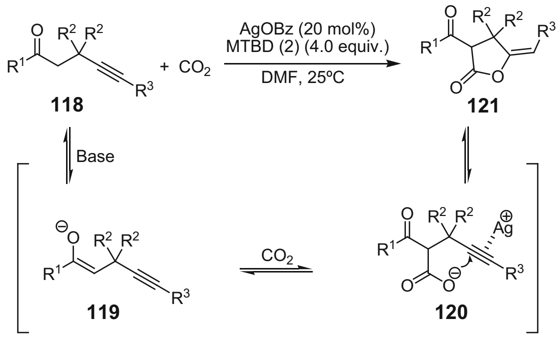

Fig. 59 Carboxylative cyclization of alkynyl ketones **118** with CO_2 to afford lactone derivatives **121** under AgOBz/MTBD catalysis

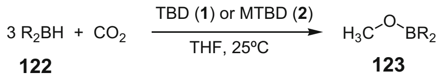

Fig. 60 Formation of methoxyboranes **123** from hydroboranes **122** and CO_2

applied to aliphatic ketone derivatives, and the corresponding γ-lactones were selectively obtained without any need for control of the enolization [135, 136]. The geometry of the C=C double bond in the lactone derivatives was confirmed by X-ray analysis and NOE experiments revealing the (*Z*)-isomer as the sole products.

In 2014, Gomes et al. [137] reported that guanidines and amidines are highly efficient metal-free catalysts for the reduction of CO_2 with hydroboranes **122**. Guanidines TBD (**1**) and MTBD (**2**) were active catalysts for this transformation, and MTBD (**2**) catalyzes the reduction of CO_2 to methoxyborane **123** (Fig. 60) at room temperature with TONs and TOFs of up to 648 and 33 h^{-1}, respectively. Formate and acetal derivatives were identified as reaction intermediates in the reduction, and the first C–H bond formation was found to be rate determining. Other nitrogen bases such as DMAP and DABCO also were tested under similar reaction conditions and showed negligible catalytic activity [137].

Recently in 2014, Zhang et al. [56] reported a reaction system using CO_2 as carboxylative reagent in a sequential carboxylation/intramolecular cyclization reaction of *o*-alkynyl acetophenone **124** to produce 1(3*H*)-isobenzofuranylidene acetic acids and esters **125** (Fig. 61). The authors studied a catalyst/base system, using copper and silver salts as catalysts and MTBD (**2**), DBU (**6**), DBN (**20**), K_2CO_3, and KO*t*Bu as bases. The optimal reaction conditions were found with 2 mol% of $AgBF_4$ as catalyst, 2.0 equiv. of MTDB (**2**), and a CO_2 balloon at room temperature for 12 h, obtaining 93% yield of product. This $AgBF_4$/MTBD system was extended to various *o*-alkynyl acetophenones, and the products were obtained in good yields (50–89%) and exclusive selectivity toward 5-*exo* oxygen cyclization [56].

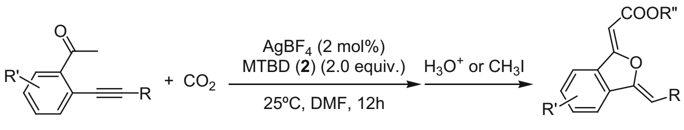

Fig. 61 Sequential carboxylation/intramolecular cyclization reaction of *o*-alkynyl acetophenones **124** to produce 1(3*H*)-isobenzofuranylidene acetic acids and esters **125**

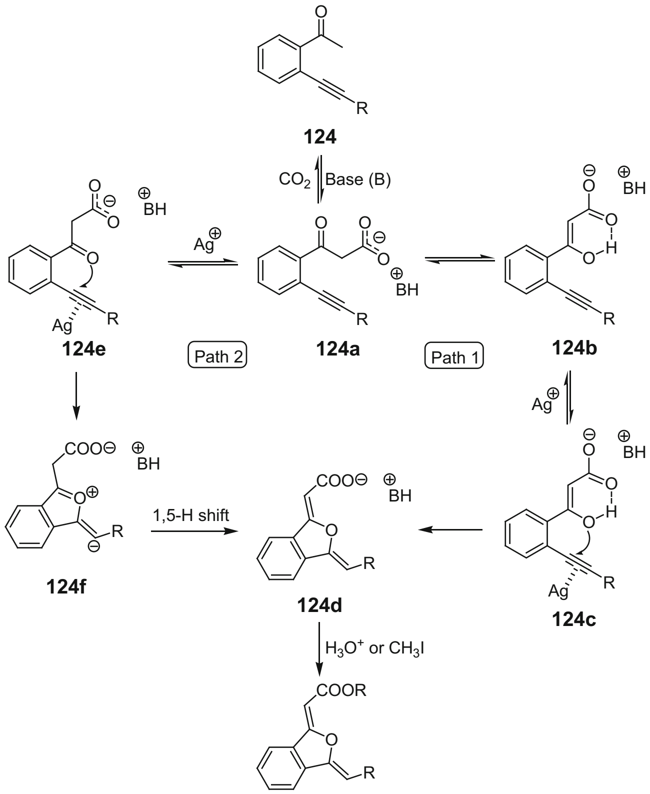

Fig. 62 Carboxylation/intramolecular cyclization mechanism proposed by Zhang et al. [56]

The authors proposed [56] a reaction mechanism shown in Fig. 62. In the presence of a suitable base such as MTBD (**2**), *o*-alkynyl acetophenone **124** is first carboxylated with CO_2 to produce a β-ketocarboxylate **124a**. For the following cyclization reaction, two possible pathways were proposed: in Path 1, **124a** undergoes keto–enol tautomerism to **124b,** and the enol oxygen atom of **124b** attacks the silver(I)-activated alkyne moiety in **124c** resulting in cyclization and formation of the 1(3*H*)-isobenzofuranylidene acetate **124d**. Path 2 involves the direct attack of the keto oxygen atom of **124a** toward the silver(I)-activated alkyne moiety **124e**, generating intermediate **124f**, and the following 1,5-hydrogen shift then gives acetate **124d**. Finally, acidification or esterification of the resulting carboxylate **124d** releases the carboxylic acid or ester **125** [56].

3 Indirect CO_2 Capture: Use of DMC in Synthesis

As mentioned in the Introduction (Sect. 1.2), organic carbonates can be used as alkylating and carbonylating agents and thus are a substitute for alkyl halides and phosgene. Dimethyl carbonate (DMC, **69**) is one of the most used organic carbonates in synthesis, and although it is synthesized from phosgene or via oxidative carbonylation of methanol, the increasing synthesis of DMC from CO_2 has converted the reactions using DMC into a means for the indirect capture CO_2.

For example, Asahi Kasei Corporation reported [36, 37] in 2003, for the first time in the world, the commercial production (50,000 ton year^{-1}) of a polycarbonate using carbon dioxide as a starting material. In this procedure, CO_2 is first converted to DMC (**69**) that is then used in the fabrication of the polymer. Accordingly, polycarbonate (PC) was made in four steps (Fig. 63): in the first step, CO_2 reacts with ethylene oxide (**126**) to form ethylene carbonate (**127**). After that, **127** reacts with methanol to produce DMC (**69**). Then, DMC (**69**) is converted to diphenyl carbonate (DPC, **128**) which reacts with bisphenol A (**129**) to generate the PC [36, 37]. Thus, DMC could be considered as an activated form of CO_2 with higher reactivity toward nucleophiles than the nonactivated CO_2 molecule.

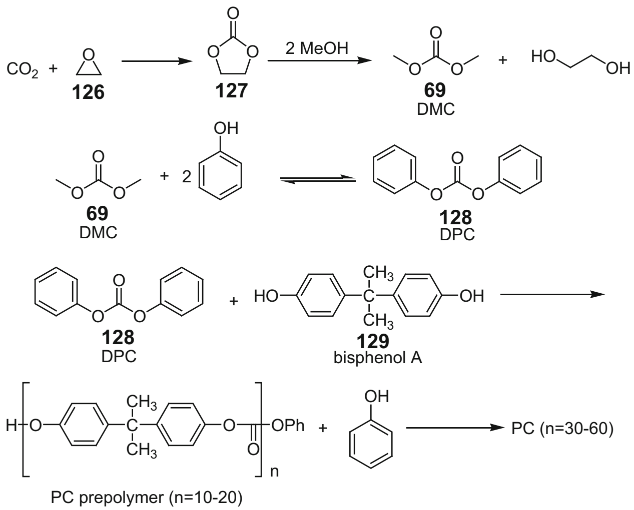

Fig. 63 Asahi Kasei polycarbonate process [36, 37]

In 2011, Tang et al. [138] reported an isocyanate-free synthesis of thermoplastic polyureas. They related for the first time that the organic superbasic guanidine TBD (**1**) is a promising catalyst for the transurethanization between dicarbamates **131a–c** and diamino-terminated poly(propylene glycol) (PPGda, **132**) for providing polyureas **133** [138]. First, they prepared the dicarbamates **131a–c** by carbomethoxylation between 1,4-diaminobutane (DAB, also called putrescine, **130**) and DMC (**69**) using TBD (**1**) as catalyst [138]. This synthetic strategy to prepare dicarbamates **131a–c** is shown in Fig. 64. The following transurethanization reaction between dicarbamates **131a–c** and diamino-terminated poly(propylene glycol) (PPGda, **132**) providing polyureas **133** [138] is shown in Fig. 65.

Thus, the authors reported the synthesis of polyureas catalyzed by TBD (**1**), starting from DAB (**130**), DMC (**69**), and PPGda (**132**), which are all potentially

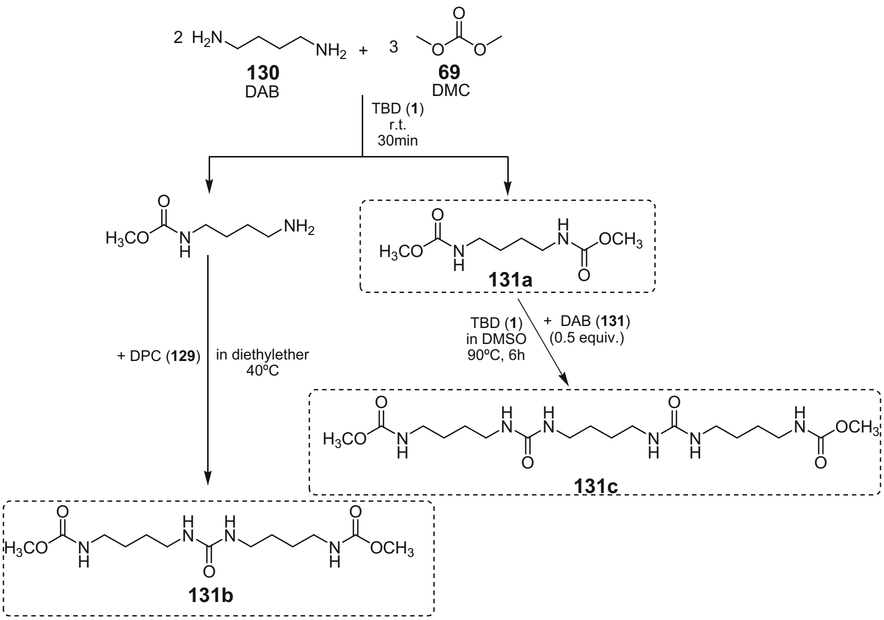

Fig. 64 Synthesis of dicarbamates **131a–c** from DAB (**130**) and DMC (**69**) using TBD (**1**) as catalyst

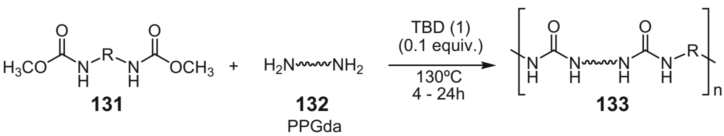

Fig. 65 Transurethanization between dicarbamates **131** and diamino-terminated poly(propylene glycol) (PPGda, **132**) providing polyureas **133**

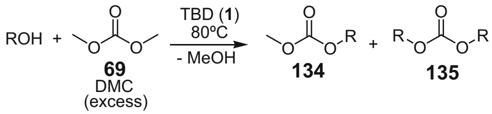

Fig. 66 General procedure for synthesis of unsymmetrical (**134**) and symmetrical (**135**) organic carbonates using TBD (**1**) and DMC (**69**)

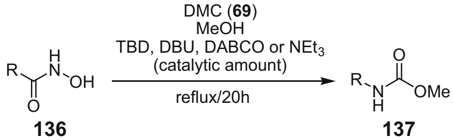

Fig. 67 General procedure to obtain methyl carbamates **137** from hydroxamic acids **136**

biomass-derived starting materials. This isocyanate-free route offers a versatile and effective way to prepare segmented polyureas with monodisperse hard segments [138].

In 2012, Mutlu et al. [139] reported the synthesis of symmetrical and unsymmetrical organic carbonates as well as polycarbonates using TBD (**1**) as a catalyst in combination with DMC (**69**) in a procedure without the use of classic toxic and harmful chemicals, such as phosgene and carbon monoxide [139]. The direct condensation of an alcohol and DMC (**69**) using TBD (**1**) in a homogeneous organocatalytic system without additional solvents affording unsymmetrical (**134**) and symmetrical (**135**) organic carbonates [139] is shown in Fig. 66. The influence of several reaction parameters such as amount of DMC, catalyst loading, and reaction time was discussed. All reactions were performed at atmospheric pressure at 80°C, and yields of up to 98% of unsymmetrical carbonates were obtained under optimized conditions (17 examples). The results obtained for the synthesis of low molecular weight building blocks could be transferred to the catalytic synthesis of high molecular weight polycarbonates [139].

In 2012, Kreye et al. [140] reported a catalytic variant of the Lossen rearrangement. They investigated if catalytic quantities of TBD (**1**) or other amine bases (DBU (**6**), TEA (**28**) and DABCO) have the potential to activate hydroxamic acids **136** with DMC (**69**) in situ to form methyl carbamates **137** [140] (Fig. 67).

The first experiments were using aliphatic hydroxamic acids. After optimization of the reaction conditions, they found that the best results were obtained when DMC (**69**) and methanol were used in a 10:1 ratio with 0.2 equiv. of TBD (**1**) at reflux for 20 h, giving yields of 52–77% (7 examples). After that, they extended the procedure to aromatic hydroxamic acids using the same conditions. However, instead of the expected methyl carbamate derivative **137**, they obtained aniline **138** (Fig. 68). Presumably, aromatic methyl carbamates are not stable under the applied basic

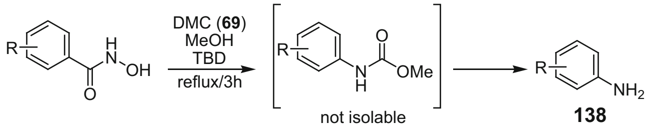

Fig. 68 General procedure to obtain anilines **138** from aromatic hydroxamic acids

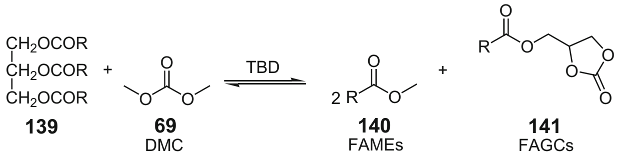

Fig. 69 Reaction between triglycerides **139** and DMC (**69**) producing a mixture of FAMEs **140** and FAGCs **141**

reaction conditions and are degraded to anilines **138** in the presence of TBD (**1**) and methanol and/or water (65–83% yield, eight examples) [140].

In summary, methyl carbamates were obtained when aliphatic hydroxamic acids were employed in this catalytic Lossen rearrangement, while aromatic hydroxamic acids yielded anilines under the same conditions. The mixture of DMC/methanol was recycled several times without observing any decrease in yields [140].

In 2013, Islam et al. [141] reported the transesterification kinetics of a homogeneous reaction system consisting of canola oil and DMC (**69**) for the productions of glycerol-free biofuels using TBD (**1**) as catalyst. The reaction between fatty acid triglycerides **139** and DMC (**69**) avoids the production of glycerol and, instead, produces a mixture of fatty acid methyl esters (FAMEs, **140**) and cyclic glycerol carbonate esters of fatty acids, known as fatty acid glycerol carbonates (FAGCs, **141**) (Fig. 69) [141].

The study was mainly focused on the influence of temperature, catalyst loading, and oil/DMC molar ratio on the progress of the transesterification reaction. The optimum conditions found were 70°C, 1.5 wt% of TBD (relative to the amount of oil), and a molar ratio of oil/DMC of 1/6 [141].

The authors proposed a mechanism for this catalytic process (Fig. 70) which is based on TBD (**1**) acting as a bifunctional nucleophilic organocatalyst. In the first step, TBD (**1**) reacts with DMC (**69**), leading to intermediate I. The methoxide anion from this intermediate attacks the triglyceride **139** to form 1 mol of FAME **140** and generates the intermediate II. The combination of diglyceride alkoxide with the intermediate II results in the regeneration of TBD (**1**), the formation of a molecule of FAGC **141** and another 1 mol of FAME **140** [141].

In 2013, Unverferth et al. [142] reported the TBD-catalyzed polycondensation reaction of fatty acid-derived dimethyl dicarbamates and diols as a versatile, non-isocyanate route toward renewable polyurethanes [142]. First, the authors

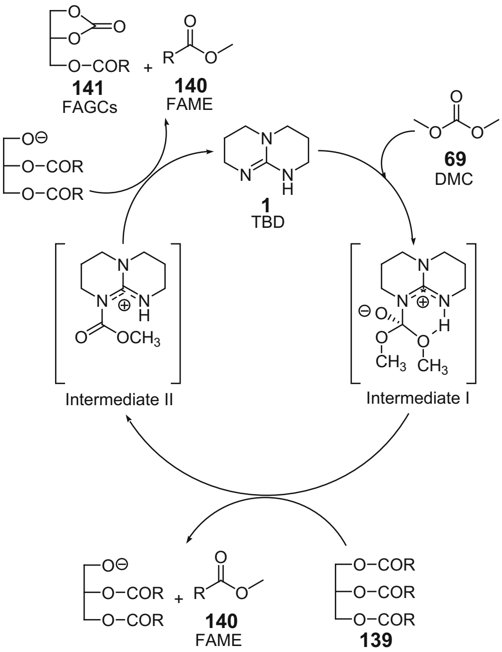

Fig. 70 Mechanism proposed by Islam et al. [141]

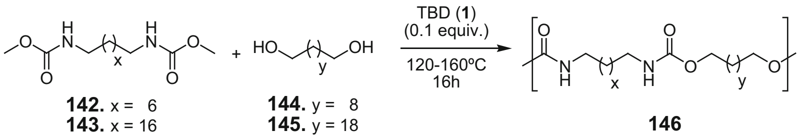

Fig. 71 General procedure for TBD-catalyzed polycondensation reactions

synthesized the dicarbamate monomers **142** and **143** by the Lossen rearrangement procedure described above (Fig. 67). The carbamate monomers **142** and **143** were then used in poly(transurethanization) reactions with diols **144** and **145** to obtain the polyurethanes **146** [142] (Fig. 71).

After optimization of the reaction conditions, polycondensations were performed at 120–160°C, continuous vacuum, and 0.1 equiv. of TBD (**1**) in three portions (0.033 equiv. at 120°C for 2 h, 0.033 equiv. at 140°C for 2 h, and 0.033 equiv. at 160°C for 12 h), and polyurethanes were obtained with molecular weights of up to 25 kDa. Other catalysts, e.g., Lewis acids such as titanium isopropoxide or tin(II) 2-ethylhexanoate, in amounts of 0.1 equiv. at temperatures of 130°C were less active than TBD (**1**), and only oligomers were obtained [142].

4 Conclusion

There are a number of energy fuel products including methanol, formic acid, and hydrocarbons and value-added chemicals including carbonates, carbamates, oxazolidinones, quinazolines, urea derivatives, isocyanates, etc. which can be produced from CO_2. These are also very important organic intermediates and building blocks in organic synthesis, pharmaceuticals and medicinal chemistry, dyes, and agricultural fields. Various catalytic systems have been found to be effective for CO_2 conversion. Heterocyclic guanidines like TBD and MTBD and linear guanidines such as TMG are an important group of compounds useful as catalysts for the capture and activation of CO_2. This chapter showed literature reports of guanidine catalysts with notorious efficiency for the synthesis of value-added chemicals by direct and indirect capture and activation of CO_2. TBD seems to be particularly useful as a catalyst both in the direct reaction with CO_2 and indirect reactions with DMC. The catalytic efficiency of TBD likely results from both the hydrogen bond activation of CO_2 and the formation of activated carbamate derivatives with enhanced electrophilicity.

References

1. Barbarini A, Maggi R, Mazzacani A, Mori G, Sartori G, Sartorio R (2003) Cycloaddition of CO_2 to epoxides over both homogeneous and silica-supported guanidine catalysts. Tetrahedron Lett 44:2931–2934
2. Dibenedetto A, Angelini A, Stufano P (2014) Use of carbon dioxide as feedstock for chemicals and fuels: homogeneous and heterogeneous catalysis. J Chem Technol Biotechnol 89:334–353
3. Mikkelsen M, Jørgensen M, Krebs FC (2010) The teraton challenge. A review of fixation and transformation of carbon dioxide. Energy Environ Sci 3:43–81
4. Behles JA, DeSimone JM (2001) Developments in CO_2 research. Pure Appl Chem 73:1281–1285
5. Aresta M, Nobile CF, Albano VG, Forni E, Manassero M (1975) New nickel-carbon dioxide complex: synthesis, properties, and crystallographic characterization of (carbon dioxide)-bis (tricyclohexylphosphine)nickel. J Chem Soc Chem Commun 15:636–637
6. Ma J, Sun N, Zhang X, Zhao N, Xiao F, Wei W, Sun Y (2009) A short review of catalysis for CO_2 conversion. Catal Today 148:221–231
7. Gomes CN, Jacquet O, Villiers C, Thuéry P, Ephritikhine M, Cantat T (2012) A diagonal approach to chemical recycling of carbon dioxide: organocatalytic transformation for the reductive functionalization of CO_2. Angew Chem Int Ed 51:187–190
8. Huang K, Sun C-L, Shi Z-J (2011) Transition-metal-catalyzed C–C bond formation through the fixation of carbon dioxide. Chem Soc Rev 40:2435–2452
9. Sakakura T, Choi J-C, Yasuda H (2007) Transformation of carbon dioxide. Chem Rev 107:2365–2387
10. Aresta M (2010) Carbon dioxide as chemical feedstock. Wiley-VCH, Weinheim
11. Metz B, Davidson O, Coninck H, Loos M, Meyer L (2005) IPCC special report on carbon dioxide capture and storage. Cambridge University Press, Cambridge
12. Liang C, Liu Q, Xu Z (2014) Surfactant-free switchable emulsions using CO_2-responsive particles. Appl Mater Interfaces 6:6898–6904

13. Pereira FS, deAzevedo ER, Silva EF, Bonagamba TJ, Agostíni DLS, Magalhães A, Job AE, González ERP (2008) Study of the carbon dioxide chemical fixation-activation by guanidines. Tetrahedron 64:10097–10106
14. Pérez ER, Silva MO, Costa VC, Rodrigues-Filho UP, Franco DW (2002) Efficient and clean synthesis of *N*-alkyl carbamates by transcarboxylation and *O*-alkylation coupled reactions using a DBU-CO_2 zwitterionic carbamic complex in aprotic polar media. Tetrahedron Lett 43:4091–4093
15. Pérez ER, Santos RHA, Gambardella MTP, Macedo LGM, Rodrigues-Filho UP, Launay J-C, Franco DW (2004) Activation of carbon dioxide by bicyclic amidines. J Org Chem 69:8005–8011
16. Alessio P, Ferreira DM, Job AE, Aroca RF, Riul A Jr, Constantino CJL, González ERP (2008) Fabrication, structural characterization, and applications of langmuir and langmuir-blodgett films of a poly(azo)urethane. Langmuir 24:4729–4737
17. Gomes CR, Ferreira DM, Constantino CJL, González ERP (2008) Selectivity of the cyclic carbonate formation by fixation of carbon dioxide into epoxides catalyzed by Lewis bases. Tetrahedron Lett 49:6879–6881
18. Hooker JM, Reibel AT, Hill SM, Schueller MJ, Fowler JS (2009) One-Pot, direct incorporation of $[^{11}C]CO_2$ into carbamates. Angew Chem Int Ed 48:3482–3485
19. Heldebrant DJ, Koech PK, Ang MTC, Liang C, Rainbolt JE, Yonker CR, Jessop PG (2010) Reversible zwitterionic liquids, the reaction of alkanol guanidines, alkanol amidines, and diamines with CO_2. Green Chem 12:713721
20. Aresta M, Berloco C, Quaranta E (1995) Biomimetic building-up of the carbamic moiety: the intermediacy of carboxyphosphate analogues in the synthesis of n-aryl carbamate esters from arylamines and organic carbonates promoted by phosphorus acids. Tetrahedron 51:8073–8088
21. Adams P, Baron FA (1965) Esters of carbamic acid. Chem Rev 65:567–602
22. Babad H, Zeiler AG (1973) The chemistry of phosgene. Chem Rev 73:75–91
23. McGhee WD, Riley D, Christ K, Pan Y, Parnas B (1995) Carbon dioxide as a phosgene replacement: synthesis and mechanistic studies of urethanes from amines, CO_2, and alkyl chlorides. J Org Chem 60:2820–2830
24. Casadei MA, Inesi A, Rossi L (1997) Electrochemical activation of carbon dioxide: synthesis of organic carbonates. Tetrahedron Lett 38:3565–3568
25. Bruneau C, Dixneuf PH (1992) Catalytic incorporation of CO_2 into organic substrates: synthesis of unsaturated carbamates, carbonates and ureas. J Mol Catal 74:97–107
26. Hoffman WA (1982) Convenient preparation of carbonates from alcohols and carbon dioxide. J Org Chem 47:5209–5210
27. Kim S-I, Chu F, Dueno EE, Jung KW (1999) Alkyl carbonates: efficient three component coupling of aliphatic alcohols, CO_2, and alkyl halides in the presence of CS_2CO_3. J Org Chem 64:4578–4579
28. Aresta M, Quaranta E (1988) Reactivity of phosphacarbamates: transfer of the carbamate group promoted by metal assisted electrophilic attack at the carbon dioxide moiety. J Org Chem 53:4154–4156
29. Casadei MA, Inesi A, Moraccia FM, Rossi L (1996) Electrochemical activation of carbon dioxide: synthesis of carbamates. Chem Commun 22:2575–2576
30. Stastny V, Rudkevich DM (2007) Separations using carbon dioxide. J Am Chem Soc 129:1018–1019
31. Hooker JM, Reibel AT, Hill SM, Schuller MJ, Fowler JS (2009) One-pot, direct incorporation of $[^{11}C]CO_2$ into carbamates. Angew Chem 121:3534–3537
32. Salvatore RN, Ledger JA, Jung KW (2001) An efficient one-pot synthesis of *N*-alkyl carbamates from primary amines using Cs_2CO_3. Tetrahedron Lett 42:6023–6025
33. Pérez ER, Garcia JR, Cardoso DR, McGarvey BR, Batista EA, Rodrigues-Filho UP, Vielstich W, Franco DW (2005) In situ FT-IR and ex situ EPR analysis for the study of the

electroreduction of carbon dioxide in N, N-dimethylformamide on a gold interface. J Electroanal Chem 578:87–94
34. Tundo P, Selva M (2002) The chemistry of dimethyl carbonate. Acc Chem Res 35:706–716
35. Pacheco MA, Marshall CL (1997) Review of dimethyl carbonate (DMC) manufacture and its characteristics as a fuel additive. Energy Fuel 11:2–29
36. Fukuoka S, Kawamura M, Komiya K, Tojo M, Hachiya H, Hasegawa K, Aminaka M, Okamoto H, Fukawa I, Konno S (2003) A novel non-phosgene polycarbonate production process using by-product CO_2 as starting material. Green Chem 5:497–507
37. Fukuoka S, Tojo M, Hachiya H, Aminaka M, Hasegawa K (2007) Green and sustainable chemistry in practice: development and industrialization of a novel process for polycarbonate production from CO_2 without using phosgene. Polym J 39:91–114
38. Dai W-L, Luo S-L, Yin S-F, Au C-T (2009) The direct transformation of carbon dioxide to organic carbonates over heterogeneous catalysts. Appl Catal A 366:2–12
39. Kolb N, Meier MAR (2012) Monomers and their polymers derived from saturated fatty acid methyl esters and dimethyl carbonate. Green Chem 14:2429–2435
40. Fuming M, Zhi P, Guangwing L (2004) The transesterification of dimethyl carbonate with phenol over Mg-Al-hydrotalcite catalyst. Org Proc Res Dev 8:372–375
41. Tong D-S, Yao J, Wang Y, Niu H-Y, Wang G-Y (2007) Transesterification of dimethyl carbonate with phenol to diphenyl carbonate over V_2O_5 catalyst. J Mol Catal A Chem 268:120–126
42. Chen T, Han H, Yao J, Wang G (2007) The transesterification of dimethyl carbonate and phenol catalyzed by 12-molybdophosphoric salts. Catal Commun 8:1361–1365
43. Kirumakki SR, Nagaraju N, Murthy KVVSBSR, Narayanan S (2002) Esterification of salicylic acid over zeolites using dimethyl carbonate. Appl Catal A Gen 226:175–182
44. Sakakura T, Choi J-C, Saito Y, Sako T (2000) Synthesis of dimethyl carbonate from carbon dioxide: catalysis and mechanism. Polyhedron 19:573–576
45. Keller N, Rebmann G, Keller V (2010) Catalysts, mechanisms and industrial processes for the dimethylcarbonate synthesis. J Mol Catal A Chem 317:1–18
46. Omae I (2006) Aspects of carbon dioxide utilization. Catal Today 115:33–52
47. Ferreira HBP, Vale DL, Andrade LS, Mota CJA, Miranda JL (2013) Dimethylcarbonate: a route for the conversion of CO_2. Rev Virtual Quim 5:188–200
48. Sakakura T, Kohno K (2009) The synthesis of organic carbonates from carbon dioxide. Chem Commun 11:1312–1330
49. Tian J-S, Miao C-X, Wang J-Q, Cai F, Du Y, Zhao Y, He L-N (2007) Efficient synthesis of dimethyl carbonate from methanol, propylene oxide and CO_2 catalyzed by recyclable inorganic base/phosphonium halide-functionalized polyethylene glycol. Green Chem 9:566–571
50. North M, Pasquale R, Young C (2010) Synthesis of cyclic carbonates from epoxides and CO_2. Green Chem 12:1514–1539
51. Taylor JE, Bull SD, Williams JMJ (2012) Amidines, isothioureas, and guanidines as nucleophilic catalysts. Chem Soc Rev 41:2109–2121
52. Ishikawa T (2009) Superbases for organic synthesis: guanidines, amidines and phosphazenes and related organocatalysts. Wiley, Chichester
53. Denmark SE, Beutner GL (2008) Lewis base catalysis in organic synthesis. Angew Chem Int Ed 47:1560–1638
54. Kiesewetter MK, Scholten MD, Kirn N (2009) Cyclic guanidine organic catalysts: what is magic about triazabicyclodecene? J Org Chem 74:9490–9496
55. Santo RDE, Simas RC, Magalhães A, Santos VG, Regiani T, Isler AC, Martins NG, Eberlin MN, González ERP (2013) Experimental NMR and MS study of benzoylguanidines. Investigation of E/Z isomerism. J Phys Org Chem 26:315–321
56. Zhang W-Z, Shi L-L, Liu C, Yang X-T, Wang Y-B, Luo Y, Lu X-B (2014) Sequential carboxylation/intramolecular cyclization reaction of o-alkynyl acetophenone with CO_2. Org Chem Front 1:275–283

57. Santo RDE, Machado MGM, Santos JL, González ERP, Chin MC (2014) Use of guanidine compounds in the treatment of neglected tropical diseases. Curr Org Chem 18:2572–2602
58. Adam F, Batagarawa MS (2013) Tetramethylguanidine-silica nanoparticles as an efficient and reusable catalyst for the synthesis of cyclic propylene carbonate from carbon dioxide and propylene oxide. Appl Catal A 454:164–171
59. Fu X, Tan C-H (2011) Mechanistic considerations of guanidine-catalyzed reactions. Chem Commun 47:8210–8222
60. Gusakova GV, Denisov GS, Smolyanskii AL (1990) Proton-acceptor power of l, l,3,3-tetramethylguanidine: hydrogen bonding and protonation in inert solvents. Zhurnal obshchei khimii 59:2343–2348
61. Barton DHR, Elliott JD, Géro SD (1981) The synthesis and properties of a series of strong but hindered organic bases. J Chem Soc Chem Commun 21:1136–1137
62. Barton DHR, Elliott JD, Géro SD (1982) Synthesis and properties of a series of sterically hindered guanidine bases. J Chem Soc Perkin Trans I 2085–2090
63. Endo T, Nagai D, Monma T, Yamaguchi H, Ochiai B (2004) A novel construction of a reversible fixation-release system of carbon dioxide by amidines and their polymers. Macromolecules 37:2007–2009
64. Darensbourg DJ, Mackiewicz RM (2005) Role of the cocatalyst in the copolymerization of CO_2 and cyclohexene oxide utilizing chromium salen complexes. J Am Chem Soc 127:14026–14038
65. Yamada T, Lukac PJ, George M, Weiss RG (2007) Reversible, room-temperature ionic liquids. Amidinium carbamates derived from amidines and aliphatic primary amines with carbon dioxide. Chem Mater 19:967–969
66. Amatore C, Savéan J-M (1981) Mechanism and kinetic characteristics of the electrochemical reduction of carbon dioxide in media of low proton availability. J Am Chem Soc 103:5021–5023
67. Villiers C, Dognon J-P, Pollet R, Thuéry P, Ephritikhine M (2010) An isolated CO_2 adduct of a nitrogen base: crystal and electronic structures. Angew Chem 122:3543–3546
68. Villiers C, Dognon J-P, Pollet R, Thuéry P, Ephritikhine M (2010) An isolated CO_2 adduct of a nitrogen base: crystal and electronic structures. Angew Chem Int Ed 49:3465–3468
69. Ma J, Zhang X, Zhao N (2010) Theoretical study of TBD-catalyzed carboxylation of propylene glycol with CO_2. J Mol Catal A Chem 315:76–81
70. Mizuno T, Okamoto N, Ito T, Miyata T (2000) Synthesis of 2,4-dihydroxyquinazolines using carbon dioxide in the presence of DBU under mild conditions. Tetrahedron Lett 41:1051–1053
71. Ishikawa T, Kumamoto T (2006) Guanidines in organic synthesis. Synthesis 5:737–752
72. Coles MP (2009) Bicyclic-guanidines, -guanidinates and -guanidinium salts: wide ranging applications from a simple family of molecules. Chem Commun 3659–3676
73. Leow D, Tan C-H (2009) Chiral guanidine catalyzed enantioselective reactions. Chem Asian J 4:488–507
74. Ishikawa T, Isobe T (2002) Modified guanidines as chiral auxiliaries. Chem Eur J 8:552–557
75. Nagasawa K, Hashimoto Y (2003) Synthesis of marine guanidine alkaloids and their application as chemical/biological tools. Chem Rec 3:201–211
76. Leow D, Tan C-H (2010) Catalytic reactions of chiral guanidines and guanidinium salts. Synlett 11:1589–1605
77. Turočkin A (2014) 1,5,7-Triazabicyclo[4.4.0]dec-5-ene (TBD) as a lewis base. Synlett 25:894–895
78. Tkatchenko DB, Sorokina S (2003) Linear organic carbonates. In: Aresta M (ed) Carbon dioxide recovery and utilization. Kluwer, Dordrecht, pp 261–277
79. Shaikh A-A G, Sivaram S (1996) Organic carbonates. Chem Rev 96:951–976
80. Pokharkar V, Sivaram S (1995) Poly(alkylene carbonate)s by the carbonate interchange reaction of aliphatic diols with dimethyl carbonate: synthesis and characterization. Polymer 36:4851–4854

81. Adams JB (1992) PCT Int Appl WO 04:318
82. Chaturvedi D (2012) Perspectives on the synthesis of organic carbamates. Tetrahedron 68:15–45
83. Ghiron C, Rossi T, Thomas RJ (1997) The stereoselective synthesis of 4-formytrinem, a key intermediate for novel trinems. Tetrahedron Lett 38:3569–3572
84. Smith AB, Freeze BS, LaMarche MJ, Hirose T, Brouard I, Rucker PV, Xian M, Sundermann KF, Shaw SJ, Burlingame MA, Horwitz SB, Myles DC (2005) Design, synthesis, and evaluation of carbamate-substituted analogues of (+)-discodermolide. Org Lett 7:311–314
85. Dangerfield EM, Timmer MSM, Stoker BL (2009) Total synthesis without protecting groups: pyrrolidines and cyclic carbamates. Org Lett 11:535–538
86. Wills AJ, Ghosh YK, Balasubramanian S (2002) Synthesis of a polymer-supported oxazolidine aldehyde for asymmetric chemistry. J Org Chem 67:6646–6652
87. Han C, Shen R, Su S, Porco JA Jr (2004) Copper-mediated synthesis of n-acyl vinylogous carbamic acids and derivatives: synthesis of the antibiotic CJ-15,801. Org Lett 6:27–30
88. Greene TW, Wuts PGM (2007) Protective group in organic synthesis, 4th edn. New York, Wiley
89. Kociensiki PJ (2003) Protective groups, 3rd edn. Thieme, Stuttgart
90. Mayer JP, Lewis GS, Curtis MJ, Zhang J (1997) Solid phase synthesis of quinazolinones. Tetrahedron Lett 38:8445–8448
91. Aresta M, Dibenedetto A (2004) The contribution of the utilization option to reducing the CO_2 atmospheric loading: research needed to overcome existing barriers for a full exploitation of the potential of the CO_2 use. Catal Today 98:455–462
92. Dibenedetto A, Angelini A (2014) Chapter two: synthesis of organic carbonates. Adv Inorg Chem 66:25–81
93. McGhee WD, Riley DP, Christ ME, Christ KM (1993) Palladium-catalyzed generation of o-allylic urethanes and carbonates from amines/alcohols, carbon dioxide, and allylic chlorides. Organometallics 12:1429–1433
94. McGhee WD, Pan Y, Riley DP (1994) Highly selective generation of urethanes from amines, carbon dioxide and alkyl chlorides. J Chem Soc Chem Commun 6:699–700
95. McGhee WD, Riley D (1995) Replacement of phosgene with carbon dioxide: synthesis of alkyl carbonates. J Org Chem 60:6205–6207
96. McGhee WD, Parnas BL, Riley DP, Talley JJ (29 June 1993) US Patent 5,223,638
97. McGhee WD, Parnas BL, Riley DP, Talley JJ (1993) Chem Abstr 118:213762
98. Kadokawa J-I, Habu H, Fukamachi S, Karasu M, Tagaya H, Chiba K (1998) Direct polycondensation of carbon dioxide with xylylene glycols: a new method for the synthesis of polycarbonates. Macromol Rapid Commun 19:657–660
99. Kadokawa J-I, Habu H, Fukamachi S, Karasu M, Tagaya H, Chiba K (1999) Direct condensation reaction of carbon dioxide with alcohols using trisubstituted phosphine-carbon tetrabromide-base system as a condensing agent. J Chem Soc Perkin Trans 1(15):2205–2208
100. Heldebrant DJ, Jessop PG, Thomas CA, Eckert CA, Liotta CL (2005) The reaction of 1,8-diazabicyclo[5.4.0]undec-7-ene (DBU) with carbon dioxide. J Org Chem 70:5335–5338
101. Pereira FS, Agostini DLS, Santo RDE, deAzevedo ER, Bonagamba TJ, Job AE, González ERP (2011) A comparative solid state ^{13}C NMR and thermal study of CO_2 capture by amidines PMDBD and DBN. Green Chem 13:2146–2153
102. Wang X, Lim YN, Lee C, Jang H-Y, Lee BY (2013) 1,5,7-Triazabicyclo[4.4.0]dec-1-ene-mediated acetylene dicarboxylation and alkyne carboxylation using carbon dioxide. Eur J Org Chem 10:1867–1871
103. Xie H, Yu X, Yang Y, Zhao ZK (2014) Capturing CO_2 for cellulose dissolution. Green Chem 16:2422–2427
104. Xie H, Duan H, Li S, Zhang S (2005) The effective synthesis of propylene carbonate catalyzed by silica-supported hexaalkylguanidinium chloride. New J Chem 29:1199–1203

105. Xie H, Li S, Zhang S (2006) Highly active, hexabutylguanidinium salt/zinc bromide binary catalyst for the coupling reaction of carbon dioxide and epoxides. J Mol Catal A Chem 250:30–34
106. Zhang X, Zhao N, Wei W, Sun Y (2006) Chemical fixation of carbon dioxide to propylene carbonate over amine-functionalized silica catalysts. Catal Today 115:102–106
107. Lu X-B, Shi L, Wang Y-M, Zhang R, Zhang Y-J, Peng X-J, Zhang Z-C, Li B (2006) Design of highly active binary catalyst systems for CO_2/epoxide copolymerization: polymer selectivity, enantioselectivity, and stereochemistry control. J Am Chem Soc 128:1664–1674
108. Li B, Zhang R, Lu X-B (2007) Stereochemistry control of the alternating copolymerization of CO_2 and propylene oxide catalyzed by SalenCrX complexes. Macromolecules 40:2303–2307
109. Zhang X, Jia Y-B, Lu X-B, Li B, Wang H, Sun L-C (2008) Intramolecularly two-centered cooperation catalysis for the synthesis of cyclic carbonates from CO_2 and epoxides. Tetrahedron Lett 49:6589–6592
110. Ren W-M, Liu Z-W, Wen Y-Q, Zhang R, Lu X-B (2009) Mechanistic aspects of the copolymerization of CO_2 with epoxides using a thermally stable single-site cobalt(III) catalyst. J Am Chem Soc 131:11509–11518
111. Huang S, Ma J, Li J (2008) Efficient propylene carbonate synthesis from propylene glycol and carbon dioxide via organic bases. Catal Commun 9:276–280
112. Prasetyanto EA, Ansari MB, Min B-H, Park S-E (2010) Melamine tri-silsesquioxane bridged periodic mesoporous organosilica as an efficient metal-free catalyst for CO_2 activation. Catal Today 158:252–257
113. Yu KMK, Curcic I, Gabriel J, Morganstewart H, Tsang SC (2010) Catalytic coupling of CO_2 with epoxide over supported and unsupported amines. J Phys Chem A 114:3863–3872
114. Yang Z-Z, Zhao Y-N, He L-N, Gao J, Yin Z-S (2012) Highly efficient conversion of carbon dioxide catalyzed by polyethylene glycol-functionalized basic ionic liquids. Green Chem 14:519–527
115. Wei-Li D, Bi J, Sheng-Lian L, Xu-Biao L, Xin-Man T, Chak-Tong A (2013) Novel functionalized guanidinium ionic liquids: efficient acid-base bifunctional catalysts for CO_2 fixation with epoxides. J Mol Catal A Chem 378:326–332
116. Liu B, Liu M, Liang L, Sun J (2015) Guanidine hydrochloride/ZnI_2 as heterogeneous catalyst for conversion of CO_2 and epoxides to cyclic carbonates under mild conditions. Catalysts 5:119–130
117. Li Y-N, He L-N, Diao Z-F, Yang Z-Z (2014) Chapter nine: carbon capture with simultaneous activation and its subsequent transformation. Adv Inorg Chem 66:289–345
118. Costa M, Chiusoli GP, Rizzardi M (1996) Base-catalysed direct introduction of carbon dioxide into acetylenic amines. Chem Commun 14:1699–1700
119. Costa M, Chiusoli GP, Taffurelli C, Dalmonego G (1998) Superbase catalysis of oxazolidin-2-one ring formation from carbon dioxide and prop-2-yn-1-amines under homogeneous or heterogenous conditions. J Chem Soc Perkin Trans 1(9):1541–1546
120. Nicholls R, Kaufhold S, Nguyen BN (2014) Observation of guanidine–carbon dioxide complexation in solution and its role in the reaction of carbon dioxide and propargylamines. Catal Sci Technol 4:3458–3462
121. Maggi R, Bertolotti C, Orlandini E, Oro C, Sartori G, Selva M (2007) Synthesis of oxazolidinones in supercritical CO_2 under heterogeneous catalysis. Tetrahedron Lett 48:2131–2134
122. Paz J, Pérez-Balado C, Iglesias B, Muñoz L (2009) Carbonylation with CO_2 and phosphorus electrophiles: a convenient method for the synthesis of 2-oxazolidinones from 1,2-amino alcohols. Synlett 3:0395–0398
123. Paz J, Pérez-Balado C, Iglesias B, Muñoz L (2010) Carbon dioxide as a carbonylating agent in the synthesis of 2-oxazolidinones, 2-oxazinones, and cyclic ureas: scope and limitations. J Org Chem 75:3037–3046

124. Yang Z-Z, Li Y-N, Wei Y-Y, He L-N (2011) Protic onium salts-catalyzed synthesis of 5-aryl-2-oxazolidinones from aziridines and CO_2 under mild conditions. Green Chem 13:2351–2353
125. Gao J, He L-N, Miao C-X, Chanfreau S (2010) Chemical fixation of CO_2: efficient synthesis of quinazoline-2,4(1*H*,3*H*)-diones catalyzed by guanidines under solvent-free conditions. Tetrahedron 66:4063–4067
126. Lu W, Ma J, Hu J, Song J, Zhang Z, Yang G, Han B (2014) Efficient synthesis of quinazoline-2,4(*1H*,*3H*)-diones from CO_2 using ionic liquids as a dual solvent-catalyst at atmospheric pressure. Green Chem 16:221–225
127. Zhao Y, Yu B, Yang Z, Zhang H, Hao L, Gao X, Liu Z (2014) A protic ionic liquid catalyzes CO_2 conversion at atmospheric pressure and room temperature: synthesis of quinazoline-2,4-(1*H*,3*H*)-diones. Angew Chem Int Ed 53:5922–5925
128. Zhao Y-N, Yu B, Yang Z-Z, He L-N (2014) Magnetic base catalysts for the chemical fixation of carbon dioxide to quinazoline-2,4(1*H*,3*H*)-diones. RSC Adv 4:28941–28946
129. Lang X-D, Zhang S, Song Q-W, He L-N (2015) Tetra-butylphosphonium arginine-based ionic liquid-promoted cyclization of 2-aminobenzonitrile with carbon dioxide. RSC Adv 5:15668–15673
130. Jessop PG, Heldebrant DJ, Li X, Eckert CA, Liotta CL (2005) Reversible nonpolar-to-polar solvent. Nature 436:1102
131. Phan L, Chiu D, Heldebrant DJ, Huttenhower H, John E, Li X, Pollet P, Wang R, Eckert CA, Liotta CL, Jessop PG (2008) Switchable solvents consisting of amidine/alcohol or guanidine/alcohol mixtures. Ind Eng Chem Res 47:539–545
132. Heldebrant DJ, Yonker CR, Jessop PG, Phan L (2008) Organic liquid CO_2 capture agents with high gravimetric CO_2 capacity. Energy Environ Sci 1:487–493
133. Koech PK, Zhang J, Kutnyakov IV, Cosimbescu L, Lee S-J, Bowden ME, Smurthwaite TD, Heldebrant DJ (2013) Low viscosity alkanolguanidine and alkanolamidine liquids for CO_2 capture. RSC Adv 3:566–572
134. Wang C, Luo H, Jiang D, Li H, Dai S (2010) Carbon dioxide capture by superbase-derived protic ionic liquids. Angew Chem Int Ed 49:5978–5981
135. Kikuchi S, Sekine K, Ishida T, Yamada T (2012) C-C bond formation with carbon dioxide promoted by a silver catalyst. Angew Chem 124:7095–7098
136. Kikuchi S, Yamada T (2014) Carbon dioxide incorporation into alkyne compounds mediated by silver catalysts. Chem Rec 14:62–69
137. Gomes CN, Blondiaux E, Thuéry P, Cantat T (2014) Metal-free reduction of CO_2 with hydroboranes: two efficient pathways at play for the reduction of CO_2 to methanol. Chem Eur J 20:7098–7106
138. Tang D, Dirk-Jan Mulder D-J, Noordover BAJ, Koning CE (2011) Well-defined biobased segmented polyureas synthesis via a TBD-catalyzed isocyanate-free route. Macromol Rapid Commun 32:1379–1385
139. Mutlu H, Ruiz J, Solleder SC, Meier MAR (2012) TBD catalysis with dimethyl carbonate: a fruitful and sustainable alliance. Green Chem 14:1728–1735
140. Kreye O, Wald S, Meier MAR (2013) Introducing catalytic lossen rearrangements: sustainable access to carbamates and amines. Adv Synth Catal 355:81–86
141. Islam MR, Kurle YM, Gossage JL, Benson TJ (2013) Kinetics of triazabicyclodecene-catalyzed canola oil conversion to glycerol-free biofuel using dimethyl carbonate. Energy Fuels 27:1564–1569
142. Unverferth M, Kreye O, Prohammer A, Meier MAR (2013) Renewable non-isocyanate based thermoplastic polyurethanes via polycondensation of dimethyl carbamate monomers with diols. Macromol Rapid Commun 34:1569–1574

Top Heterocycl Chem (2017) 51: 75–94
DOI: 10.1007/7081_2015_172

Published online: 1 October 2015

Triaminoguanidinium-Based Ligands in Supramolecular Chemistry

Carolina von Eßen, Christian R. Göb, and Iris M. Oppel

Abstract This chapter will give an insight into the chemistry of triaminoguanidinium salts (*TAG*X), their synthesis, and potential application. The main focus will be on the utilization of triaminoguanidinium salts as building blocks for C_3-symmetric ligand systems. Both the direct application and the coordination chemistry leading to molecular and supramolecular coordination compounds will be presented. The formation of basic coordination compounds and different discrete coordination cages will be described in more detail.

Keywords 2D network, C_3-Symmetric ligands, Coordination, Supramolecular chemistry, Triaminoguanidinium salts

Contents

C. von Eßen, C.R. Göb, and I.M. Oppel (✉)
Institute of Inorganic Chemistry, RWTH Aachen University, Landoltweg 1, 52074 Aachen, Germany
e-mail: iris.oppel@ac.rwth-aachen.de

Abbreviations

a	*Anti*
acac	Acetylacetonate
DMAB	Dimethylaminoborane
DMF	*N*,*N*-Dimethylformamide
en	Ethylenediamine
H_5L'	2-(4-(2-Hydroxybenzyl)amino)-5-(2-(2-hydroxybenzylidene) hydrazinyl)-4*H*-1,2,4-triazol-3-yl)phenol
H_5L	tris(2-Hydroxybenzylidene)triaminoguanidine
NaH*bar*	Sodium 5,5-diethylbarbiturate
*p*TsOH	*para*-Toluenesulfonic acid
s	*Syn*
TAG	Triaminoguanidine
*TAG*X	Triaminoguanidinium salt
$[H_6Br_3L]Cl$	tris(5-Bromo-2-hydroxybenzylidene)triaminoguanidinium chloride
$[H_3Me_3Br_3L]Cl$	tris(5-Bromo-2-methoxybenzylidene)triaminoguanidinium chloride
$[H_6(OMe)_3Br_3L]Cl$	tris(5-Bromo-2-hydroxy-3-methoxybenzylidene) triaminoguanidinium chloride
$[H_6L]Cl$	tris(2-Hydroxybenzylidene)triaminoguanidinium chloride
$[H_6Br_3L]Cl$	tris(5-Bromo-2-hydroxybenzylidene)triaminoguanidinium chloride
$[H_6Br_6(OMe)_3L]Cl$	tris(3,5-Dibromo-2-hydroxy-4-methoxybenzylidene) triaminoguanidinium chloride

1 Introduction

In 1904 Stollé mentioned the preparation of *TAG*Cl from hydrazine hydrate and carbon tetrachloride and the subsequent condensation with benzaldehyde [1]. Nowadays triaminoguanidinium salts are prepared by conversion of guanidinium salts with hydrazine hydrate (Fig. 1). Details of the basic module are presented in the chapter of S. Herres-Pawlis, which covers the guanidinium salts.

Small C_3-symmetric organic molecules, which offer three chelating coordination sites, are accessible. By deprotonation with an appropriate base, free triaminoguanidine bases (*TAG*) can be obtained. Moreover, cyclization reactions for the formation of triazoles [2, 3], tetrazoles [4, 5], and tetrazines [6] are widely used to obtain cyclic compounds with a high nitrogen content. Already in 1957, Scott described a new method for the preparation of a tetrazine derived from *TAG*NO_3 and acetylacetone [7]. Further research in this area was done by Klapötke, who was interested in tetrazoles and their usage as constituent for energetic salts [4, 5].

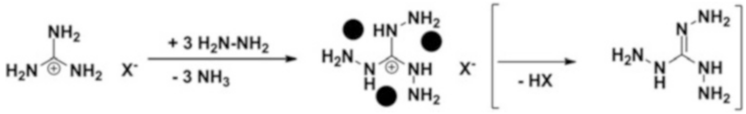

Fig. 1 Formation of *TAG*X and deprotonation to triaminoguanidine. *Black circles* show possible coordination sites

2 *TAG*-Based Ligands

There are only a few examples in which unsubstituted triaminoguanidinium salts are used directly as ligands. Romanenko et al. demonstrated the conversion of triaminoguanidinium chloride with $CuCl_2$ forming the first coordination compound $[Cu(TAG)Cl_3]Cl \cdot H_2O$ based on ionic *TAG*Cl [8]. Earlier research described Ni(II)-coordination compounds from neutral *TAG* [9]. However, all these products are unstable in both air and water because of the reducing character of the unsubstituted triaminoguanidinium salts. Therefore, protection groups have to be introduced. The terminal amine groups can easily be functionalized by condensation with aldehydes and ketones, which was already shown by Stollé in 1904 [1]. Furthermore, an enhancement of the chelating properties of the system is possible by adding additional donor atoms by the condensation with salicylaldehyde derivatives (Fig. 2).

Thus, tris-chelating ligands with a threefold symmetry are accessible. These are able to bind three metal centers with close metal–metal contacts.

Further substituents which influence the properties of the ligands can also be introduced. In this way, ligands with enhanced solubility or increased steric demand can be prepared, and building blocks with desired properties for further applications can be designed.

Regarding the crystal structures of $[H_6L]Cl$ [10] and $[H_6Br_3L]Cl$ [11] (Fig. 3), it is noticeable that the ligands can undergo conformational changes. Due to the possible rotation around the C_{imine}–$C_{1,phenyl}$ single bond, the position of the OH-substituent may be *syn* or *anti* with respect to the C=N-imine unit. Thus, four different isomeric forms are conceivable (*sss*, *ssa*, *saa*, *aaa*). In the case of $[H_6Br_3L]Cl$, the ligand exhibits the symmetric *aaa*-conformation because the hydroxyl groups form hydrogen bonds to the chloride ion. $[H_6L]Cl$, on the other hand, is present in an *saa*-conformation in solid state. Thus, intermolecular hydrogen bonding between the hydroxyl group and a polar solvent or the anion leads to the *anti*-conformation, whereas intramolecular bonding between the hydroxyl group and the imine leads to a stabilization of the *syn*-conformation. Metal binding is much stronger in the *sss*-conformation, and the undesired *aaa*-conformation in polar solvents can be inverted to *sss* by the addition of a base, which was proven by multidimensional NMR studies [11].

In addition to the utilization as ligand for metal binding, salicylaldehyde-derived *TAG* salts can also be used for the formation of two-dimensional, porous molecular networks by self-assembly on solid surfaces [12]. The introduction of a charged, trigonal core at solid surfaces results in additional bonding sites for other ions or molecules. With the coordination of metal ions, the construction of 2D metal arrays,

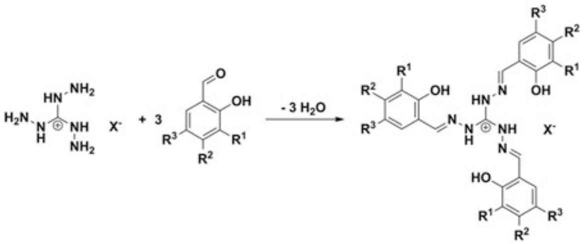

Fig. 2 Formation of the C_3-symmetric ligand $[H_6R^1{}_3R^2{}_3R^3{}_3L]X$ from *TAG*X and salicylaldehyde

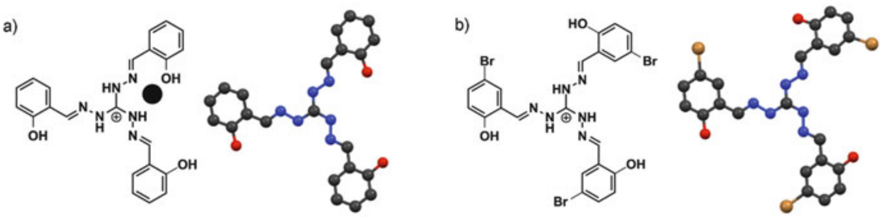

Fig. 3 (**a**) Crystal structure of $[H_6L]Cl$. *Black circle* shows a tris-chelating coordination pocket. (**b**) Crystal structure of $[H_6Br_3L]Cl$. Solvent molecules and anions are omitted for clarity

which may serve as tailor-made catalysts, would become possible. For the assembly on solid surfaces, long alkyl chains were attached to the phenyl groups because van der Waals interactions between interdigitated alkyl chains with adjacent molecules efficiently promote self-assembly. It could be observed that two different networks, a porous honeycomb and a nonporous linear network, are formed (Fig. 4). The type of network is dependent on the concentration of the ligand and on the length and number of the alkyl chains.

While the inherent lability of the imine bond is advantageous for self-assembly in supramolecular chemistry, it may also lead to decomposition or side reactions. To prevent potential decompositions, the reduction of the imine bond is necessary. This can be achieved by catalytic reduction with molecular hydrogen (Fig. 5a) [13].

Another method to reduce *TAG*X-derived ligands was described by Maas et al. [14]. While the reduction of tris(2-phenylpropyl-1-iminyl)guanidinium chloride was not possible by catalytic hydrogenation, the reaction with dimethylaminoborane (DMAB) and *p*-toluenesulfonic acid (*p*TsOH) according to Casarini et al. [15] yielded the reduced tris(2-phenylpropyl-1-amino)guanidinium tosylate (Fig. 5b). Maas used this reduced species for an *N*-carbamoylation with aryl isocyanates. The reaction with *p*-toluenesulfonyl isocyanate led to an *N-mono*-sulfonylcarbamoylation, and the reaction with aryl isothiocyanates led to the formation of triazoles. These examples show the diversity of secondary products derived from 1,2,3-tris(alkylamino)guanidinium salts using heterocumulenes as reagents. Compared to the imino-ligands mentioned before, the conformational flexibility of the reduced ligands is considerably enhanced. Solid-state structures

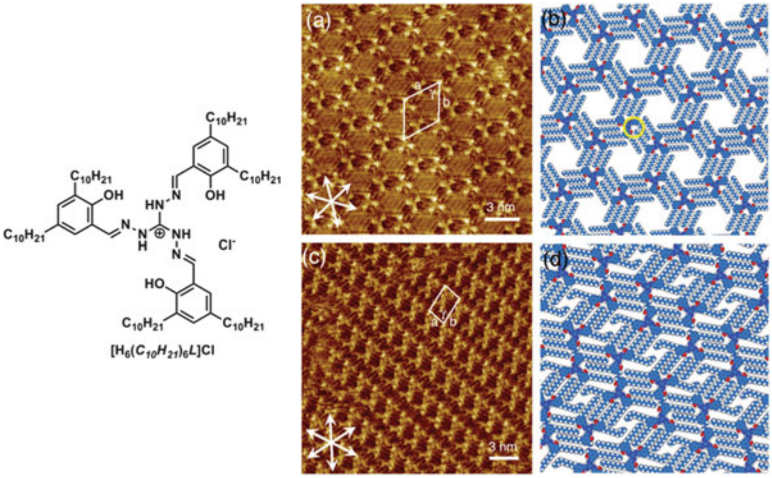

Fig. 4 Chemical structure of $[H_6(C_{10}H_{21})_6L]Cl$. STM image and network model of $[H_6(C_{10}H_{21})_6L]Cl$. (**a**, **b**) 3×10^{-6} M, (**c**,**d**) 1×10^{-3} M)

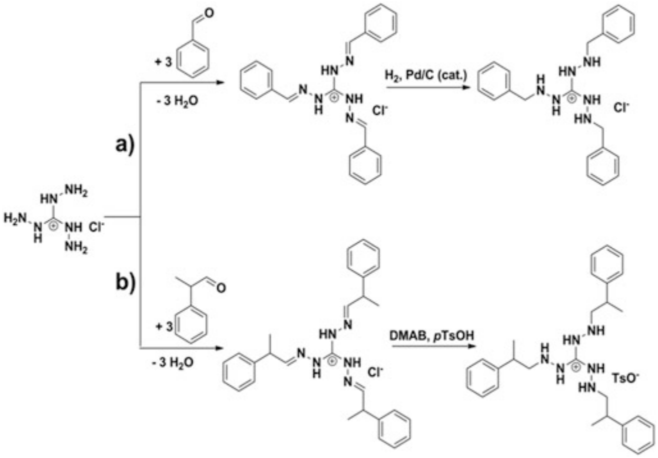

Fig. 5 Reaction scheme for the preparation of (**a**) tris(benzyliminyl)guanidinium chloride and catalytic hydrogenation to tris(benzylamino)guanidinium chloride and (**b**) tris(2-phenylpropyl-1-iminyl)guanidinium chloride and reduction to tris(2-phenylpropyl-1-amino)guanidinium tosylate

show that the phenyl groups are oriented out of plane of the CN_6 unit, and asymmetric structures can therefore be observed. Nevertheless, these ligands are still symmetric on the NMR time scale. Using salicylaldehyde derivatives instead of benzaldehyde may lead to compounds with even stronger metal coordination properties due to the additional acidic NH group.

As shown above, *TAG*X can easily be functionalized via condensation. Additional to the presented salicylaldehyde or benzaldehyde derivatives, non-aromatic ketones like acetone can also be used [16]. Moreover, the aromatic systems may be expanded by using naphthalene aldehydes [17], and it may be altered electronically by the introduction of heteroatoms like nitrogen as in pyridine carbaldehydes [18]. All these examples show that the *TAG* system is very flexible and offers a lot of possibilities for variation with regard to the desired application.

2.1 Metal Coordination

Due to the chelating character of the three coordination sites in the C_3-symmetric *TAG* ligands, metals can be bound very strongly. Here, we will show some basic coordination compounds formed from salicylaldehyde-derived *TAG*X ligand systems and different metal ions. These compounds form the basis for the design of supramolecular structures.

In 2000, the first examples of this class of coordination compounds were reported by Robson et al. [10]. The reaction of $[H_6L]Cl$ with Zn(II) or Pd (II) chlorides in the presence of a base led to the compounds shown in Fig. 6.

In these complexes, the ligands are fully deprotonated and exhibit the *sss*-conformation. Every metal ion is coordinated by the ligand in a threefold manner, and additional co-ligands are bound to complete the coordination sphere. The complex possesses a chiral, propeller-like structure in which the CN_6 unit is still planar and the phenyl rings are twisted out of plane. In 2005, another coordination compound with Zn(II) was presented (Fig. 7) [19].

In this case, the ligand contains a methoxy group instead of an acidic hydroxyl group in the 2-position. $[H_3Me_3Br_3L]Cl$ and $ZnCl_2$ were reacted in the presence of a base to give the coordination compound $(Et_3NH)_2[(ZnCl_2)_3Me_3Br_3L]$. It can be seen that the ligand remains in the *aaa*-conformation, and the methoxy group does not participate in the coordination. The Zn(II) center is coordinated tetrahedrally by the ligand and two chloride co-ligands. This example demonstrates that even in the *aaa*-conformation the ligand is able to bind metal ions.

Using copper(II) as a metal ion, different observations were made. If sterically demanding co-ligands like sodium 5,5-diethylbarbiturate (NaH*bar*) are employed, basic coordination compounds can be achieved (Fig. 8) [11].

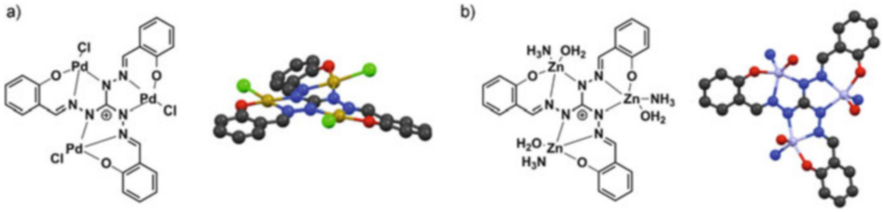

Fig. 6 (**a**) Crystal structure of the $[(PdCl)_3L]^{2-}$ ion. (**b**) Crystal structure of the $[(Zn(H_2O)(NH_3))_3L]^+$ ion

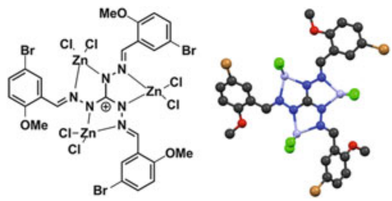

Fig. 7 Crystal structure of the $[(ZnCl_2)_3Me_3Br_3L]^{2+}$ ion

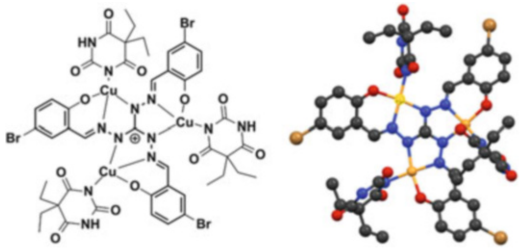

Fig. 8 Crystal structure of the $[(CuHbar)_3Br_3L]^{2-}$ ion

Again, a base was present and therefore the ligand is fully deprotonated. Every coordination site is occupied by a metal ion. The ligand adopts the common propeller-like twisting of the phenyl group, while the CN_6 unit remains planar. The coordination sphere of the Cu(II) centers is completed by partially deprotonated diethylbarbiturate anions. The distortion of the ligand is stronger as compared to the systems presented before. This shows the ligand's high degree of flexibility for further uses as predesigned building block for supramolecular cages and coordination polymers. Indeed, Plass et al. could show that the same system of $CuCl_2$ and $[H_6L]Cl$ without sterically demanding co-ligands builds up a coordination polymer consisting of two interpenetrating (10,3)-a nets with opposite chirality (Fig. 9a) [21]. The ligands are fully deprotonated and every coordination site is occupied by one metal ion. By variation of the phenyl rings through the attachment of additional OH groups at the 5-position, a porous (10,3)-a net with channels filled with solvent molecules could be obtained (Fig. 9b) [22].

Given the spatial proximity of the metal ions in all coordination compounds of about 500 pm, Plass became interested in their magnetic behavior [20]. Indeed, the porous network showed strong antiferromagnetic coupling. To observe the exchange coupling of paramagnetic Ni(II)-ions bound to the ligand, Plass reacted $[H_6Br_3L]Cl$ and Ni(II)-salts in the presence of a base and an additional sterically demanding co-ligand like 2,4,6-tris(2-pyridyl)-1,3,5-triazine and 2,2′-bipyridine [23]. Thus, the system was prevented from building coordination polymers and monomeric coordination compounds could be obtained. Magnetic measurements showed strong antiferromagnetic interactions between the metal ions, but due to the C_3-symmetry of the system, a nonmagnetic ground state was observed.

All the examples shown before are predicated on the presence of a base to enforce the *sss*-conformation and to facilitate the metal coordination. To investigate what happens if the ligand is converted with a basic metal salt without any additional base, $[H_6Br_3L]Cl$ was reacted directly with $(NH_4)_6[Mo_7O_{24}]$.

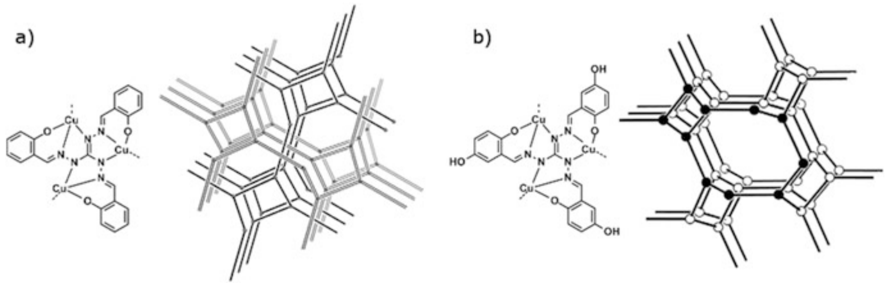

Fig. 9 (**a**) Schematic presentation of the $[Cu_3L]^+$ building block and topology of the two interpenetrated (10,3)-a nets. (**b**) $[Cu_3(OH)_3L]^+$ building block and topology of the porous framework with one of the ten-membered rings highlighted (nodes represent the central carbon atom of the triaminoguanidine ligands) [20]

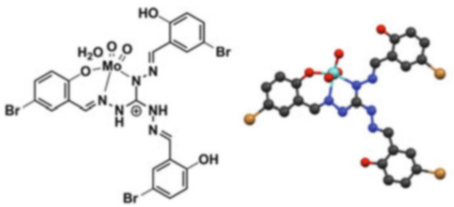

Fig. 10 Crystal structure of the asymmetric unit of $[MoO_2(H_2O)_2(H_3\mathit{Br}_3L)] \cdot 2DMF$

Figure 10 shows that in the resulting complex only one coordination pocket is occupied and the ligand is only partially deprotonated. The overall conformation is *ssa* and the *anti*-conformation is stabilized by a hydrogen bond to a DMF molecule. This proves that it is possible to coordinate metal ions even in the absence of strongly basic conditions, yet the resulting structures can no longer be reliably predicted anymore. To generate supramolecular structures with a defined shape, however, a predictable coordination behavior of the ligand is indispensable, while its flexibility must also not be disregarded. Thus, *TAG*-derived ligands are excellent building blocks for supramolecular architectures due to their well-known as well as tunable coordination behavior.

2.2 Triazole Formation

Using NaH*bar* as a co-ligand for the coordination of Pd(II) to $[H_6L]Cl$, the formation of a 1,2,4-triazole could be observed [24]. This oxidative cyclization of a triaminoguanidinium-based ligand was already found in 2000 [10] resulting in a part of a huge donut-shaped coordination oligomer (see Fig. 28). The crystal structures of an Eu(III) and an isostructural Gd(III) tetramer exhibited the same structural unit consisting of two different triazole backbones (Fig. 11).

To investigate the triazole formation, model compounds were synthesized [25]. $[H_6\mathit{Br}_3L]Cl$ was reacted with Pd(II) salts and phosphine-based co-ligands

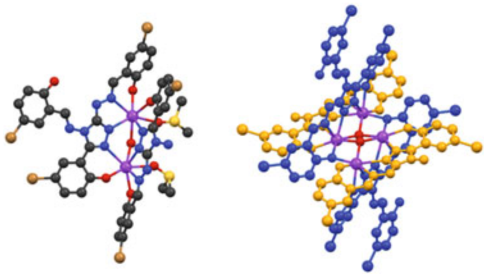

Fig. 11 Asymmetric unit and visualization of different triazole backbones in entire coordination of a Eu(III)-triazole tetramer

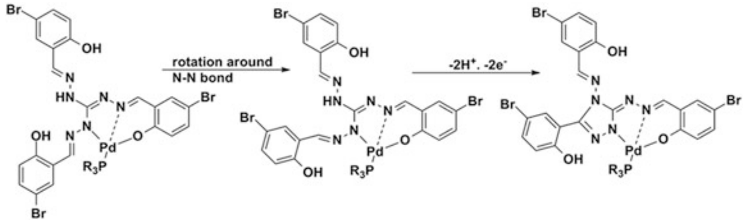

Fig. 12 Triazole formation from [(Pd(PR$_3$)H$_3$*Br*$_3$*L*] to [(Pd(PR$_3$)H*Br*$_3$*L*′]

(PPh$_3$, PEt$_3$). A basic coordination compound [(Pd(PEt$_3$)H$_3$*Br*$_3$*L*] was formed under inert conditions. After that, H_2O_2 was added stoichiometrically to allow a time-resolved monitoring of the oxidation. By means of NMR studies and single crystal diffraction, it could be demonstrated that the steric demand of the co-ligand leads to a rotation of the aromatic unit, followed by a nucleophilic attack on the imine carbon atom resulting in a proton and electron elimination and the triazole formation (Fig. 12).

Because the oxidation is also driven by oxygen from air and the ligand and triazole can easily be differentiated by ^{1}H-NMR, this reaction is a well-suitable exercise for undergraduate students to prove their skills in working under inert conditions [26].

3 Supramolecular Coordination Compounds

The following chapters will give an overview of the application of *TAG*X-based ligands in supramolecular chemistry. The focus will be on the coordination of metal ions to construct large structures from scratch.

Supramolecular coordination compounds can be differentiated into polymeric structures or discrete coordination compounds. Coordination polymers built from the Cu(II)/[H$_6$*L*]Cl system have been discussed earlier (Fig. 9).

3.1 Layered Coordination Structures

Since ligands derived from *TAG* salts and salicylaldehydes are flat with a slightly propeller-like twisting of the phenyl rings, metals can be coordinated in a tris-chelating manner (see Fig. 6). The coordinated metal ions can be linked by additional molecules to build up layered structures. For instance, a bilayer of $\{\{Zn(NH_3)\}_3Br_3L\}_2$ is stabilized by bridging OH^- groups (Fig. 13) [19].

Here, the triangular units exhibit an orientation opposite to each other. In this way, close contacts between neighboring bromine atoms are avoided. The Zn (II) ions are trigonal bipyramidally coordinated. An analogous structure is observed when pyridine carbaldehyde is used instead of 5-bromosalicylaldehyde. In that structure, the bilayered zinc compound is bridged by chlorine ligands [18].

The construction of supramolecular structures is often highly sensitive towards a change of solvent, anion, and reaction conditions. Thus, the dimeric structure of the compound shown in Fig. 13 is not observed when the same reaction mixture is crystallized from a different solvent. The observed structure exhibits two ligands that are orthogonally twisted and a central zinc ion that is octahedrally coordinated by two binding pockets (Fig. 14).

A triple-layered compound $[\{\{Ga(OH)_2\}_3Br_6L\}\{\{Ga(acac)\}_3Br_6L\}_2]$ can be obtained under solvato-thermal conditions at 120°C from $[H_6Br_6L]Cl$, gallium acetylacetonate, and triethylamine in acetonitrile (Fig. 15) [27].

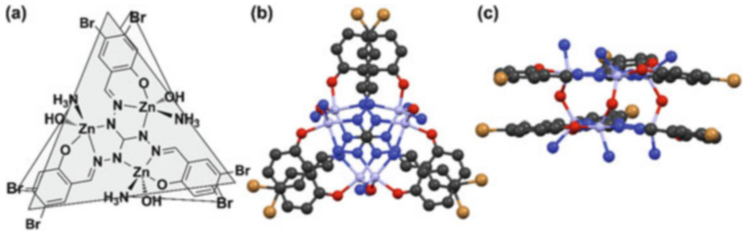

Fig. 13 $(NH_4)[\{\{Zn(NH_3)\}_3Br_3L\}_2\{\mu\text{-}(OH)_3\}_3]$ (**a**) schematic drawing, (**b**) crystal structure in the same orientation, and (**c**) side view

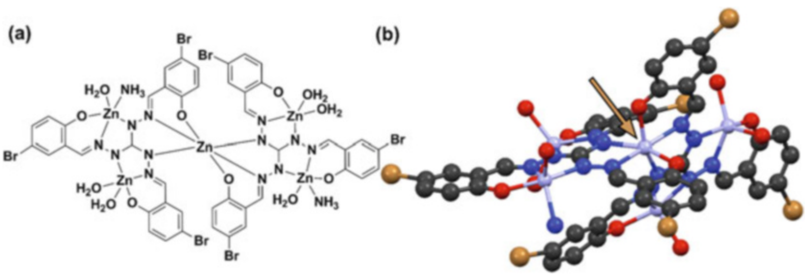

Fig. 14 (**a**) Schematic representation of $[Zn\{Zn_2(OH_2)_3(NH_3)Br_3L\}_2]$; (**b**) an *arrow* indicates the central zinc ion in the asymmetric unit

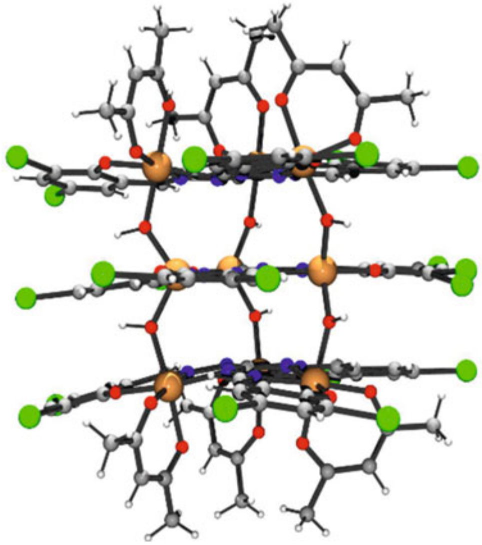

Fig. 15 Asymmetric unit of $[\{\{Ga(\mu\text{-}OH)_2\}_3 Br_6L\}\{\{Ga(acac)Br_6L\}_2]$

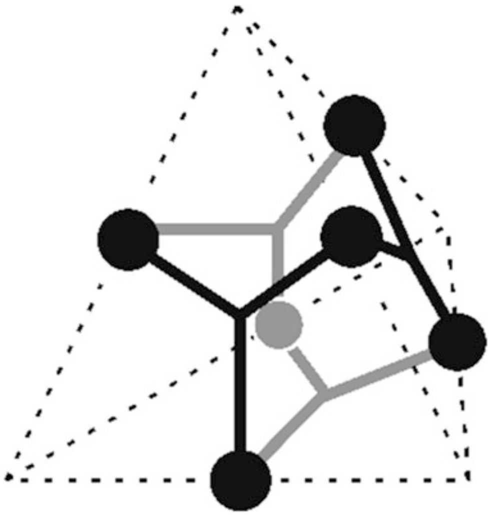

Fig. 16 Truncated or adamantanoid tetrahedron constructed by six metal ions and four C_3-symmetric *TAG*-based ligands

Three layers of the ligand are arranged in parallel with alternating orientation. The outer ligands are slightly bent. All nine binding pockets are occupied by Ga(III) ions, which are connected by bridging OH^- groups as already shown in Fig. 13.

3.2 Tetrahedral Structures

Supramolecular structures in which the ligands form a tetrahedral cage are also accessible by using *TAG*X-based ligands (Fig. 16). The aromatic substituents of the

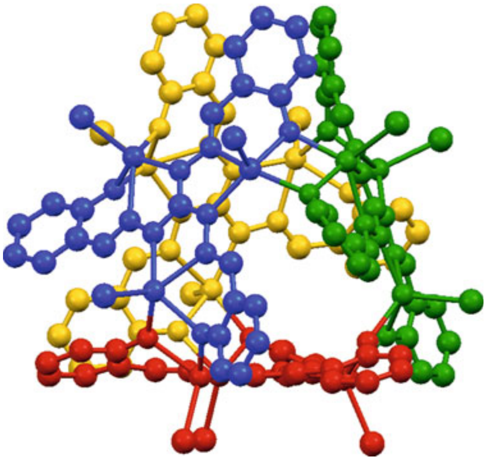

Fig. 17 $[Et_4N]_8[\{(CdCl)_3L\}_4]$, visualization of the faces of the tetrahedral structure. Counterions and solvent molecules are omitted for clarity

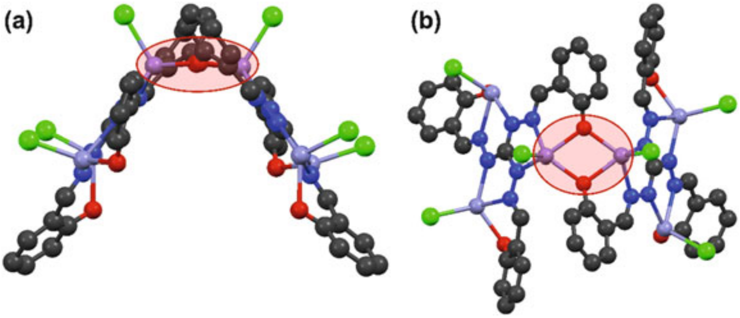

Fig. 18 Edge of the tetrahedral coordination compound $[Et_4N]_8[\{(CdCl)_3L\}_4]$ in (**a**) side and (**b**) frontal view. Bridging $(CdO)_2$ units are *highlighted*

ligands force a linkage at the edges of the tetrahedral structure which therefore form a truncated or adamantanoid tetrahedron.

The porosity of the discrete cage can be influenced by the functionalization of the aromatic rings. Thus, guest molecules are able to interact with the cavity of the host and may serve as a template for the desired structure. $[H_6L]Cl$ is one of the simplest *TAG*-based ligands in coordination chemistry. The group of Robson [28] was able to create a supramolecular tetrahedral coordination compound by the reaction of $[H_6L]Cl$ with stoichiometric quantities of cadmium(II) chloride in the presence of tetraethylammonium hydroxide (Fig. 17).

This coordination cage is an octa-anion with one tetraethylammonium ion inside the cavity which was proven by ^{1}H-NMR and ^{13}C-MAS NMR spectroscopy. A different set of signals for internal and external Et_4N^+ ions was detected. Within this cage, $(CdO)_2$ units build the edges of the tetrahedron. "O" stands for the deprotonated hydroxyl group of the aromatic rings (Fig. 18).

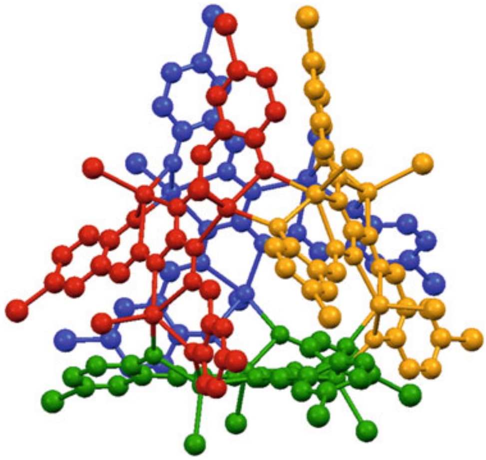

Fig. 19 $(Et_4N)_5(Et_3NH)_3$ $[\{(CdCl)_3\mathit{Br}_3L\}_4]$, visualization of the faces of the tetrahedral structure. Counterions and solvent molecules are omitted for clarity

Furthermore, Robson's group was able to isolate a similar tetrahedral coordination compound in which the coordination sphere of cadmium is completed by bromine and the cavity is filled with Me_4N^+ ions [28].

Another ligand is produced by the reaction of 5-bromosalicylaldehyde with *TAG* salts [29]. The emerged ligand $[H_6\mathit{Br}_3L]Cl$ is reacted with cadmium(II) chloride and Et_4NCl as a cationic template in the presence of triethylamine and yields a similar tetrahedral coordination cage (Fig. 19).

In addition, the tetrahedral structure can also be obtained even without the use of a tetrahedral template like NEt_4^+. $HNEt_3^+$ is also able to fill the cavity together with one molecule of water. The resulting cage structure can be verified in solid state, in solution, and also in the gas phase. NMR spectroscopy shows different $HNEt_3^+$ species, inside and outside the cavity. ESI mass spectrometry shows the tetrahedral cage with one $HNEt_3^+$ ion and one water molecule encapsulated [29].

3.3 Double-Walled Tetrahedral Structures

For the construction of tetrahedral coordination cages, an exact match of the ligands with the steric requirements of the metal centers is necessary. Zinc(II) ions exhibit a smaller diameter as compared to cadmium(II) and palladium(II) ions. This would force the faces of a theoretical tetrahedral coordination structure to come in close contact, which is sterically unfavorable. Since zinc(II) ions are situated up to 0.87 Å above the planar CN_6 unit (Fig. 13), they can form a $(ZnO)_2$ bridging edge. By utilizing an equimolar mixture of the two ligands $[H_6\mathit{Br}_3L]^+$ and $[H_6\mathit{Br}_6\mathit{(OMe)}_3L]^+$ (Fig. 20), the formation of a double-walled tetrahedral structure (Fig. 21) in which the layers are linked by methanolate ions can be achieved [30].

Fig. 20 Ligands used in the preparation of a double-walled tetrahedron

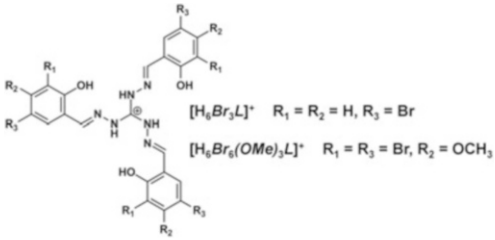

Fig. 21 Double-walled tetrahedral cage

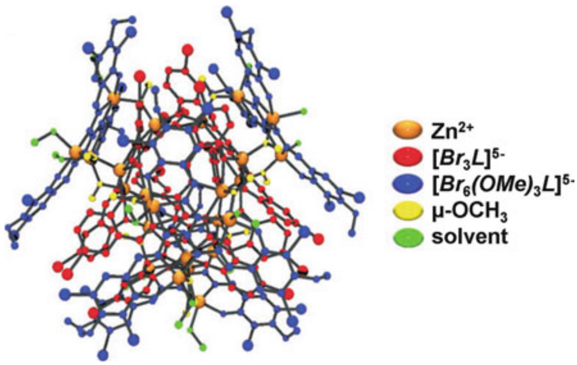

From Fig. 21 it can be seen that the double-walled tetrahedron exhibits nearly closed corners. The sterically more demanding ligand $[Br_6(OMe)_3L]^{5-}$ occupies the outer shell of the tetrahedral coordination cage. The four negative charges of this compound are compensated by four $HNEt_3^+$ ions, of which one is located inside the cage.

3.4 Octahedral Structures

Octahedral coordination cages are accessible by using an approach similar to the construction of tetrahedral structures (Fig. 22).

The dihedral angles at the edges of octahedral coordination cages are larger in comparison with tetrahedral structures. Therefore, the binding angle of the bridging element needs to be customized by a suitable twofold bridging ligand such as sodium 5,5-diethylbarbiturate (NaH*bar*, Fig. 23a) [24].

Thus, when $[H_6L]Cl$ is reacted with palladium(II) chloride and NaH*bar* in aqueous acetonitrile solution in the presence of NEt_3, an octahedral coordination compound is formed. The resulting large cavity is occupied by four sodium ions and approximately twenty water molecules (Fig. 23b).

Even though the aromatic rings of the ligands are tilted out of the face planes to avoid close H–H contacts, the corners of the octahedral structure are tightly closed.

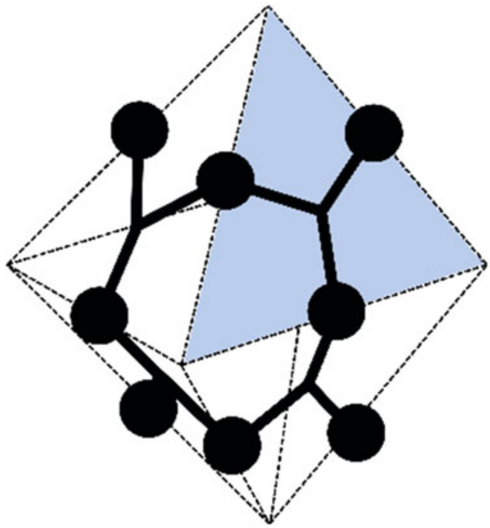

Fig. 22 Schematic representation of an octahedral coordination cage

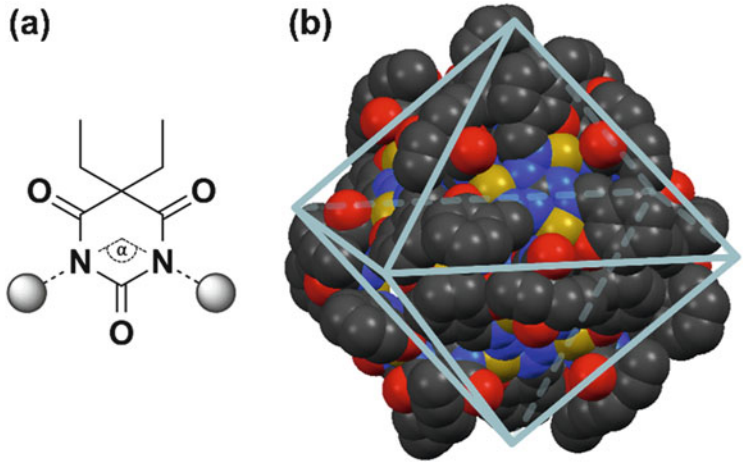

Fig. 23 (**a**) *bar*$^{2-}$, bridging angle $\alpha = 108–117°$, (**b**) schematic drawing of the octahedral coordination compound

3.5 Trigonal Bipyramidal Structures

The construction of trigonal bipyramidal structures by using *TAG*-derived ligands follows the same design concept needed for the construction of octahedral structures. Ligands occupy the faces of the trigonal bipyramid, and twofold bridging units are used to connect at the edges (Fig. 24).

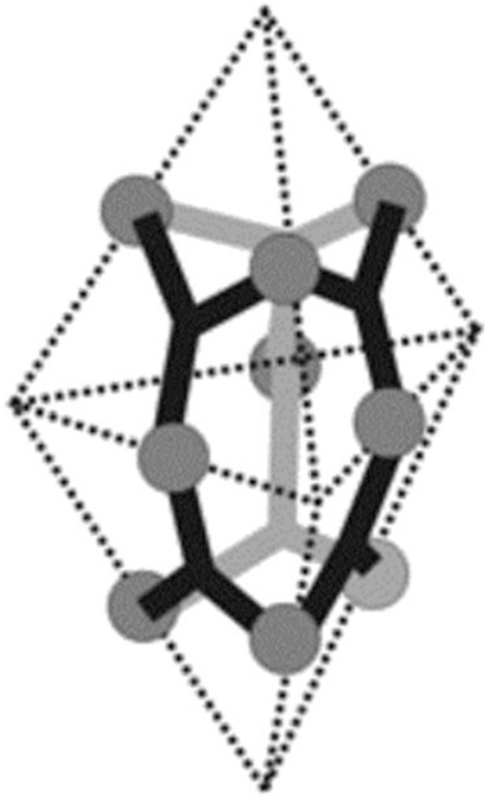

Fig. 24 Schematic drawing of a trigonal bipyramidal structure

To force a system into a trigonal bipyramidal structure, it is necessary to increase the steric demand at the corners of the polygon by the right choice of ligand. The equatorial angles at the corners of a trigonal bipyramid are small (60°); thus, the atoms tend to avoid each other. This effect can further be increased by modifying the aromatic substituents with large groups such as the bromine atoms in $[H_6Br_3L]^+$. Accordingly, the reaction of palladium(II) chloride, $[H_6Br_3L]Cl$, NaH*bar*, and NEt_4Cl in the presence of NEt_3 leads to the formation of a trigonal bipyramidal structure. The cavity is occupied by four Et_3NH^+ ions and one Et_4N^+ ion (Fig. 25).

From Fig. 25 it can be seen that the aromatic rings of the ligands are slightly tilted due to the steric demand of the bromine substituents. bar^{2-} is bridging two palladium(II) ions and the ethyl groups are pointing outwards.

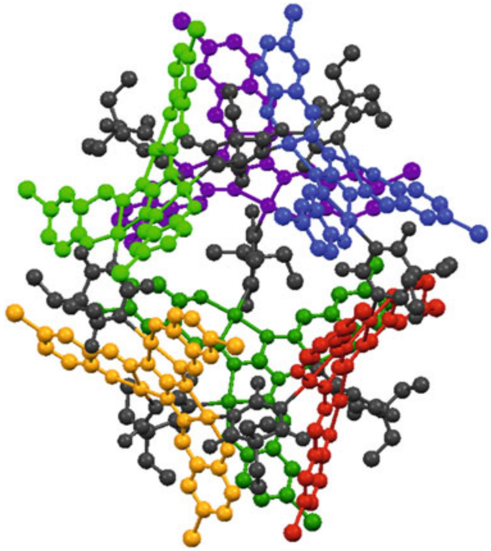

Fig. 25 Visualization of the faces of the trigonal bipyramidal structure, *bar*$^{2-}$ highlighted *black*. Counterions and solvent molecules are omitted for clarity

3.6 Irregularly Shaped Coordination Compounds

3.6.1 A Box-Shaped Coordination Compound

In the complex $[Co(en)_3]Br_3$, Co(III) is octahedrally coordinated. It can potentially be used as a template for the construction of an octahedral supramolecular compound. With $[H_6L]Cl$ and Pd(II), a box-shaped coordination compound is formed. Each ligand molecule binds two palladium(II) ions and one cobalt(III) ion (Fig. 26) [24].

The Co(III) ions are coordinated octahedrally by two ligands. Two Pd(II) ions are connected by bridging *bar*$^{2-}$ ligands. The remaining two Pd(II) ions complete their coordination sphere with one chloride anion each.

3.6.2 A Donut-Shaped Coordination Compound with Cd

Although ligand H_5L remains intact during the formation of trimetallic complexes (Fig. 6), it is able to undergo an cycloisomerization to form a triazole in the presence of Cd(II) ions and low quantities of triethylamine. Furthermore, the reduction of one imine bond to the corresponding secondary amine is observed (H_5L', Fig. 27) [10].

This structural motive is part of a coordination oligomer shown in Fig. 28. The donut-shaped coordination oligomer exhibits a molecular weight of over 10,000 g mol^{-1} and a diameter of 30 Å. The oligomer contains 24 Cd(II) centers, 12 H_2L^{3-} , and 6 $H_2L'^{3-}$ ligands in total.

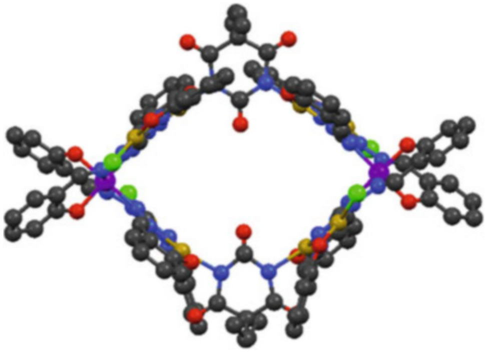

Fig. 26 Box-shaped coordination compound $(Et_4N)_6[\{Co\{(PdCl)(Pd)L\}_2(\mu\text{-}bar)\}_2]$

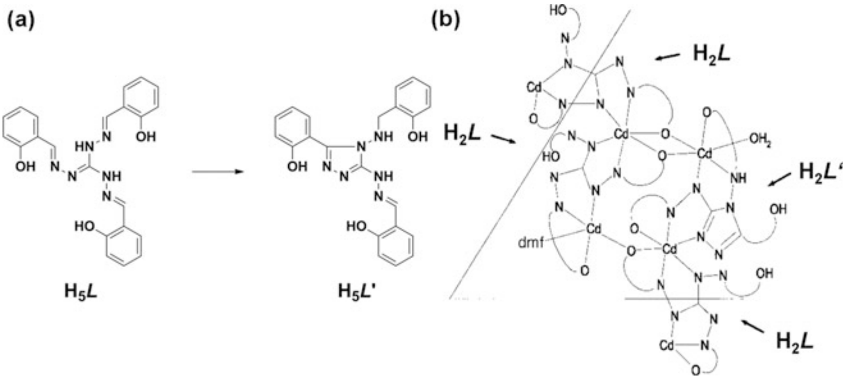

Fig. 27 (**a**) Triazole formation of H_5L to H_5L'; (**b**) schematic representation of a donut segment

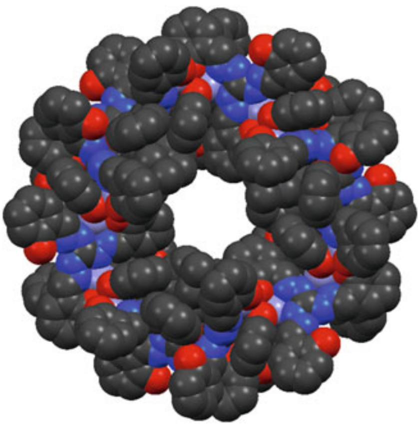

Fig. 28 Donut-shaped coordination oligomer

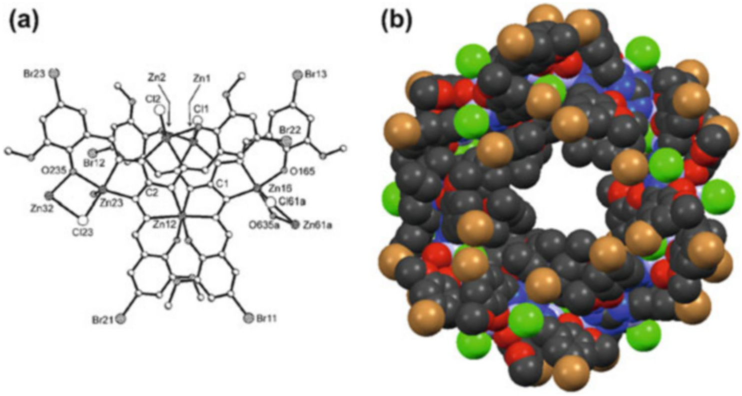

Fig. 29 (**a**) Dimeric building block; (**b**) donut-shaped coordination oligomer

3.6.3 A Donut-Shaped Coordination Compound with Zn

The reaction of $[H_6(OMe)_3Br_3L]Cl$ and zinc(II) chloride in the presence of triethylamine leads to the formation of a protein-sized ($d = 32$ Å), donut-shaped coordination compound (Fig. 29b) [19].

The coordination oligomer consists of six dimeric building blocks shown in Fig. 29a. In total, the structure contains 30 Zn(II) ions, 12 ligands, and 18 chloride ligands leading to an overall charge of −18, which is compensated by $HNEt_3^+$ ions. The donut-shaped coordination oligomer exhibits a higher symmetry as compared to the oligomer in Fig. 28. This ligand does not undergo triazole formation under the reaction conditions. The coordination compound has a sufficiently high solubility for ^{1}H-NMR spectroscopy. The obtained spectrum proves that the coordination compound is also stable in solution.

4 Conclusion

Triaminoguanidinium salts are the basis for miscellaneous multidentate ligands. As three metal centers can be bound strongly in a chelating manner, these ligands can be used in supramolecular coordination chemistry. A large variety of supramolecular coordination compounds, both desired and unexpected, have already been obtained. Given the structural diversity and complexity of these already known compounds, *TAG*X-based complexes will certainly offer a lot of exciting opportunities for further applications in the future.

References

1. Stollé R (1904) Ber Dtsch Chem Ges 37:3548–3549
2. Potts KT, Hirsch CA (1968) J Org Chem 33:143–150
3. Cardillo P, Dellavedova M, Gigante L, Lunghi A, Pasturenzi C, Salatelli E, Zanirato P (2012) Eur J Org Chem 2012:1195–1201
4. Fischer N, Klapötke TM, Stierstorfer J (2011) Eur J Inorg Chem 2011:4471–4480
5. Klapötke TM, Martin FA, Stierstorfer J (2011) Angew Chem Int Ed 50:4227–4229
6. Gao H, Wang R, Twamley B, Hiskey MA, Shreeve JM (2006) Chem Commun 4007–4009
7. Scott FL (1957) Angew Chem 69:506
8. Savel'eva ZA, Romanenko GV, Sheludyakova LA, Larionov SV (2000) Polyhedron 19:1737–1740
9. Jensen KA, Nygaard B (1994) Acta Chem Scand 3:481–486
10. Müller IM, Robson R (2000) Angew Chem Int Ed 39:4357–4359
11. Müller IM, Möller D (2005) Eur J Inorg Chem 2005:257–263
12. Tahara K, Abraham ML, Igawa K, Katayama K, Oppel IM, Tobe Y (2014) Chem Commun 50:7683–7685
13. Bucher N, Szabo J, Oppel IM, Maas G (2012) Z Naturforsch 67b:631–642
14. Szabo J, Karger K, Bucher N, Maas G (2014) Beilstein J Org Chem 10:2255–2262
15. Casarini ME, Ghelfi F, Libertini E, Pagnoni UM, Parsons AF (2002) Tetrahedron 58:7925–7932
16. Szabo J, Maas G (2013) Z Naturforsch 68b:207–213
17. Chaudhari AK, Sharma A, Mukherjee S, Joarder B, Ghosh SK (2014) Cryst Eng Commun 16:4691–4695
18. Zhou Y, Li Z-X, Zang S-Q, Zhu Y-Y, Zhang H-Y, Hou H-W, Mak TCW (2012) Org Lett 14:1214–1217
19. Müller IM, Möller D, Föcker K (2005) Chem Eur J 11:3318–3324
20. Plass W (2009) Coord Chem Rev 253:2286–2295
21. Zharkouskaya A, Görls H, Vaughan G, Plass W (2005) Inorg Chem Commun 8:1145–1148
22. Zharkouskaya A, Buchholz A, Plass W (2005) Eur J Inorg Chem 2005:4875–4879
23. Ion AE, Spielberg ET, Görls H, Plass W (2007) Inorg Chim Acta 360:3925–3931
24. Müller IM, Spillmann S, Franck H, Pietschnig R (2004) Chem Eur J 10:2207–2213
25. Abraham ML, Schulze AC, Korthaus A, Oppel IM (2013) Dalton Trans 42:16066–16072
26. Abraham ML, Oppel IM (2014) J Chem Educ 91:2174–2177
27. Föcker K (2008) PhD thesis, Ruhr-Universität Bochum
28. Müller IM, Robson R, Separovic F (2001) Angew Chem Int Ed 40:4385–4386
29. Müller IM, Möller D, Schalley CA (2005) Angew Chem Int Ed 44:480–484
30. Oppel IM, Föcker K (2008) Angew Chem Int Ed 47:402–405

Top Heterocycl Chem (2017) 51: 95–164
DOI: 10.1007/7081_2015_173

Published online: 3 October 2015

Guanidine Metal Complexes for Bioinorganic Chemistry and Polymerisation Catalysis

Julia Stanek, Thomas Rösener, Angela Metz, Johannes Mannsperger, Alexander Hoffmann, and Sonja Herres-Pawlis

Abstract Guanidines are highly useful ligands which have conquered coordination chemistry within the last 20 years. Their CN_3 moiety allows multiple substitution patterns which enables tailoring them to a large variety of applications, ranging from bioinorganic coordination chemistry via medicinal chemistry to polymerisation catalysis. In bioinorganic chemistry, guanidines gave important stimuli in the modelling of copper type 1, 2 and 3 enzymes. This review provides with a comprehensive overview on complexes which have been reported with neutral guanidine ligands. Peralkylated guanidines as well as bicyclic or more complex guanidine-comprising entities are described in their coordination chemistry with transition and main-group metals. The structural features of the complexes as well as their most prominent features in bioinorganic chemistry or polymerisation catalysis are highlighted. Hereby, the role of the delocalisation of the positive charge within the guanidine unit gained during coordination is discussed in its importance for efficient and robust coordination. The delocalisation within the CN_3 unit can be measured by the structural value ρ which is discussed for numerous systems. The charge delocalisation makes neutral guanidines versatile and efficient for the stabilisation of highly different coordination modes and a large variety of oxidation states.

Keywords Atom transfer radical polymerisation · Copper enzyme models · Electron transfer · Lactide polymerisation

J. Stanek, A. Metz, and J. Mannsperger
Department Chemie, Ludwig-Maximilians-Universität München, Butenandtstr. 5-13, 81377 Munich, Germany

T. Rösener, A. Hoffmann, and S. Herres-Pawlis (✉)
Lehrstuhl für Bioanorganische Chemie, Rheinisch-Westfälische Technische Hochschule Aachen University, Institut für Anorganische Chemie, Landoltweg 1, 52074 Aachen, Germany
e-mail: sonja.herres-pawlis@ac.rwth-aachen.de

Contents

Abbreviations

ATRP	Atom transfer radical polymerisation
DβM	Dopamine β-monooxygenase
Fc*	Decamethylferrocene
LMCT	Ligand to metal charge transfer
MLCT	Metal to ligand charge transfer
PD	Polydispersity
PhIO	Iodosylbenzene
^{s}PhIO	2-(*tert*-butylsulfonyl)-iodosylbenzene
PHM	Peptidylglycine α-hydroxylating monooxygenase
ROP	Ring-opening polymerisation
TEMPO	2,2,6,6-Tetramethylpiperidyl-1-oxyl
XAS	X-ray absorption spectroscopy

1 Introduction

Within the last 15 years, the coordination chemistry of neutral guanidines enjoyed a rapid expansion. Guanidine transition metal complexes have been applied in diverse fields of bioinorganic chemistry as well as polymerisation catalysis. The N_{imine} donor function resembles the δ-imine donor function of histidine which makes them highly valuable for the synthesis of bioinorganic copper complexes mimicking type 2 and type 3 copper proteins [1].

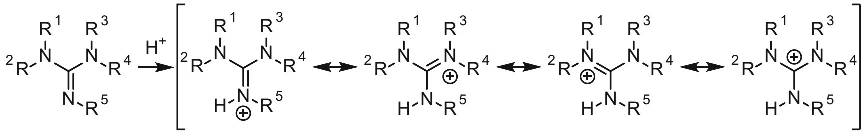

Scheme 1 Stabilisation of a positive charge through delocalisation in a guanidine

The chemistry of the neutral guanidines is very different from that of the formally related guanidinate anions which have already been known for a rich variety of coordination modes and excellent donor properties since the 1960s [2–4]. A special class of guanidinates are the imidazolin-2-iminato ligands which have been established as powerful ancillary ligands in catalysis [5]. Guanidines have found widespread use in coordination and organic chemistry, as pharmaceuticals, sweeteners, catalysts, etc., and a multitude of synthetic approaches has been reported [6, 7].

The electron-rich guanidines and guanidinates owe their excellent donor properties to a good charge delocalisation within the Y-shaped CN_3 moiety (Scheme 1). This CN_3 moiety shows a special delocalisation behaviour of the 6 π-electrons which has been discussed as Y-aromaticity [8]. This resonance stabilisation is a major reason for the high basicity of guanidines (pK_{BH+} of [H–NMe–C(NMe$_2$)$_2$] in MeCN: 25.00) [9, 10]. Due to their strong donation properties, guanidines are capable of forming stable complexes with many metals in various oxidation states.

For the description of the degree of delocalisation within the guanidine moiety, Sundermeyer et al. introduced the ρ-value [11]. It describes the changes of the C–N bond lengths (elongation of the C=N double bond and shortening of the C–NR$_2$ bonds) within the guanidine unit. It is calculated by the formula $\rho = 2a/(b + c)$ with a as C=N bond length and b and c as C–NR$_2$ bond lengths. ρ equals to 1 for a C_3-symmetrical guanidine unit. In free guanidine ligands, ρ amounts to 0.92 [12], whereas in complexes, it is raised to 0.96 up to 1.04 (vide infra) due to the stabilisation of the metal charge. The guanidine moiety tries to maintain a high degree of planarity of all substituents for ideal delocalisation, but this is hindered by the steric interaction between the substituents. This steric hindrance twists the amine parts of the guanidine in a propeller-like fashion which decreases the delocalisation. It was observed that even in the unsubstituted guanidine HN=C(NH$_2$)$_2$, the NH_2 units are twisted slightly against each other [13, 14]. This effect is more pronounced in peralkylated systems [15].

This review focuses on the coordination chemistry of neutral guanidines containing a substituted RN=C(NR$_2$)$_2$ moiety because the coordination chemistry of this specific ligand class has been developed very successfully towards numerous applications in bioinorganic chemistry and catalysis. The wealth of guanidine-stabilised complexes has been classified into different groups depending on the number of guanidine units and further appended donor groups.

More exciting applications of guanidines as redox-active compounds in the stabilisation of diboranes and in supramolecular approaches are reviewed by Himmel and Oppel et al. in this book.

2 Guanidines for Bioinorganic Coordination Chemistry

Owing to their excellent donor properties, guanidines are capable to stabilise various transition metals in several oxidation states which renders them very valuable for bioinorganic chemistry. Guanidines can be categorised by the number of guanidine units or type of the coordinating atom of the non-guanidine function. Historically, the earliest studies in bioinorganic coordination chemistry focused on mono(guanidines), followed by a lively progress of bis- and tris(guanidines) and combinations of guanidines with other N and S donor functions. The following sections retrace this development from the very beginning.

Historically, the first acyclic guanidine adducts were reported in 1965 [16], when Longhi et al. presented a series of complexes of 1,1,3,3-tetramethylguanidine (TMG) at divalent transition metals. In the 1990s, Schmidbaur et al. used TMG as ancillary ligand for the stabilisation of gold complexes [17]. The substitution pattern of the CN_3 unit can easily be changed by various methods yielding, for example, the chiral pyrrolidine-1-carboximidamides [2, 18–21]. They possess good chelating properties explored in zinc and molybdenum chemistry by Anders et al. [19–21]. These early examples revealed the superior donor properties, but only the combination into poly(guanidines) paved the way to a broader use in coordination chemistry.

2.1 Bis(guanidines)

Bis(guanidine) ligands are composed of two guanidine functions which are connected by a backbone linker. The first bis(guanidine) was published in 2000 simultaneously by the groups of Pohl, Henkel and Sundermeyer [22–24]. 1,3-Bis(*N*,*N*,*N*′,*N*′-tetramethylguanidino)propane (btmgp, TMG_2p) is based on two tetramethylguanidine units bridged with a propylene linker. The groups synthesised the molecule using totally different synthetic routes. Henkel and Pohl et al. used the reaction of 1,3-dibromopropane with an excess of tetramethylguanidine (HN=C$(NMe_2)_2$ = TMG) for at least 12 h at 100–150°C (Scheme 2, right). Followed by distillation of the TMG excess, deprotonation with sodium ethoxide and purification by distillation, they obtained yields of 30–40%, whereas the Sundermeyer group used the synthetic approach of Kantlehner et al. [25]. Here, they used the reaction of tetramethylchloroformamidinium chloride with 1,3-propylenediamine in acetonitrile for several hours at reflux. After two deprotonation steps, the pure ligand was obtained with 95% yield (Scheme 2, left).

btmgp convinces with its favourable coordinative bite and especially its high N donor strength, which leads to a wide field of applications such as the stabilisation of biomimetic copper complexes [22, 26].

Besides the initially described btmgp, more propylene-bridged chelate guanidine ligands have been synthesised. The examples in Fig. 1 show different coordination

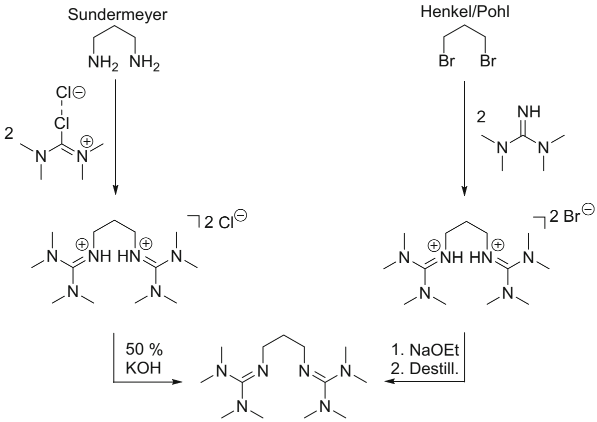

Scheme 2 Synthetic routes towards bis(tetramethylguanidino)propane (btmgp or TMG_2p)

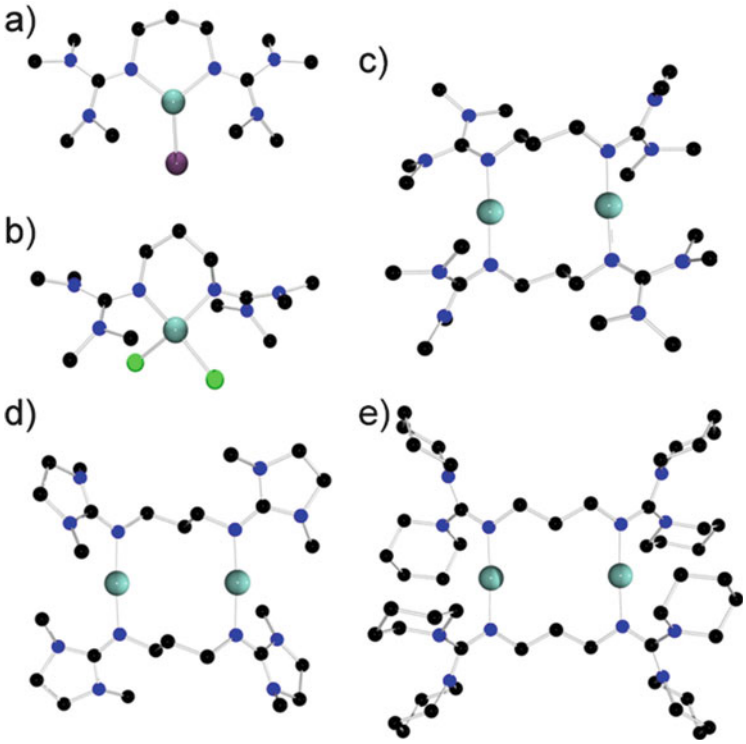

Fig. 1 Molecular structures of (**a**) [Cu(btmgp)I], (**b**) $[Cu(btmgp)Cl_2]$, (**c**) $[Cu_2(btmgp)_2]^{2+}$ in crystals of $[Cu_2(btmgp)_2][PF_6]_2$, (**d**) $[Cu_2(DMEG_2p)_2]^{2+}$ in crystals of $[Cu_2(DMEG_2p)_2][PF_6]_2$ and (**e**) $[Cu_2(DPipG_2p)_2]^{2+}$ in crystals of $[Cu_2(DPipG_2p)_2][PF_6]_2$

Table 1 Selected bond lengths (Å) and angles (°) of selected propylene-bridged bis(guanidine) complexes

	[Cu (btmgp)I]	[Cu (btmgp)Cl_2]	[Cu_2(btmgp)$_2$] [PF_6]$_2$	[Cu_2 (DMEG$_2$p)$_2$] [PF_6]$_2$	[Cu_2 (DPipG$_2$p)$_2$] [PF_6]$_2$
M–N_{imine}	2.010(5), 2.002(5)	1.988(5), 1.992(4)	1.876(2), 1.878(2)	1.878(2), 1.873(2)	1.856(3), 1.876(3)
N_{imine}=C_{imine}	1.287(8), 1.302(8)	1.315(7), 1.306(7)	1.323(3), 1.315(3)	1.310(3), 1.318(3)	1.320(5), 1.297(4),
C_{imine}–N_{amine}	1.363–1.387	1.351–1.354	1.356–1.363	1.345–1.370	1.356–1.374
N_{imine}–M–N_{imine}	103.3(2)	89.7(2)	176.7(1)	175.3(1)	176.8(2)
ρ	0.94	0.97	0.97	0.97	0.96
References	[22]	[22]	[27]	[27]	[27]

geometries of selected bis(guanidine) ligands with one or two copper centres [22, 26, 27]. Bis(guanidines) can act as chelating or bridging ligands caused by their strong donor properties. They also stabilise linear copper coordination under formation of binuclear compounds or coordination polymers. Table 1 shows the most important geometrical parameters of selected complexes for comparison of the different propylene-bridged guanidines. The M–N_{imine} bond length decreases with smaller coordination number and higher oxidation state of the metal centre. The shortening of the bond length describes a change in donation between metal and ligand which causes structural changes of the CN_3 unit. The stronger interaction is accompanied by the elongation of the C_{imine}–N_{imine} bond, shortening of the C_{imine}–N_{amine} bonds and concomitant increase of the ρ-value. Due to delocalisation, any changes of oxidation states and geometry of the complex are stabilised by the whole guanidine unit. These special donor properties make the guanidine ligands very important in coordination chemistry.

Another frequently used backbone for bis(guanidine) ligands is the ethylene unit. Owing to the suited distance between the coordinating N donor atoms, these ligands build stable complexes, which have a favourable coordination "bite". The geometric parameters (Table 2) for several ethylene-bis(guanidine) copper complexes (Fig. 2) show similar trends; the Cu–N_{imine} bond length is shortened with higher oxidation states, and therefore, the delocalisation parameter ρ increases [29–31].

Additionally to the well-known copper complexes of bis(guanidine) ligands with aliphatic backbone linkers, there are various complexes with other transition metals like Mn, Co, Ni, Zn, Cd, Hg and Ag and propylene- and ethylene-bridged ligands (Fig. 3). Table 3 displays their geometric parameters. The complexes show two different coordination modes depending on oxidation state and coordination geometry: distorted tetrahedral [M(L)Y_2] (i.e. [Co(btmgp)Cl_2] and [Zn(DMEG$_2$e)Cl_2]) and linear complexes with two metal centres ([Cu_2(btmgp)$_2$][PF_6]$_2$) [22, 28].

The bite angles of all transition metal complexes with ethylene-bridged ligands are smaller in comparison to the values of btmgp complexes. Therefore, the

Table 2 Selected bond lengths (Å) and angles (°) of ethylene-bridged bis(guanidine) copper complexes

	$[Cu^I(DMEG_2e)_2][CuCl_2]$	$[Cu^{II}(DMEG_2e)_2][Cu_2I_4]$	$[Cu(DMEG_2e)I]$	$[Cu(TMG_2e)_2][Cu_2I_4]$	$[Cu(TMG_2e)Cl_2]$
$Cu–N_{imine}$	2.078(2), 2.062(2)	1.960(2), 1.979(2)	2.046(1), 2.029(1)	1.994–2.000	1.975(1)
$N_{imine}=C_{imine}$	1.294–1.296	1.305(4), 1.298(4)	1.293(2), 1.291(2)	1.310–1.327	1.310
$C_{imine}–N_{amine}$	1.377–1.397	1.362–1.372	1.384(2), 1.381(3)	1.351–1.379	1.361–1.368
$N_{imine}–Cu–N_{imine}$	84.0(1)	84.4(1)	85.48(6)	83.8(1)	83.9(1)
ρ	0.93	0.95	0.95	0.97	0.96
References	[28]	[29]	[30]	[31]	[31]

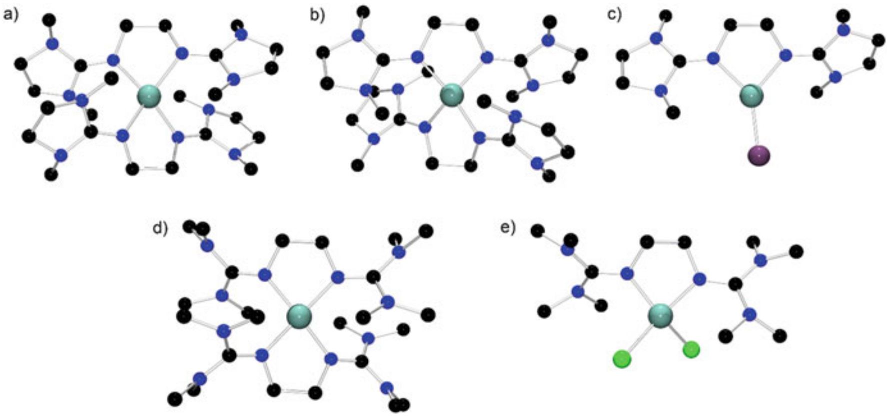

Fig. 2 Molecular structures of (**a**) $[Cu(DMEG_2e)_2]^+$ in crystals of $[Cu(DMEG_2e)_2][CuCl_2]$, (**b**) $[Cu(DMEG_2e)_2]^{2+}$ in crystals of $[Cu(DMEG_2e)_2][Cu_2I_4]$, (**c**) $[Cu(DMEG_2e)I]$, (**d**) $[Cu(TMG_2e)_2]^{2+}$ in crystals of $[Cu(TMG_2e)_2][Cu_2I_4]$ and (**e**) $[Cu(TMG_2e)Cl_2]$

coordination of two guanidine ligands and the formation of bis(chelate) complexes are promoted (i.e. $[Fe(DMEG_2e)_2]^{2+}$ or $[Ni(DMEG_2e)_2]^{2+}$). In general, the differences of the other geometric parameters of btmgp and $DMEG_2e$ complexes are not significant [28].

Next to the aliphatically bridged bis(guanidine) ligands, a variety of ligands with aromatic backbone linkers was developed [33, 34]. Diphenylene-amine, phenylene and pyridine are three representative backbones for bis(guanidine) complexes.

2′-Bis(2*N*-(1,1′,3,3′-tetramethylguanidino))diphenylene-amine (TMG_2PA) is an example for an aromatic copper-coordinating ligand. The Cu^{II} complex $[Cu^{II}(TMG_2PA^{amid})I]$ is synthesised by the reaction of the ligand with Cu^I in acetonitrile. This implies an oxidation of the metal centre by the N–H proton of

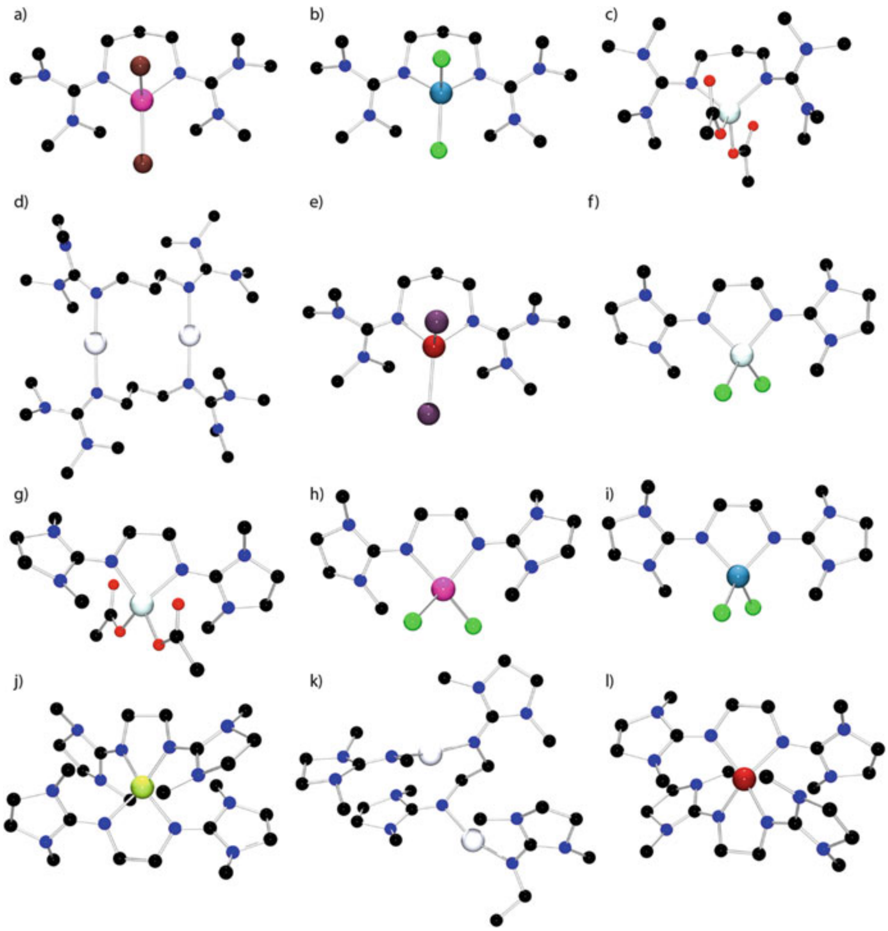

Fig. 3 Molecular structures of (**a**) [Mn(btmgp)Br_2], (**b**) [Co(btmgp)Cl_2], (**c**) [Zn(btmgp)($CH_3COO)_2$], (**d**) [Ag_2(btmgp)$_2$][ClO_4]$_2$, (**e**) [Fe(btmgp)I_2], (**f**) [Zn($DMEG_2$e)Cl_2], (**g**) [Zn($DMEG_2$e)($CH_3COO)_2$], (**h**) [Mn($DMEG_2$e)Cl_2], (**i**) [Co($DMEG_2$e)Cl_2], (**j**) [Ni($DMEG_2$e)$_2$]$^{2+}$ in crystals of [Ni($DMEG_2$e)$_2$]I_2, (**k**) {[Ag($DMEG_2$e)]BF_4}$_n$ and (**l**) [Fe($DMEG_2$e)$_2$]$^{2+}$ in crystals of [Fe($DMEG_2$e)$_2$][$Fe_2(CO)_8$]

the ligand which itself is converted to molecular hydrogen. If the copper reagent contains a non-coordinating counterion (i.e. [PF_6]$^-$), Cu^I is prevented from oxidation. Instead it induces a cyclisation reaction within the ligand, which results in the formation of a benzimidazole–guanidine ligand, and [Cu^I_2(TMGbenz)$_2$][PF_6]$_2$ is formed. In Fig. 4, the molecular structures of the distorted tetrahedral complex [Cu^{II}(TMG_2PA^{amid})I] and the [Cu^I_2(TMGbenz)$_2$][PF_6]$_2$ complex with linear copper coordination are shown [35].

The aromatic ligand TMG_2b forms stable complexes with copper halides. [Cu(TMG_2b)Cl_2] and [Cu(TMG_2b)Br_2] (Fig. 5) have distorted copper centres with τ_4

Table 3 Selected bond lengths (Å) and angles (°) of ethylene-bridged bis(guanidine) transition metal complexes

	Mn		Co		Ni		Zn	
	[Mn(btmgp)Br2]	$[Mn(DMEG_2e)_2Cl_2]$	$[Co(btmgp)Cl_2]$	$[Co(DMEG_2e)Cl_2]$	$[Ni(btmgp)I_2]$	$[Ni(DMEG_2e)_2]I_2$	$[Zn(btmgp)Cl_2]$	$[Zn(DMEG_2e)Cl_2]$
$M–N_{imine}$	2.098(14), 2.103(14)	2.1389(18), 2.1390(18)	1.997(2), 1.999(2)	2.0317(13)	1.956(3), 1.969(3)	1.977(2), 1.987(2)	1.997(2), 2.008(2)	2.038(2)
$N_{imine}=C_{imine}$	1.312(2), 1.313(2)	1.308(3)	1.313(3), 1.316(3)	1.308(2)	1.328(5), 1.325(4)	1.306(3), 1.313(3)	1.307(3), 1.316(3)	1.309(3)
$C_{imine}–N_{amine}$	1.356–1.361	1.367(3), 1.374(3)	1.349–1.361	1.363(2), 1.374(2)	1.351–1.361	1.373(3), 1.371(3),	1.354–1.363	–
$N_{imine}–M–N_{imine}$	93.0(1)	82.84(9)	97.2(1)	85.76(7)	95.7(1)	84.03(7)	97.0(1)	86.18(10),
ρ	0.97	0.96	0.97	0.96	0.98	0.96	0.97	0.96
References	[29]	[27]	[29]	[27]	[29]	[27]	[29]	[30]

	Zn		Ag		Fe		Cd	Hg
	$[Zn(btmgp)(CH_3COO)_2]$	$[Zn(DMEG_2e)(CH_3COO)_2]$	$[Ag_2(btmgp)_2][ClO_4]_2$	$\{[Ag(DMEG_2e)]BF_4\}_n$	$[Fe(btmgp)I_2]$	$[Fe(DMEG_2e)_2][Fe_2(CO)_8]$	$[Cd(btmgp)Cl_2]$	$[Hg(btmgp)Cl_2]$
$M–N_{imine}$	1.998(2), 2.000(2)	2.011(2), 2.038(2)	2.107(1); 2.116(1)	2.144(3), 2.119(3)	2.038(3), 2.040(3)	2.019(2)–2.067(2)	2.211(2), 2.212(2)	2.245(6), 2.246 (6)
$N_{imine}=C_{imine}$	1.307(3), 1.307(3)	1.308(2), 1.305(2)	1.304(2), 1.303(2)	1.311(4), 1.314(4),	1.317(4), 1.320(4)	1.302(3)–1.310(3)	1.390(3), 1.390(3)	1.282(9), 1.305 (9)
$C_{imine}–N_{amine}$	1.353–1.368		1.365–1.373	1.373(4), 1.361(4)	1.357–1.365	–	1.357–1.366	1.355–1.367
$N_{imine}–Cu–N_{imine}$	100.2(1)	86.16(6)	174.6(1)	163.10(11)	94.0(1)	83.17(7), 83.86(7)	90.1(1)	88.8(2)
ρ	0.96	0.96	0.95	0.96	0.97	0.96	0.96	0.95
References	[28]	[32]	[28]	[30]	[22]	[29]	[28]	[28]

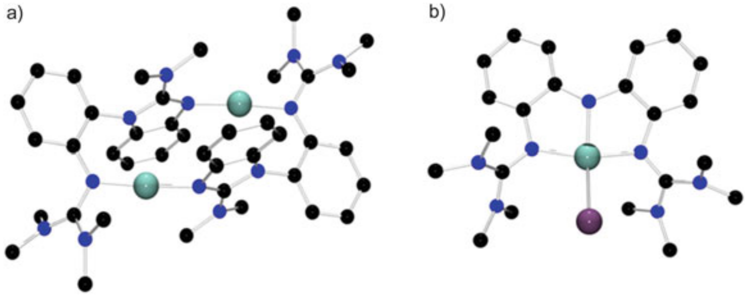

Fig. 4 Molecular structures of (**a**) the $[Cu_2(TMGbenz)_2]^{2+}$cation in crystals of $[Cu^I_2(TMGbenz)_2][PF_6]_2$ ($Cu–N_{imine,benz}$ 1.879(5), $Cu–N_{imine,gua}$ 1.895(6), $N_{imine,benz}–C_{imine}$ 1.307(8), $N_{imine,gua}–C_{imine}$ 1.324(9) Å) and (**b**) $[Cu(TMG_2PA^{amid})I]$ ($Cu–N_{amide}$ 1.903(5), $Cu–N_{imine}$ 1.961(5), $N_{imine}–C_{imine}$ 1.348 Å)

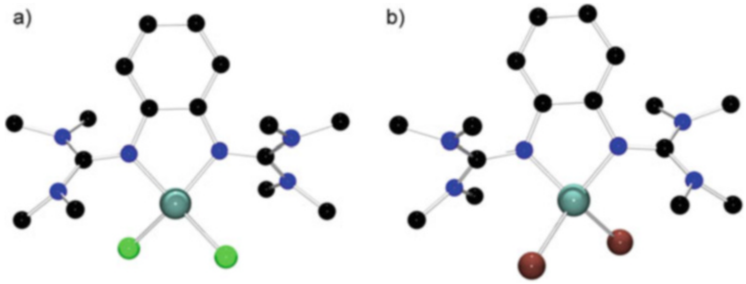

Fig. 5 Molecular structures of (**a**) $[Cu(TMG_2b)Cl_2]$ and (**b**) $[Cu(TMG_2b)Br_2]$

Table 4 Selected bond lengths (Å) and angles (°) of phenylene-bridged bis (guanidine) copper complexes

	$[Cu(TMG_2b)Cl_2]$	$[Cu(TMG_2b)Br_2]$
$Cu–N_{imine}$	1.972(2), 1.980(2)	1.959(3), 1.971(3)
Cu–X	2.251(1), 2.231(1)	2.361(1), 2.380(1)
C=N	1.340(3), 1.343(3)	1.311(5), 1.343(5)
$N_{imine}–Cu–N_{imine}$	83.5(1)	83.9(2)
ρ	1.00	1.00
References	[37]	[37]

values of 0.51 and 0.55 (with $\tau_4 = 1$ for an ideal tetrahedron and $\tau_4 = 0$ for an ideal square planar coordination) [36, 37]. The geometric parameters (Table 4) show trends similar to ligands with aliphatic backbones. It has to be noted that upon attachment to an aromatic unit, the guanidine moiety tends to a stronger delocalisation which appears in the large ρ of 1. Those copper guanidine complexes are used for the atom transfer radical polymerisation of styrene (see Sect. 3.2) [37].

Many more complexes of ligands with aromatic backbones with other transition metals have been synthesised. Himmel et al. developed a zinc complex with the bis (guanidine) ligand bdmegb (or $DMEG_2b$) which consists of two DMEG groups connected via a benzene linker. $[Zn(DMEG_2b)(Et)_2]$ crystallises with distorted

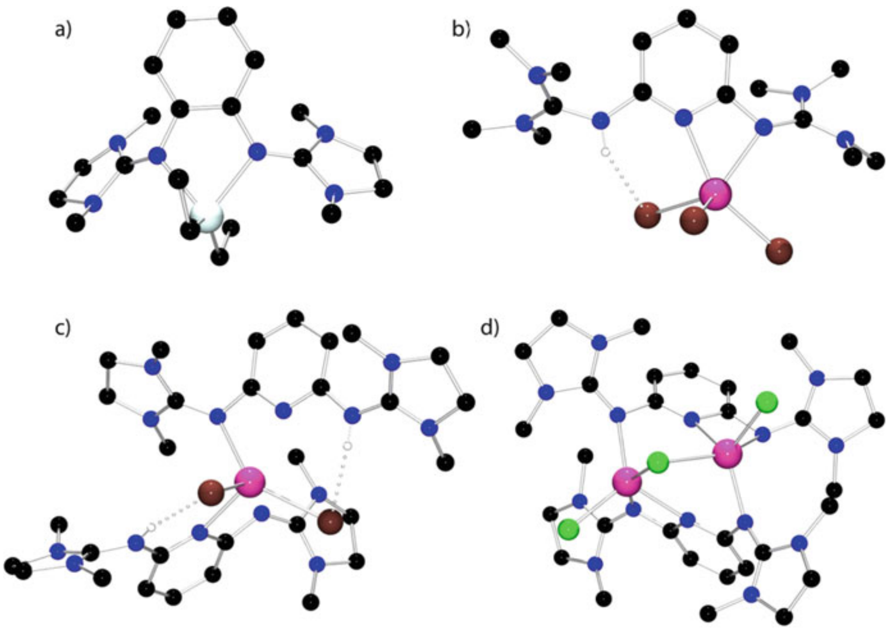

Fig. 6 Molecular structures of (**a**) $[Zn(DMEG_2b)(Et)_2]$, (**b**) $[MnBr_3(TMG_2pyH)]$, (**c**) $[MnBr_2(DMEG_2pyH)_2]^{2+}$ in crystals of $[MnBr_2(DMEG_2pyH)_2][MnBr_4]$ and (**d**) $[Mn_2Cl_3(DMEG_2py)_2]^{+}$ in crystals of $[Mn_2Cl_3(DMEG_2py)_2][MnCl_4]$

tetragonal geometry [38]. In studies on manganese complexes, Herres-Pawlis and Henkel et al. observed that pyridine-bridged bis(guanidines) occur in protonated and unprotonated forms within the same complexes: the reaction of TMGpy or DMEGpy with manganese halides leads to the complexes $[MnBr_3(TMG_2pyH)]$, $[MnBr_2(DMEG_2pyH)_2]^{2+}$ and $[Mn_2X_3(DMEG_2py)_2]^{+}$ (with X=Cl/Br). The Mn atoms of $[MnBr_3(TMG_2pyH)]$ and $[MnBr_2(DMEG_2pyH)_2]_2$ are coordinated each to one guanidine and one pyridine N ligand. In the binuclear complex $[Mn_2X_3(DMEG_2py)_2]$, each Mn atom is coordinated to N_{gua} and N_{py} of one ligand and to one guanidine of the second ligand, and the two metal centres are connected via a halogen bridge (Fig. 6) [39]. In the coordinating guanidine moieties, ρ amounts to approximately 1, whereas it is even larger in the protonated guanidine units (Table 5).

However, the majority of guanidine complexes comprise copper. Some of the bis (guanidine) copper complexes react with O_2 at low temperatures and generate different forms of binuclear Cu_2O_2 motifs (Fig. 7): the bis(μ-oxo)dicopper(III) and μ-η^2:η^2-peroxo-dicopper(II) complexes [26, 27]. Those complexes act as bioinorganic model complexes for type 3 copper proteins like hemocyanin. Due to characteristic ligand-to-metal charge transfer (LMCT), they can be identified using UV/Vis spectroscopy: the $[Cu^{III}{}_2(\mu\text{-}O)_2]^{2+}$ core shows oxo→Cu(III) LMCTs at 300 and 400 nm and the $[Cu^{II}{}_2(\mu\text{-}O_2)]^{2+}$ core the analogous peroxo→Cu(II)

Table 5 Selected bond lengths (Å) and angles (°) of aromatic-bridged bis(guanidine) transition metal complexes

	$[Zn(DMEG_2b)(Et)_2]$	$[MnBr_3(TMG_2pyH)]$	$[MnBr_2(DMEG_2pyH)_2]^{2+}$	$[Mn_2Cl_3(DMEG_2py)_2]^+$
$M–N_{imine}$	2.2288(18), 2.2057(15)	2.264(5)	2.367(3), 2.263(3)	2.270(5), 2.130(6), 2.141(6), 2.242(5)
$M–N_{py}$	–	2.267(5)	2.289(3), 2.333(3)	2.308(6), 2.275(5),
$N_{imine}=C_{imine}$ [a]	1.307(2), 1.306(2)	1.329(8)	1.334(4), 1.343(5)	1.286–1.337
M–X/Et	2.0122(19), 2.015(2)	2.5806(12), 2.4970(12), 2.5010(12)	2.6150(7), 2.6362(7),	2.348(2), 2.422(2), 2.350(2),
$N_{imine}–M–N_{py}$	–	58.22(19)	–	–
ρ^a	0.95	0.99	1.00	0.99
ρ^b	–	1.04	1.02	–
References	[38]	[39]	[39]	[39]

[a] Coordinated guanidine unit(s)
[b] Protonated guanidine unit

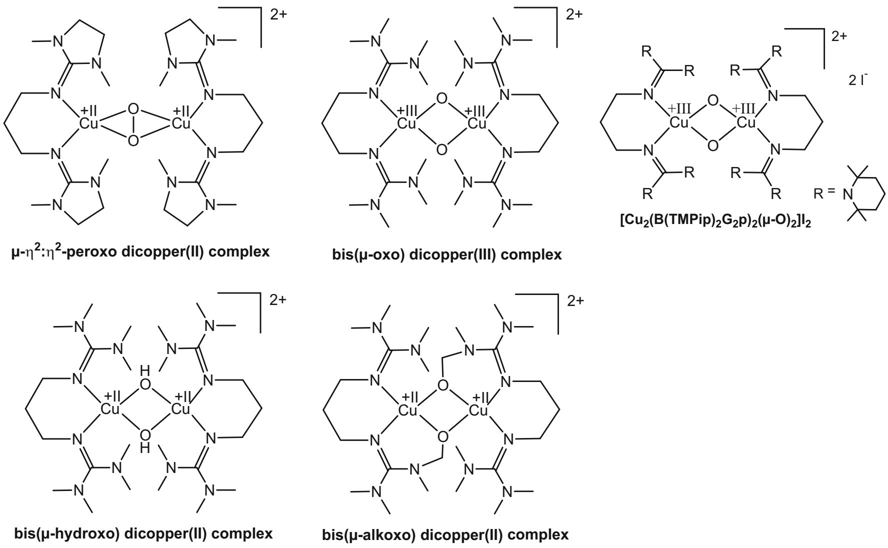

Fig. 7 Bis(guanidine)-stabilised Cu_2O_2 motifs

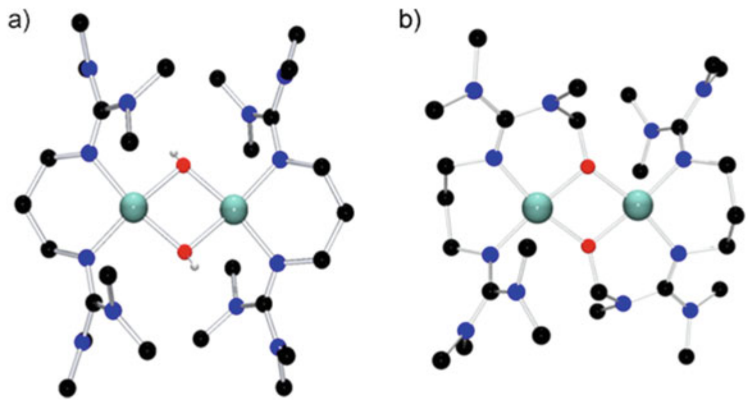

Fig. 8 Molecular structures of (**a**) $[Cu_2(btmgp)_2(\mu\text{-}OH)_2]^{2+}$ in crystals of $[Cu_2(btmgp)_2(\mu\text{-}OH)_2][PF_6]_2$ and (**b**) $[Cu_2(btmgpO)_2]^{2+}$ in crystals of $[Cu_2(btmgpO)_2][PF_6]_2$

LMCTs at 350 and 550 nm [40]. The guanidine-stabilised $[Cu^{III}{}_2(\mu\text{-}O)_2]^{2+}$ core shows an additional absorption band of $\pi_{gua}\rightarrow$Cu(III) LMCTs at 550 nm [41]. In those bis(guanidine)-stabilised Cu_2O_2 species, the preferred formation of bis (μ-oxo)dicopper(III) complexes or μ-η^2:η^2-peroxo-dicopper(II) complexes is correlated with the torsion within the guanidine groups [27]. The warming of the solutions of Cu_2O_2 complexes above −40°C leads to hydroxylation of the guanidine methyl groups forming bis(μ-alkoxo)dicopper(II) and bis(μ-hydroxo) dicopper (II) complexes (Fig. 8, Table 6) [26]. When the substituents at the guanidine are

Table 6 Selected bond lengths (Å) and angles (°) of hydroxo and alkoxo dicopper complexes

	$[Cu_2(btmgp)_2(OH)_2][PF_6]_2$	$[Cu_2(btmgpO)_2][PF_6]_2$
$Cu–N_{imine}$	1.962(2), 1.968(2)	1.937(2), 1.961(2)
$N_{imine}=C_{imine}$	1.321(3), 1.313(3)	1.314(3), 1.311(3)
$C_{imine}–N_{amine}$	1.356–1.364	1.348–1.374
$N_{imine}–Cu–N_{imine}$	94.0(2)	93.3(1)
ρ	0.97	0.97
References	[26]	[26]

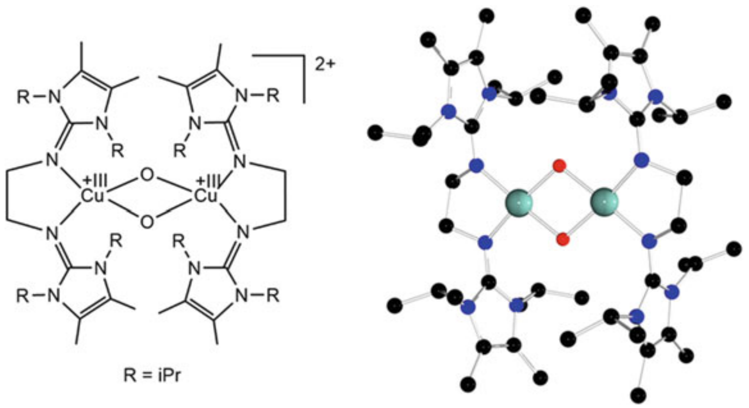

Fig. 9 $[Cu_2(\mu\text{-}O)_2(BL^{iPr})_2]^{2+}$ (*left*) and molecular structure of $[Cu_2(\mu\text{-}OH)_2(BL^{iPr})_2]^{2+}$ (Cu–N1 1.916(2), Cu–N2 1.950(2), Cu–O 1.932(2), Cu–OA 1.930(2), Cu–CuA 3.0487(6), N1–C3 1.342(3), N2–C14 1.340(3); N1–Cu–N2 84.52(8), O–Cu–OA 75.72(8), Cu–O–CuA 104.28(8), N1–Cu–O 100.78(8), N2–Cu–OA 99.32(8)) (*right*, H atoms omitted for clarity)

significantly enlarged, the Cu_2O_2 core unit is shielded which precludes reactions with substrates or solvent molecules such as in the bis(μ-oxo)dicopper(III) complex with the ligand N^1,N^3-bis[bis(2,2,6,6-tetramethylpiperidin-1-yl)methylen]propan-1,3-diamine (B(TMPip)G_2p) [42]. By combining resonance Raman and XAS spectroscopy, it was possible to characterise the optically excited state of the bis(μ-oxo)dicopper(III) complex: owing to the large substituents, only 10% of structural distortion on the way to a peroxo core is achieved.

Besides the Cu_2O_2 complexes with TMG$_2$p and DMEG$_2$p ligands, Tamm et al. developed bis(μ-oxo/hydroxo) cores with the ethylene-bridged ligand *N*,*N′*-bis(1,3-diisopropyl-4,5-dimethylimidazolin-2-ylidene)-1,2-ethanediamine BL^{iPr}. The presence of the bis(μ-oxo)dicopper(III) at low temperatures was determined by UV/Vis spectroscopy, and it exhibits absorption bands at 400, 585 and 760 nm. Upon warming to room temperature, the more stable bis(μ-hydroxo) dicopper(II) is formed. Its molecular structure is shown in Fig. 9 [43].

Furthermore, the Tamm group prepared more complexes of BL^{iPr} with other transition metals. Each metal centre is coordinated by two N_{gua} donors of the ligand

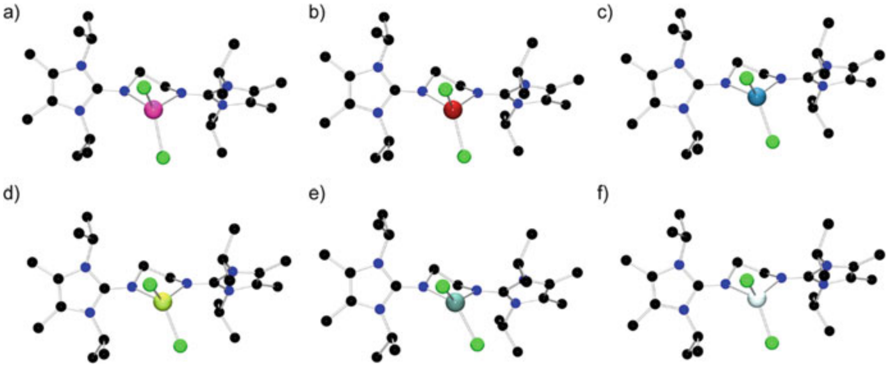

Fig. 10 Molecular structures of (**a**) [Mn(BL^{iPr})Cl_2], (**b**) [Fe(BL^{iPr})Cl_2], (**c**) [Co(BL^{iPr})Cl_2], (**d**) [Ni(BL^{iPr})Cl_2], (**e**) [Cu(BL^{iPr})Cl_2] and (**f**) [Zn(BL^{iPr})Cl_2]

Table 7 Selected bond lengths (Å) and angles (°) of transition metal complexes with BL^{iPr}

	[Mn(BL^{iPr})Cl_2]	[Fe(BL^{iPr})Cl_2]	[Co(BL^{iPr})Cl_2]	[Ni(BL^{iPr})Cl_2]	[Cu(BL^{iPr})Cl_2]	[Zn(BL^{iPr})Cl_2]
M–N1	2.1224(12)	2.0668(16)	2.0142(14)	1.9951(9)	1.9709(12)	2.0342(9)
M–Cl	2.3356(5)	2.2795(7)	2.2585(5)	2.2502(4)	2.2460(5)	2.2500(4)
N1–C2	1.3248(17)	1.330(2)	1.329(2)	1.3308(14)	1.3286(18)	1.3264(14)
N2–C2	1.3651(18)	1.364(2)	1.362(2)	1.3680(14)	1.3592(17)	1.3664(14)
N3–C2	1.3645(18)	1.367(2)	1.362(2)	1.3614(14)	1.3644(18)	1.3615(13)
N1–M–N1′	81.46(6)	81.28(6)	84.00(8)	83.58(5)	83.39(7)	84.39(5)
Cl–M–Cl′	118.64(3)	118.05(3)	113.95(3)	114.64(3)	104.35(3)	115.46(2)
N1–M–Cl	122.45(3)	124.14(5)	124.83(4)	127.38(3)	140.14(4)	122.54(3)
N1–M–Cl′	103.70(3)	102.70(5)	103.83(4)	101.43(3)	98.52(4)	104.67(3)
Angle between MCl_2 and MN_2 planes	74.5	72.2	72.8	68.6	53.9	75.5
ρ	0.971	0.974	0.976	0.975	0.976	0.972
$\tau4$	0.82	0.79	0.78	0.75	0.57	0.82
Angle between imidazole planes	67.1	66.0	66.1	66.6	64.8	66.2

and two chloride anions (Fig. 10). They crystallise in a distorted geometry with τ_4 values between 0.57 and 0.82 (Table 7). With $\tau_4 = 0.57$, the copper complex is most distorted, and the other complexes, especially [Mn(BL^{iPr})Cl_2] and [Zn(BL^{iPr})Cl_2], are more tetrahedrally coordinated. All guanidine CN_3 centres have similar ρ-values [44].

The sulphur analogue of a μ-η^2:η^2-peroxo-dicopper(II) complex could be successfully synthesised and characterised by the Houser group. In the obtained μ-η^2:η^2-disulfido-dicopper(II) complexes (Fig. 11), the copper centres are coordinated with btmgp and *N*,*N*′-(2-methyl-2-(2-pyridyl)propan-1,3-diyl)bis

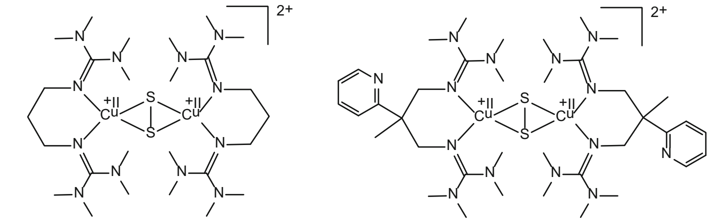

Fig. 11 Bis(guanidine) μ-η^2:η^2-disulfido-dicopper(II) complexes

Table 8 Selected bond lengths (Å) and angles (°) of bis(guanidine) μ-η^2:η^2-disulfido-dicopper (II) complexes

	$[Cu_2(btmgp)_2(S_2)][PF_6]_2$	$[Cu_2(Py\text{-}btmgp)_2(S_2)][PF_6]_2$
$Cu–N_{imine}$	1.932(2), 1.936(2)	1.919(4), 1.926(3)
$N_{imine}=C_{imine}$	1.314	1.323
$C_{imine}–N_{amine}$	1.361	1.352
Cu–S	2.1533(9)	2.1264(15)
S–S	2.1993(14)	2.204(2)
$N_{imine}–Cu–N_{imine}$	99.77(9)	98.95(16)
S–Cu–S	61.44(3)	62.44(5)
ρ	0.97	0.98

(tetramethylguanidine) and show characteristic charge-transfer transitions at 376 and 477 nm in the UV/Vis spectrum. Concerning the geometrical parameters of the μ-η^2:η^2-disulfido-dicopper(II) complexes (Table 8), the $Cu–N_{imine}$ bond lengths are shorter than in the comparable bis(μ-hydroxo) dicopper complexes. Houser et al. additionally synthesised the cupric chloride complex and the bis (μ-hydroxo) dicopper complex with *N*,*N*′-(2-methyl-2-(2-pyridyl)propan-1,3-diyl) bis(tetramethylguanidine) [45].

Further aromatic bis(guanidines) without metal coordination studied so far are the proton sponges based on diaminonaphthalenes intensively investigated by Sundermeyer et al. [11].

2.2 Tris(guanidines)

The class of tris(guanidines) comprises ligands with three guanidine units which are connected through a tertiary amino group. The most important tris(guanidine) ligand TMG_3tren was synthesised using the method of Kantlehner et al. by the Sundermeyer group in 2001 [46]. It found attention as “superligand” for transition metal chemistry and could form complexes with various transition metals, i.e. Cu and Fe [46, 47]. A very interesting ability of this ligand is the stabilisation of

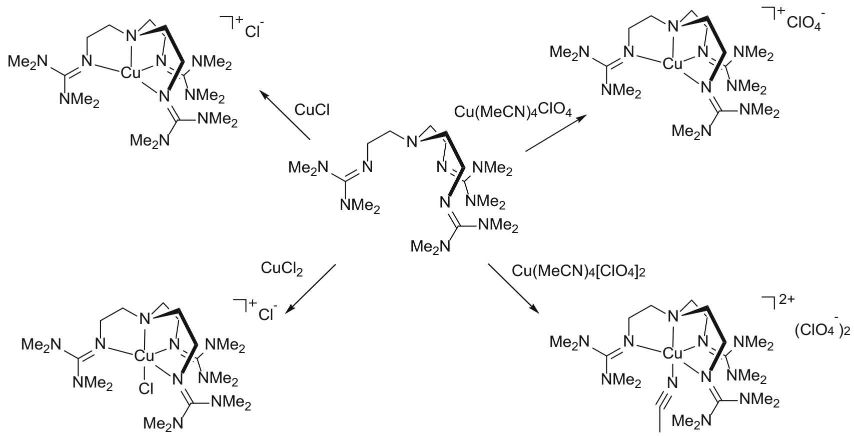

Scheme 3 Synthesis of copper complexes with TMG_3tren

copper–superoxo complexes which was examined in various studies by Sundermeyer, Schindler and Holthausen et al. [48–53]. Another tris(guanidine) ligand is $DMPG_3tren$ which forms the $[Cu(DMPG_3tren)]ClO_4$ complex with copper(I) [47].

The precursor structures of copper–superoxo complexes allow interesting insights into the guanidine binding situations. The metal centre is tetrapodally coordinated by all three guanidine units; therefore, they form a cavity around the copper atom. In some copper(I) complexes (shown in Scheme 3), the metal centre is only coordinated by the TMG_3tren ligand. In copper(II) complexes, this tetrapodal coordination is not sufficient, and ancillary ligands such as chloride or acetonitrile complement the coordination sphere. Therefore, the parameter ρ is larger in copper (II) than in copper(I) complexes (Table 9).

The copper–superoxo 1:1 CuO_2 species is formed reversibly from the corresponding $[Cu(TMG_3tren)]$ analogue at low temperatures (Scheme 4), it was spectroscopically and theoretically characterised in 2004 [48, 51], and the structure of the end-on superoxo $[Cu^{II}(\eta^1\text{-}O_2^-)(TMG_3tren)][SbF_6]$ complex was determined in 2006 (Fig. 12) [49, 52]. The electronic and geometric properties of the superoxo–Cu(II) unit were characterised by isotopic probing [55], different spectroscopic techniques (i.e. magnetic circular dichroism and resonance Raman) and DFT calculations [56]. It is noteworthy that this superoxo–copper(II) complex possesses a triplet ground state which is due to the two corresponding perpendicular magnetic orbitals, the d_{z2}-π_σ* and the π_v* orbitals. Hence, any antiferromagnetic coupling is precluded. Moreover, resonance Raman profiles of the Cu–O and O–O stretches proved the dominant absorption feature of the complex as a superoxo π^*_σ to copper d_{z2} (LMCT) transition. Upon warming to room temperature, the superoxo complex loses the bound oxygen within seconds which proves the stability of the tetramethylguanidine groups against C–H activation. In flash-photolysis studies

Table 9 Selected bond lengths (Å) and angles (°) of TMG_3tren copper complexes

	$[Cu^{I}(TMG_3tren)]Cl$	$[Cu^{II}(TMG_3tren)Cl]Cl$	$[Cu^{II}(TMG_3tren)(NCMe)][ClO_4]_2$	$[Cu(O_2)(TMG_3tren)][SbF_6]$	$[Cu^{II}(NO_2)(TMG_3tren)][B(C_6F_5)_4]$	$[Cu^{II}(TMG_3trenO)][B(C_6F_5)_4]$
$Cu–N_{imine}$	2.052(2)	2.091–2.109	2.054–2.082	2.080–2.095	2.084–2.090	2.053–2.117
$Cu–N_{amine}$	2.190(3)	2.111(3)	2.078(5)	2.128	2.068	2.091(2)
$N_{imine}=C_{imine}$	1.295	1.309–1.316	1.299–1.313	1.307–1.320	1.306	1.302–1.303
$C_{imine}–N_{amine}$	1.370, 1.381	1.357–1.374	1.350–1.374	1.359–1.375	1.361–1.370	1.365–1.380; 1.415
$Cu–L_{ax}$	–	2.285(1)	2.002(5)	1.927(2)	1.940	1.972(5)
ρ	0.94	0.96	0.96	0.96	0.96	0.95, 0.94
References	[47]	[47]	[47]	[49, 52]	[54]	[50, 53]

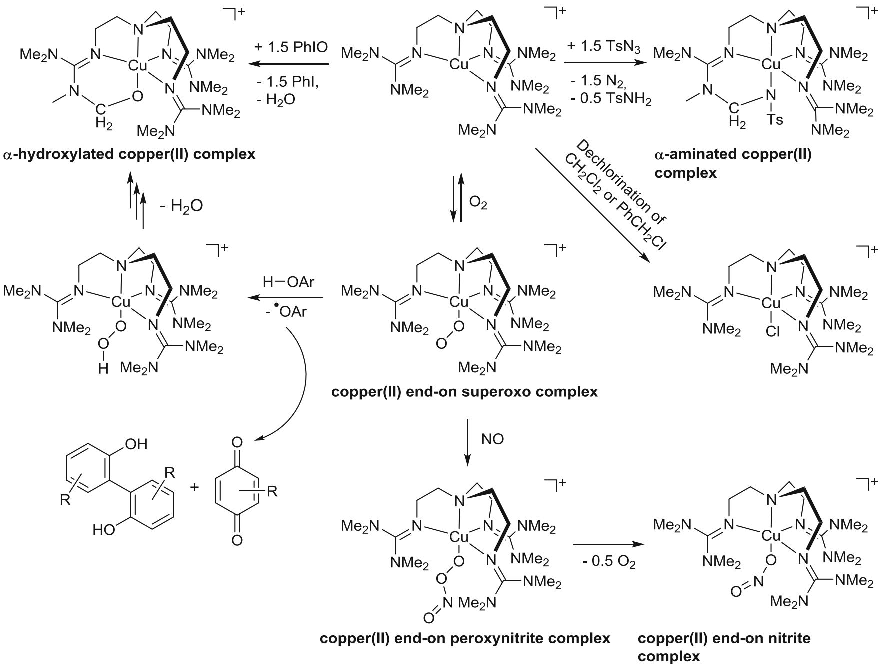

Scheme 4 Different reactions of $[Cu(TMG_3tren)]^+$ with various small molecules

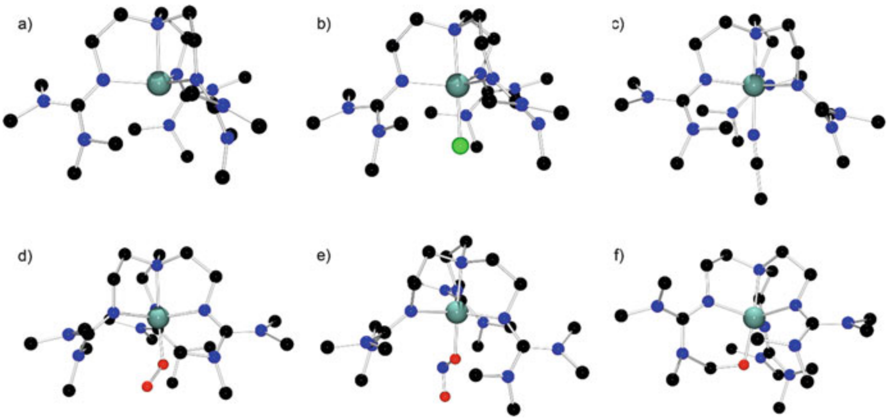

Fig. 12 Molecular structures of (**a**) $[Cu(TMG_3tren)]^+$ in crystals of $[Cu(TMG_3tren)]Cl$, (**b**) $[Cu(TMG_3tren)Cl]^+$ in crystals of $[Cu(TMG_3tren)Cl]Cl$, (**c**) $[Cu(TMG_3tren)(MeCN)]^{2+}$ in crystals of $[Cu(TMG_3tren)(MeCN)][ClO_4]_2$, (**d**) $[Cu(O_2)(TMG_3tren)]^+$ in crystals of $[Cu(O_2)(TMG_3tren)][SbF_6]$, (**e**) $[Cu(NO_2)(TMG_3tren)]^+$ in crystals of $[Cu(NO_2)(TMG_3tren)]$ $[B(C_6F_5)_4]$ and (**f**) $[Cu(TMG_3trenO)]^+$ in crystals of $[Cu(TMG_3trenO)][B(C_6F_5)_4]$

and theoretical calculations on the involved excited states, Karlin and Neese et al. showed that the bound dioxygen can be relieved by photodissociation even at low temperatures of −40°C [57]. This effect is wavelength dependent (in contrast to myoglobin-O_2 systems) because upon excitation at 436 nm, the triplet-Cu(II)-superoxide is promoted to a Cu(I)-$^3O_2$-species with extremely weakened Cu–O bond. With an O–O bond length of 1.280(3) Å and a O–O–Cu angle of 123.5(2), the [CuO_2(TMG_3tren)] complex has a similar geometry as the crystallographic structure of the peptidylglycine α-hydroxylating monooxygenase (PHM), a hydroxylating and amidating enzyme for selected aliphatic C–H positions [58]. The end-on superoxo–copper(II) species also appears as a crucial intermediate in dopamine β-monooxygenase (DβM). DβM and PHM are important enzymes in neuropeptide and neurotransmitter biosynthesis and catalyse the stereospecific hydroxylation of C–H bonds. PHM catalyses the hydroxylation of the glycine α-carbon of glycine-extended peptides, and DβM catalyses the conversion of dopamine to norepinephrine [59].

The reaction of the [Cu(O_2)(TMG_3tren)] complex with phenolic substrates results in substrate oxidation to *ortho*-quinones or radically coupled bisphenols [50, 53]. The [Cu^{II}(TMG_3trenO)][$B(C_6F_5)_4$] complex is formed as by-product by hydroxylation of a guanidine methyl position [50, 53]. This hydroxylation reaction could be evoked by an hydrogen atom source like TEMPO and a subsequent O–O bond cleavage or by applying PhIO to TMG_3tren copper(I) complexes [50, 53]. Poater and Cavallo relate this hydroxylation behaviour in DFT studies to a highly reactive intermediate hydroperoxo species [Cu^{II}(TMG_3tren)OOH^-]$^+$ which abstracts the methyl-H-atom at a guanidine group [60].

Similar to the PhIO activation, TMG_3tren copper(I) complexes reacted with tosyl azide (TsN_3) to a copper complex which is aminated at a methyl group of one of the guanidine groups [9]. Furthermore, the reaction of the end-on superoxo–copper species with NO was examined by the Karlin group. The generated peroxynitrite copper(II) complex is stable at low temperatures and decays into a copper(II) nitrito complex [54].

Besides its biomimetic properties, the [Cu(TMG_3tren)]Cl complex could also function as a catalyst in the oxidative carbonylation of methanol to dimethyl carbonate and water. This reaction is a non-phosgene route to dimethyl carbonate, a precursor in many industrial processes. During this reaction, the copper (I) complex reacts with O_2 in the presence of methanol under formation of a copper(II) methoxy species. The masked coordinated methoxy radicals are transferred to CO to give dimethyl carbonate and the initial copper(I) complex which allows to start the next cycle [61].

In 2013, Karlin and Solomon et al. examined the protonation and electron transfer reduction of [Cu(O_2)(TMG_3tren)]$^+$ with trifluoroacetic acid (CF_3CO_2H) and exogenous decamethylferrocene (Fc*) reductants. The reaction products are the copper(II)–CF_3CO_2 complex and H_2O_2 (Scheme 5) [62].

Que et al. focused their studies on the tris(guanidine) ligand TMG_3tren and its iron reactivity. In 2009, a trigonal bipyramidal iron(II) complex was developed. The metal centre in [Fe(TMG_3tren)(TfO)](TfO) is coordinated by three N_{gua} donors

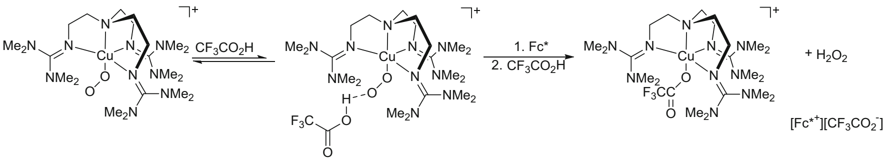

Scheme 5 Reaction of $[Cu(O_2)(TMG_3tren)]^+$ with CF_3CO_2H and Fc*

Table 10 Selected bond lengths (Å) and angles (°) of TMG_3tren iron complexes

	[Fe (TMG_3tren) (TfO)]$^+$	[Fe(O) (TMG_3tren)]$^{2+}$ (deuterated)	[Fe^{II}(CN) (TMG_3tren)]	[Fe^{III}(CN) (TMG_3tren)]$^+$	[Fe (TMG_3tren) (CH_3CN)]$^{2+}$
Fe–L_{ax}	2.156(2)	1.661(2)	2.1293(15)	2.094(4)	2.151(4)
Fe–N_{gua}	2.094 (Ø)	2.005 (Ø)	2.109 (Ø)	2.014 (Ø)	2.073(Ø)
Fe–N_{amine}	2.118(3)	2.112(3)	2.3017(12)	2.214(3)	2.254(3)
N_{gua}=C_{gua}	1.316 (Ø)	1.337 (Ø)	1.319 (Ø)	1.340 (Ø)	1.311 (Ø)
References	[63, 64]	[65]	[66]	[66]	[46]

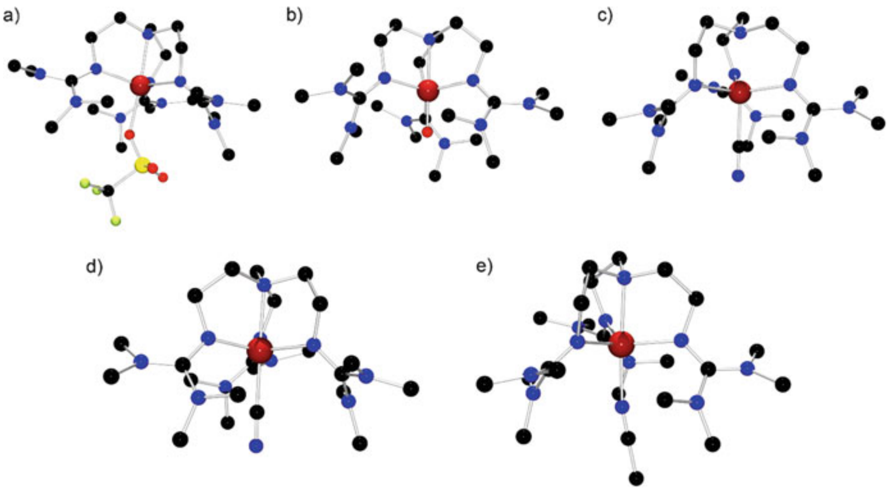

Fig. 13 Molecular structures of (**a**) $[Fe(TMG_3tren)(TfO)]^+$ in crystals of $[Fe(TMG_3tren)(TfO)]$(TfO), (**b**) $[Fe(O)(TMG_3tren)]^{2+}$ in crystals of D_{36}-$[Fe(O)(TMG_3tren)][TfO]_2$, (**c**) $[Fe^{II}(CN)(TMG_3tren)]$, (**d**) $[Fe^{III}(CN)(TMG_3tren)]^+$ and (**e**) $[Fe(TMG_3tren)(CH_3CN)]^{2+}$ in crystals of $[Fe(TMG_3tren)(CH_3CN)](ClO_4)_2$

in equatorial and by the N_{amine} donor and the coordinating anion in axial position (Table 10). The reaction of this complex with 2-(*tert*-butylsulfonyl)-iodosylbenzene (^{S}PhIO) leads to the oxoiron(IV) species $[Fe(O)(TMG_3tren)]^{2+}$ (Fig. 13). The presence of the oxoiron double bond was confirmed by resonance Raman spectroscopy [63, 64]. One year later, the Que group obtained the molecular

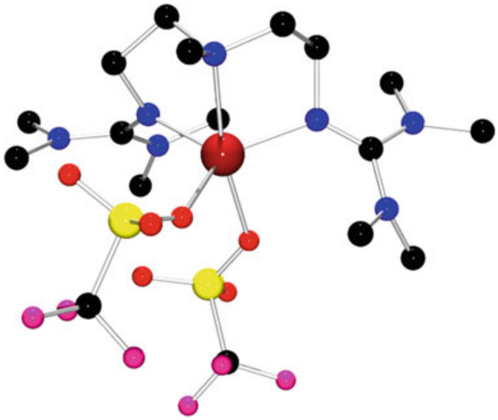

Fig. 14 Molecular structure of [Fe(TMG$_2$dien)(TfO)$_2$] (Fe–O$_{ax}$ 2.2012(15), Fe–O$_{eq}$ 2.0816(15), Fe–N$_{amine}$ 2.2835(17); Fe–N$_{gua}$(Ø), 2.0597(17))

structure after deuteration [65]. The Fe(IV)=O complex with the TMG$_3$tren ligand shows only weak C–H activation reactivity, and in its self-decay pathway, hydroxylation activity occurs which is directed towards the guanidine methyl substituents as observed for their copper analogues [65, 67]. The existence and reactivity of the Fe(IV)=O species with this high oxidation state of the metal centre were confirmed by different analytical methods [68]. These systems function as biomimetic models for an intermediate of nonheme iron (NHFs) enzymes, which are responsible for many C–H bond activations [68]. Additionally, the Que group synthesised iron (IV) TMG$_3$tren complexes with other small coordinating molecules. [Fe^{IV}(CN)(TMG$_3$tren)]$^{2+}$ was generated starting with the iron(II) complex [Fe^{II}(CN)(TMG$_3$tren)] via [Fe^{III}(CN)(TMG$_3$tren)]$^{+}$ by electrolytic oxidation. The formation was observed by UV/Vis spectroscopy through the growth of characteristic UV/Vis transitions of Fe(IV)=CN at 403/393 and 609/584 nm [66].

Another closely related oxoiron precursor complex developed by the Que group has to be mentioned here, although [Fe(TMG$_2$dien)(TfO)$_2$] comprises a bis(guanidine). The complex has trigonal bipyramidal geometry like their tris(guanidine) analogues, and the iron centre is coordinated equatorially by two N$_{gua}$ donors and a coordinating anion; the N$_{amine}$ and a TfO^{-} occupy the axial positions (Fig. 14). The Fe(IV)=O species [Fe(O)(TMG$_2$dien)(CH$_3$CN)]$^{2+}$ occurs after the reaction with ^{s}PhIO in acetonitrile and shows characteristic UV/Vis transitions at 380 (8,200 M^{-1} cm^{-1}) and 805 nm (270 M^{-1} cm^{-1}) [69].

Additionally, the TMG$_3$tren ligand can coordinate the transition metals cobalt, nickel, manganese, zinc and molybdenum. Ray et al. synthesised the trigonal bipyramidal complexes [Co^{II}(TMG$_3$tren)(TfO)](TfO) and [Ni^{II}(TMG$_3$tren)(TfO)]$^{+}$ (Fig. 15), which formed metal oxo species. The Co(IV)-O species is stabilised by a Sc(TfO)$_3$ group, whereas the Ni(III)-O complex is formed by the reaction of the precursor complex with *m*CPBA (*meta*-chloroperbenzoic acid) and subsequent O–O homolysis [70–72]. The Zn and Mn complexes with TMG$_3$tren crystallise like their iron analogue with trigonal bipyramidal geometry (Fig. 15). The metal centre is coordinated by three N$_{gua}$ donors in equatorial position and by

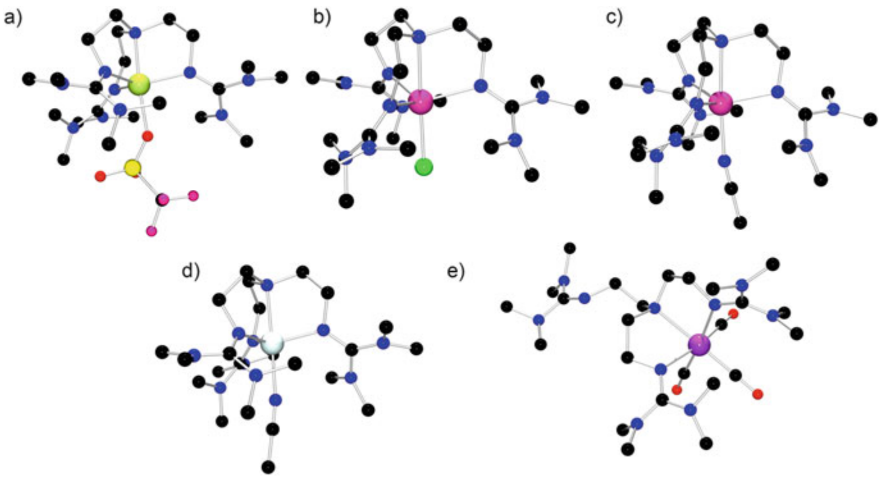

Fig. 15 Molecular structures of (**a**) $[Ni^{II}(TMG_3tren)(TfO)]^+$ in crystals of $[Ni(TMG_3tren)(OTf)]OTf$, (**b**) $[Mn(TMG_3tren)Cl]^+$ in crystals of $[Mn(TMG_3tren)Cl]Cl$, (**c**) $[Mn(TMG_3tren)(CH_3CN)]^{2+}$ in crystals of $[Mn(TMG_3tren)(CH_3CN)](ClO_4)_2$, (**d**) $[Zn(TMG_3tren)(CH_3CN)]^{2+}$ in crystals of $[Zn(TMG_3tren)(CH_3CN)](ClO_4)_2$ and (**e**) $[Mo(TMG_3tren)(CO)_3]$

Table 11 Selected bond lengths (Å) and angles (°) of TMG_3tren transition metal complexes

	$[Mn(TMG_3tren)Cl]Cl$	$[Mn(TMG_3tren)(CH_3CN)]^{2+}$	$[Zn(TMG_3tren)(CH_3CN)]^{2+}$	$[Mo(TMG_3tren)(CO)_3]$
M–X	2.430(1)	2.215(3)	2.187(3)	1.926(Ø)
$M–N_{gua}$	2.183(Ø)	2.135(Ø)	2.039(Ø)	2.328(Ø)
$M–N_{amine}$	2.378(1)	2.328(3)	2.269(2)	2.354(2)
$(C=N)_{gua}$	1.313(Ø)	1.311(Ø)	1.310(Ø)	1.314(Ø)
$(C–N)_{gua}$	1.355–1.373	1.358–1.365	1.351–1.369	1.364–1.377
References	[46]	[46]	[46]	[46]

N_{amine} and the coordinating anion or a solvent molecule in axial position (Table 11). In $[Mo(TMG_3tren)(CO)_3]$, the Mo centre is coordinated tetragonal bipyramidally by two N_{gua} and two CO ligands in equatorial and N_{amine} and CO in axial position. One guanidine unit is not coordinating [46].

Another special tris(guanidine) ligand is the $TMGm_3et$ (1,1,1-tris[2*N*-(1,1,3,3-tetramethylguanidino)methyl]ethane), which is based on three guanidine units connected by an aliphatic backbone linker. It forms complexes with the transition metals Zn and Mn. In $[Zn(TMGm_3et)Cl_2]$ and $[Mn(TMGm_3et)Cl_2]$, the metal centres each are coordinated by only two N_{gua} units and two chloride anions, the third guanidine does not coordinate (Fig. 16). The complex crystallises with distorted tetrahedral geometry [24].

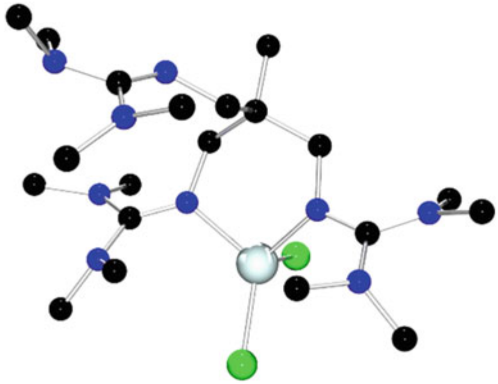

Fig. 16 Molecular structure of [Zn(TMGm$_3$et)Cl$_2$] (Zn–Cl 2.267(Ø), Zn–N$_{gua}$ 2.008(Ø), C=N 1.315 (Ø), C–N 1.355(Ø), Cl–Zn–Cl 107.90(4), Cl–Zn–N$_{gua}$ 102.93(Ø)/121.97(Ø), N$_{gua}$–Zn–N$_{gua}$ 96.29(10))

2.3 Hybridguanidines

The combination of guanidine functions with other donor functions can be very useful for tailoring coordination sites. In this context, hybridguanidines have been designed which combine amine or imine functions with various guanidines and backbones.

The first examples of this class are shown in Fig. 17: *N*-(1,3-dimethylimidazolidine-2-ylidene)pyridine-8-amine (DMEGpy), 1,1,3,3-tetramethyl-2-((pyridin-2-yl)methyl)guanidine (TMGpy), *N*-(1,3-dimethylimidazolidin-2-ylidene)quinoline-8-amine (DMEGqu) and 1,1,3,3-tetramethyl-2-(quinolin-8-yl)guanidine (TMGqu) combine guanidine groups with pyridinyl or quinolinyl groups. The ligands were synthesised by the reaction of chloroformamidium chlorides with 2-picolylamine or 8-aminoquinoline [73].

With these ligands, numerous complexes with cobalt, copper, manganese and zinc have been structurally characterised. Figure 18 depicts selected TMGqu containing complexes, and Table 12 collects the key bond lengths of these complexes. The complexes with metals in oxidation state +II attain relatively high ρ-values of 0.98–1.00. The manganese complexes have been shown to be active catalysts for the epoxidation of 1-octene with peracetic acid [74]. The zinc complexes are highly active lactide polymerisation catalysis and are summarised in Sect. 3.1. Elongation of the pyridine side arm yields the ligands TMGepy and DMEGepy which gave mono(chelate) copper and cobalt complexes [77].

The most important feature of the TMGqu copper complexes (Fig. 18d) is the structural similarity of copper(I) and copper(II) states which renders them models for the entatic state. The guanidine donors answer strongly to the change in oxidation state (0.1 Å), whereas the quinoline maintains its distance to the copper. The angle between the chelate planes changes from 67° in TMGqu copper (I) complexes to 43° in TMGqu copper(II) complexes due to steric encumbrance which hinders a stronger structural change. Their structural similarity in solid state and solution has been confirmed by X-ray absorption spectroscopy. In principle, the

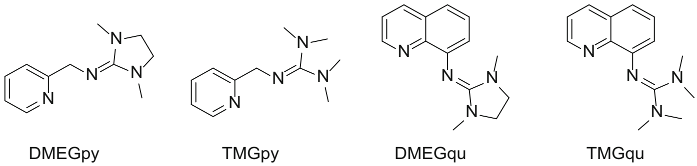

Fig. 17 Guanidine ligands DMEGpy, TMGpy, DMEGqu and TMGqu [73]

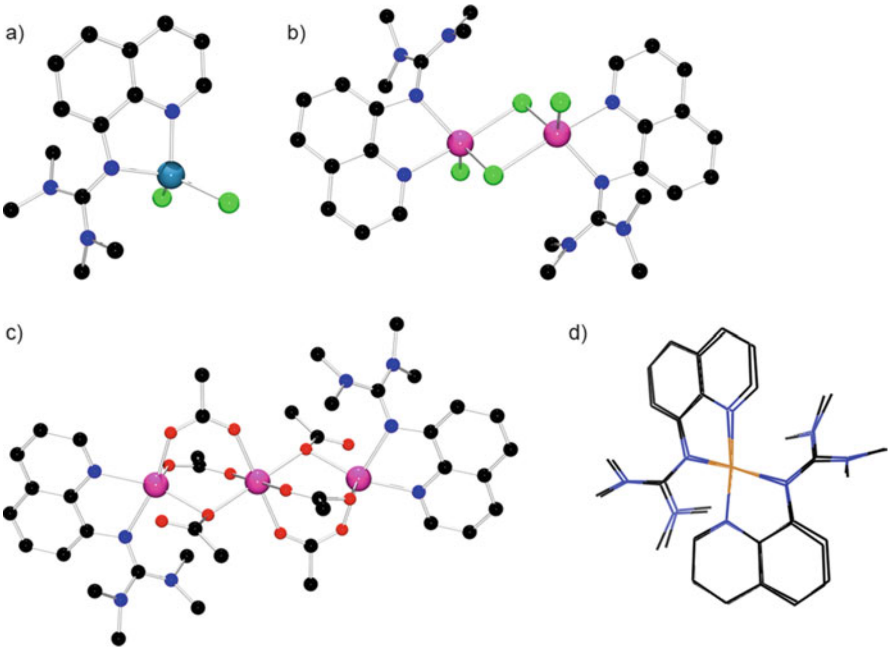

Fig. 18 Selected TMGqu complexes: (**a**) $[Co(TMGqu)Cl_2]$, (**b**) $[Mn_2(TMGqu)_2(\mu\text{-}Cl)_2Cl_2]$, (**c**) $[Mn_3(TMGqu)_2(\mu\text{-}CH_3COO)_6]$ and (**d**) overlay of $[Cu(TMGqu)_2]^{+/2+}$ in crystals of $[Cu(TMGqu)_2]ClO_4$ and $[Cu(TMGqu)_2][PF_6]_2$

Table 12 Selected bond lengths of TMGqu complexes

	$[Co(TMGqu)Cl_2]$	$[Mn_2(TMGqu)_2(\mu\text{-}Cl)_2Cl_2]$	$[Mn_3(TMGqu)_2(\mu\text{-}CH_3COO)_6]$	$[Cu(TMGqu)_2]^+$ (average)	$[Cu(TMGqu)_2]^{2+}$ (average)
$M–N_{gua}$	2.045(6)	2.189(1)	2.283(2)	2.082	1.963
$M–N_{imine}$	2.122(6)	2.220(1)	2.203(2)	1.991	1.975
$(C{=}N)_{gua}$	1.361(9)	1.352(2)	1.332(4)	1.320	1.349
$(C–N)_{gua}$	1.346(2)/1.352(2)	1.354(2)/1.339(2)	1.348(4)/1.360(4)	1.364	1.341
ρ	0.99	1.00	0.98	0.96	1.00
References	[73]	[74]	[74]	[75, 76]	[75, 76]

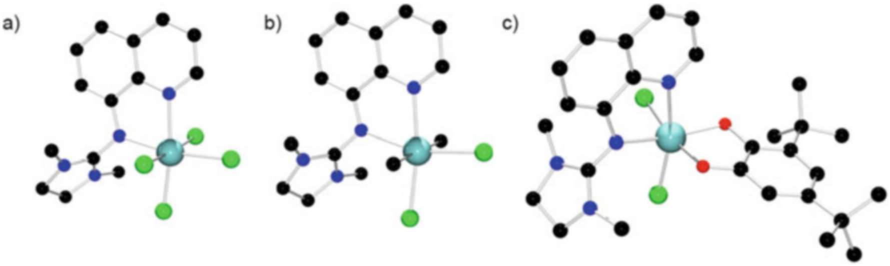

Fig. 19 Molecular structures of (**a**) [Sn(DMEGqu)Cl_4], (**b**) [Me_2Sn(DMEGqu)Cl_2] and (**c**) [Sn (DMEGqu)(3,5-DBCat)Cl_2] [81]

concepts of charge transfer through optical excitation and electron transfer are combined in these complexes. Here, the transition state of the electron transfer is accessible by resonant excitation of the two entatic copper complexes through vibrational modes which are coupled to metal ligand charge transfer (MLCT) and ligand metal charge transfer (LMCT) states. Raman spectroscopy helped to identify the resonance and the crucial vibrations which connect the two states. The charge-transfer behaviour of these complexes has been intensively studied by density functional theory and many-body perturbation theory, and TD-DFT was found to reproduce the experimental spectra faithfully when using triple-zeta basis sets and hybrid functionals [78–80].

DMEGqu is even able to stabilise tin(IV) complexes (Fig. 19) where the guanidine C=N bond is considerably elongated to 1.355–1.365 Å due to charge transfer to the formal tin(IV) [81]. This leads to a large ρ-value of 1.04 and an enhanced planarity of the DMEGqu moiety.

In parallel, aliphatic hybridguanidines have been developed, e.g. (tetramethylguanidino)(dimethylamino)-propane (TMGdmap). Here, biomimetic phenolate hydroxylation was observed via the bis(μ-oxo) dicopper(III) complex $[Cu_2(\mu\text{-}O)_2(TMGdmap)_2]^{2+}$ [41]. This reactivity proves that $[Cu_2(\mu\text{-}O)_2(TMGdmap)_2]^{2+}$ can be regarded as a good model system for the binuclear copper protein tyrosinase which mediates the *ortho*-hydroxylation of phenols [1]. The comparison between the parent bisamine and bis(guanidine) species highlights the attributes that lead to biomimetic phenolate hydroxylation with a bis(μ-oxo) dicopper(III) complex: the congested complex with bis(guanidine) ligation of btmgp reacts neither with phenols nor phenolates revealing the importance of core accessibility in such oxidations. The least congested complex with bisamine ligation yields exclusively the C–C radical-coupled bis-phenol product with both phenols and phenolates, a reactivity observed with most bis (μ-oxo) dicopper(III) complex species. The hybrid guanidine complex unites mild oxidative capability with steric accessibility. The distinct sideband in the UV/Vis absorption of $[Cu_2(\mu\text{-}O)_2(TMGdmap)_2]^{2+}$ at 450 nm (compared to classical bis (μ-oxo) complexes) could be identified as $\pi \rightarrow Cu_2O_2$ LMCT.

With this ligand, copper(I) complexes and a bis(μ-hydroxo) dicopper (II) complex could be structurally characterised. Here, the different donor strengths

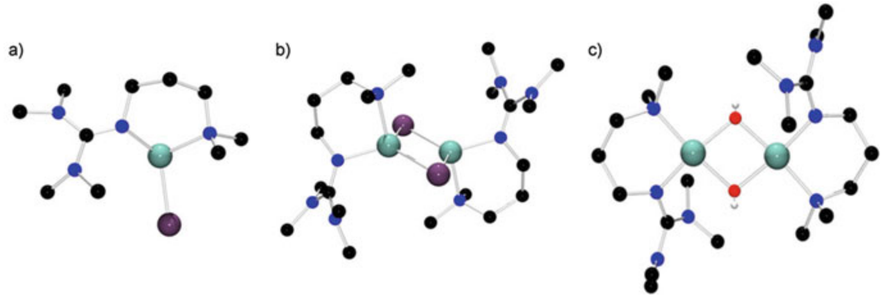

Fig. 20 Molecular structures of (**a**) [Cu(TMGdmap)I], (**b**) $[Cu(TMGdmap)I]_2$ and (**c**) $[Cu_2(TMGdmap)_2(\mu\text{-}OH)_2]^{2+}$ in crystals of $[Cu_2(TMGdmap)_2(\mu\text{-}OH)_2][CuI_3]$

of the two N donor functions appear very distinct with Cu–N_{imine} bond lengths of 1.961(2) and 2.037(2) Å in the copper(I) iodido complexes and 1.981(3) Å in the hydroxo complex compared to Cu–N_{amine} bond lengths of 2.119(2), 2.160(2) and 2.046(3) Å, respectively (Fig. 20).

When the ligand backbone is shortened to an ethylene bridge, oxygen can still be activated, but no defined Cu_2O_2 species could be observed [82]. However, numerous bis(μ-hydroxo) dicopper complexes could be structurally characterised (Fig. 21 and Table 13). Here, the distinct donor difference between simple aliphatic amine groups and the strong guanidine donor becomes obvious: the Cu–N_{gua} bond length is 0.07–0.14 Å shorter than the Cu–N_{amine} bond.

In a different research field, tripodal ligands have been used for the stabilisation of potential spin-crossover iron(II) complexes. Here, the pyridinyl–guanidine complex $[Fe(TMG\text{-}uns\text{-}penp)(NCS)_2]$ was structurally characterised and investigated within a series of tripodal ligands [83].

2.4 *Guanidine-thio Ligands*

Besides the bis- and tris(guanidine) ligands with different backbone linkers, more guanidine ligands contain further N, O or S donor functions. Through the additional heteroatom functionalities linked by a flexible backbone, new coordination geometries and bonding modes are created.

The guanidine hybrid ligands with a sulphur donor were developed by the Henkel group and form biomimetic model complexes for the Cu_A centre. The thiolate–guanidines and thioester–guanidines (Fig. 22) act as ligands for mono- and polynuclear copper centres. Therefore, the bis(guanidine) ligands react with the copper reactant generating the required complexes after the reductive splitting of the ligand's disulphide bridge and formation of a thiolate donor [84].

In the obtained complexes, the copper centres are coordinated by the N_{gua} of the guanidine units and one or two S donor atoms of the non-guanidine unit (Fig. 23 and

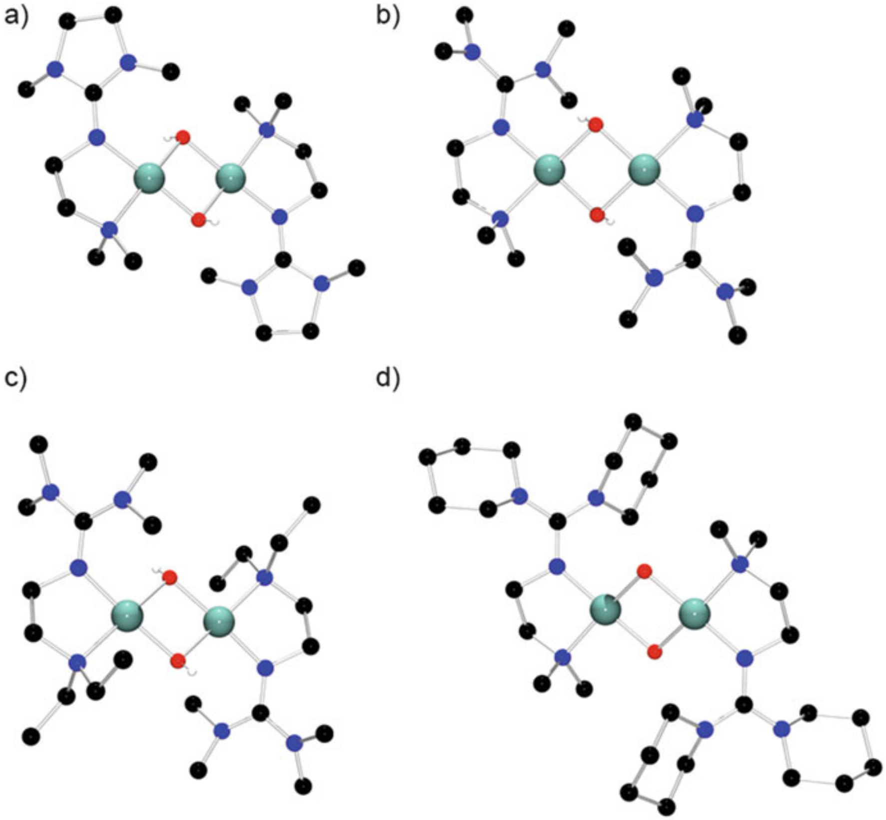

Fig. 21 Molecular structures of (**a**) $[Cu_2(DMEGdmae)_2(\mu\text{-}OH)_2]^{2+}$ in crystals of $[Cu_2(DMEGdmae)_2(\mu\text{-}OH)_2]I_2$, (**b**) $[Cu_2(TMGdmae)_2(\mu\text{-}OH)_2]^{2+}$ in crystals of $[Cu_2(TMGdmae)_2(\mu\text{-}OH)_2]I_2$, (**c**) $[Cu_2(TMGdeae)_2(\mu\text{-}OH)_2]^{2+}$ in crystals of $[Cu_2(TMGdeae)_2(\mu\text{-}OH)_2]Cu_2I_4$ and (**d**) $[Cu_2(DPipGdmae)_2(\mu\text{-}OH)_2]^{2+}$ in crystals of $[Cu_2(DPipGdmae)_2(\mu\text{-}OH)_2](CF_3SO_3)_2$

Table 13 Selected bond lengths of hybrid guanidine bis(μ-hydroxo) dicopper complexes [82]

	$[Cu_2(DMEGdmae)_2(\mu\text{-}OH)_2]I_2$	$[Cu_2(TMGdmae)_2(\mu\text{-}OH)_2]I_2$	$[Cu_2(TMGdeae)_2(\mu\text{-}OH)_2]Cu_2I_4$	$[Cu_2(DPipGdmae)_2(\mu\text{-}OH)_2](CF_3SO_3)_2$
M–O	1.935(2)/1.928(2)	1.932(2)/1.948(2)	1.927(2)/1.967(2)	1.911(2)/1.933(2)
$M–N_{gua}$	1.961(2)	1.949(3)	1.933(2)	1.937(2)
$M–N_{amine}$	2.031(2)	2.033(3)	2.071(2)	2.046(2)
$(C=N)_{gua}$	1.308(3)	1.311(4)	1.316(3)	1.325(3)
$(C–N)_{gua}$	1.345(3)/1.373(3)	1.365(4)/1.368(4)	1.364(3)/1.366(3)	1.357(3)/1.364(3)
ρ	0.96	0.96	0.96	0.97

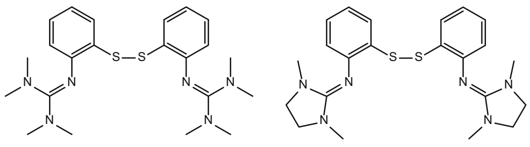

Fig. 22 Examples of thio-guanidine ligands: $(TMGS)_2$ (*left*) and $(DMEGS)_2$ (*right*) [84, 85]

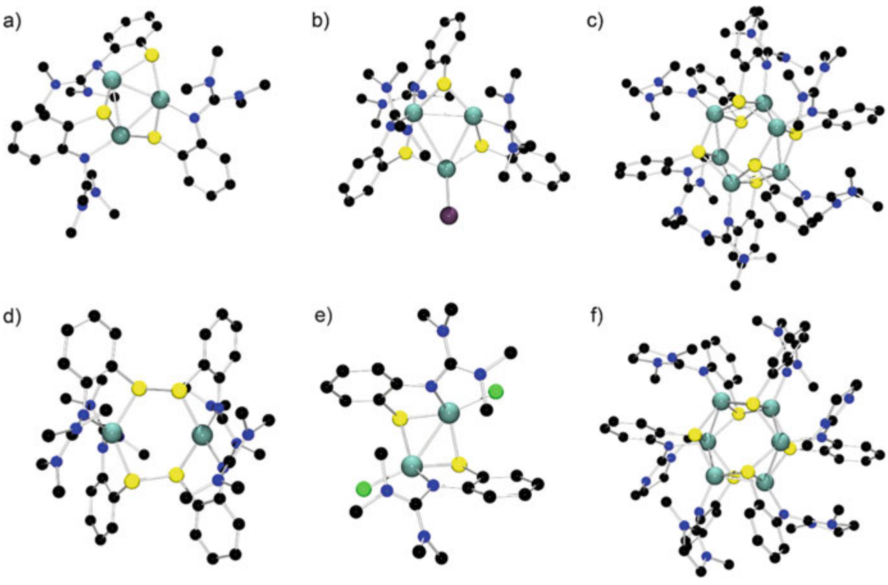

Fig. 23 Molecular structures of (**a**) $[Cu_3(TMGS)_3]$, (**b**) $[Cu_3(TMGS)_3I]$, (**c**) $[Cu_6(TMGS)_6]^{2+}$ in crystals of $[Cu_6(TMGS)_6][PF_6]_2$, (**d**) $[Cu_2\{(TMGS)_2\}_2]^{2+}$ in crystals of $[Cu_2\{(TMGS)_2\}_2][TfO]_2$, (**e**) $[Cu_2(TMGS)_2Cl_2]$ and (**f**) $[Cu_6(DMEGS)_6]^{2+}$ in crystals of $[Cu_6(DMEGS)_6][PF_6]_2 \cdot 2CH_3CN \cdot 2CH_2Cl_2$

Table 14). In $[Cu_3(TMGS)_3]$, each copper is part of a five-membered chelate ring, and the metal centres are connected through S-bridges. The $[Cu_6(TMGS)_6]^{2+}$ is formally comparable to the dimeric form of $[Cu_3(TMGS)_3]$ and builds Cu_6S_6 cages [84]. $[Cu_6(DMEGS)_6]^{2+}$ could be synthesised as analogous Cu_6S_6 complex with the DMEGS ligand [85]. The binuclear complexes $[Cu_2\{(TMGS)_2\}_2][TfO]_2$ and $[Cu_2(TMGS)_2Cl_2]$ are synthetically connected by a chloride-induced disulphide–thiolate interconversion. Disulphide cleavage and addition of chloride anions lead to significant structural changes; the six-membered Cu_2S_4-ring is transformed into a bis(μ-S) dicopper unit [86].

Table 14 illustrates the general tendency: upon oxidation of the coordinated copper ion, the C=N bond stretches and the ρ-value increases.

Furthermore, Henkel and Schindler et al. developed modified TMG_3tren ligands replacing one guanidine with a thio unit. The resulting copper compounds function

Table 14 Selected bond lengths of guanidine-thio copper complexes (minimal and maximal values are given)

	$[Cu_3(TMGS)_3]$	$[Cu_3(TMGS)_3I]$	$[Cu_6(TMGS)_6]^{2+}$	$[Cu_2\{(TMGS)_2\}_2]^{2+}$	$[Cu_2(TMGS)_2Cl_2]$	$[Cu_6(DMEGS)_6]^{2+}$
Cu–S	2.200–2.296	2.1951–2.2821	2.2939–2.4573	2.2755–2.3000	2.2204	2.2939–2.3117
$Cu–N_{gua}$	2.025–2.084	1.980–2.032	2.005–2.018	2.013–2.037	2.0034	2.005–2.018
$(C{=}N)_{gua}$	1.306–1.348	1.132–1.353	1.333–1.339	1.343–1.359	1.355	1.333–1.339
$(C–N)_{gua}$	1.362–1.385	1.334–1.368	1.339–1.357	1.309–1.371	1.338, 1.348	1.339–1.357
ρ	0.97	0.99	0.99	1.00	1.01	0.99
References	[84]	[84]	[84]	[86]	[86]	[85]

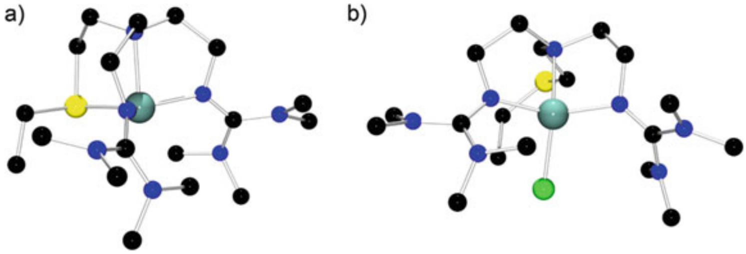

Fig. 24 Molecular structures of (**a**) $[Cu((TMG_{et})_2N_{et}SEt)]^+$ in crystals of $[Cu((TMG_{et})_2N_{et}SEt)]BPh_4$ and (**b**) $[Cu((TMG_{et})_2N_{et}SEt)Cl]^+$ in crystals of $[Cu((TMG_{et})_2N_{et}SEt)Cl]Cl$

Table 15 Selected bond lengths (Å) and angles (°) of $(TMG_{et})_2N_{et}SEt$ -complexes

	$[Cu((TMG_{et})_2N_{et}SEt)]^+$	$[Cu((TMG_{et})_2N_{et}SEt)Cl]^+$
Cu–N_{imine}	2.039(1), 2.031(1)	1.958(2), 1.964(2)
Cu–N_{amine}	2.196(1)	2.054(2)
N_{imine}=C_{imine}	1.304(2), 1.307(2)	1.310(3), 1.323(3)
C_{imine}–N_{amine}	1.384(2), 1.375(2), 1.376(2)	1.364(3), 1.352(3), 1.354(3), 1.365(3)
Cu–S	2.260(1)	–
References	[87]	[87]

as model complexes of the peptidglycine-α-hydroxylating monooxygenase (PHM) (Fig. 24, Table 15) [87].

2.5 *Tetrakis(guanidines)*

1,2,4,5-Tetrakis-(tetramethylguanidino)benzene (ttmgb) was developed by the group of Himmel in 2008 [88]. The general redox and spectroscopic chemistry of these so-called guanidine-functionalised aromatic compounds (GAFs) is comprehensively discussed in the chapter by Himmel. This section focuses on structural aspects of the redox chemistry of complexes containing 1,2,4,5-tetrakis-(tetramethylguanidino)benzene with special attention to the stretching of the C–N_{imine} bond length in different complexes with different metal and ligand oxidation states (Scheme 6). The reaction of the ligand with an excess of copper (II) tetrafluoroborate yields the binuclear complex $[\{Cu(MeCN)_4\}_2(ttmgb)][BF_4]_6$ under oxidation of the ligand and precipitation of elemental copper. The reaction with copper(II) nitrate yields $[\{Cu(NO_3)_2\}_2(ttmgb)]$ which decomposes under ligand oxidation to give $[\{Cu(NO_3)_2\}_2(ttmgb)][Cu(NO_3)_4]$. Slightly different reaction conditions provide $[\{Cu(NO_3)_2\}_2(ttmgb)][NO_3]$ including a radical form of ttmgb. With halide ligands, a nonoxidised and an oxidised form of $[Cu_2Br_2(ttmgb)]$ have been reported, and the oxidation of $[Cu_2I_2(ttmgb)]$ leads to the coordination polymer $\{[(CuI)_2(ttmgb)](I_3)_2\}_n$. Recently, the Himmel group demonstrated that $[\{Cu(OAc)_2\}_2(ttmgb)]$ can be oxidised to complexes with radical monocationic or

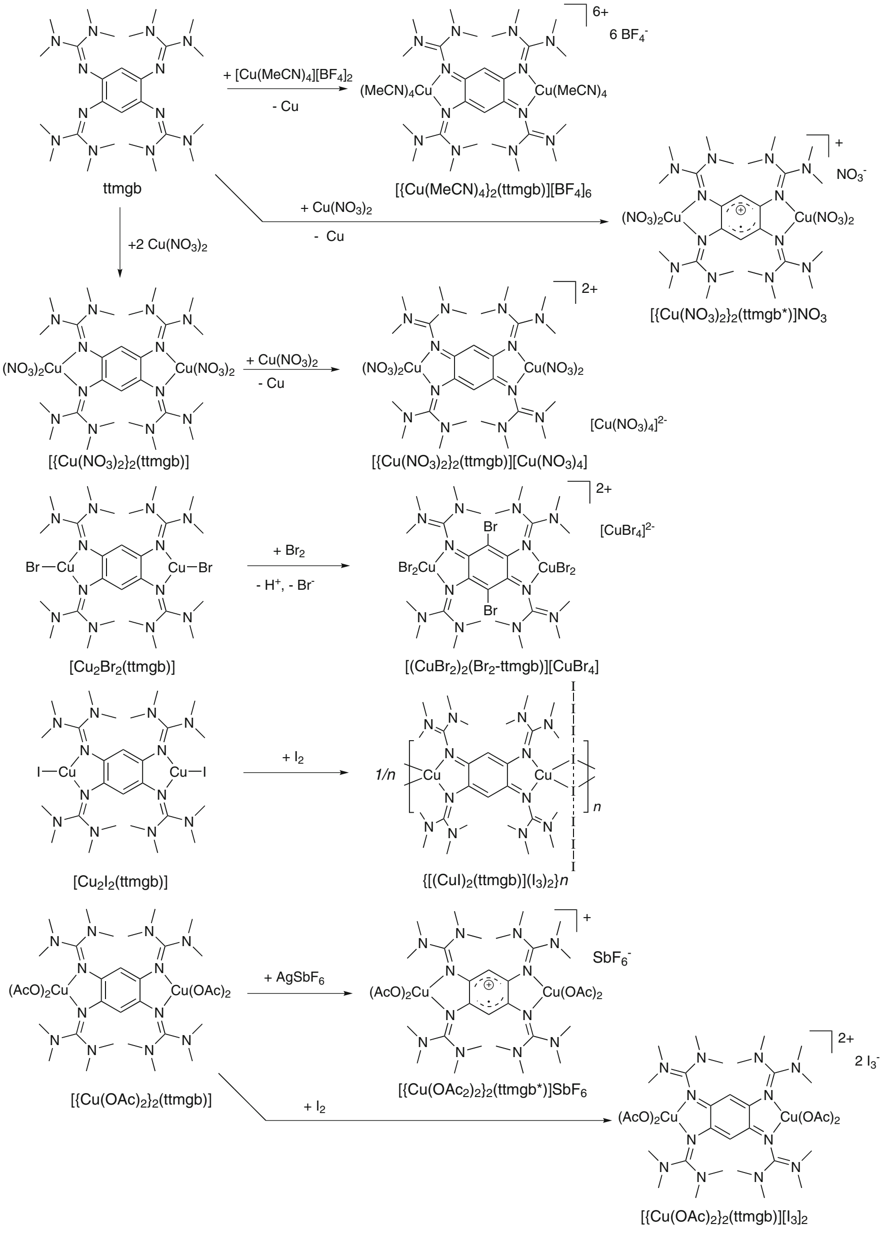

Scheme 6 Copper complexes with tetrakis(guanidines)

dicationic ligands depending on the oxidising agent [89]. Selected bond lengths of these complexes are summarised in Table 16. It is worth mentioning that each of these ligand states can stabilise copper complexes. Shortest $N_{imine}{=}C_{gua}$ bond lengths are found (as expected) in the pure ligand (1.29 Å) and in the copper

Table 16 Selected bond lengths (Å) of different copper ttmgb complexes

	[{Cu $(MeCN)_4\}_2$ (ttmgb)] $[BF_4]_6$	$[Cu_2Br_2$ (ttmgb)]	$[(CuBr_2)_2$ $(Br_2$-ttmgb)] $[CuBr_4]$	$[Cu_2I_2$ (ttmgb)]	$\{[(CuI)_2$ (ttmgb)] $(I_3)_2\}_n$	[{Cu $(NO_3)_2\}_2$ (ttmgb)]	[{Cu $(NO_3)_2\}_2$ (ttmgb)] [Cu $(NO_3)_4]$	[{Cu $(NO_3)_2\}_2$ (ttmgb*)] $[NO_3]$	[{Cu $(OAc)_2\}_2$ (ttmgb)]	[{Cu $(OAc)_2\}_2$ (ttmgb*)] (PF_6)	[{Cu $(OAc)_2\}_2$ (ttmgb)] $(I_3)_2$	ttmgb
Classification	$[Cu^{II}$-GFA^{2+}-$Cu^{II}]$	$[Cu^{I}$-GFA-$Cu^{I}]$	$[Cu^{II}$-$(Br_2$-$GFA)^{2+}$-$Cu^{II}]$	$[Cu^{I}$-GFA-$Cu^{I}]$	$[Cu^{I}$-GFA^{2+}-$Cu^{I}]$	$[Cu^{II}$-GFA-$Cu^{II}]$	$[Cu^{II}$-GFA^{2+}-$Cu^{II}]$	$[Cu^{II}$-GFA^{+}-$Cu^{II}]$	$[Cu^{II}$-GFA-$Cu^{II}]$	$[Cu^{II}$-GFA^{+}-$Cu^{II}]$	$[Cu^{II}$-GFA^{2+}-$Cu^{II}]$	GFA
Cu–N_{imine}	1.9985(14)	1.992(3)	1.998(3)	2.0159(18)	2.064(4)	1.963(2)	1.971(3)	1.9533(16)	1.988(2)	1.977	2.000(3)	–
	1.9984(16)	2.059(3)	2.013(3)	2.0165(17)		1.969(2)	1.963(2)	1.9535(16)	1.983(2)		2.001(3)	
N_{imine}=C_{gua}	1.4085(19)	1.311(5)	1.391(5)	1.324(2)	1.383(7)	1.333(3)	1.412(5)	1.371(2)	1.343(3)	1.366(3)	1.403(5)	1.291(2)
	1.4050(18)	1.327(5)	1.405(5)	1.322(2)		1.346(3)	1.386(4)	1.373(2)	1.344(3)		1.400(5)	1.288(2)
C_{gua}–N_{amine}	1.3232(19)	1.363(5)	1.331(5)	1.358(3)	1.328(6)	1.358(4)	1.328(4)	1.328(3)	1.347(3)	1.328(3)	1.336(5)	1.384(2)
	1.325(2)	1.352(5)	1.319(5)	1.364(3)	1.344(7)	1.344(3)	1.333(5)	1.339(3)	1.354(3)	1.346(3)	1.325(4)	1.394(2)
N_{imine}–C_{arom}	1.3370(18)	1.409(5)	1.343(5)	1.415(2)	1.334(6)	1.414(3)	1.313(4)	1.366(2)	1.411(3)	1.367(3)	1.323(4)	1.423(2)
	1.3337(18)	1.413(4)	1.327(4)	1.405(2)			1.340(4)		1.416(3)		1.333(4)	1.414(2)
References	[90]	[91]	[91]	[91]	[91]	[92]	[92]	[92]	[89]	[89]	[89]	[88]

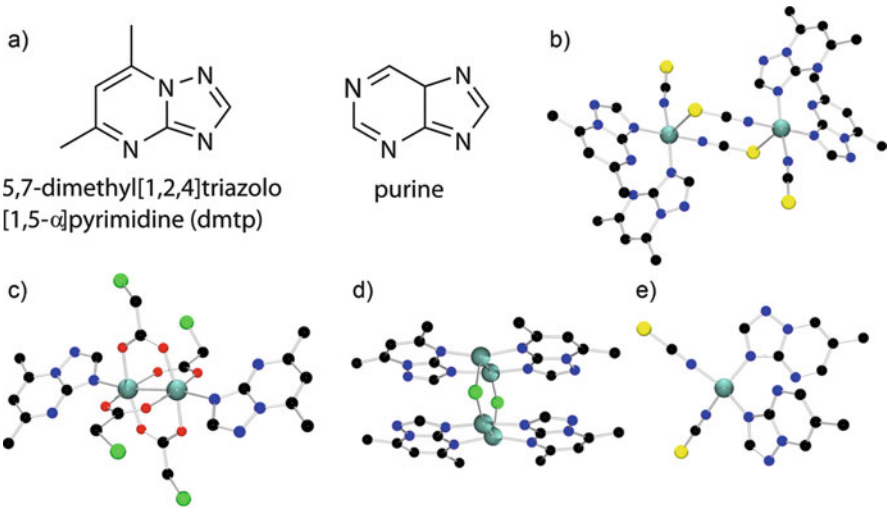

Fig. 25 (**a**) dmtp and its natural model purine, (**b**) molecular structure of $[Cu_2(dmtp)_2(NCS)_2]$, (**c**) molecular structure of $[Cu_2(dmtp)_2(CH_2ClCOO)_4]$, (**d**) molecular structure of $[Cu_4(dmtp)_4Cl_2]$ and (**e**) molecular structure of $[Cu(NCS)_2(6mtp)_2]$

(I) complexes (1.32 Å). All copper(II) complexes with the neutral ttmgb ligand contain guanidine moieties with distinct delocalisation of the Y-aromatic system but with an expanded $N_{imine}{=}C_{gua}$ bond in the range of 1.32–1.34 Å. The N_{amine}–C_{gua} bonds are slightly longer in a comparable range of 1.34–1.36 Å (see Table 16). The one-electron oxidation leads to an inversion of this situation with $N_{imine}{=}C_{gua}$ bond lengths in the range of 1.37 Å and N_{amine}–C_{gua} bonds in the range of 1.33–1.34 Å. The withdrawal of another electron leads to an even more inverted guanidine situation with formal $N_{imine}{=}C_{gua}$ bonds in the range of 1.39–1.41 Å and formal N_{amine}–C_{gua} bonds in the range of 1.31–1.34 Å. Additionally, it can be noted that the N_{imine}–C_{arom} distance decreases with the sequential oxidation of the ligand owing to the delocalisation of the charge into the aromatic ring [89–92]. For detailed information about this kind of complexes and the chemistry behind, the reader is referred to the chapter by Himmel.

2.6 Triazolopyrimidine as Purine Analogue

5,7-Dimethyl[1,2,4]triazolo[1,5-α]pyrimidine is a nitrogen-rich ligand system which includes a guanidine function (in the following abbreviated as dmtp). In 1983, Reedijk and co-workers began to investigate the coordination chemistry of this type of ligand. It has been used as a purine analogue with several advantages in comparison with its natural model (Fig. 25a). One of the pyrimidine N-atoms which provides an additional coordination position in the natural purine framework occupies the bridge-head position in dmtp. Thus, one possibility of coordination is ruled out. Another important feature in contrast to purines is the fact that none of the N donor atoms in dmtp is protonated under neutral or weakly acidic conditions. With its structure, dmtp should mimic the N(3), N(9) coordination of purines, so that the coordination chemistry of nucleic acid fragments could be easily modelled and investigated. Dmtp provides three coordination sites. Due to sterical reasons, the coordination via N(3) is preferred and thus observed in most of the complexes. One of the first crystallised compounds, $[Cu_2(dmtp)_2(NCS)_2]$, contains a dimeric unit of copper centres bridged via two thiocyanates (Fig. 25b). The Cu–N(3) bond lengths are 2.019(8) and 2.000(7) Å. After extensive studies with different metal salts, Reedijk et al. concluded that the coordination chemistry of dmtp essentially depends on the used anion [93–95].

Szlyk et al. used dmtp in the synthesis of an analogous copper(II) chloroacetate complex $[Cu_2(dmtp)_2(CH_2ClCOO)_4]$ (Fig. 25c). Two copper centres are connected by four carboxyl functions of the chloroacetate anions. The coordination sphere around every copper ion contains an axially coordinated dmtp ligand. As usual, the ligand coordinates via N(3). The Cu–N(3) bond length is 2.150(1) Å and thus significantly longer than in the complexes investigated by Reedijk et al. [96].

Besides the complexes described above, dmtp also stabilises complexes in a bridging mode. One example of such a complex is $[Cu_4(dmtp)_4Cl_2]$ (Fig. 25d). This compound includes an interesting complex cation comprising four copper atoms. Two of the metal atoms are connected by the dmtp ligand. Dmtp coordinates with N (3) (Cu–N(3), 1.918 Å) and N(4) (Cu–N(4), 1.965 Å). The Cu–Cu distance is 2.909 Å. Two of such moieties are associated by bridging chlorido anions. The cation could also be crystallised with different anions, such as $[PtCl_4]^{2-}$. Complexes with other halogenido anions could, so far, not be crystallised. Similar spectral properties imply a similar structure of the corresponding complex cation [97].

The group of Reedijk performed coordination studies with differently substituted triazolopyrimidine ligands to investigate the influence of the substituents. Complexes including the ligand 5-ethyl[1,2,4]triazolo[1,5-α]pyrimidin-7-ol revealed good stacking abilities that influence their solid-state structure and magnetic properties [98]. The C5 modification into 5-methyl[1,2,4]triazolo[1,5-α] pyrimidine (5mtp) has only a small influence on the copper(II) coordination chemistry in regard to the unsubstituted [1,2,4]triazolo[1,5-α]pyrimidine (tp). In contrast to that, the C6 modification in 6-methyl [1,2,4]triazolo [1,5-α]pyrimidine (6mtp) gave a much larger effect. $[Cu(NCS)_2(6mtp)_2]$ shows a rather uncommon structure and interesting spectral properties. The central metal is surrounded by two thiocyanates and two 6mtp molecules in a distorted tetrahedron (Fig. 25e). The formal copper(II) complex seems to have a more monovalent character which is also reflected in an intense charge transfer band at approx. 500 nm [99].

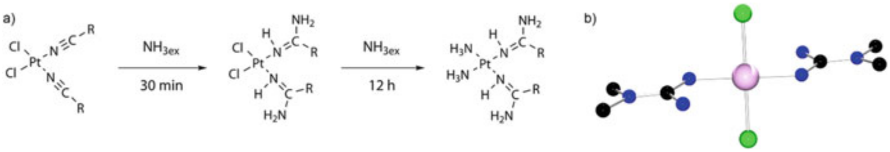

Fig. 26 (**a**) The general synthesis of guanidine platinum complexes and (**b**) *trans*-[Pt(*N*,*N*-DMG)$_2$Cl$_2$], an example for a cytostatic guanidine platinum complex

2.7 Guanidines in Medicinal Complexes

Cisplatin is by far the best-known cytostatic based on a transition metal complex. The compound behind the name cisplatin, *cis*-[Pt(NH$_3$)$_2$(Cl)$_2$], binds to and causes an irreversible structural change in DNA, which triggers the desired apoptosis of malignant cells. The mechanisms behind the cisplatin–DNA interaction seemed to be well understood. Thus, it was not surprising that the cytotoxicity of the analogous *trans*-[Pt(NH$_3$)$_2$(Cl)$_2$] is significantly lower. Nevertheless, several exceptional Pt complexes were found that exhibit a higher cytotoxicity when their leaving groups occupy the *trans*-positions in the ligand sphere. The mechanism behind the effect of Pt-based cytostatics thus seems not completely clear. This and several side effects in the medical application of cisplatin are reasons for constant research on new transition metal and especially Pt-based cytostatics. The teams around Bokach and Kukushkin screened multiple Pt guanidine complexes with regard to their cytotoxicity. Several complexes have been synthesised (Fig. 26) [100]. In contrast to *cis*-[Pt(NH$_3$)$_2$(Cl)$_2$] and *trans*-[Pt(NH$_3$)$_2$(Cl)$_2$], some *trans*-complexes were found by these groups and Keppler that possess significantly higher cytotoxicity than their *cis*-congeners. *Trans*-complexes revealed a higher accumulation than the respective *cis*-complexes. This could be another reason for their increased cytotoxicity [101].

Additionally, Karvembu et al. recently developed guanidine-containing bioactive complexes. Copper(II) is of special importance as central metal because of its biocompatibility. The group of Karvembu screened different copper(II) complexes with trisubstituted guanidine ligands (example in Fig. 27) with respect to their DNA and protein interaction. Their cytotoxicity in vitro also has been investigated. Spectroscopic measurements gave indication about a non-covalent intercalative DNA interaction. A good protein binding ability was revealed by fluorescence spectroscopy. The cytotoxicity study stands in contrast with the results from the DNA interaction assay, which leads to the assumption that the cytotoxic activity proceeds differently [102].

2.8 Bicyclic Guanidines

1,3,4,6,7,8-Hexahydro-2*H*-pyrimido[1,2-*α*]pyrimidine (hpp) represents an interesting class of guanidine ligands. Coles and co-workers were the first to use this kind

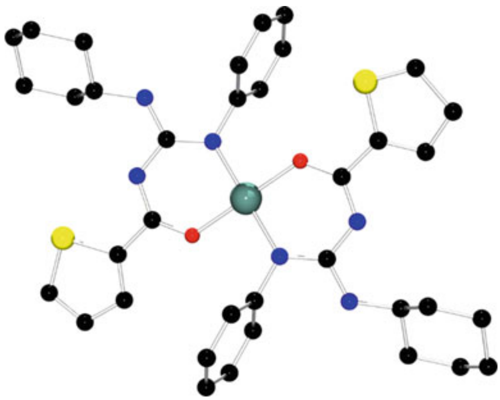

Fig. 27 Example for a complex containing trisubstituted guanidine ligands

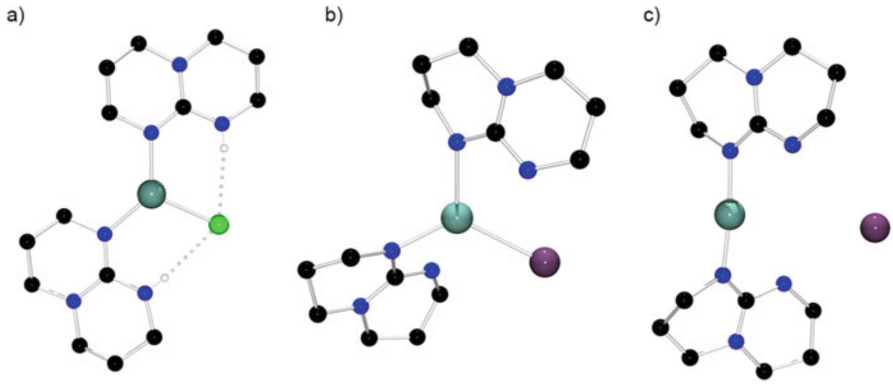

Fig. 28 (**a**) Molecular structure of [Cu(hppH)$_2$Cl], (**b**) [Cu(hppH)$_2$I] and (**c**) with ion pair of [Cu (hppH)$_2$]I

of ligand to stabilise copper(I) cyanide structures [103]. Before that, the protonated derivative hppH has never been used as a neutral ligand. The complex [Cu (hppH)$_2$Cl] was structurally and spectroscopically examined and additionally tested as catalyst in ATRP (see Sect. 3.2). The complex includes some interesting structural features that seem worth mentioning (Fig. 28).

The central metal is surrounded by two hppH ligands coordinating via N_{imine} and an additional chlorido anion completing the trigonal planar coordination sphere. Two additional hydrogen bridges enhance the stability of this complex. The complex molecule of [Cu(hppH)$_2$Br] exhibits a similar structure, whereas [Cu(hppH)$_2$I] crystallises differently. In this complex, the unit cell contains both complex molecules with a Cu bond (Fig. 28b) and ion pairs composed of a complex cation and an iodine anion (Fig. 28c). There are no additional hydrogen bridges stabilising this type of structure [104].

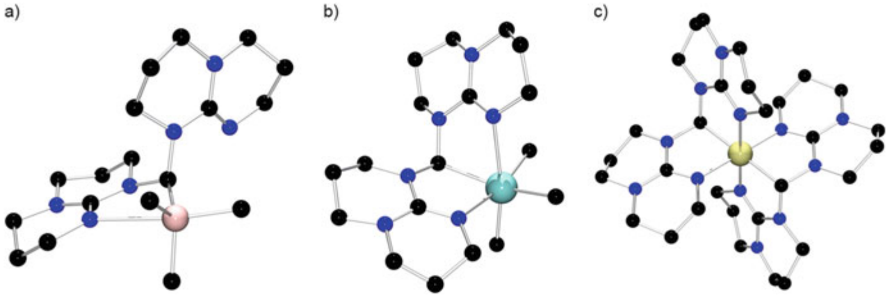

Fig. 29 (**a**) Molecular structures of HC{$SiMe_3$}{hpp}$_2$, (**b**) [Sn(CH{hpp}$_2$)Me_3] and (**c**) [Al(HC{hpp}$_2$)$_2$]$^+$ in crystals of [Al(HC{hpp}$_2$)$_2$][$AlCl_4$]

Further studies elucidated sterical and electronic factors influencing the bonding of hppH compared to the well-established PPh_3 ligand. With the replacement of a single hppH by PPh_3 in [Cu(hppH)$_2$Cl], a shortening of the Cu–Cl bond from 2.40 to 2.21 Å was observed. Compared to PPh_3, hppH seems to be the stronger donor [18]. In the following, the influence of the hydrogen bridges described previously was further investigated by the synthesis of the hppH derivatives hppMe and hppSiMe and their copper complexes [105].

In further work, the group of Coles developed compounds with two or three hpp moieties combined within one ligand. With Me_2Si\{hpp\}$_2$ and H_2C\{hpp\}$_2$, they obtained copper chelate complexes such as [Cu(H_2C\{hpp\}$_2$)Cl] and [Cu(Me_2Si\{hpp\}$_2$)Cl]. Complexes of an analogous MeSi\{hpp\}$_3$ could not be obtained so far. In comparison with [Cu(hppH)$_2$Cl], [Cu(H_2C\{hpp\}$_2$)Cl] shows many similarities. In [Fe(hppH)$_2Cl_2$], hydrogen bonds again play an important role in determining the structure of the complex molecule. The molecular structure of [Fe(H_2C\{hpp\}$_2$)Cl_2] is analogous to the structure of [Cu(H_2C\{hpp\}$_2$)Cl] except that there is an additional chlorido anion coordinated. In palladium(II) complexes, a square planar coordination sphere could also be stabilised by H_2C\{hpp\}$_2$. The bis(guanidine) ligand H_2C\{hpp\}$_2$ can stabilise trigonal planar, tetrahedral and square planar complexes [106, 107]. H_2C\{hpp\}$_2$ also can serve as a *N*,*C*,*N*′-pincer ligand as demonstrated by Coles and co-workers in 2014. Reaction of the ligand firstly with *t*BuLi and then with $SiMe_3Cl$ or $SnMe_3Cl$ yields the complexes shown in Fig. 29.

HC\{$SiMe_3$\}\{hpp\}$_2$ includes a pentacoordinated silicon atom with four participating Si–C interactions and an additional Si–N_{imine} interaction. In [Sn(CH\{hpp\}$_2$)Me_3], the Sn atom is coordinated by the pincer ligand in a pseudo-facial manner and three additional methyl groups. The coordination sphere can be better described as a bicapped tetrahedron. The complex cation of the analogous aluminium complex [Al(HC\{hpp\}$_2$)$_2$][$AlCl_4$] is depicted in Fig. 29c. The authors reported it as the first six-coordinate organoalumocenium cation [108].

The bulky silyl-substituted hpp ligand (C\{$SiMe_3$\}$_2$\{$SiMe_2$hpp\})$^-$ developed in 2007 yielded a number of main-group metal and mercury complexes depicted in

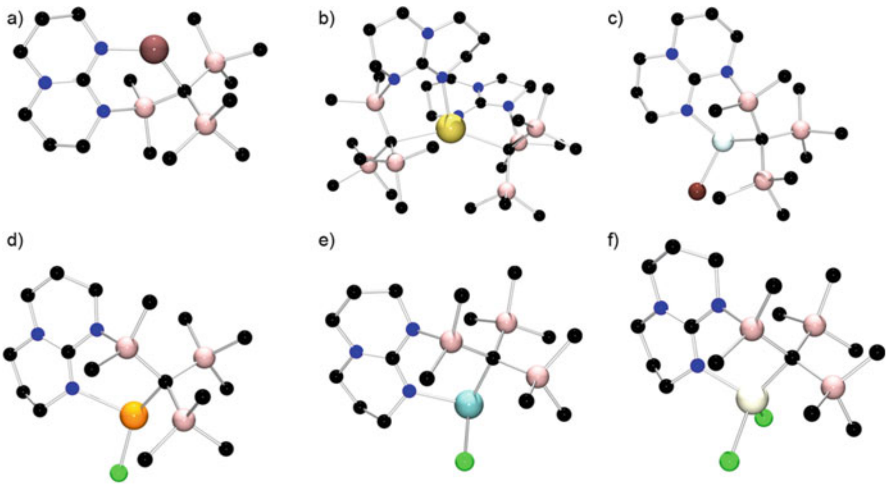

Fig. 30 Molecular structures of main-group metal and mercury complexes including (C{$SiMe_3$}$_2${$SiMe_2$hpp}): (**a**) Li(C{$SiMe_3$}$_2${$SiMe_2$hpp}), (**b**) Ca(C{$SiMe_3$}$_2${$SiMe_2$hpp})$_2$, (**c**) Zn(C{$SiMe_3$}$_2${$SiMe_2$hpp})Br of the dimer {Zn(C{$SiMe_3$}$_2${$SiMe_2$hpp})Br}$_2$, (**d**) Hg(C{$SiMe_3$}$_2${$SiMe_2$hpp})Cl, (**e**) Sn(C{$SiMe_3$}$_2${$SiMe_2$hpp})Cl and (**f**) In(C{$SiMe_3$}$_2${$SiMe_2$hpp})Cl_2

Fig. 30 [109–112]. With zinc, bromido-bridged binuclear complexes and extended clusters are also known.

2.9 *Azoimidazole Ligands*

The combination of nitrogen-rich organic compounds often leads to the formal construction of a guanidine system. The attachment of azo groups at imidazole yields so-called azoimidazole ligands containing a guanidine moiety and the azo group as an additional donor function. This class of ligands is synthesised by coupling of imidazole with substituted phenyl- or β-naphtyldiazoniumions in an aqueous solution of sodium carbonate. Subsequent alkylation of the imidazole unit generates a broad library of azoimidazole ligands. The group of Sinha investigated this new class of ligands in platinum and copper coordination chemistry. [Pt(β-NaiEt)Cl_2], for example, is a platinum mono(chelate) complex containing one β-NaiEt ligand and two chlorido anions in a square planar coordination sphere (Fig. 31a) [113].

In combination with Cu(I) perchlorate, the same group synthesised a complex containing two β-NaiEt ligands preferentially coordinated by N_{imine} (Cu–N_{imine} 1.851 Å). The central metal and N_{Azo} possess a loose contact (Cu–N_{Azo} 2.655 Å), so that the copper is coordinated in an almost linear manner (Fig. 31b). The analogous complex bis[1-methyl-2-(naphthyl-α-azo)imidazole] copper perchlorate contains a

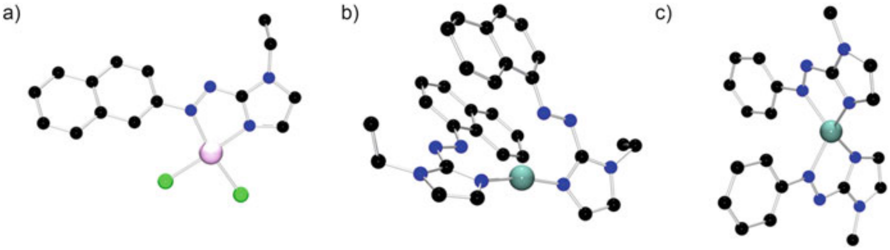

Fig. 31 (**a**) Molecular structure of [Pt(β-NaiEt)Cl_2], (**b**) and (**c**) comparison of the molecular structure of copper complexes containing structurally different azoimidazole ligands

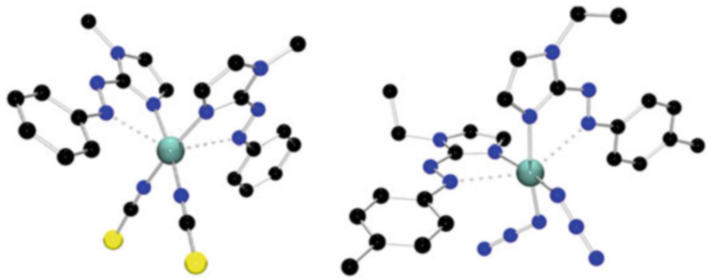

Fig. 32 Azoimidazole complexes containing additional pseudohalide ligands

sterically less demanding ligand. The azoimidazoles form a bis(chelate) under formation of five-membered metallacycles (Fig. 31c). The distances between copper and both N_{imine} and N_{Azo} are almost identical (Cu–N_{imine} 2.004 Å, Cu–N_{Azo} 2.021 Å) [114].

Sinha et al. also synthesised copper(II) complexes containing the pseudohalide azide and thiocyanate. Both octahedral complexes contain two pseudohalide anions in a *cis*-fashion (Fig. 32). The rest of the coordination sphere is occupied by two azoimidazole ligands. The equatorial plane is formed by the N_{imine} atoms and the pseudohalides. Very different Cu–N distances for N_{imine} and N_{Azo} (Cu–N_{imine} ca. 2.0 Å, Cu–N_{Azo} ca. 2.7 Å) lead to a distortion of the formed metallacycle and the octahedron. Both the large difference between the Cu–N distances in the complexes just described and the almost linear Cu–N_{imine} coordination in the complexes described earlier lead to the assumption that N_{imine} represents the stronger donor [115].

Using copper(II) azide, tetranuclear complexes were also synthesised and investigated structurally and magnetically [116]. Incorporation of an additional donor, in this case a thioether functionality, enables access to five-coordinated complexes like 1-alkyl-2-{(*o*-thioalkyl)phenylazo}imidazole copper(II) chloride. The objective was to develop a ligand that can stabilise both copper(I) and copper (II) complexes [117].

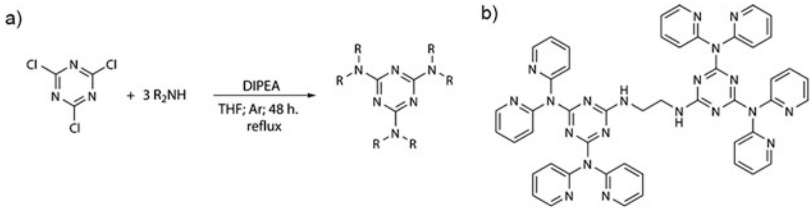

Scheme 7 (**a**) The general synthesis of polydentate guanidine ligands starting from 2,4,6-trichloro-1,3,5-triazine and (**b**) example for a bridged polydentate triazine ligand

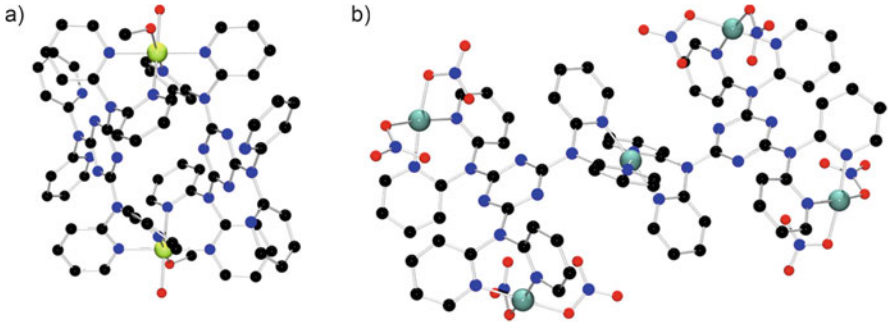

Fig. 33 (**a**) A nickel and (**b**) a copper complex containing the N^2,N^2,N^4,N^4,N^6,N^6-hexa(pyridin-2-yl)-1,3,5-triazine-2,4,6-triamine ligand

2.10 Triazine-Based Guanidine Ligands

A new class of polydentate ligands containing the guanidine functionality was developed by Reedijk et al. in 2002. The ligands are based on a 1,3,5-triazine scaffold. Starting from 2,4,6-trichloro-1,3,5-triazine, the sequential substitution of chlorido units by simple amines yields a large library of new polydentate ligands. The basic reaction and reaction conditions are shown in Scheme 7a. By adjustment of the reaction conditions, it is also possible to synthesise bidentate ligands. The conjunction of two of such units with bridging amines leads to complex polydentate compounds (example given in Scheme 7b) [118].

The new ligands described above were used in complex syntheses with nickel and copper. The copper complexes were tested in the catalysed oxidation of 3,5-di-*tert*-butylcatechol. With nickel(II) perchlorate hexahydrate, crystals of $[Ni_2(N^2,N^2,N^4,N^4,N^6,N^6\text{-hexa(pyridin-2-yl)-1,3,5-triazine-2,4,6-triamine})_2(H_2O)_2(MeOH)_2](ClO_4)_4(MeOH)_6$ (Fig. 33a) were obtained. The two ligands coordinate in a bidentate bridging manner and connect two nickel ions. The slightly disordered octahedral coordination sphere is completed by a methanol molecule and a water molecule. An additional metal coordination seems possible due to the fact that both N^2,N^2,N^4,N^4,N^6,N^6-hexa(pyridin-2-yl)-1,3,5-triazine-2,4,6-triamine ligands have

Fig. 34 A mixed-valent $Cu^{II}{}_4Cu^{I}$ complex containing 1,3,5-triazine ligands

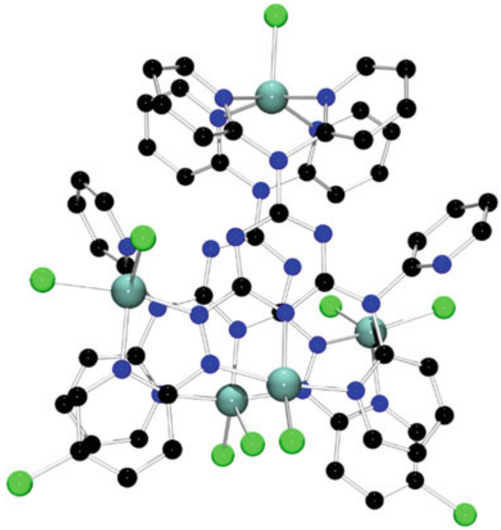

another unoccupied coordination site. The central guanidine moieties are not involved in coordination.

Analogous copper(II) complexes form one-dimensional ladderlike structures (Fig. 33b shows one building block or "rung" of this ladder). Here again, the guanidine moieties are not involved in coordination. Different complexes were tested in the oxidation of 3,5-di-*tert*-butylcatechol and showed catalytic activity [119, 120]. In further studies, Reedijk and co-workers have shown that the complex architecture strongly depends on the reaction conditions. The crystallisation solvent had an influence on whether mononuclear or trinuclear complexes of *N*,*N*′-{2,4-di-[(di-pyridin-2-yl)amine]-1,3,5-triazine}ethylene diamine with zinc(II) nitrate would be obtained [121]. In 2008, the group of Reedijk published a new ligand system based on 1,3,5-triazine. The new ligand includes a pyrazolyl–pyridine moiety for copper coordination and a TEMPO radical unit. The aim was to develop an ecologically friendly catalyst for the aerobic oxidation of primary alcohols to the corresponding aldehydes [122].

In the mixed-valent $Cu^{II}{}_4Cu^{I}$ complex shown in Fig. 34, 1,3,5-triazine ligands coordinate with their central triazine/guanidine site. A copper(II)-mediated one-electron oxidation and deprotonation of the ligand leads to an azo radical anion, which contains a typical N–N bond length of 1.33 Å. This results in a remarkable radical anion ligand. The complexes have been comprehensively studied by various analytical methods [123].

Ligands containing an additional thioether coordination site also showed triazine/guanidine coordination. The ligands are depicted in Fig. 35a and b, examples of a corresponding complex in Fig. 35c–e. It is worth mentioning that one of the bromido ligands in [Cu(2-chloro-4,6-bis-*N*-[2-methylsulfanyl-*N*-(pyridin-2-ylmethyl)aniline]-1,3,5-triazine)] is in close contact to the central electron-poor

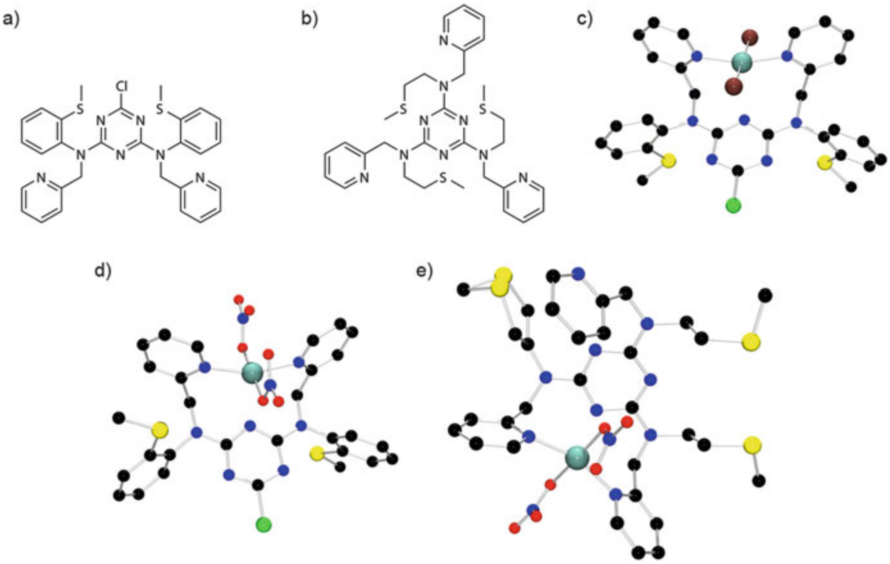

Fig. 35 (**a**) and (**b**) Triazine ligands with additional thioether coordination sites, (**c**)–(**e**) complexes including different triazine–thioether complexes

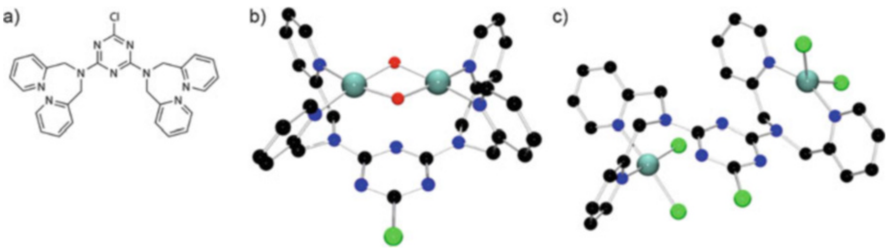

Fig. 36 (**a**) 2-Chloro-4,6-bis(di-2-picolylamino)-1,3,5-triazine, (**b**) The copper(II) perchlorate and (**c**) the copper(II) chloride complex of 2-chloro-4,6-bis(di-2-picolylamino)-1,3,5-triazine

triazine ring. It should also be noted that the relatively small distance between the bromido ligand can be enforced by geometrical restrictions [124].

Massoud et al. investigated structural, magnetic and DNA cleavage properties of copper(II) complexes with the bisguanidine ligand 2-chloro-4,6-bis(di-2-picolylamino)-1,3,5-triazine (Fig. 36a). With copper(II) perchlorate hexahydrate and copper(II) chloride dihydrate, they obtained two compounds that were studied comprehensively (Fig. 36b and c). Di-μ-hydroxido $[Cu_2(\mu bdpaT^{Cl})(\mu\text{-}OH)_2\text{-}(H2O)_{0.5}(ClO_4)_{0.5}](ClO_4)_{1.5}\cdot(H_2O)_{1.5}$ is a dimeric copper complex containing two bridging hydroxido ligands. In $[Cu_2(\mu\text{-}bdpaT^{Cl})Cl_4],\cdot 2CH_3OH$ bdpaT^{C} itself acts as a binucleating bridging ligand. The two complexes show different magnetic and electrochemical properties. The chlorido complex is a moderately active

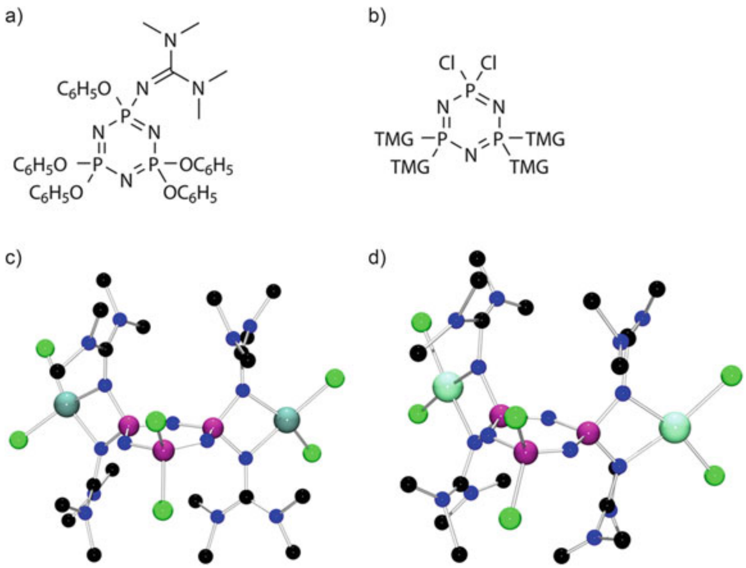

Fig. 37 (**a**) The cyclotriphosphazene ligands 2-(*N*,*N*,*N*′,*N*′-tetramethylguanidine)-2,4,4,6,6-pentaphenoxy-2 λ5,4 λ5,6 λ5-cyclotriphosphaza-1,3,5-trien, (**b**) 2,2-dichlor-4,4,6,6-tetra-(*N*,*N*,*N*′,*N*′-tetramethylguanidine)-2 λ5,4 λ5,6 λ5-cyclotriphosphaza-1,3,5-trien, (**c**) molecular structures of the copper(II) and (**d**) palladium(II) complex of 2,2-dichlor-4,4,6,6-tetra-(*N*,*N*,*N*′,*N*-′-tetramethylguanidine)-2 λ5,4 λ5,6 λ5-cyclotriphosphaza-1,3,5-trien

nuclease, whereas the μ-hydroxido shows no DNA cleavage activity. The strong magnetic coupling between the two copper centres mediated by the hydroxido ligands seems to play a fundamental role in inhibiting its reactivity [125].

2.11 Further Coordination Chemistry with Guanidine Ligands

The following section deals with further interesting coordination chemistry with guanidine ligands.

Diefenbach and Bloy synthesised and investigated cyclotriphospazenes with additional tetramethylguanidine groups. The reaction of monochloropentaphenoxycyclotriphosphazene with *N*,*N*,*N*′,*N*′-tetramethylguanidine in dioxane yields 2-(*N*,*N*,*N*′,*N*′-tetramethylguanidine)-2,4,4,6,6-pentaphenoxy-2 λ5,4 λ5,6 λ5-cyclotriphosphaza-1,3,5-trien (Fig. 37a). Attempts to synthesise an analogous hexasubstituted cyclotriphosphazene derivative failed so far. The tetrasubstituted 2,2-dichlor-4,4,6,6-tetra-(*N*,*N*,*N*′,*N*′-tetramethylguanidine)-2 λ5,4 λ5,6 λ5-cyclotriphosphaza-1,3,5-trien was obtained instead (Fig. 37b).

The tetraguanidine ligand has been used in complex synthesis with $CuCl_2$ and Pd $(CH_3CN)_2Cl_2$ (Fig. 37c and d). The ligand connects two square planar metal

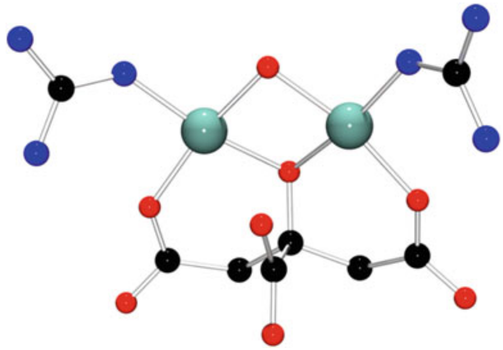

Fig. 38 The complex system [GuH][Cu_2(OH)(cit)$(Gu)_2$] studied by Parsons et al.

centres, and the coordination spheres are completed by the corresponding anion ligands. The square planar coordination spheres of the copper complex exhibit a distinct tetrahedral distortion. Geometrical restrictions lead to distorted bond angles within the metallacycles and exceptional short Cu–P distances of 2.763(4) and 2.778(4) Å. The analogous Pd complex has not been further discussed due to unsatisfactory crystal quality [126].

In 2009, Parsons et al. performed high pressure experiments with the copper (II) guanidine complex [GuH][Cu_2(OH)(cit)$(Gu)_2$] (Fig. 38). Under increased pressure, the Cu(II) dimer polymerises into one-dimensional chains [127].

Experiments by Knipp and co-workers had a more biochemical background. In 2012, they mutated the heme protein nitrophorin 4 (NP4) in *Rhodnius prolixus*, a bloodsucking parasite. They chose to mutate Leu130 under the assumption that this alteration has no significant influence on the folding of NP4. The original leucine was replaced by arginine, an amino acid containing a guanidine function. The incorporation took place in proximity to the ferroheme centre of the protein, which demonstrates the principal possibility for guanidine ferroheme coordination. There are only few arginine metal interactions known in nature and even fewer arginine iron coordination examples. This is due to the reason that arginine typically occurs protonated. In the L130R mutant of NP4, an iron coordinated by Arg130 with an interatomic distance of 2.1 Å could be observed. This implies a strong interaction between the donor and metal centre. Furthermore, it seems to be the first arginine–ferroheme interaction ever observed. The special environment provided by the ferroheme cavity in NP4 might be one of the reasons why arginine serves as a ligand in this context [128].

Siemeling and co-workers not only combined N-heterocyclic carbenes with a non-coordinating guanidine moiety [129], but they also developed ferrocene-based bisguanidine ligands. Such ligands can be easily obtained starting from 1,1′-diaminoferrocene and suited chloroformamidinium chlorides. The molecular structure of such a ligand and its hydrated form are shown in Fig. 39. The molecular structure of the palladium complex *trans*-[PdCl(1,1′DiTMG-ferrocene $\kappa Fe,\kappa^2 N$)$]_2$[$PdCl_4$] is shown in Fig. 39c. The distance between iron and palladium is 2.714(1) Å and is ascribed to a weak dative Fe → Pd bond. Therefore, this class of

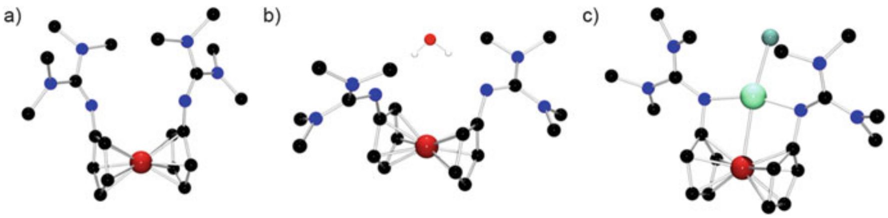

Fig. 39 (**a**) The molecular structure of a 1,1′diguanidinoferrocene ligands, (**b**) the same ligands hydrated and (**c**) the molecular structure of *trans*-[PdCl(1,1′DiTMG-ferrocen $\kappa Fe,\kappa^2 N$)]$_2$[PdCl$_4$]

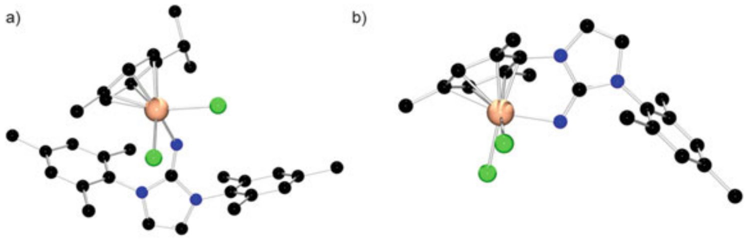

Fig. 40 (**a**) Example for a complex of the type [Ru(*p*-cymene)LCl$_2$] before and (**b**) after the reaction under the influence of UV light

ligands seem to act as tridentate ligands that provide two strong guanidine donors and an additional weak Fe donor. The inserted guanidine function alters the electrochemical behaviour of the ferrocene system dramatically. In 1,1′-diTMG-ferrocene, for example, the ferrocene-based half-wave is found at −0.68 V vs ferrocenium/ferrocene. The cyclovoltammetric measurement of the palladium-centred transition results in decomposition of the majority of the complexes [130].

Coordination chemistry with late transition metals was conducted by the group of Severin. For their studies, they synthesised several imidazolin-2-imine and imidazolidin-2-imine ligands. When reacted with [Ru(*p*-cymene)Cl$_2$]$_2$, mononuclear complexes of the type [Ru(*p*-cymene) LCl$_2$] were obtained (example shown in Fig. 40a). Under the influence of UV light, these compounds lose *p*-cymene to give complexes in which one of the aryl groups acts as a π-ligand (Fig. 40b) [131].

Recent investigations by Stavropoulos et al. resulted in copper(I) guanidine complexes as catalysts that mediate nitrene transfer from corresponding precursors to aliphatic hydrocarbons and olefins. The ligand used was TMG$_3$trphen. The molecular structure of the complex cation [Cu(TMG$_3$trphen)]$^+$ is shown in Fig. 41. The catalyst shows a wide substrate range and product yields that are comparable with those reported for Rh and Ru catalysts. Comprehensive mechanistic studies have also been carried out. They gave hints that the mechanism differentiates from that of the rhodium-mediated nitrene transfer. Hammett correlations support a mechanism where carboradicals generated by H atom abstraction play a crucial role [132].

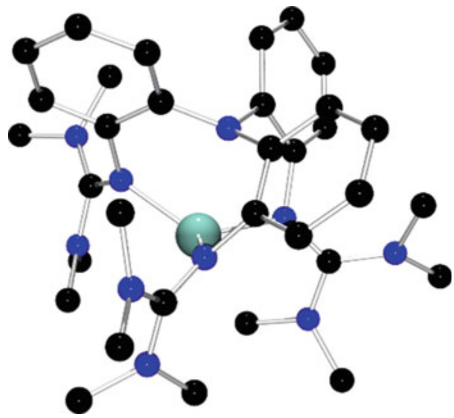

Fig. 41 The complex cation $[Cu(TMG_3trphen)]^+$ of the catalyst $[Cu(TMG_3trphen)][PF_6]$ used by Stavropoulos et al.

3 Guanidines in Transition Metal Polymerisation Catalysis

3.1 Ring-Opening Polymerisation (ROP) of Lactide with Zinc Guanidine Complexes

Polylactide (PLA) is an aliphatic, biodegradable polyester which can be produced from renewable resources such as corn, sugar beets, corn straw or agricultural waste [133, 134]. The polymer can be manufactured to plastics similar to conventional materials such as poly(ethylene terephthalate) (PET) or poly(propylene) (PP) [135–137]. These excellent properties raise the interest in new ecologically friendly catalysts for polylactide synthesis. PLA has found application in many fields, for example, in food packaging, in medical implants and in agricultural areas [138, 139]. Producing biodegradable polymers from renewable raw materials will reduce the use of fossil resources and decrease the accumulation of waste in future.

Polylactide can be synthesised from lactide by ring-opening polymerisation (ROP). The cyclic diester lactide is produced from lactic acid which is obtained from bacterial fermentation of a carbohydrate feed. After use, PLA can be either recycled, combusted or composted. Thus, the CO_2 emission in relation to the starting materials is neutral [136–151].

3.1.1 Coordination–Insertion Mechanism

There are different mechanisms for polylactide synthesis. Polycondensation and addition reactions, for example, are uncontrolled polymerisation reactions. In these, high temperatures and long reaction times are necessary. Furthermore, the lack of kinetic control generates polymers with a high polydispersity and rather short

Scheme 8 Coordination–insertion mechanism

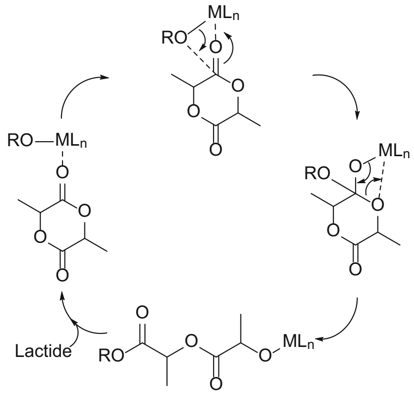

polymer chains [141, 144–151]. During the last decades, many new ROP processes have been developed. Cationic, anionic, organocatalytic and coordination–insertion mechanisms are considered as controlled chain growth polymerisation reactions. Since the coordination–insertion mechanism is controlled with regard to molecular weight, microstructure and composition, it is regarded as the most efficient process for ring-opening polymerisation of lactide. The polymerisation can be conducted under living conditions, and the absence of ionic intermediates excludes racemisation processes [141, 144–151].

The reaction is initiated by coordination of an exocyclic oxygen atom of a lactide monomer to the metal centre of a catalyst complex. Afterwards, a nucleophilic attack of the alkoxide on the acyl carbon atom and an insertion of lactide into the metal alkoxide species with retention of configuration take place (Scheme 8) [141, 144–151].

Nowadays, mostly homoleptic catalysts are being used, such as tin (II) ethylhexanoate, zinc(II) lactate and aluminium isopropoxide [152–154]. These are used in combination with initiators such as benzyl alcohol. Due to side reactions like transesterification and epimerisations, which lead to broad molar mass distribution, new single-site metal catalysts are of high interest [133–139, 141, 144–151, 155]. As an advantage, this class of catalysts can initiate and catalyse the reaction at the same time. Therefore, they should exhibit great control, activity and selectivity during the polymerisation. As a result, the research and development of single-site catalysts for the ring-opening polymerisation of lactide increases substantially. The ideal catalyst is nontoxic, tolerant towards air, lactide melt and acidic impurities in the monomer. Furthermore, it should be cheap, colourless and odourless [141, 144–151].

A variety of catalysts for ROP reactions of lactide are already known. Most complexes contain zinc, tin, magnesium or aluminium as metal centres and anionic ligands such as thiolates, aminates, salens, ß-ketiminates, alkoxides and carboxylates [156–167]. Most of these catalysts exhibit good activity in the ROP of lactide. As a major disadvantage, the anionic ligands render their complexes very sensitive towards air, moisture and impurities. Although these complexes often exhibit a high

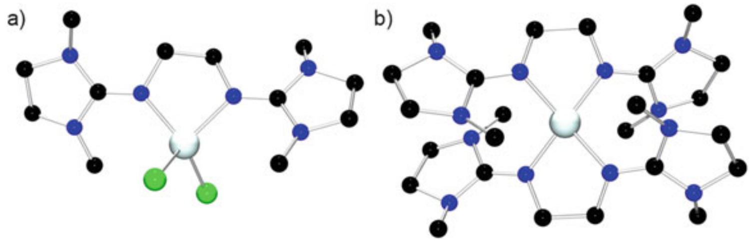

Fig. 42 Molecular structure of (**a**) [Zn(DMEG$_2$e)Cl$_2$] and (**b**) [Zn(DMEG$_2$e)$_2$]$^{2+}$ in crystals of [Zn(DMEG$_2$e)$_2$][OTf]$_2$ [32]

activity, they are mostly not suitable for industrial use [133, 134, 140–151]. In contrast to the poor properties of anionic ligands in ROP, a small number of neutral ligands are less sensitive towards impurities, air and moisture and stabilise ROP active complexes [165]. Here, especially guanidines have been found to stabilise very robust zinc complexes with high ROP activity.

3.1.2 Zinc Guanidine Complexes

Guanidines possess a large Lewis basicity and good donor properties – both features are crucial for efficient ROP catalysis [27, 28, 135]. The large variety of fully characterised guanidine ligands comprises different modifications on each of the nitrogen atoms.

In 2007, the first cationic, bis(chelate) complex [Zn(DMEG$_2$e)$_2$][OTf]$_2$ which is active in the ROP of lactide in melt was reported (Fig. 42) [32]. The angles between the chelate planes of this complex indicate a coordination between tetrahedral and square planar geometry. At 150°C, polymers with molecular weights around 24,000 g/mol could be obtained within 24 h [32]. Besides bis(chelate) zinc triflato complexes, complexes with chloride and acetate anions ([Zn(DMEG$_2$e)Cl$_2$] and [Zn(DMEG$_2$e)OAc$_2$]) were synthesised and successfully tested in the ROP. ROP studies of these complexes in lactide melt yielded polymers with molar masses between 18,000 and 59,000 g/mol. It was further found that the catalytic performance of these complexes strongly depends on the anionic component of the zinc salt. Complexes with chloride or bis(triflate) anions showed an improved catalytic activity compared to acetato complexes.

The basicity of the ligand is important for the ROP catalysis. Thus, the complexes [Zn(8MeBL)Cl$_2$] and [Zn(8MeBL)(OAc)$_2$] bearing a more basic imino imidazoline ligand 8MeBL have been tested as well [137]. It was found that the partial charge on the zinc atom and on the donating N_{imine} atom is very important for lactide polymerisation activity (Fig. 43) [137, 168]. Polymerisations with complexes [Zn(8MeBL)Cl$_2$] and [Zn(8MeBL)(OAc)$_2$] yielded PLA polymers with molecular weights of 25,000 and 12,000 g/mol at a conversion of around 90% (Table 18).

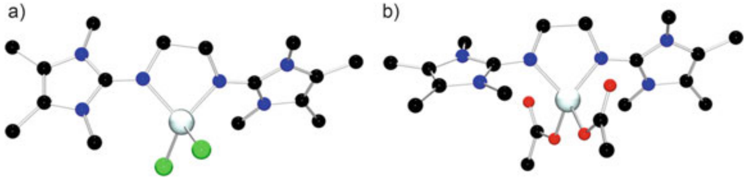

Fig. 43 Molecular structure of (**a**) [Zn(8MeBL)Cl_2] and (**b**) [Zn(8MeBL)$(OAc)_2$] [137]

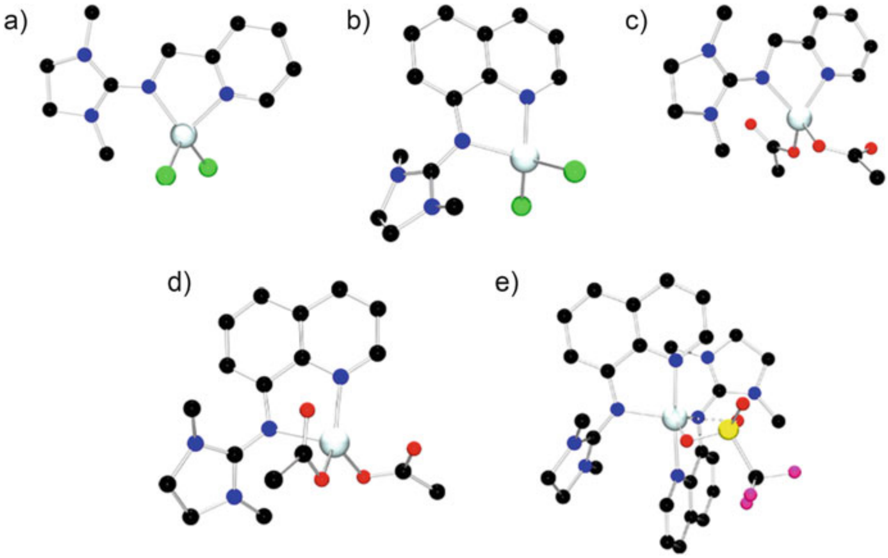

Fig. 44 Molecular structures of (**a**) [Zn(DMEGpy)Cl_2], (**b**) [Zn(DMEGqu)Cl_2], (**c**) [Zn(DMEGpy)$(OAc)_2$], (**d**) [Zn(DMEGqu)$(OAc)_2$] and (**e**) [Zn$(DMEGqu)_2$(CF_3SO_3)][CF_3SO_3] [168]

The aromatic guanidine ligands discussed in Sect. 2.3 [73] have been used in reactions with zinc chloride, acetate or triflate for subsequent polymerisation studies (Table 18) [168]. The resulting complexes were investigated in ROP reactions, where picolylamine-based zinc chlorido catalysts exhibited a higher polymerisation activity than comparable quinoline-based zinc chlorido complexes (Fig. 44) [168]. Furthermore, complexes with a coordinated pyridine ligand containing chlorido ligands show a much higher catalytic activity than those which contain acetate instead of chloride. If the complexes contain quinoline ligands, then it is the other way round. However, the highest activity for the polymerisation of lactide is achieved with quinoline complexes containing triflate ([Zn$(DMEGqu)_2$(CF_3SO_3)][CF_3SO_3] and [Zn$(TMGqu)_2$(CF_3SO_3)][CF_3SO_3]). Molecular weights up to 176,000 g/mol could be obtained.

In the chlorido and acetato complexes, the zinc centre is four-coordinate. The Zn–N bond lengths of the two nitrogen donor atoms differ slightly with no obvious

Table 17 Selected bond lengths of [Zn(DMEGpy)Cl_2], [Zn(DMEGqu)Cl_2], [Zn(DMEGpy)($CH_3COO)_2$], [Zn(DMEGqu)($CH_3COO)_2$] and [Zn(DMEGqu)$_2$(CF_3SO_3)][CF_3SO_3] [168]

	[Zn (DMEGpy) Cl_2]	[Zn (DMEGqu) Cl_2]	[Zn (DMEGpy) $(OAc)_2$]	[Zn (DMEGqu) $(OAc)_2$]	[Zn (DMEGqu)$_2$(CF_3SO_3)] [CF_3SO_3]
Zn–N_{py}	2.047(1)	2.045(1)	2.036(2)	2.048(1)	2.089(3), 2.091(3)
Zn–N_{gua}	2.036(1)	2.039(1)	2.038(2)	2.106(1)	2.035(3), 2.049(3)
C_{gua}=N_{gua}	1.317(2)	1.327(2)	1.313(2)	1.336(2)	1.357(5), 1.342(5)
C_{gua}–N_{amine}	1.375(2)	1.355(2)	1.367(2)	1.336(2)	1.329(5), 1.352(5)
	1.362(2)	1.352(2)	1.348(2)	1.364(2)	1.344(5), 1.338(5)
ρ	0.96	0.98	0.97	0.99	1.00

Table 18 Results of the ROP of lactide with zinc guanidine complexes

Catalyst	*t* (h)	Conversion (%)	M_n (g/mol)	*PD*	P_r [a]	References
[Zn($DMEG_2e$)$_2$][OTf]$_2$	24	83	24,000	1.6	n.d.	[32]
[Zn($DMEG_2e$)Cl_2]	24	79	22,000	1.7	0.50	[32]
[Zn($DMEG_2e$)OAc_2]	24	69	15,000	1.6	0.50	[32]
[Zn(8MeBL)Cl_2]	24	85	25,000	2.0	0.53	[137]
[Zn(8MeBL)OAc_2]	24	88	12,000	2.0	0.50	[137]
[Zn(TEGqu)Cl_2]	48	17	16,000	2.0	0.55	[15]
[Zn(DMorphGqu)Cl_2]	24	51	30,000	1.6	0.57	[15]
[Zn(MorphDMGqu)Cl_2]	24	72	31,000	1.8	0.56	[15]
[Zn(TMGqu)OAc_2]	48	41	9,000	2.1	n.d.	[168]
[Zn(DMEGqu)OAc_2]	48	58	9,000	2.0	n.d.	[168]
[Zn(DMPGqu)OAc_2]	48	60	19,000	1.8	n.d.	[15]
[Zn(DMorphGqu)OAc_2]	48	51	15,000	1.7	0.49	[15]
[Zn(MorphDMGqu)OAc2]	48	29	13,000	1.7	0.49	[15]
[Zn(DMEGqu)$OMes_2$]	48	0	–	–	–	[169]
[Zn(TMGqu)$_2$(OMes)] [OMes]	48	33	18,000	1.6	n.d.	[169]
[Zn(TMGqu)$_2$(OTf)][OTf]	24	93	70,000	2.2	n.d.	[168, 170]
[Zn(DMEGqu)$_2$(OTf)][OTf]	24	92	77,000	2.1	n.d.	[168, 170]
[(TMG_4(baem)$_2$b)($ZnCl_2$)$_2$]	24	81	19,000	1.9	0.54	[171]
[Zn(TMG_3tren)(Cl)][Cl]	24	71	12,000	1.9	0.52	[171]
[Zn($DMEG_3$tren)(Cl)][Cl]	24	72	12,000	1.8	0.53	[171]

Conditions for *rac*-LA polymerisation with zinc guanidine complexes: solvent-free melt polymerisation at 150°C, monomer/initiator ratio 500:1

[a] P_r: probability of racemic enchainment calculated by analysis of the homonuclear decoupled ^{1}H-NMR spectra

trend (Table 17). In the five-coordinate triflato complexes, a larger partial charge at the zinc centre is obtained which results in slightly shorter Zn–N_{gua} bond lengths and a larger ρ-value of 1.00 [168]. This indicates a stronger donation of the guanidine nitrogen atom compared to the pyridine nitrogen atom, which is directly related to the Y-aromaticity. Consequently, the C=N$_{gua}$ bonds are elongated compared to those in the chlorido and acetato complexes.

It has to be noted that the increasing size of the substituents, e.g. in tetraethylguanidine zinc complexes, at the guanidine renders it difficult to maintain this aromaticity. Analysing the molecular structures with density functional methods proved that rotational conformers with a lower degree of intra-guanidine twisting are energetically more favourable which demonstrates that the guanidine part tries to maintain the delocalisation [15].

Focusing on quinoline–guanidine complexes, mono(chelate) chlorido complexes ([Zn(TMGqu)Cl$_2$], [Zn(DMEGqu)Cl$_2$], [Zn(DMPGqu)Cl$_2$], [Zn(TEGqu)Cl$_2$], [Zn(DMorphGqu)Cl$_2$], [Zn(MorphDMGqu)Cl$_2$]) show a lower ROP activity than comparable mono(chelate) acetato complexes ([Zn(TMGqu)OAc$_2$], [Zn(DMEGqu)OAc$_2$], [Zn(DMPGqu)OAc$_2$], [Zn(DMorphGqu)OAc$_2$], [Zn(MorphDMGqu)OAc$_2$]) (Fig. 44) [15, 168]. However, bis(chelate) triflato complexes ([Zn(TMGqu)$_2$(OTf)][OTf], [Zn(DMEGqu)$_2$(OTf)][OTf]) possess a much higher activity in the polymerisation of lactide (Fig. 45, Table 18). Furthermore, they show a high robustness towards impurities in the monomer. During ROP of technical lactide with complexes ([Zn(TMGqu)$_2$(OTf)][OTf] and [Zn(DMEGqu)$_2$(OTf)][OTf]), PLA with polydispersities around two and molecular weights of up to 77,000 g/mol can be synthesised. Consequently, these catalysts are of high interest for industrial use.

For further improvements of the polymerisation properties, the guanidine–quinoline ligands have been modified in the 2-position of the quinolinyl moiety. The aim is to reach a steric hindrance at the zinc metal in the resulting zinc triflato or chlorido complexes. The activity studies of the complexes in the lactide polymerisation imply that the substitution at the 2-position (methyl or *tert*-butyl) has a critical influence on the tacticity, polydispersity and polymerisation rate. Using methyl-substituted quinoline–guanidine bis(chelate) zinc triflato complexes (Fig. 46), shorter polymer chains were obtained compared to unsubstituted catalysts. Concluding, methyl-substituted quinoline ligands have a major effect on the stereoselectivity and catalytic activity during ROP processes [172].

Previous studies showed that in the mono(chelate) mesylato complexes ([Zn(DMEGqu)OMes$_2$] and [Zn(TMGqu)$_2$(OMes)][OMes]) and bis(chelate) triflate complexes ([Zn(TMGqu)$_2$(OTf)][OTf] and [Zn(DMEGqu)$_2$(OTf)][OTf]), the zinc atoms possess higher positive partial charges compared to the respective chlorido and acetato complexes ([Zn(TMGqu)Cl$_2$], [Zn(DMEGqu)Cl$_2$], [Zn(TMGqu)OAc$_2$] and [Zn(DMEGqu)OAc$_2$]) [169]. In these cases, the partial charge of the guanidine follows a reversed trend. The smaller positive charge at the zinc atom results in a lower catalytic activity. In addition to electronic effects, the Zn–O bond length of the solid-state structure correlates with the activity during the polymerisation reaction. In the mesylato complex [Zn(TMGqu)$_2$(OMes)][OMes], the zinc–oxygen bond is shorter (2.103(1) Å) and stronger compared to the respective triflato complex (2.684(3) Å in [Zn(TMGqu)$_2$(OTf)][OTf]), which leads to a lower ROP activity. As a result, the larger Lewis acidity of the zinc complex facilitates the ring-opening step of the lactide during lactide ROP [168].

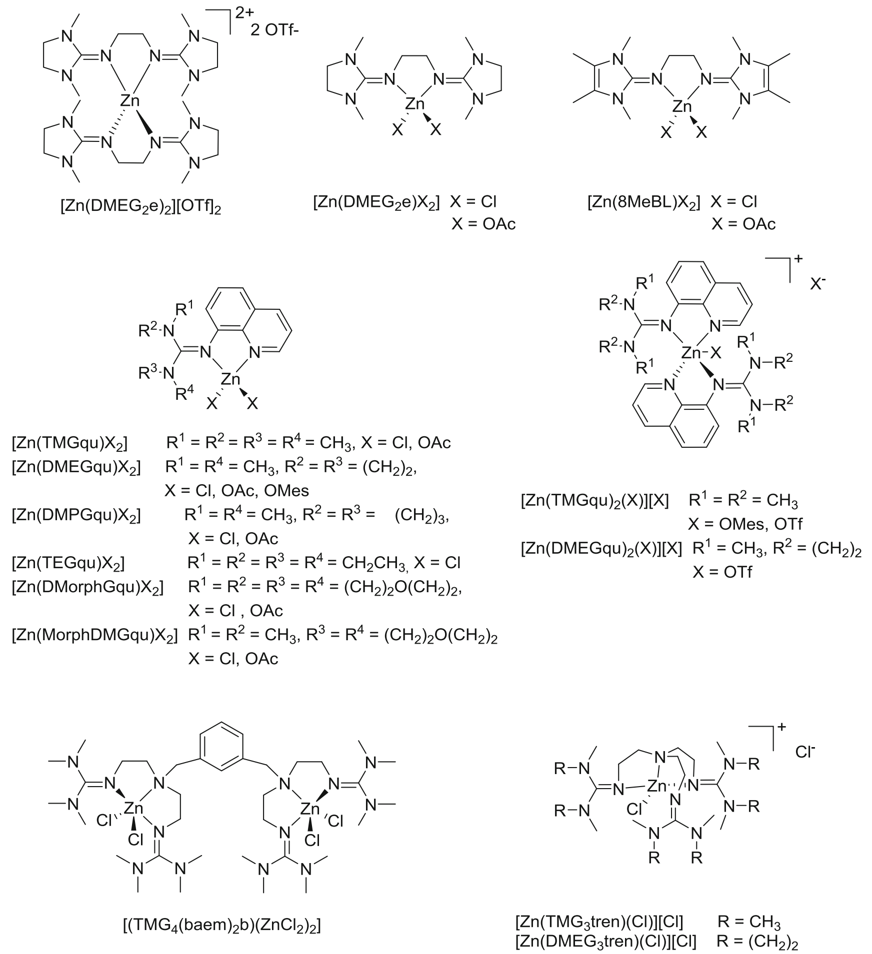

Fig. 45 Overview of zinc guanidine complexes

The dinuclear tetrakis(guanidine) complex [(TMG$_4$(baem)$_2$b)(ZnCl$_2$)$_2$] and the tris(guanidine) zinc complex [Zn(TMG$_3$tren)Cl][Cl] and [Zn(DMEG$_3$tren)Cl][Cl] are examples for poly(guanidines). These poly(guanidines) were tested in the polymerisation of lactide and showed moderate activity [171]. In all these polymerisations, no external initiator is needed. The same results are obtained regardless of using technical or sublimated lactide. Therefore, no impurities in the technical lactide can act as a chain starter [173]. The donor strength of guanidines is similar to that of ketiminates. Thus, they are supposed to act as ring-opening reagents. The next mechanistic hint was given by the fluorescence activity of the guanidine–quinoline ligands [73]. The quinoline-related emission can be detected in the zinc complexes and in the resulting polymer. The fluorescence intensity of samples with different chain lengths was investigated. Samples with shorter chain

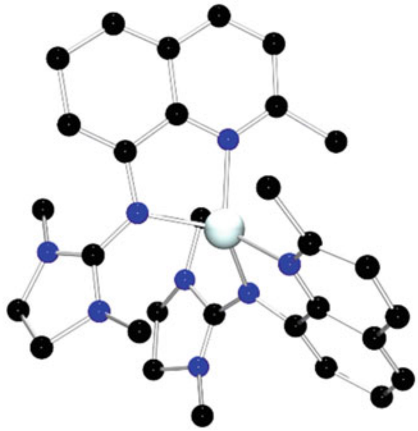

Fig. 46 Molecular structure of [Zn(DMEGmqu)$_2$]$^{2+}$ in crystals of [Zn(DMEGmqu)$_2$][CF$_3$SO$_3$]$_2$ [172]

lengths show higher fluorescence intensity compared to longer chains. As a result, the ligands act as end groups, and after workup, they can be found at the end of the polymer. Furthermore, in the UV–vis spectra, the absorption of the guanidine–quinoline ligands was observed in the corresponding polylactide samples. The reason is the $\pi - \pi^*$ transition of the aromatic quinoline system in the polymer [170].

The polymerisation with complexes [Zn(TMGqu)$_2$(OTf)][OTf], [Zn(DMEGqu)$_2$(OTf)][OTf] follows a first-order kinetic with activation parameters of $\Delta H^{\ddagger} = 79(4)$ kJ mol^{-1} and $\Delta S^{\ddagger} = -33(4)$ J K^{-1} mol^{-1} up to 165°C [170]. These values are in good agreement with those of other single-site catalysts [174]. A polymerisation at room temperature with these catalysts is energetically hindered. It has been observed that the molecular weights increase with the conversion, and thus, a controlled polymerisation can be assumed. However, the polydispersity amounts to a value around two which is a result of transesterification reactions. With the results from polymerisation kinetics and computational studies on the [Zn(TMGqu)$_2$(OTf)][OTf] system, a mechanism for zinc guanidine complexes could be proposed (Figs. 47 and 48) which proceeds without any co-initiator. The hypothesis is that the guanidines act as ring-opening reagents because of their high nucleophilicity and strong donor properties. Previous studies showed that a good basis set and functional for describing zinc N-donor complexes is 6-31G(d) or 6-311 g+(d) and B3LYP [137, 168, 175–179]. The first step is the exothermic coordination of the lactide monomer by one of the carbonyl oxygen atoms to the zinc atom (C1). Due to its high Lewis acidity, Zn^{2+} exhibits a particularly suited coordination sphere. In the transition state TS0, one of the guanidine N-atoms moves away from the zinc centre. This results in a stronger coordination of the lactide to the zinc metal C2. During the next transition state TS1, the N_{gua} atom

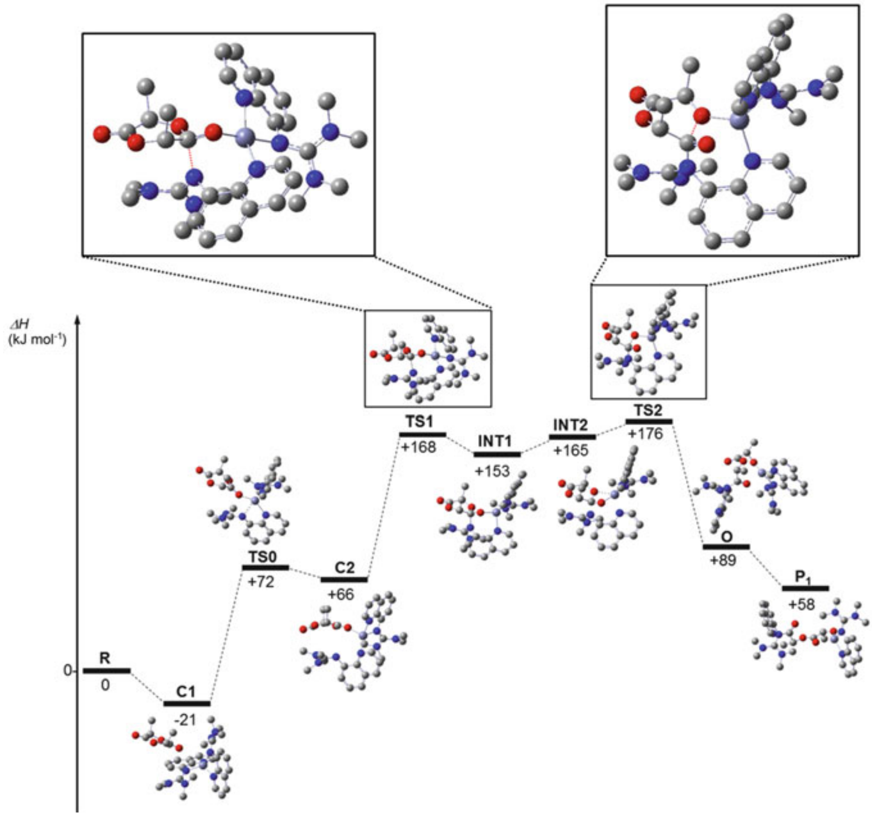

Fig. 47 Insertion of the first lactide monomer (*R* reactants, *C* zinc coordinated lactide, *TS* transition state, *INT* tetrahedral intermediate, *O* opened species, *P* propagating species)

transfers electron density to the carbonyl carbon atom at the lactide monomer under formation of a tetrahedral intermediate (INT1). This step needs an activation enthalpy of 102 kJ/mol which is reachable at the temperature used for the polymerisation. Going from INT1 to INT2, the coordination sphere changes, and the second oxygen atom of the lactide molecule participates in the zinc coordination. In both intermediate states, the Zn–N_{gua} distance is very long. In TS2, the $C_{carbonyl}$–$O_{alkoxide}$ bond in the lactide molecule breaks with formation of an eight-membered heterocycle followed by the ring-opened species P1. This detailed mechanism is similar to other reported single-site catalyst coordination–insertion mechanisms [156, 180–183]. In summary, the nucleophilicity of the guanidines is obviously strong enough to open the lactide ring.

For the chain propagation, a further study had to be performed, because the coordination sphere changes after the first step. In the initiation step, the ring opening is accomplished by the alcoholate function of the lactate part. In the propagation steps, the lactate group is linked to the zinc atom which is now

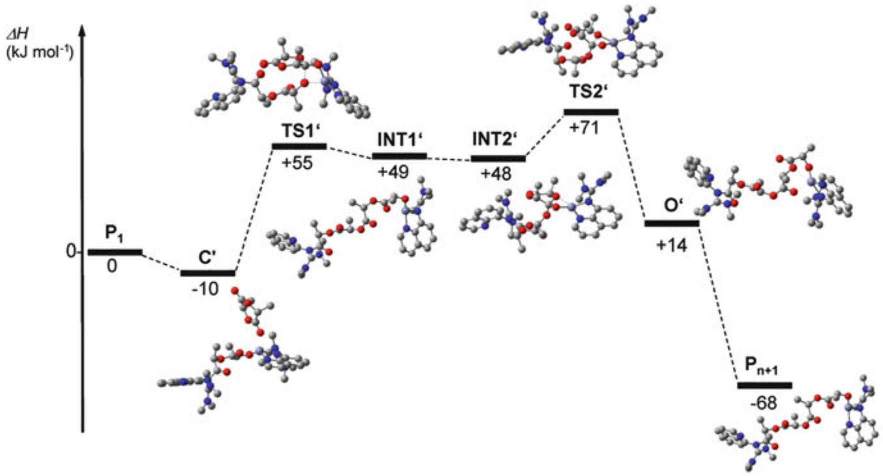

Fig. 48 Complete reaction coordinate diagram for the propagation step (*C′* zinc coordinated lactide, *TS* transition state, *INT* tetrahedral intermediate, *O′* opened species, *P* propagating species)

responsible for the nucleophilic attack and opens the ring of the second lactide monomer (Fig. 48). For the propagation steps, a similar mechanism was calculated as for the initiation step, starting with the lactate species. In the propagation mechanism, the pre-transition state TS0 does not appear because no coordination rearrangement is needed. The transition states TS1′ and TS2′ are similar to the initiation steps. At first a nucleophilic attack occurs (TS1′) followed by the ring-opening part with the $C_{carbonyl}$–$O_{alkoxide}$ bond release (TS2′). The alcoholate function of the lactate acts as a stronger nucleophile, and therefore, the activation barrier of TS1′ is lowered to 65 kJ/mol. In comparison to the experimental value for the activation enthalpy ($\Delta H^{\ddagger} = 79(4)$ kJ/mol), the theoretical value compares very well. All in all, the propagation step is energetically more preferred than the initiation step. As a result of the high initiation barrier, only a few catalysts are active in the ROP at lower temperature. This leads to higher experimental molecular weights than expected from the theoretical molecular weights [170].

In conclusion, a great advantage of using guanidine zinc systems is that they are robust against air and monomer impurities. Only few further robust systems are known, for example, tris(phenolate) titanium complexes [184–187]. As a result of the excellent donor properties and high nucleophilicity, guanidines have the ability to open the lactide ring.

In summary, it has been shown that guanidine ligands are well suited for the complexation of zinc salts and that these complexes show good catalytic activity in the polymerisation of lactide. In comparison to anionic ligands, neutral ligands are strongly preferred since the industrial use demands for complexes that are robust against impurities in the lactide monomer, air and elevated temperatures. Another advantage of using guanidine ligands is the high synthetic flexibility with ligand tailoring at all sides.

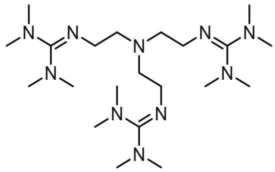

Fig. 49 TMG_3tren as reactive ligand in copper-mediated ATRP [189]

3.2 Guanidines in Copper-Mediated Atom Transfer Radical Polymerisation

Atom Transfer Radical Polymerisation (ATRP) reactions are a class of Controlled Radical Polymerisation (CRP) reactions. In CRP reactions, an equilibrium of activators and deactivators implements controlled conditions to radical polymerisations. As a result, polymers with narrow molecular weight distributions and precise molecular structures can be synthesised. In ATRP, a vast variety of transition metal complexes can be used; however, copper complexes with chelating N donor ligands are present in the literature predominantly [188].

During ATRP reactions, the catalysts undergo numerous oxidation and reduction reactions changing the metal's oxidation state, its coordination number and its geometrical parameters. For a catalyst, only stable ligands with a strong coordination are able to sustain these conditions for an elongated period of time. Many metal cations are stabilised by strong electron donating ligands. Guanidine copper complexes, for example, can be stabilised in both of its stable cationic oxidation states (Cu^I and Cu^{II}) [27]. Even frequent oxidation changes, which exert steric or geometrical stress on the coordination sphere, do not lead to dissociation of the coordination. These properties make guanidines great ligands for copper ATRP.

In 2005, Brar and Kaur used a tetramethylguanidine (TMG) derivative of the tren ligand (tris(2-aminoethyl)amine) called TMG_3tren as ligand in copper-mediated ATRP (Fig. 49) [189]. The complex of TMG_3tren with CuBr was successfully applied in polymerisations of methyl methacrylate (MMA), *n*butyl acrylate (BA), styrene (sty) and acrylonitrile. The catalyst behaved similarly to Me_6tren in BA polymerisation although a decreased activity in styrene polymerisations was observed. The high activity of this ligand was utilised in polymerisation reactions with low catalyst loadings (0.05 mol% of the initiator).

Tamm et al. synthesised an ethylene-bridged bis(imidazolin-2-imine) ligand (BL*i*Pr) derived from a cyclic N-heterocyclic carbene in 2008 [43]. The guanidine ligand incorporated strong donating N donor atoms which stabilised Cu^I metal centres and exhibited trigonal coordination. The respective copper complexes with non-coordinating anions were used in oxygen activation (SbF_6^-, PF_6^-) (see Sect. 2.2), whereas the CuCl derivative (Fig. 50) was successfully used in ATRP of styrene. The catalyst yielded polystyrene with low polydispersities and molecular weights up to 30,000 g mol^{-1}.

The bis(chelate) guanidine ligand [N^1,N^2-bis(1,3-dimethylimidazolin-2-ylidene) ethane-1,2-diamine] ($DMEG_2$e) was synthesised and characterised by Herres-

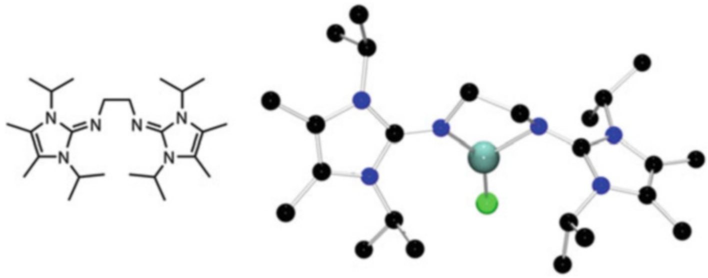

Fig. 50 *Left*, the bidentate ethylene-bridged bis(imidazolin-2-imine) ligand (BL*i*Pr) synthesised by Petrovic et al.; *right*, the CuCl complex used in ATRP of styrene [43]

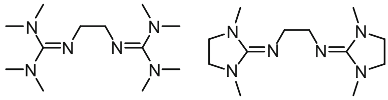

Fig. 51 The ligands TMG_2e (*left*) and $DMEG_2e$ (*right*)

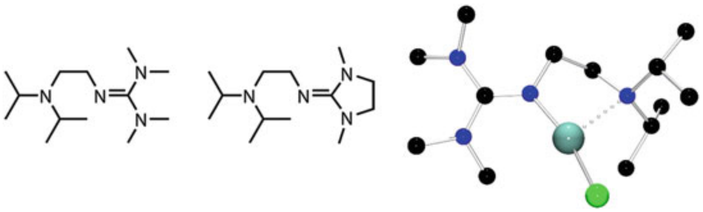

Fig. 52 *Left*, the ATRP active ligands TMGd^{i}pae and DMEGd^{i}pae; *right*, the molecular structure of the ATRP catalyst [Cu(TMGd^{i}pae)Cl] [190]

Pawlis et al. in 2008 (see Sect. 2.1 for the transition metal complexes) [29]. Later, in 2010, a tetramethylguanidine derivative [bis(*N*,*N*,*N*′,*N*′-tetramethylguanidino)ethane] (TMG_2e) was synthesised, and both ligands were coordinated to CuCl and applied in ATRP of styrene (Fig. 51) [31]. The complexes exhibited coordination environments between tetrahedral and square planar geometries. In ATRP, the complexes yielded polymers with high conversions and good molecular weight distributions indicating a controlled polymerisation mechanism.

In 2011, Herres-Pawlis et al. synthesised and characterised copper halide complexes with the ligands 2-(2-(diisopropylamino)ethyl)-1,1,3,3-tetramethylguanidine (TMGd^{i}pae) and *N*-(2-((1,3-dimethylimidazolidin-2-ylidene)amino)ethyl)-*N*-isopropylpropan-2-amine (DMEGd^{i}pae) (Fig. 52) [190]. The molecular structure of the complex as well as DFT calculations revealed a stronger donation of the TMG unit in TMGd^{i}pae than the respective DMEG unit. The polymerisation of styrene under ATRP standard conditions with CuCl and CuBr resulted in good molecular weights with reasonable reaction control. For bidentate ligands, it should be noted that they are generally used in a 2:1 ratio towards copper for controlled

Fig. 53 *Left*, TMGpy; *right*, TMG_2b used in copper-mediated ATRP [37, 191]

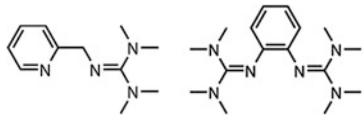

polymerisation reactions. However, in this particular case, polymerisations were also conducted successfully in a 1:1 ratio.

In 2014, the same group published a series of copper halide complexes with different bidentate guanidine hybrid ligands [37, 191]. Of those, the hybrid ligands (tetramethylguanidine)methylenepyridine (TMGpy), (dimethylethyleneguanidine) methylenepyridine (DMEGpy) and the bisguanidine ligand 2,20-(1,2-phenylenebis (1,1,3,3-tetramethyl)guanidine) (TMG_2b) (Fig. 53) were applied in atom transfer radical polymerisation. The methylenepyridine derivatives (TMGpy and DMEGpy) exhibited a fast polymerisation with good control and PD values around 1.2, in which the higher polymerisation rate was obtained with DMEGpy. While TMG_2b showed a slower polymerisation rate, it revealed excellent reaction control with PD values as low as 1.06.

Another class of guanidines, the hexahydropyrimidopyrimidine ligands, were applied in ATRP in 2003 by Coles et al. [104]. The bicyclic guanidine ligand 1,3,4,6,7,8-hexahydro-2*H*-pyrimido-[1,2-a]pyrimidine (hppH) stabilised copper (I) halides by coordination of the imine nitrogen and additional NH-halide interactions (see Sect. 2.8).

4 Conclusion

Neutral guanidines have been proven to be highly useful ligands for the stabilisation of transition metals in various oxidation states and even rather high oxidation states such as Cu(III), Co(IV) and Fe(IV) in bioinorganic model complexes. They are able to coordinate a large number of transition metals and main-group metals in a vast multitude of coordination motifs. Bis(guanidine) copper complexes are useful as tyrosinase models, whereas tris(guanidine) copper complexes mimic the dopamine β-monooxygenase. The same TMG_3tren ligand stabilises a nonheme iron enzyme model as well as high-valent nickel and cobalt complexes. Hybridguanidines combine guanidine functions with other N donor functions and are able to model electron transfer systems but also stabilise efficient lactide polymerisation and ATRP catalysts. In parallel, the guanidine unit has been incorporated in larger scaffolds such as triazolopyrimidines which act as purine analogue, bicyclic guanidines, azoimidazole ligands and triazine guanidines.

For all of these complexes, the excellent ability to delocalise the positive charge within the whole guanidine unit is the key to their multifaceted coordination chemistry.

Standing for a long time in the shadow of their anionic congeners, neutral guanidines have taken a permanent place in coordination chemistry, and many more exciting applications are to be expected in the future.

References

1. Solomon EI, Heppner DE, Johnston EM, Ginsbach JW, Cirera J, Qayyum M, Kieber-Emmons MT, Kjaergaard CH, Hadt RG, Tian L (2014) Copper active sites in biology. Chem Rev 114:3659–3853
2. Bailey PJ, Pace S (2001) The coordination chemistry of guanidines and guanidinates. Coord Chem Rev 214:91–141
3. Edelmann FT (2008) Advances in the coordination chemistry of amidinate and guanidinate ligands. In: Hill AF, Fink MJ (eds) Advances in organometallic chemistry, vol 57. Elsevier, Oxford, pp 183–352
4. Edelmann FT (2013) Recent progress in the chemistry of metal amidinates and guanidinates: syntheses, catalysis and materials. In: Hill AF, Fink MJ (eds) Advances in organometallic chemistry, vol 61. Elsevier, Oxford, pp 55–374
5. Wu X, Tamm M (2014) Transition metal complexes supported by highly basic imidazolin-2-iminato and imidazolin-2-imine N-donor ligands. Coord Chem Rev 260:116–138
6. Zhang W-X, Xua L, Xi Z (2015) Recent development of synthetic preparation methods for guanidines via transition metal catalysis. Chem Commun 51:254–265
7. Elorriaga D, Carrillo-Hermosilla F, Antinolo A, Suarez FJ, Lopez-Solera I, Fernandez-Galan R, Villaseno E (2013) Asymmetric niobium guanidinates as intermediates in the catalytic guanylation of amines. Dalton Trans 42:8223–8230
8. Gobbi A, Frenking G (1993) Y-conjugated compounds: the equilibrium geometries and electronic structures of guanidine, guanidinium cation, urea, and 1,1-diaminoethylene. J Am Chem Soc 115:2362–2372
9. Sundermeyer J, Raab V, Gaoutchenova E, Garrelts U, Abicilar N, Harms K (1990) The chemistry of superbasic guanidines. In: Bolm C, Hahn FE (eds) Activating unreactive substrates: the role of secondary interactions. Wiley, Weinheim, pp 17–35
10. Schwesinger R (1990) Starke ungeladene Stickstoffbasen. Nachr Chem Tech Lab 38:1214–1226
11. Raab V, Harms K, Sundermeyer J, Kovacevic B, Maksic ZB (2003) 1,8-Bis(dimethylethyleneguanidino)naphthalene: tailoring the basicity of bisguanidine “proton sponges” by experiment and theory. J Org Chem 68:8790–8797
12. Herres S, Flörke U, Henkel G (2004) N,N′-Bis(dipiperidin-1-ylmethylene)-propane-1,3-diamine and N,N′-bis-(1,3-dimethylperhydropyrimidin-2-ylidene)propane-1,3-diamine. Acta Crystallogr C60:o358–o360
13. Yamada T, Liu X, Englert U, Yamane H, Dronskowski R (2009) Solid-state structure of free base guanidine achieved at last. Chem Eur J 15:5651–5655
14. Sawinski PK, Meven M, Englert U, Dronskowski R (2013) Single-crystal neutron diffraction study on guanidine, CN_3H_5. Cryst Growth Des 13:1730–1735
15. Börner J, dos Santos Vieira I, Jones MD, Döring A, Kuckling D, Flörke U, Herres-Pawlis S (2011) Zinc complexes with guanidine–pyridine hybrid ligands – guanidine effect and catalytic activity. Eur J Inorg Chem 4441–4456
16. Longhi R, Drago RS (1965) Transition metal ion complexes of tetramethylguanidine. Inorg Chem 4:11–14
17. Schneider W, Bauer A, Schier A, Schmidbaur H (1997) Tetramethylguanidine and benzophenoneimine as ligands in gold chemistry. Chem Ber 130:1417–1422

18. Oakley SH, Soria DB, Coles MP, Hitchcock PB (2004) Structural diversity in the coordination of amidines and guanidines to monovalent metal halides. Dalton Trans 537–546
19. Köhn U, Günther W, Görls H, Anders E (2004) Preparation of chiral thioureas, ureas and guanidines from (S)-2-(N, N-dialkylaminomethyl)pyrrolidines. Tetrahedron Asymmetry 15:1419–1426
20. Köhn U, Schulz M, Görls H, Anders E (2005) Neutral zinc(II) and molybdenum(0) complexes with chiral guanidine ligands: synthesis, characterisation and applications. Tetrahedron Asymmetry 16:2125–2131
21. Köhn U, Klopffleisch M, Görls H, Anders E (2006) Synthesis of hindered chiral guanidine bases starting from (S)-(N, N-dialkyl-aminomethyl)pyrrolidines and BrCN. Tetrahedron Asymmetry 17:811–818
22. Pohl S, Harmjanz M, Schneider J, Saak W, Henkel G (2000) 1,3-Bis(*N*,*N*,*N*,*N*-tetramethylguanidino)propane: synthesis, characterization and bonding properties of the first bidentate, peralkylated guanidine ligand. J Chem Soc, Dalton Trans 3473–3479
23. Pohl S, Harmjanz M, Schneider J, Saak W, Henkel G (2000) Syntheses and structures of transition metal thiolate complexes containing the new bis(tetramethylguanidine) ligand btmgp. Inorg Chim Acta 311:106–112
24. Wittmann H, Schorm A, Sundermeyer J (2000) Chelatliganden auf Basis peralkylierter Bis- und Tris-Guanidine. Z Anorg Allg Chem 626:1583–1590
25. Kantlehner W, Haug E, Mergen WW, Speh P, Maier T, Kapassakalidis JJ, Bräuner HJ, Hagen H (1984) Herstellung von 1,1,2,3,3-pentasubstituierten und 1,1,2,2,3,3-hexasubstituierten Guanidiniumsalzen sowie von 1,1,2,3,3-Pentaalkylguanidinen. Liebigs Ann Chem 1:108–125
26. Herres S, Heuwing AJ, Flörke U, Schneider J, Henkel G (2005) Hydroxylation of a methyl group: synthesis of $[Cu_2(btmmO)_2I]^+$ and of $[Cu_2(btmmO)_2]^{2+}$ containing the novel ligand {bis(trimethylmethoxy)guanidino}propane (btmmO) by copper-assisted oxygen activation. Inorg Chim Acta 358:1089–1095
27. Herres-Pawlis S, Flörke U, Henkel G (2005) Tuning of copper(I)–dioxygen reactivity by bis (guanidine) ligands. Eur J Inorg Chem 3815–3824
28. Neuba A, Herres-Pawlis S, Seewald O, Börner J, Heuwing AJ, Flörke U, Henkel G (2010) Systematische Studie zu den Koordinationseigenschaften des Guanidin-Liganden Bis (tetramethylguanidino)propan mit den Metallen Mangan, Cobalt, Nickel, Zink, Cadmium, Quecksilber und Silber. Z Anorg Allg Chem 636:2641–2649
29. Herres-Pawlis S, Haase R, Akin E, Flörke U, Henkel G (2008) Syntheses and x-ray structure analyses of the first bis(chelated) copper and iron bis(guanidine) complexes. Z Anorg Allg Chem 634:295–298
30. Neuba A, Haase R, Bernard M, Flörke U, Herres-Pawlis S (2008) Systematische Studie zu den Koordinationseigenschaften des Guanidin-Liganden N1, N2-Bis(1,3-dimethylimidazolidin-2-yliden)-ethan-1,2-diamin mit den Metallen Mn, Co, Ni, Ag und Cu. Z Anorg Allg Chem 634:2511–2517
31. Bienemann O, Haase R, Flörke U, Döring A, Kuckling D, Herres-Pawlis S (2010) New bis (guanidine)-copper complexes and their application in ATRP. Z Naturforsch 65b:798–806
32. Börner J, Herres-Pawlis S, Flörke U, Huber K (2007) [Bis(guanidine)]zinc complexes and their application in lactide polymerization. Eur J Inorg Chem 5645–5651
33. Pruszynski P, Leffek KT, Borecka B, Cameron TS (1992) Synthesis and structure of the picrate salt of 2,2′-bis[2*N*-(1,1,3,3-tetramethylguanidino)]biphenyl. Acta Crystallogr C 48:1638–1641
34. Herres-Pawlis S, Neuba A, Seewald O, Seshadri T, Egold H, Flörke U, Henkel G (2005) A library of peralkylated bis-guanidine ligands for use in biomimetic coordination chemistry. Eur J Org Chem 4879–4890
35. Herres-Pawlis S, Seshadri T, Flörke U, Henkel G (2009) Reactivity of 2,2′-bis(2N-(1,1′,3,3-′-tetramethyl-guanidino))diphenylene-amine with CuI and $[Cu(MeCN)_4][PF_6]$: benzimidazole formation vs. Cu oxidation. Z Anorg Allg Chem 635:1209–1214

36. Yang L, Powell DR, Houser RP (2007) Structural variation in copper(I) complexes with pyridylmethylamide ligands: structural analysis with a new four-coordinate geometry index, τ_4. Dalton Trans 955–964
37. Hoffmann A, Bienemann O, dos Santos Vieira I, Herres-Pawlis S (2014) Neue aromatische Bisguanidin-Kupfer-Komplexe und ihre Anwendung in der ATRP. Z Naturforsch 69b:589–595
38. Reinmuth M, Neuhäuser C, Walter P, Enders M, Kaifer E, Himmel H-J (2010) The flexible coordination modes of guanidine ligands in Zn Alkyl and halide complexes: chances for catalysis. Eur J Inorg Chem 83–90
39. Neuba A, Herres-Pawlis S, Flörke U, Henkel G (2008) Synthese und Strukturen der ersten mehrkernigen Mangan-Guanidin-Komplexe und der ersten Mangan-Komplexe mit monoprotonierten Bis-Guanidinliganden. Z Anorg Allg Chem 634:771–777
40. Mirica LM, Ottenwaelder X, Stack TDP (2004) Structure and spectroscopy of copper-dioxygen complexes. Chem Rev 104:1013–1045
41. Herres-Pawlis S, Verma P, Haase R, Kang P, Lyons CT, Wasinger EC, Flörke U, Henkel G, Stack TDP (2009) Phenolate hydroxylation in a bis(μ-oxo)dicopper(III) complex: lessons from the guanidine/amine series. J Am Chem Soc 131:1154–1169
42. Herres-Pawlis S, Binder S, Eich A, Haase R, Schulz B, Wellenreuther G, Henkel G, Rübhausen M, Meyer-Klaucke W (2009) Stabilisation of a highly reactive bis(μ-oxo) dicopper (III) species at room temperature by electronic and steric constraint of an unconventional nitrogen donor ligand. Chem Eur J 15:8678–8682
43. Petrovic D, Hill LMR, Jones PG, Tolman WB, Tamm M (2008) Synthesis and reactivity of copper(I) complexes with an ethylene-bridged bis(imidazolin-2-imine) ligand. Dalton Trans 887–894
44. Glöge T, Petrovic D, Hrib CG, Daniliuc C, Herdtweck E, Jones PG, Tamm M (2010) Synthesis and structural characterisation of an isomorphous series of bis(imidazolin-2-imine) metal dichlorides containing the first row transition metals Mn, Fe, Co, Ni, Cu and Zn. Z Anorg Allg Chem 636:2303–2308
45. Chaudhuri UP, Powell DR, Houser RP (2009) New examples of μ-η2:η2-disulfido dicopper (II, II) complexes with bis(tetramethylguanidine) ligands. Inorg Chim Acta 362:2371–2378
46. Wittmann H, Raab V, Schorm V, Plackmeyer J, Sundermeyer J (2001) Complexes of manganese, iron, zinc, and molybdenum with a superbasic tris(guanidine) derivative of tris (2-ethylamino)amine (tren) as a tripod ligand. Eur J Inorg Chem 1937–1948
47. Raab V, Kipke J, Burghaus O, Sundermeyer J (2001) Copper complexes of novel superbasic peralkylguanidine derivatives of tris(2-aminoethyl)amine as constraint geometry ligands. Inorg Chem 40:6964–6971
48. Schatz M, Raab V, Foxon SP, Brehm G, Schneider S, Reiher M, Holthausen MC, Sundermeyer J, Schindler S (2004) Combined spectroscopic and theoretical evidence for a persistent end-on copper superoxo complex. Angew Chem 116:4460–4464
49. Würtele C, Gaoutchenova E, Harms K, Holthausen MC, Sundermeyer J, Schindler S (2006) Crystallographic characterization of a synthetic 1:1 end-on copper dioxygen adduct complex. Angew Chem 118:3951–3954
50. Maiti D, Lee D-H, Gaoutchenova K, Würtele C, Holthausen MC, Narducci Sarjeant AA, Sundermeyer J, Schindler S, Karlin KD (2008) Reactions of a copper(II) superoxo complex lead to C-H and O-H substrate oxygenation: modeling copper-monooxygenase C-H hydroxylation. Angew Chem 120:88–91
51. Schatz M, Raab V, Foxon SP, Brehm G, Schneider S, Reiher M, Holthausen MC, Sundermeyer J, Schindler S (2004) Combined spectroscopic and theoretical evidence for a persistent end-on copper superoxo complex. Angew Chem Int Ed 43:4360–4363
52. Würtele C, Gaoutchenova E, Harms K, Holthausen MC, Sundermeyer J, Schindler S (2006) Crystallographic characterization of a synthetic 1:1 end-on copper dioxygen adduct complex. Angew Chem Int Ed 45:3867–3869

53. Maiti D, Lee D-H, Gaoutchenova K, Würtele C, Holthausen MC, Narducci Sarjeant AA, Sundermeyer J, Schindler S, Karlin KD (2008) Reactions of a copper(II) superoxo complex lead to C-H and O-H substrate oxygenation: modeling copper-monooxygenase C-H hydroxylation. Angew Chem Int Ed 47:82–85
54. Maiti D, Lee D, Narducci Sarjeant AA, Pau MYM, Solomon EI, Gaoutchenova K, Sundermeyer J, Karlin KD (2008) Reaction of a copper-dioxygen complex with nitrogen monoxide (•NO) leads to a copper(II)-peroxynitrite species. J Am Chem Soc 130:6700–6701
55. Lanci MP, Smirnov VV, Cramer CJ, Gauchenova EV, Sundermeyer J, Roth JP (2007) Isotopic probing of molecular oxygen activation at copper(I) sites. J Am Chem Soc 129:14697–14709
56. Woertink JS, Tian L, Maiti D, Lucas HR, Himes RA, Karlin KD, Neese F, Würtele C, Holthausen MC, Bill E, Sundermeyer J, Schindler S, Solomon EI (2010) Spectroscopic and computational studies of an end-on bound superoxo-Cu(II) complex: geometric and electronic factors that determine the ground state. Inorg Chem 49:9450–9459
57. Saracini C, Liakos DG, Zapata Rivera JE, Neese F, Meyer GJ, Karlin KD (2014) Excitation wavelength dependent O2 release from copper(II)−superoxide compounds: laser flash-photolysis experiments and theoretical studies. J Am Chem Soc 136:1260–1263
58. Prigge ST, Eipper BA, Mains RE, Amzel LM (2004) Dioxygen binds end-on to mononuclear copper in a precatalytic enzyme complex. Science 304:864–867
59. Klinman JP (1996) Mechanisms whereby mononuclear copper proteins functionalize organic substrates. Chem Rev 96:2541–2562
60. Poater A, Cavallo L (2009) Probing the mechanism of O_2 activation by a copper (I) biomimetic complex of a C-H hydroxylating copper monooxygenase. Inorg Chem 48:4062–4066
61. Raab V, Merz M, Sundermeyer J (2001) Ligand effects in the copper catalyzed aerobic oxidative carbonylation of methanol to dimethyl carbonate (DMC). J Mol Catal A Chem 175:51–63
62. Peterson RL, Ginsbach JW, Cowley RE, Qayyum MF, Himes RA, Siegler MA, Moore CD, Hedman B, Hodgson KO, Fukuzumi S, Solomon EI, Karlin KD (2013) Stepwise protonation and electron-transfer reduction of a primary copper−dioxygen adduct. J Am Chem Soc 135:16454–16467
63. England J, Martinho M, Farquhar ER, Frisch JR, Bominaar EL, Münck E, Que L Jr (2009) A synthetic high-spin oxoiron(IV) complex: generation, spectroscopic characterization, and reactivity. Angew Chem 121:3676–3680
64. England J, Martinho M, Farquhar ER, Frisch JR, Bominaar EL, Münck E, Que L Jr (2009) A synthetic high-spin oxoiron(IV) complex: generation, spectroscopic characterization, and reactivity. Angew Chem Int Ed 48:3622–3626
65. England J, Guo Y, Farquhar ER, Young VG Jr, Münck E, Que L Jr (2010) The crystal structure of a high-spin oxoiron(IV) complex and characterization of its self-decay pathway. J Am Chem Soc 132:8635–8644
66. England J, Farquhar ER, Guo Y, Cranswick MA, Ray K, Münck E, Que L Jr (2011) Characterization of a tricationic trigonal bipyramidal iron(IV) cyanide complex, with a very high reduction potential, and its iron(II) and iron(III) congeners. Inorg Chem 50:2885–2896
67. Janardanan D, Wang Y, Schyman P, Que L Jr, Shaik S (2010) The fundamental role of exchange-enhanced reactivity in C-H activation by S=2 oxo iron(IV) complexes. Angew Chem Int Ed 49:3342–3345
68. Wong SD, Bell CB III, Liu LV, Kwak Y, England J, Alp EE, Zhao J, Que L Jr, Solomon EI (2011) Nuclear resonance vibrational spectroscopy on the Fe^{IV}=O S=2 non-heme site in TMG3tren: experimentally calibrated insights into reactivity. Angew Chem Int Ed 50:3215–3218

69. England J, Guo Y, Van Heuvelen KM, Cranswick MA, Rohde GT, Bominaar EL, Münck E, Que L Jr (2011) A more reactive trigonal-bipyramidal high-spin oxoiron(IV) complex with a cis-labile site. J Am Chem Soc 133:11880–11883
70. Pfaff FF, Kundu S, Risch M, Pandian S, Heims F, Pryjomska-Ray I, Haack P, Metzinger R, Bill E, Dau H, Comba P, Ray K (2011) An oxocobalt(IV) complex stabilized by lewis acid interactions with scandium(III) ions. Angew Chem 123:1749–1753
71. Pfaff FF, Kundu S, Risch M, Pandian S, Heims F, Pryjomska-Ray I, Haack P, Metzinger R, Bill E, Dau H, Comba P, Ray K (2011) An oxocobalt(IV) complex stabilized by lewis acid interactions with scandium(III) ions. Angew Chem Int Ed 50:1711–1715
72. Pfaff FF, Heims F, Kundu S, Mebs S, Ray K (2012) Spectroscopic capture and reactivity of $S = 1/2$ nickel(III)–oxygen intermediates in the reaction of a Ni^{II}-salt with mCPBA. Chem Commun 48:3730–3732
73. Hoffmann A, Börner J, Flörke U, Herres-Pawlis S (2009) Synthesis and properties of guanidine-pyridine hybridligands and structural characterisation of their mono- and bis (chelated) cobalt complexes. Inorg Chim Acta 362:1185–1193
74. Wortmann R, Flörke U, Sarkar B, Maheshwari U, Gescheidt G, Herres-Pawlis S, Henkel G (2011) Synthesis and characterisation of novel manganese guanidine complexes and their application in the epoxidation of 1-octene. Eur J Inorg Chem 121–130
75. Hoffmann A, Binder S, Jesser A, Haase R, Flörke U, Gnida M, Salomone Stagni M, Meyer-Klaucke W, Lebsanft B, Grünig LE, Schneider S, Hashemi M, Goos A, Wetzel A, Rübhausen M, Herres-Pawlis S (2014) Catching an entatic state – a pair of copper complexes. Angew Chem 126:305–310
76. Hoffmann A, Binder S, Jesser A, Haase R, Flörke U, Gnida M, Salomone Stagni M, Meyer-Klaucke W, Lebsanft B, Grünig LE, Schneider S, Hashemi M, Goos A, Wetzel A, Rübhausen M, Herres-Pawlis S (2014) Catching an entatic state – a pair of copper complexes. Angew Chem Int Ed 53:299–304
77. Wortmann R, Hoffmann A, Haase R, Flörke U, Herres-Pawlis S (2009) Synthese und Charakterisierung von Cobalt(II)- und Kupfer(I)-Komplexen mit Guanidin-Pyridin-Hybridliganden. Z Anorg Allg Chem 635:64–69
78. Jesser A, Rohrmüller M, Schmidt WG, Herres-Pawlis S (2014) Geometrical and optical benchmarking of copper guanidine–quinoline complexes: insights from TD-DFT and many-body perturbation theory. J Comput Chem 35:1–17
79. Hoffmann A, Rohrmüller M, Jesser A, dos Santos Vieira I, Schmidt WG, Herres-Pawlis S (2014) Geometrical and optical benchmarking of copper(II) guanidine-quinoline complexes: insights from TD-DFT and many-body perturbation theory (part II). J Comput Chem 35:2146–2161
80. Hoffmann A, Grunzke R, Herres-Pawlis S (2014) Insights into the influence of dispersion correction in the theoretical treatment of guanidine-quinoline copper(I) complexes. J Comput Chem 35:1943–1950
81. Jesser A, dos Santos Vieira I, Herres-Pawlis S (2013) Novel tin(IV) complexes with the hybrid guanidine ligand DMEGqu. Z Naturforsch 68b:653–665
82. Haase R, Beschnitt T, Flörke U, Herres-Pawlis S (2011) Bidentate guanidine ligands with ethylene spacer in copper-dioxygen chemistry: structural characterization of bis(l-hydroxo) dicopper complexes. Inorg Chim Acta 374:546–557
83. Kisslinger S, Kelm H, Zheng S, Beitat A, Würtele C, Wortmann R, Bonnet S, Herres-Pawlis S, Krüger H-J, Schindler S (2012) Synthesis and characterization of iron (II) thiocyanate complexes with derivatives of the tris(pyridine-2-ylmethyl)amine (tmpa) ligand. Z Anorg Allg Chem 638:2069–2077
84. Neuba A, Flörke U, Meyer-Klaucke W, Salomone-Stagni M, Bill E, Bothe E, Höfer P, Henkel G (2011) The trinuclear copper(I) thiolate complexes $[Cu_3(NGuaS)_3]^{0/1+}$ and their dimeric variants $[Cu_6(NGuaS)_6]^{1+/2+/3+}$ with biomimetic redox properties. Angew Chem Int Ed 50:4503–4507

85. Neuba A, Flörke U, Henkel G (2013) The mixed-valent copper thiolate complex hexakis{l3-2-[(1,3-dimethylimidazolidene)amino]benzenethiolato}-dicopper(II)tetracopper(I) bis (hexafluoridophosphate) acetonitrile disolvate dichloromethane disolvate. Acta Crystallogr E69:m54–m55
86. Neuba A, Haase R, Meyer-Klaucke W, Flörke U, Henkel G (2012) A halide-induced copper (I) disulfide/copper(II) thiolate interconversion. Angew Chem Int Ed 51:1714–1718
87. Hoppe T, Josephs P, Kempf N, Wölper C, Schindler S, Neuba A, Henkel G (2013) An approach to model the active site of peptidglycine-α-hydroxylating monooxygenase (PHM). Z Anorg Allg Chem 639:1504–1511
88. Peters A, Kaifer E, Himmel H-J (2008) 1,2,4,5-Tetrakis(tetramethylguanidino)benzene: synthesis and properties of a new molecular electron donor. Eur J Org Chem 2008:5907–5914
89. Trumm C, Hübner O, Walter P, Leingang S, Wild U, Kaifer E, Eberle B, Himmel H-J (2014) One- versus two-electron oxidation of complexed guanidino-functionalized aromatic compounds. Eur J Inorg Chem 2014:6039–6050
90. Peters A, Trumm C, Reinmuth M, Emeljanenko D, Kaifer E, Himmel H-J (2009) On the chemistry of the strong organic electron-donor 1,2,4,5-tetrakis(tetramethylguanidino)benzene: electron transfer in donor–acceptor couples and binuclear late transition metal complexes. Eur J Inorg Chem 2009:3791–3800
91. Emeljanenko D, Peters A, Wagner N, Beck J, Kaifer E, Himmel H-J (2010) Successive ligand and metal oxidation: redox reactions involving binuclear Cu^{I} complexes of chelating guanidine ligands. Eur J Inorg Chem 2010:1839–1846
92. Trumm C, Kaifer E, Hübner O, Himmel H-J (2010) Trapped in a complex: the 1,2,4,5-tetrakis (tetramethylguanidino)benzene radical cation ($ttmgb^{+\cdot}$) with a bisallylic structure. Eur J Inorg Chem 2010:3102–3108
93. Biagini Cingi M, Manotti Lanfredi AM, Tiripicchio A, Haasnoot JG, Reedijk J (1983) Spectral properties and crystal structure of bis(μ-thiocyanato-N, S)bis-(thiocyanato-N) tetrakis(5,7-dimethyl[1,2,4]triazolo[1,5α]pyrimidine-N3)-dicopper(II) and of tetrakis (5,7-dimethyl[1,2,4]triazolo-[1,5α]pyrimidine-N3)-platinum(II) hexa(thiocyanato-S)palatinate(IV). Inorg Chim Acta 72:81–88
94. Haasnoot JG, Driessen WL, Reedijk J (1984) Distortion isomerism in a thiocyanate-bridged copper(II) dimer. X-ray structure of β-bis(μ- thiocyanato-N, S) bis[bis(5,7-dimethyl[1,2,4]-triazolo[1,5-α]pyrimidine) (thiocyanato-N)copper(II)] and comparison of its spectral and structural properties with those of other copper(II) 5,7-dimethyl[1,2,4]triazolo[1,5-α]pyrimidine thiocyanates. Inorg Chem 23:2803–2807
95. Favre TLF, Haasnoot JG, Reedijk J (1986) Characterization of copper(II) coordination compounds of 5,7-dimethyl[1,2,4]triazolo[1,5-*α*]pyrimidine: the crystal structure of diaquatetrakis-(5,7-dimethyl[1,2,4]triazolo[1,5-*α*]pyrimidine-N^3)-copper (II) hexafluorophosphate. Polyhedron 5:1405–1411
96. Grodzicki A, Szlyk E, Wojtczak A, Wrzeszcz G, Pazderski L, Muziol T (1999) The molecular structures of copper(II) chloroacetate complexes with 5,7-dimethyl- 1,2,4-triazolo-[1,5-*α*]-pyrimidine and 5,7-diphenyl-1,2,4-triazolo-[1,5-*α*]-pyrimidine. Polyhedron 18:519–527
97. Haasnoot JG, Favre TLF, Hinrichs W, Reedijk J (1988) A novel tetranuclear copper(I) cluster with alternate bridging halide and triazolopyrimidine ligands. Angew Chem Int Ed 27:856–858
98. Dirks EJ, Haasnoot JG, Kinnegin AJ, Reedijk J (1987) Coordination compounds of 5-methyl [1,2,4]triazolo[1,5*α*]pyrimidin-7-ol. Structures, spectra, and unusual magnetic properties of tetraaquabis(5-methyl[1,2,4]triazolo[1,5-*α*]pyrimidin-7-olato)copper(II) and the structurally analogous diammine diaqua compound. Inorg Chem 26:1902–1906
99. Cornelissen JP, De Graaff RAG, Haasnoot JG, Prins R, Reedijk J (1989) Structures and properties of bis(thiocyanato-*N*)bis(6-methyl[1,2,4]triazolo[1,5-*α*]pyrimidine-N^3)copper(II), a distorted tetrahedral copper(II) thiocyanate compound, and bis(thiocyanato-*N*)bis(5-methyl

[1,2,4]triazolo[1,5-α]pyrimidine-N^3)copper(II), a polynuclear pseudo-layered system. Polyhedron 8:2313–2320
100. Tyan MR, Bokach NA, Wang M-J, Haukka M, Kuznetsov ML, Kukushkin VY (2008) Facile cyanamide-ammonia coupling mediated by *cis*- and *trans*-[$Pt^{II}L_2$] centers and giving metal-bound guanidines. Dalton Trans 2008:5178–5188
101. Legin AA, Jakupec MA, Bokach NA, Tyan MR, Kukushkin VY, Keppler BK (2014) Guanidine platinum(II) complexes: synthesis, *in vitro* antitumor activity, and DNA interactions. J Inorg Biochem 133:33–39
102. Jeyalakshmi K, Selvakumaran N, Bhuvanesh NSP, Sreekanth A, Karvembu R (2014) DNA/protein binding and cytotoxicity studies of copper(II) complexes containing N, N′, N″-trisubstituted guanidine ligands. RSC Adv 4:17179–17195
103. Coles MP, Hitchcock PB (2001) Synthesis and X-ray crystal structure of polymeric and dimeric copper(I) cyanide complexes incorporating a bicyclic guanidine ligand. Polyhedron 20:3027–3032
104. Oakley SH, Coles MP, Hitchcock PB (2003) Structural and catalytic properties of bis(guanidine)copper(I) halides. Inorg Chem 42:3154–3154
105. Oakley SH, Coles MP, Hitchcock PB (2004) Structural consequences of the prohibition of hydrogen bonding in copper-guanidine systems. Inorg Chem 43:5168–5172
106. Oakley SH, Coles MP, Hitchcock PB (2004) Poly(guanidyl)silanes as a new class of chelating, *N*-based ligand. Dalton Trans 2004:1113–1114
107. Oakley SH, Coles MP, Hitchcock PB (2004) Multiple coordination geometries supported by methylene-linked guanidines. Inorg Chem 43:7564–7566
108. Coles MP, Khalaf MS, Hitchcock PB (2014) A new aliphatic N, C, N′-pincer ligand with pendant guanidine groups. Inorg Chim Acta 422:228–234
109. Coles MP, Sözerli SE, Smith JD, Hitchcock PB (2007) Metal complexes of guanidine-substituted alkyl ligands: an unsolvated monomeric two-coordinate organolithium. Organometallics 26:6691–6693
110. Coles MP, Sözerli SE, Smith JD, Hitchcock PB, Day IJ (2009) An ether-free, internally coordinated dialkylcalcium(II) complex. Organometallics 28:1579–1581
111. Coles MP, El-Hamruni AM, Smith JD, Hitchcock PB (2008) An organozinc hydride cluster: an encapsulated tetrahydrozincate. Angew Chem Int Ed 47:10147–10150
112. El-Hamruni SM, Sözerli SE, Smith JD, Coles MP, Hitchcock PB (2014) Tin and mercury compounds supported by a bulky organometallic ligand incorporating a pendant guanidine functionality. Aust J Chem 67:1071–1080
113. Pal S, Das D, Chattopadhyay P, Sinha C, Panneerselvam K, Lu T-H (2000) Synthesis, spectral and electrochemical properties of 1-alkyl-2-(naphthyl-β-azo)imidazole complexes of platinum(II) and the reaction with pyridine bases. Single-crystal X-ray structure of dichloro-[1-ethyl-2-(naphthyl-β-azo)imidazole]platinum(II). Polyhedron 19:1263–1270
114. Dinda J, Ray U, Mostafa G, Lu T-H, Usman A, Razak IA, Chantrapromma S, Fun H-K, Sinha C (2003) Copper(I)-azoimidazoles: a comparative account on the structure and electronic properties of copper(I) complexes of 1-methyl-2-(phenylazo)imidazole and 1-alkyl-2-(naphthyl-(α/β)-azo)imidazoles. Polyhedron 22:247–255
115. Ray U, Banerjee D, Mostafa G, Lu T-H, Sinha C (2004) Copper coordination compounds of chelating imidazole-azo-aryl ligand. The molecular structures of bis[1-ethyl-2-(*p*-tolylazo)imidazole]-bis-(azido)copper(II) and bis[1-methyl-2-(phenylazo) imidazole]-bis(thiocyanato)copper(II). New J Chem 28:1437–1442
116. Ray U, Sarker KK, Mostafa G, Lu T-H, Fallah MSE, Sinha C (2006) Copper(II) azide complexes of 1-alkyl-2-(arylazo)imidazoles: structure and magnetism. Polyhedron 25:2764–2772
117. Banerjee D, Ray U, Jasimuddin S, Liou J-C, Lu T-H, Sinha C (2006) Copper(II) complexes of thioether containing an azoimidazolyl system. X-ray structure of $Cu(SEtaaiNEt)Cl_2$ (SEtaaiNEt = 1-ethyl-2-{(*o*-thioethyl)phenylazo}imidazole). Polyhedron 25:1299–1306

118. de Hoog P, Gamez P, Driessen WL, Reedijk J (2002) New polydentate and polynucleating N-donor ligands from amines and 2,4,6-trichloro-1,3,5-triazine. Tetrahedron Lett 43:6783–6786
119. de Hoog P, Gamez P, Roubeau O, Lutz M, Driessen WL, Spek AL, Reedijk J (2002) Novel zigzag 1D coordination polymer from copper(II) chloride and N, N′-{2,4-di[(di-pyridin-2-yl) amine]-1,3,5-triazine}ethylenediamine exhibiting ferromagnetic interactions. New J Chem 27:18–21
120. Gamez P, de Hoog P, Lutz M, Spek AL, Reedijk J (2003) Coordination compounds from 1,3,5-triazine-derived multidirectional ligands: application in oxidation catalysis. Inorg Chim Acta 351:319–325
121. Casellas H, Gamez P, Reedijk J, Massera C (2006) Solvent control in the synthesis of Zn (II) and Cd(II) supramolecular compounds with N, N′-{2,4-di-[(di-pyridin-2-yl)amine]-1,3,5-triazine}ethylenediamine. Polyhedron 25:2959–2966
122. Lu Z, Costa JS, Roubeau O, Mutikaine I, Turpeine U, Teat JS, Gamez P, Reedijk J (2008) A copper complex bearing a TEMPO moiety as catalyst for the aerobic oxidation of primary alcohols. Dalton Trans 2008:3567–3573
123. Mooibroek TJ, Aromi G, Quesada M, Roubeau O, Gamez P, George SD, van Slageren J, Yasin S, Ruiz E, Reedijk J (2009) A mixed-valent pentanuclear $Cu^{II}{}_4Cu^{II}$ compound containing a radical-anion ligand. Inorg Chem 48:10643–10651
124. Costa JS, Castro AG, Pievo R, Roubeau O, Modec B, Kozlevecar B, Teat SJ, Gamez P, Reedijk J (2010) Proficiency of the electron-deficient 1,3,5-triazine ring to generate anion–π and lone pair–π interactions. Inorg Chem 48:10643–10651
125. Massoud SS, Louka FR, Xu W, Perkins RS, Vicente R, Albering JH, Maautner FA (2011) DNA cleavage by structurally characterized dinuclear copper(II) complexes based on triazine. Eur J Inorg Chem 2011:3469–3479
126. Bloy M, Diefenbach U (2000) Synthese, Komplexbildung und Kristallstrukturen von Cyclotriphosphazenen mit N, N, N′, N′-Tetramethylguanidingruppen. Z Anorg Allg Chem 626:885–891
127. Moggach SA, Galloway KW, Lennie AR, Parois P, Rowantree N, Brechin EK, Warren JE, Murrie M, Parsons S (2009) Polymerisation of a Cu(II) dimer into 1D chains using high pressure. CrystEngComm 11:2601–2604
128. He C, Fuchs MR, Ogata H, Knipp M (2012) Guanidine-ferroheme coordination in the mutant protein nitrophorin 4(L130R). Inorg Chem 51:4470–4473
129. Färber C, Leibold M, Bruhn C, Maurer M, Siemeling U (2012) Nitron: a stable *N*-heterocyclic carbene that has been commercially available for more than a century. Chem Commun 48:227–229
130. Klapp LRR, Bruhn C, Leibold M, Siemeling U (2013) Ferrocene-based bis(guanidines): superbases for tridentate N, Fe, N-coordination. Organometallics 32:5862–5872
131. Tönnemann J, Scopelliti R, Severin K (2014) (Arene)ruthenium complexes with imidazolin-2-imine and imidazolidin-2-imine ligands. Eur J Inorg Chem 2014:4287–4293
132. Bagchi V, Paraskevopoulou P, Das P, Chi L, Wang Q, Choudhury A, Mathieson JS, Cronin L, Pardue DB, Cundari TR, Mitrikas G, Sanakis Y, Stavropoulos P (2014) A versatile tripodal Cu(I) reagent for C–N bond construction via nitrene-transfer chemistry: catalytic perspectives and mechanistic insights on C–H aminations/amidinations and olefin aziridinations. J Am Chem Soc 136:11362–11381
133. Nair LS, Laurencin CT (2007) Biodegradable polymers as biomaterials. Prog Polym Sci 32:762–798
134. Sudesh K, Iwata T (2008) Sustainability of biobased and biodegradable plastics. Clean 36:433–442
135. dos Santos Vieira I, Herres-Pawlis S (2012) Lactide polymerisation with complexes of neutral N-donors – new strategies for robust catalysts. Eur J Inorg Chem 765–774
136. Endres HJ, Siebert-Raths A (2011) Engineering biopolymers. Hanser, Munich, p 225

137. Börner J, Flörke U, Glöge T, Bannenberg T, Tamm M, Jones MD, Döring A, Kuckling D, Herres-Pawlis S (2010) New insights into the lactide polymerisation with neutral N-donor stabilised zinc complexes. J Mol Catal A Chem 316:139–145
138. Auras R, Lim LT, Selke SEM, Tsuji H (2010) Poly(lactic acid) – synthesis, structures, properties, processing, and applications. Wiley, Hoboken
139. Inkinen S, Hakkarainen M, Albertsson AC, Södergard A (2011) From lactic acid to poly (lactic acid) (PLA): characterization and analysis of PLA and its precursors. Biomacromolecules 12:523–532
140. Gupta AP, Kumar V (2007) New emerging trends in synthetic biodegradable polymers – polylactide a critique. Eur Polym J 43:4053–4074
141. Platel RH, Hodgson LM, Williams CK (2008) Biocompatible initiators for lactide polymerization. Polym Rev 48:11–63
142. Garlotta D (2001) A literature review of poly(lactic acid). J Polym Environ 9:63–84
143. Ahmed J, Varshney SK (2011) Polylactides-chemistry, properties and green packaging technology: a review. Int J Food Prop 14:37–58
144. Dechy-Cabaret O, Martin-Vaca B, Bourissou D (2004) Controlled ring-opening polymerization of lactide and glycolide. Chem Rev 104:6147–6176
145. Wheaton CA, Hayes PG, Ireland BJ (2009) Complexes of Mg, Ca and Zn as homogeneous catalysts for lactide polymerization. Dalton Trans 4832–4846
146. Wu J, Yu TL, Chen CT, Lin CC (2006) Recent developments in main group metal complexes catalyzed/initiated polymerization of lactides and related cyclic esters. Coord Chem Rev 250:602–626
147. Drumright R, Gruber P, Henton D (2000) Polylactic acid technology. Adv Mater 12:1841–1846
148. Mehta R, Kumar V, Bhunia H, Upadhyay SN (2005) Synthesis of poy(lactic acid): a review. J Macromol Sci C Polym Rev 45:325–349
149. Kricheldorf HR (2001) Syntheses and application of polylactides. Chemosphere 43:49–54
150. Dijkstra PJ, Dum H, Feijen J (2011) Single site catalysts for stereoselective ring-opening polymerization of lactides. Polym Chem 2:520–527
151. Stanford MJ, Dove AP (2010) Stereocontrolled ring-opening polymerisation of lactide. Chem Soc Rev 39:486–494
152. Kricheldorf HR, Meier-Haak J (1993) Polylactones, 22 ABA triblock copolymers of L-lactide and poly(ethylene glycol). Macromol Chem 194:715–725
153. Yuan M, Liu D, Xiong C, Deng X (1999) Synthesis of polylactide and polyethylene glycol-co-poly-lactide copolymer with allylmagnesium chloride. Eur Polym J 35:2139–2145
154. Kricheldorf HR, Damrau DO (1997) Polymerizations of L-lactide initiated with Zn(II) - L-lactate and other resorbable Zn salts. Macromol Chem Phys 198:1753–1766
155. Thomas CM (2010) Stereocontrolled ring-opening polymerization of cyclic esters: synthesis of new polyester microstructures. Chem Soc Rev 39:165–173
156. Dove AP, Gibson VC, Marshall EL, Rzepa HS, White AJP, Williams DJ (2006) Synthetic, structural, mechanistic and computational studies on single-site β-diketiminate tin (II) initiators for the polymerization of rac-lactide. J Am Chem Soc 128:9834–9843
157. Williams CK, Breyfogle LE, Choi SK, Nam W, Young VG, Hillmyer MA, Tolman WB (2003) A highly active zinc catalyst for the controlled polymerization of lactide. J Am Chem Soc 125:11350–11359
158. Chamberlain BM, Cheng M, Moore DR, Ovitt TM, Lobkovsky EB, Coates GW (2001) Polymerization of lactide with zinc and magnesium ß-diiminate complexes: stereo control and mechanism. J Am Chem Soc 123:3229–3238
159. Ejfler J, Zafert S, Mierzwicki K, Jerzykiewicz LB, Sobota P (2008) Homo- and heteroleptic zinc aminophenolates as initiators for lactide polymerization. Dalton Trans 6556–6562
160. Wu JC, Huang BH, Hsueh ML, Lai SL, Lin CC (2005) Ring-opening polymerization of lactide initiated by magnesium and zinc alkoxides. Polymer 46:9784–9792

161. Jones MD, Davidson MG, Keir CG, Hughes LM, Mahon MF, Apperley DC (2009) Zinc (II) homogenous and heterogeneous species and their application for the ring-opening polymerization. Eur J Inorg Chem 635–642
162. Zhong ZY, Dijkstra PJ, Feijen J (2002) [(salen)Al]-Mediated, controlled and stereoselective ring-opening polymerization of lactide in solution and without solvent: synthesis of highly isotactic polylactide stereocopolymers from racemic d, l-lactide. Angew Chem 114:4692–4695
163. Zhong ZY, Dijkstra PJ, Feijen J (2003) Controlled and stereoselective polymerization of rac-(D, L)-lactide: kinetics, selectivity and microstructures. J Am Chem Soc 125:11291–11298
164. Pratt RC, Lohmeijer BGG, Long DA, Waymouth RM, Hedrick JL (2006) Triazabicyclodecene: a simple bifunctional organocatalyst for acyl transfer and ring-opening polymerization of cyclic esters. J Am Chem Soc 128:4556–4557
165. Kamber NE, Jeong W, Waymouth RM, Pratt RC, Lohmeijer BGG, Hedrick JL (2007) Organocatalytic ring-opening polymerization. Chem Rev 107:5813–5840
166. Becker JM, Tempelaar S, Stanford MJ, Pounder RJ, Covington JA, Dove AP (2010) Development of amino-oxazoline and amino-thiazoline organic catalysts for the ring-opening polymerisation of lactide. Chem Eur J 16:6099–6105
167. Chuma A, Horn HW, Swope WC, Pratt RC, Zhang L, Lohmeijer BGG, Wade CG, Waymouth RM, Hedrick JL, Rice JE (2008) The reaction mechanism for the organocatalytic ring-opening polymerization of L-lactide using a guanidine-based catalyst: hydrogen-bonded or covalently bound? J Am Chem Soc 130:6749–6754
168. Börner J, Flörke U, Huber K, Döring A, Kuckling D, Herres-Pawlis S (2009) Synthesis and characterisation of zinc complexes with guanidine-pyridine hybrid ligands: new catalysts for the ring-opening polymerisation of D, L-lactide. Chem Eur J 15:2362–2376
169. Börner J, Flörke U, Döring A, Kuckling D, Herres-Pawlis S (2010) Tracking the structure-reactivity relationship of zinc guanidine-pyridine hybrid complexes initiating lactide polymerisation. Macromol Symp 296:354–365
170. Börner J, dos Santos Vieira I, Pawlis A, Döring A, Kuckling D, Herres-Pawlis S (2011) Mechanism of the living lactide polymerisation mediated by robust zinc guanidine complexes. Chem Eur J 17:4507–4512
171. Börner J, dos Santos Vieira I, Flörke U, Döring A, Kuckling D, Herres-Pawlis S (2011) Zinc complexes with mono- and polydentate behaving guanidine ligands and their application in lactide polymerization. In: Smith PB (ed) Renewable and sustainable polymers. American Chemical Society, Division of Polymer Chemistry/Oxford University Press, Washington, pp 169–200
172. dos Santos Vieira I, Herres-Pawlis S (2012) Novel guanidine-quinoline hybrid ligands and the application of their zinc complexes in lactide polymerisation. Z Naturforsch 67:320–330
173. Börner J, dos Santos Vieira I, Flörke U, Döring A, Kuckling D, Herres-Pawlis S (2010) Studies on the lactide polymerization initiated by DMEGqu-containing zinc complexes. Polym Prepr (Am Chem Soc Div Polym Chem) 51:743–744
174. Douglas AF, Patrick BO, Mehrkhodavandi P (2008) A highly active chiral indium catalyst for living lactide polymerization. Angew Chem 120:2322–2325
175. Sousa SF, Carvalho ES, Ferreira DM, Tavares IS, Fernandes PA, Ramos MJ, Gomes JANF (2009) Comparative analysis of the performance of commonly available density functionals in the determination of geometrical parameters for zinc complexes. J Comput Chem 30:2752–2763
176. Picot D, Ohanessian G, Frison G (2008) The alkylation mechanism of zinc-bound thiolates depends upon the zinc ligands. Inorg Chem 47:8167–8178
177. Frison G, Ohanessian G (2008) A comparative study of semiempirical, ab initio, and DFT methods in evaluating metal-ligand bond strength, proton affinity, and interactions between first and second shell ligands in Zn-biomimetic complexes. J Comput Chem 29:416–433

178. Amin EA, Truhlar DG (2008) Zn coordination chemistry: development of benchmark suites for geometries, dipole moments and bond dissociation energies and their use to test and validate density functionals and molecular orbital theory. J Chem Theory Comput 4:75–85
179. Eger WA, Jahn BO, Anders E (2009) The zinc complex catalyzed hydration of alkyl isothiocyanates. J Mol Model 15:433–446
180. Ryner M, Stridsberg K, Albertsson AC, von Schenck H, Svensson M (2001) Mechanism of ring-opening polymerization of 1,5-Dioxepan-2-one and L-lactide with stannous 2-ethylhexanoate. A theoretical study. Macromolecules 34:3877–3881
181. von Schenck H, Ryner M, Albertsson AC, Svensson M (2002) Ring-opening polymerization of lactones and lactides with Sn(IV) and Al(III) initiators. Macromolecules 35:1556–1562
182. Marshall EL, Gibson VC, Rzepa HS (2005) A computational study on the ring-opening polymerization of lactide initiated by β-diketiminate metal alkoxides: the origin of heterotactic stereocontrol. J Am Chem Soc 127:6048–6051
183. Ling J, Shen J, Hogen-Esch TE (2009) A density functional theory study of the mechanisms of scandium-alkoxide initiated coordination–insertion ring-opening polymerization of cyclic esters. Polymer 50:3575–3581
184. Bull SD, Davidson MG, Johnson AL, Robinson DEJE, Mahon MF (2003) Synthesis, structure and catalytic activity of an air-stable titanium triflate, supported by an amine tris (phenolate) ligand. Chem Commun 1750–1751
185. Davidson MG, O'Hara CT, Jones MD, Keir CG, Mahon MF, Kociok-Köhn G (2007) Synthesis and structure of a molecular barium aminebis(phenolate) and its application as an initiator for ring-opening polymerization of cyclic esters. Inorg Chem 46:7686–7688
186. Chmura AJ, Cousins DM, Davidson MG, Jones MG, Lunn MD, Mahon MF (2008) Robust chiral zirconium alkoxide initiators for the room-temperature stereoselective ring-opening polymerisation of rac-lactide. Dalton Trans 1437–1443
187. Jones MD, Davidson MG, Kociok-Köhn G (2010) New titanium and zirconium initiators for the production of polylactide. Polyhedron 29:697–700
188. Matyjaszewski K, Tsarevsky NV (2014) Macromolecular engineering by atom transfer radical polymerization. J Am Chem Soc 136:6513–6533
189. Brar AS, Kaur S (2005) Tetramethylguanidino-tris(2-aminoethyl)amine: a novel ligand for copper-based atom transfer radical polymerization. J Polym Sci Part A Polym Chem 43:5906–5922
190. Bienemann O, Haase R, Jesser A, Beschnitt T, Döring A, Kuckling D, dos Santos Vieira I, Flörke U, Herres-Pawlis S (2011) Synthesis and application of new guanidine copper complexes in atom transfer radical polymerisation. Eur J Inorg Chem 15:2367–2379
191. Hoffmann A, Bienemann O, dos Santos Vieira I, Herres-Pawlis S (2014) New guanidine-pyridine copper complexes and their application in ATRP. Polymers 6:995–1007

Top Heterocycl Chem (2017) 51: 165–204
DOI: 10.1007/7081_2015_168

Published online: 11 September 2015

Redox-Active Guanidines and Guanidinate-Substituted Diboranes

Hans-Jörg Himmel

Abstract Guanidino groups and guanidinate substituents are used to stabilise positive charges, both through mesomeric and through inductive effects. The interplay between several guanidino groups is employed to create redox-active compounds. One realisation concept leads to guanidino-functionalised aromatic compounds (GFAs), which comprise aromatic systems substituted with several guanidino groups and constitute a relatively new class of strong organic electron donors as well as redox-active ligands. Some properties of these compounds and applications are presented, e.g. photochemical reductive C–C coupling, redox switches and stabilisation of polyanions. In addition, we allude to dinuclear copper complexes of bridging GFA ligands with several oxidation states of copper and the GFA ligand. In a second concept, two guanidinyl groups are connected, leading to bisguanidines which are generally termed urea azines. They could be oxidised in two separated one-electron steps. GFAs and bisguanidines are compared with other organic electron donors, and a relationship is established between the (gas-phase) adiabatic ionisation energy and the redox potential in solution. Lewis acid-base adducts between boranes and bicyclic guanidines could be subjected to dehydrocoupling reactions, leading to new sp^3–sp^3-hybridised diboranes of special reactivity. Their coordination chemistry and oxidative insertion reactions into the B–B bond are discussed. The electron-rich bridging guanidinate substituents allow for the synthesis of unprecedented cationic boron hydride compounds.

Keywords Diboranes · Guanidino-functionalised aromatic compounds · Organic electron donors · Urea azines

H.-J. Himmel (✉)
Anorganisch-Chemisches Institut, Ruprecht-Karls-Universität Heidelberg, Im Neuenheimer Feld 270, 69120 Heidelberg, Germany
e-mail: hans-jorg.himmel@aci.uni-heidelberg.de

Contents

Abbreviations

9-BBN	9-Borabicyclo[3.3.1]nonane
COSMO	Conductor-like screening model
CV	Cyclic voltammetry
Fc/Fc^+	Ferrocene/Ferrocenium
GFA	Redox-active guanidino-functionalised aromatic compound
hppH	1,3,4,6,7,8-Hexahydro-2H-pyrimido[1,2-a]pyrimidine. The compound is also known as triazabicyclodecene (1,5,7-triazabicyclo[4.4.0]dec-5-ene or TBD)
Htbn	1,5,7-Triazabicyclo[4.3.0]non-6-ene
Htbo	1,4,6-Triazabicyclo[3.3.0]oct-4-ene
TCNQ	Tetracyanoquinodimethane
TDAE	Tetrakis(dimethylamino)ethylene

1 Introduction

Neutral guanidines as well as guanidinates are excellent ligands, which are applied in coordination chemistry for manifold purposes [1–10]. Cu^I complexes of tripodal tris(2-guanidinylethyl)amine ligands were used for the preparation of end-on bonded superoxo complexes which exhibit a rich chemistry [11–16]. Other guanidine ligands were used as catalysts, e.g. in lactide polymerisation [17–21] or Heck-type reactions [22]. Acyclic guanidinates with sterically demanding organic groups served as substituents in dimeric Mg^I compounds [23, 24]. Bicyclic guanidinate ligands stabilise dinuclear transition metal complexes with multiple bonding between two highly oxidised metal atoms [25–28] and were applied for the design of molecular catalysts for several reactions [7, 29].

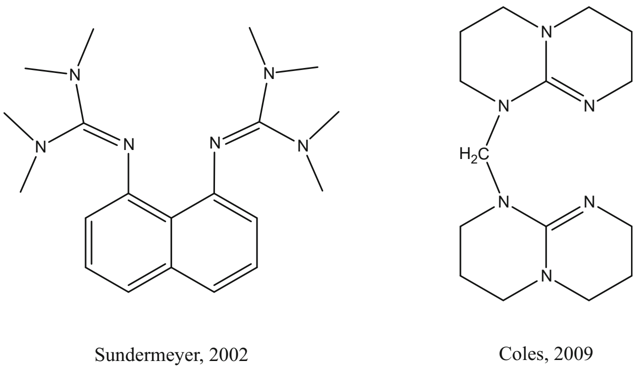

Scheme 1 Lewis structures of the two proton sponges 1,8-bis(tetramethylguanidino)-naphthalene and $H_2C(hpp)_2$ (hppH = 1,3,4,6,7,8-hexahydro-2H-pyrimido[1,2-a]pyrimidine)

The superior Brønsted basicity of guanidines is employed to build super bases ([30] and references given therein) and proton sponges ([31]). Proton sponges exhibit a very high proton affinity, but are otherwise much less nucleophilic. The archetypical proton sponge is 1,8-bis(dimethylamino)-naphthalene, which was first reported by Alder [32]. Both the bridging position of the bound proton and the reduction of the lone-pair repulsion between the two amino groups are factors to explain the high proton affinity. From the many examples for proton sponges [22, 33–40], Scheme 1 shows the Lewis structures of two examples, namely, 1,8-bis(tetramethylguanidino)naphthalene, which was studied by the group of Sundermeyer [34], and $H_2C(hpp)_2$ (hppH = 1,3,4,6,7,8-hexahydro-2H-pyrimido [1,2-a]pyrimidine) from the group of Coles [35]. In both cases, the interplay of two guanidino groups, acyclic or bicyclic ones, is responsible for the proton sponge characteristics. The same guanidino groups will also be relevant for the discussion in this chapter. Also, the interplay between several guanidino groups is used to realise a special reactivity.

For the discussion in this chapter, the capability of guanidino groups and guanidinate substituents to stabilise positive charges both through mesomeric and inductive effects is of significance. If guanidino groups are attached to electron-rich systems, special redox properties result. In the second section of this chapter, we discuss the creation of strong organic electron donors by the interplay of several guanidino groups. The simplest realisation concept is to connect directly two guanidinyl groups, resulting in bisguanidines (usually termed urea azines). Surprisingly little is known about these species. An alternative concept that envisages substitution of aromatic systems with several guanidino groups leads to a new class of strong organic electron donors, which is denoted GFA (guanidino-functionalised aromatic compound). Within this concept, it is even possible to turn electron acceptors such as *p*-benzoquinones into electron donors. Some applications of GFAs will be discussed. In the third section of this chapter, bicyclic guanidino groups will be applied as bridging substituents in sp^3–sp^3-hybridised diboranes featuring a direct B–B bond. They lend a special reactivity to the B–B bond, which manifests itself especially in the formation of unprecedented mono- and dicationic boron hydrides.

2 Redox-Active Guanidines

2.1 Guanidino-Functionalised Aromatic Compounds (GFAs)

Organic electron donors are attractive for a variety of applications which span from synthesis [41] to materials. A prominent (and archetypical) example for an electron donor is tetrakis(dimethylamino)ethylene (TDAE, **1**), which was first synthesised in 1950 [42]. The CV curve of **1** in CH_3CN shows two reversible one-electron waves [43, 44], while in DMF one reversible two-electron wave is observed [44, 45]. Its redox potential ($E_{1/2}$) in DMF amounts to -1.07 V vs. Fc/Fc$^+$ (Fc = ferrocene) [46]. The related compound 1,1′,3,3′-tetraphenyl-2,2′-biimidazolidinylidene (**2**) followed 10 years later [47]. Both compounds were extensively used in redox reactions and also for the formation of carbene complexes [48]. Further modifications led to compound **3** (see Scheme 2) [49, 50], which was termed “super electron donor”. An $E_{1/2}$ value (for two-electron oxidation) of -1.60 V vs. Fc/Fc$^+$ was determined for this compound. Upon oxidation of **3**, aromaticity is created (see Scheme 2), and this aromatic stabilisation of the monocationic and dicationic forms was made responsible for the stronger reduction power compared to **1** or **2** [51].

In 2008 our group reported the first member of a new class of strong electron donors, which was termed GFAs (guanidino-functionalised aromatic compounds) [52, 53]. The compound 1,2,4,5-tetrakis(tetramethylguanidino)benzene **4** (see Scheme 2) exhibits an $E_{1/2}$ value of 0.70 V vs. Fc/Fc$^+$ in dichloromethane, when ferrocene is used as external standard [46], and -0.76 V, when ferrocene is used as internal standard [54]. The neutral compound **4** as well as complexes of the radical monocation $\mathbf{4}^{+\cdot}$ and the dication $\mathbf{4}^{2+}$ were synthesised and structurally characterised. The structure of $\mathbf{4}^{2+}$ is in line with a description as a pair of bisguanidino-allyl cations which are connected by two C–C single bonds (see the Lewis structure in Scheme 2). The alternative description as a quinone-diiminium dication does not correctly describe the electronic situation (see the examples provided below). In the case of **4** and most other GFAs, aromaticity is present in the *neutral* form, but *removed* upon oxidation to the monocation or dication (see Scheme 2). In the following years, we synthesised a number of GFA compounds and studied their chemistry [52].

It might be tempting to explain the higher redox potential in solution of **4** compared with **1** and **3** with the loss of aromaticity upon oxidation [51, 55]. However, this explanation is wrong. The (gas-phase) ionisation energy (calculated with B3LYP/TZVP) of **4** (4.66 eV) is slightly lower than that of **1** (5.03 eV) and not much higher than that of **3** (4.43 eV). The second ionisation energy of **4** (7.31 eV) is even much lower than that of **1** (9.08 eV) or **3** (8.52 eV). Hence, intrinsic effects cannot explain the order in the redox potentials determined in solution.

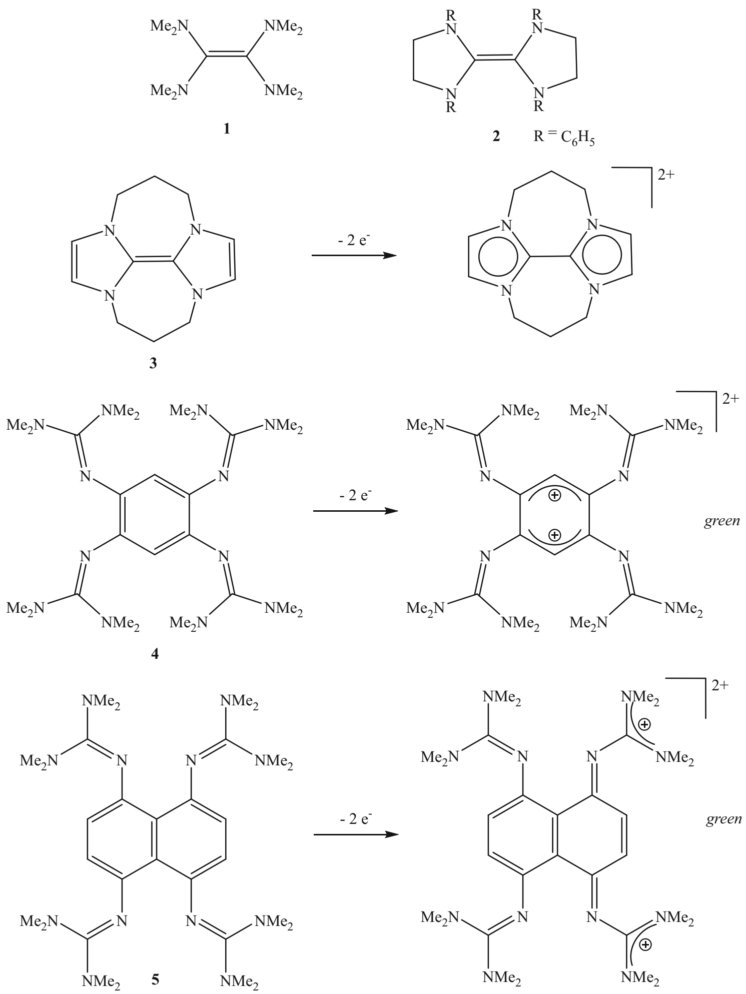

Scheme 2 Five typical organic electron donors: tetrakis(dimethylamino)ethylene (TDAE, **1**), 1,1′,3,3′-tetraphenyl-2,2′-biimidazolidinylidene (**2**), the special tetrakis(dialkylamino)-ethylene (**3**) and the GFA compounds 1,2,4,5-tetrakis(tetramethylguanidino)benzene (**4**) and 1,4,5,8-tetrakis(dimethylguanidino)naphthalene (**5**)

The relatively large volume of **4** (707 Å^3) compared with **1** (296 Å^3) or **3** (254 Å^3) reduces the stabilisation of the charged species by a polar solvent. Hence, solvent stabilisation and not the gain or loss of aromaticity is the decisive factor. We will discuss this issue in some more depth in Sect. 2.3 (for a comprehensive discussion, see Eberle et al. [46]).

In the case of compound **5**, the 10π-aromatic system is removed upon oxidation, but a 6π-aromatic system is formed. Compound **5** and stable salts of the dication **5**$^{2+}$ and even the tetracation **5**$^{4+}$ (in this case the 6π-aromatic system which is created

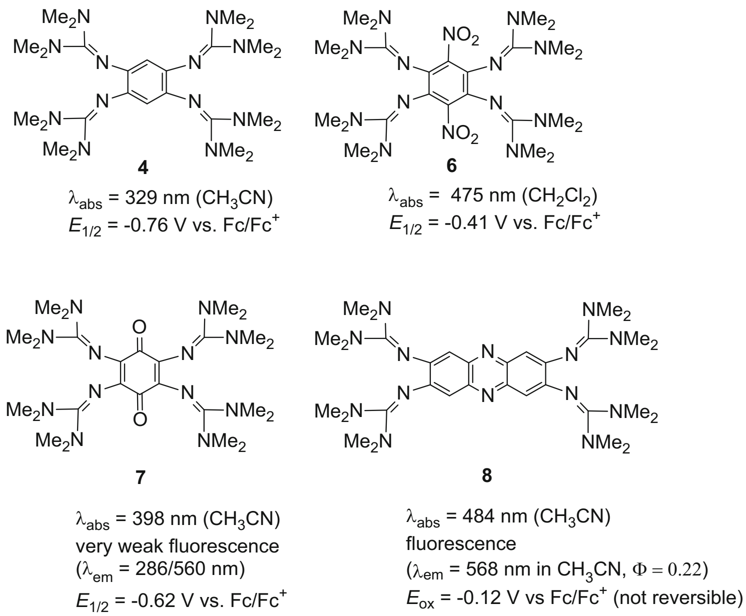

Scheme 3 Lewis structures of some GFAs and related compounds with distinct optical properties before oxidation. The wavelength at the maximum of the band due to the lowest-energetic electronic transition detected in the UV/Vis spectrum (λ_{abs}) and the redox potential ($E_{1/2}$ values in V vs. Fc/Fc^+, with ferrocene (Fc) added as internal standard to the solution) is given underneath

upon two-electron oxidation is removed) were already synthesised and structurally characterised [56, 57]. The redox potential of **5** ($E_{1/2} = -0.65$ V vs. Fc/Fc^+ in CH_2Cl_2) is slightly higher than that of **4**. Usually, (uncoordinated) GFAs eliminate two electrons at similar potential, and consequently a two-electron wave is observed in the CV curves. A rare exception is the compound 3,3′,4,4′-tetrakis (tetramethylguanidino)1,1′-biphenyl, for which two well-separated one-electron redox waves are observed (at $E_{1/2}$ values of 0.06 and 0.61 V in CH_3CN vs. SCE), translating into values of −0.34 and 0.21 V vs. Fc/Fc^+ [58].

Compounds **4** and **5** are colourless in their neutral state, but become intensely coloured after oxidation. Other GFAs are already coloured in their neutral state. Scheme 3 gives some examples, namely, 1,2,4,5-tetrakis(tetramethylguanidino)-3,6-dinitro-benzene (**6**) [54], 2,3,5,6-tetrakis(tetramethylguanidino)-*p*-benzoquinone (**7**) [59] and 2,3,7,8-tetrakis(tetramethylguanidino)-phenazine (**8**) [60]. The phenazine derivative **8** shows intense solvent-dependent fluorescence. Coordination with $ZnCl_2$ leads to a blue shift of the emission maximum (from 568 nm in **8** to 506 nm in [**8**$(ZnCl_2)_2$]) and enhances the quantum yield for fluorescence (22% for **8** and 36% for [**8**$(ZnCl_2)_2$]). Further coordination of $ZnCl_2$ at the nitrogen atoms of the phenazine ring quenches fluorescence and leads to a significant red-shift in the electronic absorption spectra [60].

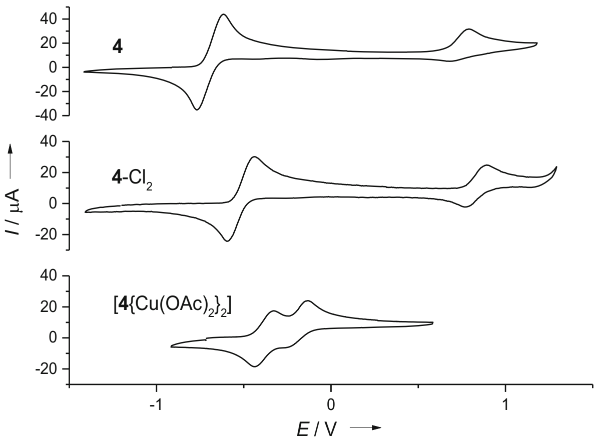

Fig. 1 CV curves (measured in CH_2Cl_2, potentials given vs. Fc/Fc^+) as recorded for **4**, dichloro-substituted **4** (**4**-Cl_2) and the dicopper complex [**4**{Cu $(OAc)_2\}_2$]

The redox properties and the optical properties of GFA compounds could be tuned by aromatic substitution, complexation or protonation. As an example, Fig. 1 displays the CV curves as measured for **4**, dichloro-substituted **4** (1,2,4,5-tetrakis (tetramethylguanidino)-3,6-dichloro-benzene, **4**-Cl_2) and the dinuclear Cu^{II} complex [**4**{$Cu(OAc)_2\}_2$] [46]. The $E_{1/2}$ value for two-electron oxidation shifts from −0.70 V for **4** to −0.52 for **4**-Cl_2 (vs. Fc/Fc^+, added as external standard). A further one-electron oxidation wave is observed in both cases at higher potentials. In the case of [**4**{$Cu(OAc)_2\}_2$], two separated one-electron oxidation waves are visible at −0.39 and −0.20 V vs. Fc/Fc^+.

In some cases, the reduction power of GFAs is too strong for a desired outcome of the redox reaction, and in this case, one could use complexation as a means to reduce the reduction power [61, 62]. Complex salts $[(GFA)(BF_2)_2]^{2+}(BF_4{}^-)_2$ were synthesised by reaction of the GFA (e.g. **4** or **5**) with 4 equiv. of BF_3. Exchange spectroscopy (EXSY) ^{19}F NMR experiments show exchange between the $BF_2{}^+$ groups in the dication and the $BF_4{}^-$ anions, with an exchange rate of $(4 \pm 1)\,s^{-1}$ [61]. Due to the relatively high charge, the N–B bonds in the dication are fairly weak. Solutions of this salt behave as a source of uncomplexed GFA, which is delivered in small amounts to provide especially mild reducing conditions:

$$\left[(GFA)(BF_2)_2\right]^{2+} + 2BF_4{}^- + nX_2 \rightarrow (GFA)^{2+} + 4BF_3 + 2X_n{}^-$$

Generally, the $X_n{}^-$ anion crystallises together with the $[(GFA)(BF_2)_2]^{2+}$ dication from the reaction mixture. This could be used, e.g. to synthesise polyhalides [61]. Reaction between uncomplexed GFAs and I_2 or Br_2 leads typically to the salts $(GFA)(I_3)_2$ and $(GFA)Br_2$ (in some cases oxidation is accompanied by aromatic substitution). On the other hand, reaction with complexed GFAs leads to polyhalides. For X = I, one obtains a network of $I_7{}^-$ anions. In the case of X = Br and GFA **5**, $Br_5{}^-$ anions are formed which interact with each other in the solid state. This strategy could also be employed to synthesise organic semiconducting materials. Uncomplexed GFAs react with TCNQ to give salts $(GFA)(TCNQ)_2$ with isolated $[(TCNQ)_2]^{2-}$ units. When $[\mathbf{4}(BF_2)_2](BF_4)_2$ or $[\mathbf{5}(GaCl_2)_2](GaCl_4)_4$ are used for TCNQ reduction, π-stacks of TCNQ-units with a formal charge of −0.5 e per unit are formed, and the resulting materials are electrical semiconductors with a band gap of ca. 0.5 eV [62].

Photochemical reductive C–C coupling reactions of alkyl halides could be accomplished with the GFA 2,3,5,6-tetrakis(tetramethylguanidino)-pyridine (**9**) [63]. So far this reaction resorts to benzyl and allyl halides.

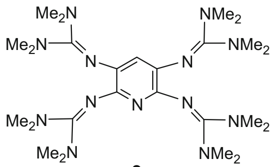

9

$$\mathbf{9} + 2\ RX \xrightarrow{h\nu} \mathbf{9}^{2+} + 2\,X^- + R\text{-}R$$

A possible reaction pathway is sketched in Fig. 2. The first step is without doubt the formation of a pyridinium-alkyl salt. If GFA **9** is replaced by GFA **4**, no photoreaction occurs, since **4** could not bind to the alkyl halide. Irradiation of this salt leads to cleavage of the GFA-R bond and formation of a radical $R^{\cdot}$ together with the radical monocation $GFA^{+\cdot}$, which promptly disproportionates into GFA and GFA^{2+}. Quantum chemical calculations were carried out to compare the pyridinium-alkyl cation dissociation into an alkyl radical and a pyridinium cation with that into an alkyl cation and pyridine (see Scheme 4). In the case of pyridine, the formation of an alkyl cation and pyridine is energetically favoured. On the other hand, in the presence of the guanidino groups, the formation of an alkyl radical and a pyridinium cation is favoured. It is not yet clear if two radicals R, released in the photoreaction, react with each other to give the coupling product or if the radical $R^{\cdot}$ attacks a further pyridinium-alkyl salt. The dication GFA^{2+} could be reduced again to neutral GFA with hydrazine or cobaltocene ($CoCp_2$, Cp = cyclopentadienyl) to close the cycle in Fig. 2. Up to date, GFA reduction has to be done in a separated step. Research is ongoing with the aim to develop the process further to a photocatalytic reaction.

GFAs are strong Brønsted bases and were even shown to deprotonate CH_3CN in the presence of PhAuCl, resulting in the formation of a gold-cyanomethyl complex [64]. On the other hand, GFAs with partially alkylated guanidino groups could be turned into strong hydrogen-bond donors by two-electron oxidation. By design of the guanidino groups, one could also synthesise redox switches, in which hydrogen bonding is reversibly switched on by oxidation (see Scheme 5) [65]. As an example, Fig. 3 displays the structure of the aggregate $[(\mathbf{10})_3]^{2+}$. The dication $\mathbf{10}^{2+}$ also forms aggregates with other hydrogen-bond acceptors, including GFA **4**.

On the other hand, if $\mathbf{10}^{2+}$ is reacted with the proton sponge **5**, it is deprotonated (see Scheme 6). The product of deprotonation is an intensely red-coloured dye.

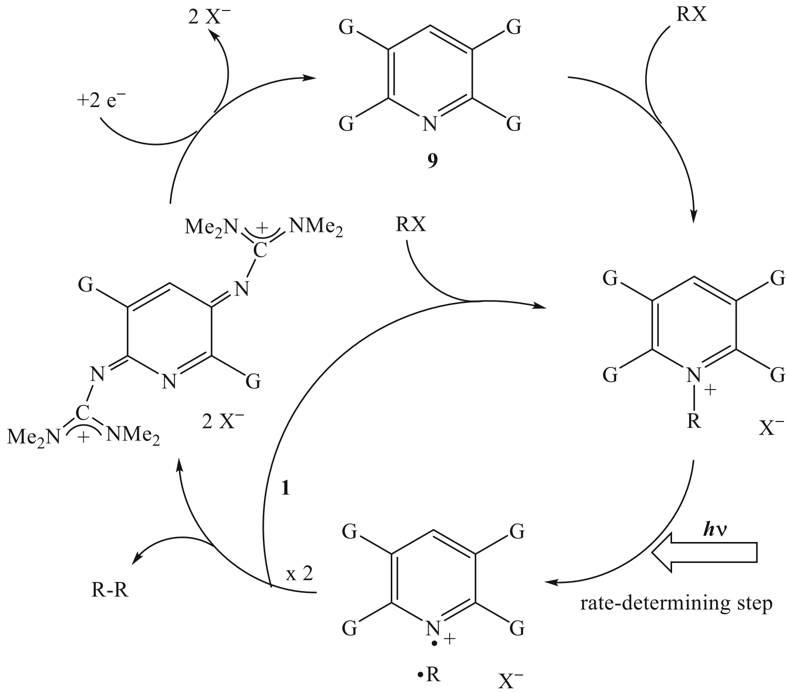

Fig. 2 Possible reaction pathway for the photochemical reductive C–C coupling of alkyl halides with GFA **9** (G = tetramethylguanidino, e.g. R = benzyl or allyl derivatives)

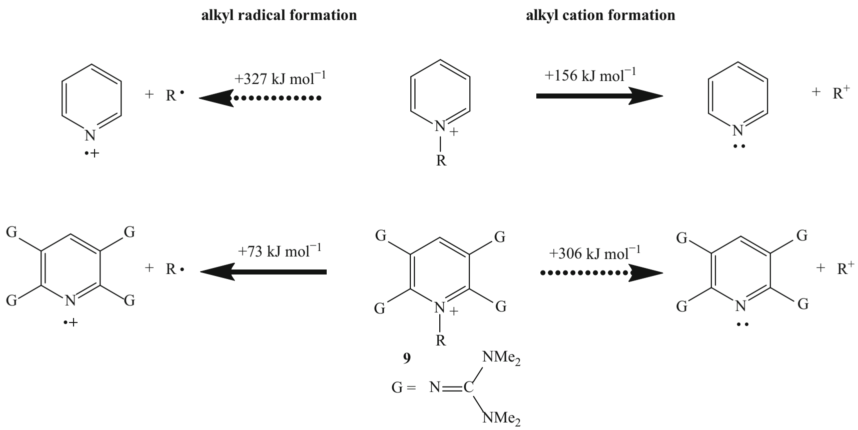

Scheme 4 N–C bond cleavage reactions showing the preference of *N*-alkyl pyridinium ions for alkyl cation formation. By contrast, **9**-alkyl cations prefer to form alkyl radicals. The energies are Δ*G* values (1 bar, 198 K) for R = benzyl from B3LYP/6-311G** calculations

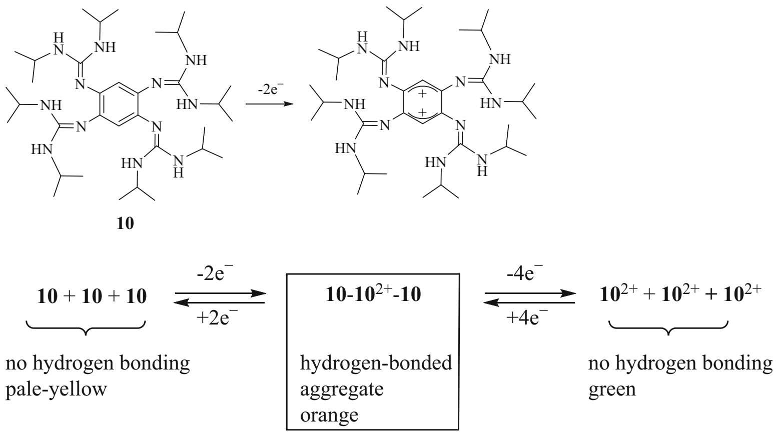

Scheme 5 Lewis structure of GFA **10** and oxidation-induced aggregate formation and deaggregation

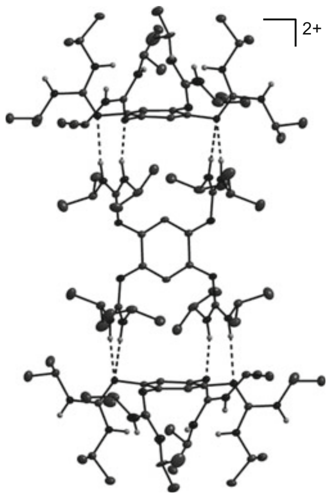

Fig. 3 Structure of the hydrogen-bonded aggregate $[(\mathbf{10})_3]^{2+}$. Vibrational ellipsoids drawn at the 50% probability level. Hydrogens attached to carbon omitted

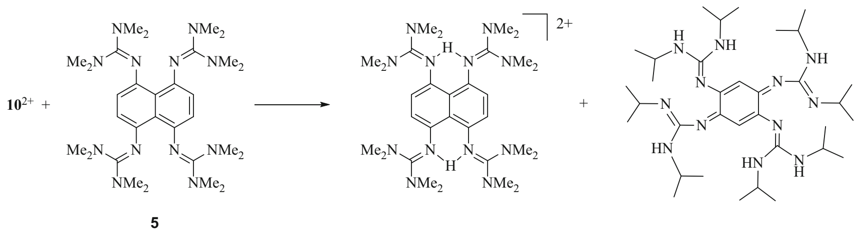

Scheme 6 Deprotonation of $\mathbf{10}^{2+}$ by reaction with the proton sponge GFA **5**

Table 1 Fully characterised (including crystal structure) examples in the formal "charge-transfer" series of dinuclear copper complexes with GFA **4** (only examples with $Cu^{I/II}$ and $GFA^{0/+/2+}$ are considered)

"Red. form"	$-e^- \rightarrow$	$-2e^- \rightarrow$	$-3e^- \rightarrow$	$-4e^- \rightarrow$
[Cu^I-GFA-Cu^I]	[Cu^{II}-GFA-Cu^I]	[Cu^{II}-GFA-Cu^{II}]	[Cu^{II}-GFA^+-Cu^{II}]	[Cu^{II}-GFA^{2+}-Cu^{II}]
[**4**$(CuX)_2$] [66]	charge localization or delocalization, no example so far	[**4**$\{Cu(OAc)_2\}_2$] [67] [**4**$\{Cu(NO_3)_2\}_2$] [68]	[**4**$\{Cu(OAc)_2\}_2]^+$ [67]	[**4**$\{Cu(CH_3CN)_4\}_2]^{6+}$ [69]
(X = Br, I)		Weak antiferromagn. coupl.	LLCT band,[a] strong ferromagn. coupl.	[**4**$\{Cu(OAc)_2\}_2]^{2+}$ [67]
Trig. planar coord. geom.			[**4**$\{Cu(NO_3)_2\}_2]^+$ [68]	[**4**$\{Cu(NO_3)_2\}_2]^{2+}$ [68]
			Strong ferromagn. coupl.	Weak antiferromagn. coupl.
	[Cu^I-GFA^+-Cu^I]	[Cu^{II}-GFA^+-Cu^I]	[Cu^{II}-GFA^{2+}-Cu^I]	
	No example so far	charge localization or delocalization, no example so far	charge localization or delocalization, no example so far	
		[Cu^I-GFA^{2+}-Cu^I]		
		$\{[$**4**$(CuI)_2](I_3)_2\}_n$ [66]		
		Semiconduct. chain, band gap 1.1 eV		

[a]*LLCT* ligand–ligand charge transfer

GFAs form dinuclear transition metal complexes not only in their neutral state but also upon oxidation. Especially, copper complexes are in the focus of actual research. Table 1 provides an overview of the different types of complexes which are possible and which were already synthesised with GFA **4**. Starting with the electron-rich complex type [Cu^I-GFA-Cu^I], the other types are formally obtained by removal of up to four electrons. The synthesised complexes of the type [Cu^I-GFA-Cu^I] (with GFA **4** and other GFAs) all feature trigonal-planar-coordinated Cu^I atoms. Such a coordination geometry is especially interesting for possible catalytic applications, since the open structure at the copper atoms should facilitate oxidative addition reactions. Examples of the type [Cu^{II}-GFA^{2+}-Cu^{II}] are also readily available. They could either be synthesised in one step by reaction with a Cu^{II} compound (e.g. synthesis of [**4**$\{Cu(CH_3CN)_4\}_2](BF_4)_6$ from **4** and $Cu(BF_4)_2$ in CH_3CN) or by coordination followed by oxidation (e.g. synthesis of [**4**$\{Cu(OAc)_2\}_2](I_3)_2$ by reaction between **4** and $Cu(OAc)_2$, followed by oxidation with I_2; see Scheme 7). Especially interesting is the "$-2e^-$ case" (see Table 1), for which three electronic descriptions are possible. For the complexes [**4**$\{Cu(OAc)_2\}_2$] and [**4**$\{Cu(NO_3)_2\}_2$], the analytical data unambiguously showed the presence of neutral GFA ligand units

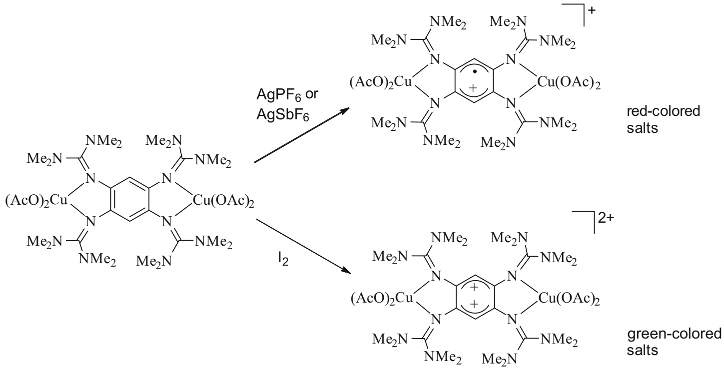

Scheme 7 One-electron and two-electron oxidation of the complex [**4**{Cu(OAc)$_2$}$_2$]

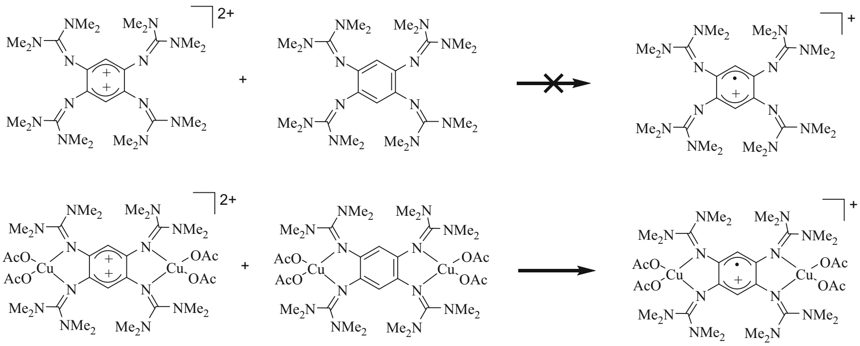

Scheme 8 While the free radical monocation **4**$^{+\cdot}$ cannot be formed by adding neutral **4** to a solution of a salt of the dication **4**$^{2+}$, the corresponding reaction for dinuclear Cu(OAc)$_2$ complexes proceeds quantitatively

and Cu^{II} atoms (type [Cu^{II}-GFA-Cu^{II}]). On the other hand, in the coordination polymer {[**4**(CuI)$_2$](I$_3$)$_2$}$_n$, the GFA ligand is oxidised and the copper atoms are in the +1 oxidation state. The polymer therefore belongs to the type [Cu^{I}-GFA^{2+}-Cu^{I}].

GFAs are generally two-electron donors in organic solvents, and in CV experiments, two electrons are eliminated at similar potential. A comproportionation reaction to generate the radical monocation (see Scheme 8 for the example of GFA **4**) does not work. However, upon complexation, comproportionation becomes feasible, leading quantitatively to the complexed radical monocation (see Scheme 8) [46, 67].

Dinuclear Cu^{I} complexes of neutral GFAs could readily be oxidised. In the case of GFA **4**, oxidation leads selectively to oxidation of the ligand, but not of the copper atoms. The resulting dinuclear Cu^{I} complex of the dicationic ligand polymerises to give a semiconducting chain polymer (see Fig. 4a) with a band gap of ca. 1.1 eV (estimated from an Arrhenius fit of the temperature-dependent conductivity σ; see Fig. 4b) [66]. The increase in the coordination number (from three to four), owing to the lower Lewis basicity of the GFA ligand upon oxidation, effects polymerisation.

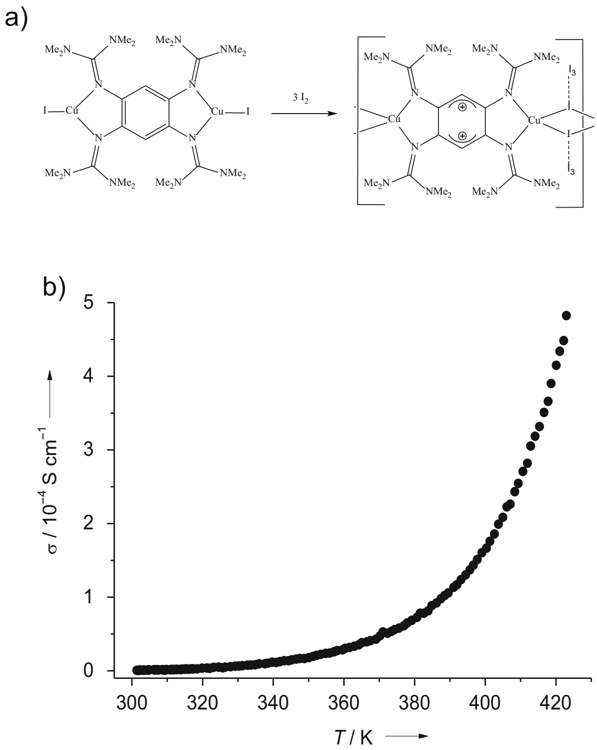

Fig. 4 (**a**) Example for the oxidation of a dinuclear Cu^{I} complex with a GFA (**4**) ligand. Oxidation leads to ligand oxidation, but not copper oxidation. The product is a chain polymer with GFA^{2+} ligand units. (**b**) The temperature-dependence of the electrical conductivity σ that was used to estimate the band gap of a compressed pellet of the chain polymer

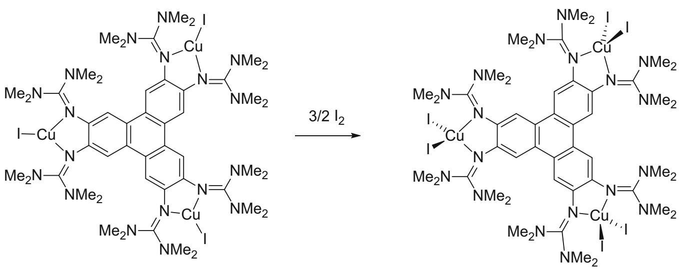

Scheme 9 Oxidation of trinuclear Cu^{I} complexes of the GFA 2,3,6,7,10,11-hexakis(tetramethylguanidino)triphenylene lead to metal oxidation to give trinuclear Cu^{II} complexes. The ligand remains neutral, in contrast to the reaction given in Fig. 4a

The trinuclear Cu^{I} complex of the GFA 2,3,6,7,10,11-hexakis(tetramethylguanidino)-triphenylene could be oxidised with I_2 to the trinuclear Cu^{II} complex (see Scheme 9) [70]. In this case, the copper atoms rather than the GFA ligand are oxidised. The $E_{1/2}$ value in CH_2Cl_2 for two-electron oxidation of the free GFA is −0.39 V vs. Fc/Fc^+, a value which is significantly higher than the −0.76 V measured for **4**. In the case of the CuI_2 complex, a considerable percentage of the spin-density is located at the I atoms.

2.2 *Urea Azines (Bisguanidines)*

As already mentioned (see Sect. 1), an alternative strategy for generating organic electron donors is to link two guanidinyl units directly together. The resulting bisguanidines are usually denoted urea azines. Surprisingly little is known up to date about this interesting class of compounds. Scheme 10 shows the four compounds **11–14** which were synthesised up to date [71–73], together with the elusive compound **15**.[1] Our group was the first to inspect their redox properties ([73]; 2,2′-azines were studied previously by Hünig et al. [74, 75]). In CV experiments, urea azines could be oxidised in two separated one-electron steps. For the first (one-electron) oxidation, potentials of $E_{1/2} = -0.50$, −0.29 and −0.40 V vs. Fc/Fc^+ were obtained for compounds **12**, **13** and **14**, respectively. Chemical oxidation of compound **14** by TCNQ (tetracyanoquinodimethane) gives the radical salt **14**(TCNQ). The structural elucidation showed that mixed stacks are formed in the solid state

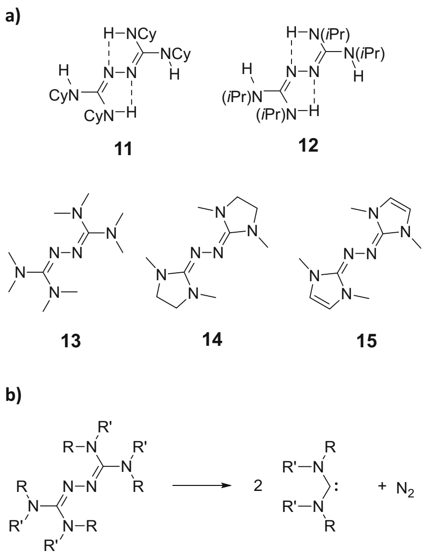

Scheme 10 (**a**) Lewis structures of four examples for urea azines (bisguanidines). Of these, compound **15** was not yet synthesised. (**b**) Hypothetical decomposition of a urea azine with two organic substituents R and R′ into N_2 and carbene

[1] Attempts to synthesise this compound were so far unsuccessful. The standard route ("activation" of the urea by reaction with oxalyl chloride and subsequent reaction with hydrazine) fails due to the reduced electrophilicity of the imidazolium salt ("activated urea"). See the Supporting Information in Herrmann et al. [73].

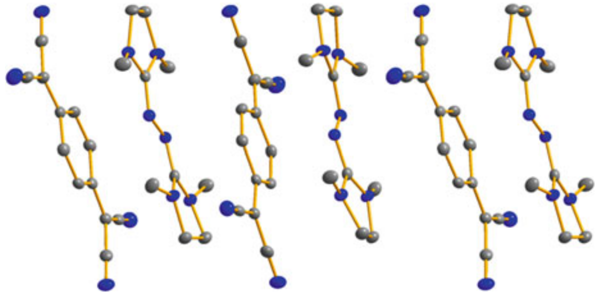

Fig. 5 Illustration of the packing within the chains of solid **14**(TCNQ), as determined by X-ray diffraction

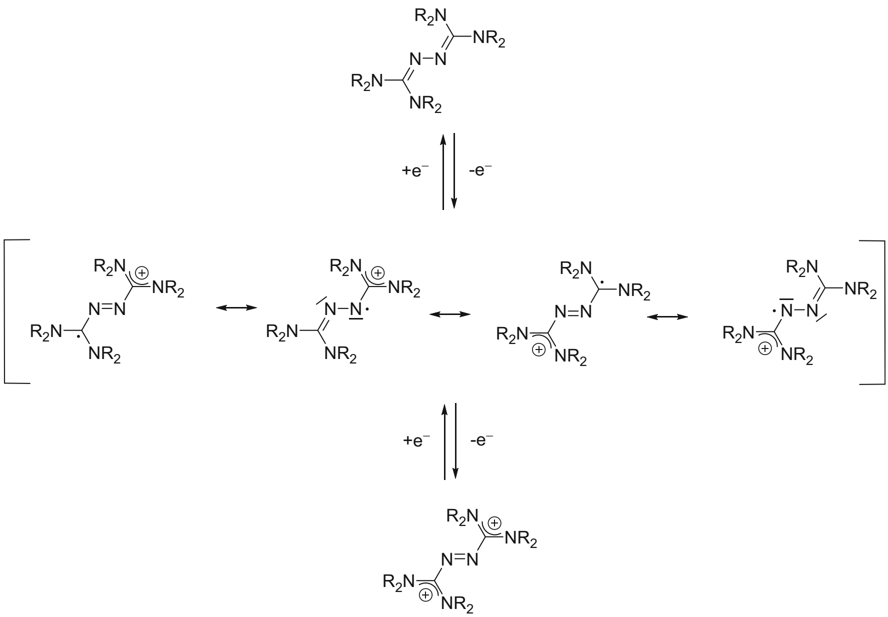

Scheme 11 Lewis structures upon one-electron and two-electron oxidation of urea azines. After two-electron oxidation, the central N–N single bond is converted into a double bond

Scheme 12 (**a**) "Classical" Lewis structures and (**b**) dative bond descriptions (double-base stabilised highly excited dinitrogen)

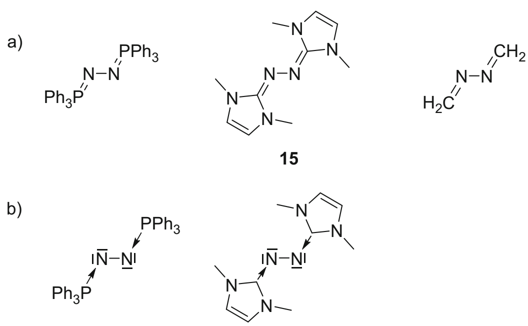

(see Fig. 5). The length of the central N–N bond in **14** decreases upon one-electron oxidation from 1.416(1) to 1.335(4) Å. This is in agreement with the Lewis formula (see Scheme 11), suggesting a bond order between 1 and 2 in the radical monocation and of 2 in the dication.

The electronic properties of urea azines are worth a comment in the light of the actual discussion about dative bonding in main-group element chemistry. Recently the compound $Ph_3PNNPPh_3$, which was already reported 50 years ago [76], was described as two PPh_3 donors bound to N_2, leading to the Lewis structure shown in Scheme 12b [77].

In this description, the complex is built of N_2 in its highly excited $(1)^1\Gamma_g$ electronic state (valence configuration $(1\sigma_g)^2(1\sigma_u)^2(1\pi_u)^2(2\sigma_g)^2(1\pi_g)^2$) with an energy 1,427 kJ mol^{-1} higher than the $X^1\Sigma_g{}^+$ ground state (a value which exceeds significantly the dissociation energy of N_2!), stabilised by two PPh_3 donors. The authors argue that a high activation barrier prohibits decomposition into N_2 and PPh_3, which was calculated to be exergonic ($\Delta G = -312$ kJ mol^{-1} by RI-PB86/TZVPP [77] and -367 kJ mol^{-1} by MP2/TZVP//B3LYP/TZVP [78] (single-point MP2 calculations for the electronic energies with the optimised structure from B3LYP)). In this context, *N*-heterocyclic carbene (NHC)-stabilised N_2 was also mentioned. Moreover, a theoretical work studied “NHC-stabilised diatomics” including N_2 [78], and within this work, compound **15** was explicitly mentioned as an example. The enthalpy and Gibbs-free energy for decomposition of the urea azine into N_2 and singlet carbene (reaction in Scheme 10b) is plotted in Fig. 6 for compounds **12–15**. The values show a clear trend towards decreasing energies in the series **12–15**. Compound **14** already exhibits a negative ΔH^0 value for decomposition, and for **15** both ΔH^0 and ΔG^0 become negative. However, a thorough analysis under consideration of the vibrational modes [73] clearly shows that in all cases the dative bond description is inadequate, the classical Lewis structure being a much better description. The clear trend in the decomposition enthalpies and Gibbs-free energies simply reflects the stability of the carbene products, but not the electronic structure in the bisguanidines, which is similar in all compounds (see the discussion in [73]).

Partially alkylated urea azines could be used for the synthesis of new heteronuclear ring compounds. As an example, Fig. 7 shows the reaction between 9-BBN (9-borabicyclo[3.3.1]nonane) and **12**.

2.3 Electron Donor Strength: Intrinsic and Extrinsic Factors

As already mentioned, GFAs such as **4** and **5** (see Scheme 2) are quite large molecules in comparison with, e.g. the electron donors **1** and **3** and also with urea azines. The relatively large size is responsible for their higher redox potential in solution. Under certain assumptions (zero or small static dipole moment, relatively uniform charge distribution in the oxidised species), the first ionisation energy in solution could be linked with the first ionisation energy in the gas-phase through a

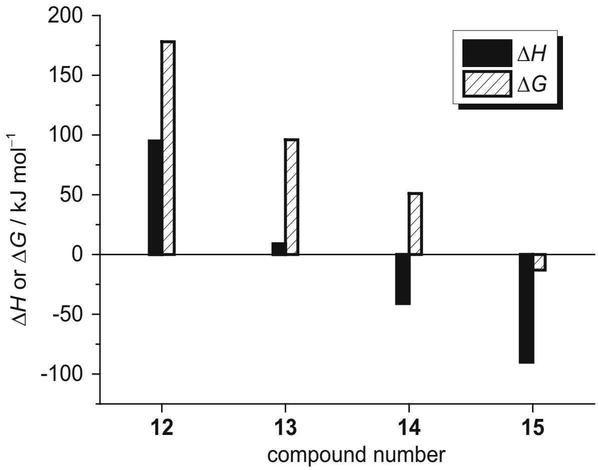

Fig. 6 Calculated gas-phase enthalpy and Gibbs energy changes (at 273 K and 0.1 MPa) for the decomposition of compounds **12–15** to give N_2 and two diamino-carbene units (calculations with B3LYP/TZVP)

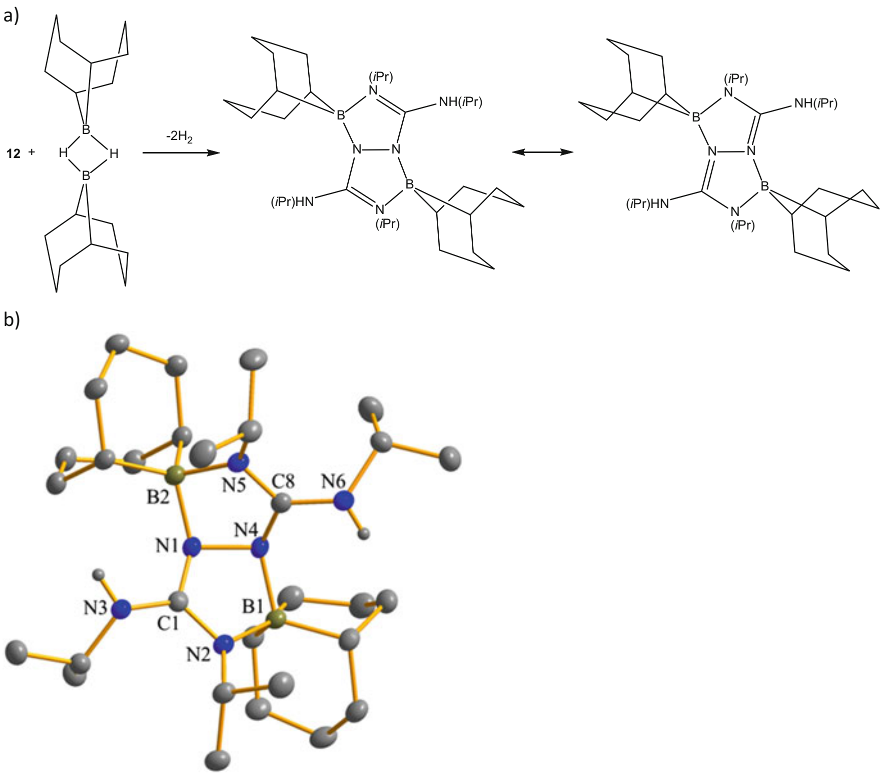

Fig. 7 (**a**) Reaction of **12** with 9-BBN to give a new bora-heterobicycle (two mesomeric structures are shown, of which the structure on the left dominates). (**b**) Illustration of the product structure. Vibrational ellipsoids drawn at the 50% probability level. Hydrogens attached to carbon omitted

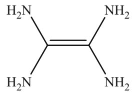

16

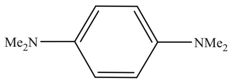

17

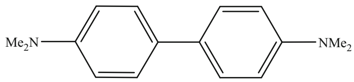

18

Scheme 13 Lewis structures for compounds **16–18** included in the correlation

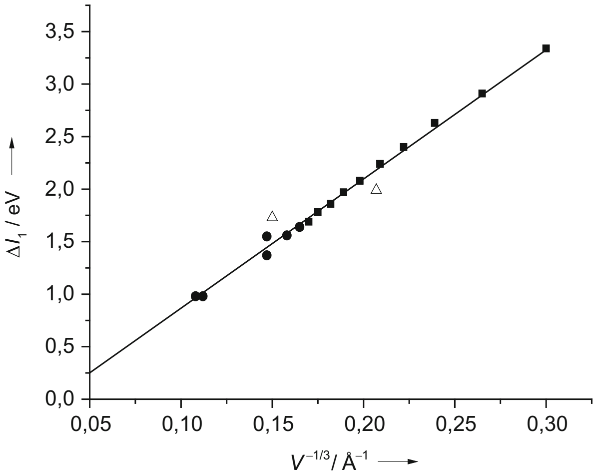

Fig. 8 Linear regression of ΔI_1 for compounds **1**, **3–5**, **13** and **16–18** and some *all-trans* conjugated carbon chains plotted versus $V^{-1/3}$ to show the relationship between solvation energy and the molecular volume. The data for the conjugated carbon chains are included as *rectangles*, for **3–5**, **13**, **17** and **18** as *circles* and for compounds **1** and **16** as *triangles*

simple relationship [46]. To establish a formula, we considered conjugated carbon chains of the general formula C_nH_{n+2} ($2 \leq n \leq 10$) in *all-trans* conformation and the methyl radical, $CH_3^{\cdot}$, as well as compounds **1**, **3–5** (Scheme 2), **13** (Scheme 10) and **16–18** (Scheme 13). Figure 8 plots ΔI_1, which is the difference between the calculated first ionisation energy in the gas-phase and in solution, as a function of $V^{-1/3}$, where V is the molecular volume (see [46] for details).

From the plot in Fig. 8, the following relationship could be established between the first ionisation energy in the gas-phase and in solution for a molecular electron donor [46]:

$$I_1(\text{solution}) = I_1(\text{gas-phase}) - \frac{C_1}{\sqrt[3]{V}} + C_2$$

The dielectric constant of the solvent is not included in the formula. If the ionisation energy (calculated with the conductor-like screening model (COSMO)) is plotted versus the dielectric solvent ε_r, one obtains a steep decrease at low ε_r values.

However, from ε_r values of ca. 10 onwards, the changes in the ionisation energy become very small, and therefore, in practically all solvents which could be applied for this redox chemistry, the ionisation energy is almost independent of the ε_r value [46].

A linear regression (see Fig. 7) yields $C_1 = 12.29$ eV · Å and $C_2 = -0.36$ eV. The correlation coefficient R is 0.989, and the mean absolute deviation of datapoints from the linear regression is 0.053 eV. Hence, the general level of agreement is extremely pleasing. Compounds **1** and **16** (triangles in Fig. 8) deviate most from the linear correlation. The reason for the deviation of **1** is discussed below. The 0.19 eV derivation of compound **16** from the expected value might be a reasonable estimate for the (maximal) deviation one has to expect for different classes of redox-active compounds.

Table 2 compares the predicted difference in the redox potentials for two organic electron donors, $\Delta E_{1/2} = e \cdot \Delta I_1$(solution), with the experimentally determined $\Delta E_{1/2}$ values in solution from CV measurements. It can be seen that the calculated $\Delta E_{1/2}$ values fit to the experimentally obtained ones. The only exception, for which the volume term does not operate in the right direction, is compound **1**. This is an important exception, and the reason for the failure of the simple relationship can easily be understood. The eight methyl groups of **1** affect the ionisation potential through their inductive effect, but are not involved in the delocalised system (that comprises only six atoms). A comparison between the volumes of **1** (tetraaminoethylene with methyl groups, 296 Å^3) and **16** (without methyl groups, 113 Å^3) shows that the "redox-active part" in **1** constitutes only ca. 40% of the volume. This means that the effective volume, which should be used in the equation, is considerably smaller than the total volume. For all other compounds, the increase in the volume by the methyl groups has no significant consequences since the redox-active part is considerably larger. In general, this result means that the above relationship could not be applied if the molecule exhibits large "redox-inactive" groups. In such cases, one should instead use an "effective volume".

Often, data for the (adiabatic) ionisation energy in the gas-phase are not available. Then, the correlation could be used to estimate this value from the redox potential measured in solution. For two *organic electron donors* A and B with molecular volumes V_A and V_B (zero or small static dipole moment, relatively uniform charge distribution in the oxidised species), one obtains [46]

$$\Delta I_1 = e \cdot \Delta E_{1/2} + C_1 \left(\frac{1}{\sqrt[3]{V_A}} - \frac{1}{\sqrt[3]{V_B}} \right)$$

where $\Delta I_1 = I_1(\mathrm{A}) - I_1(\mathrm{B})$ is the difference in the adiabatic gas-phase first ionisation energies, $\Delta E_{1/2}$ is the difference in the redox potential in solution (e.g. measured by CV measurements) and $C_1 = 12.29$ eV · Å.

Since the solvent effects (as modelled by the COSMO model) are equal for positive and negative charge (if chemical bonding (significant orbital overlap) between the compound and solvent molecules could be neglected), a similar formula could be derived for electron acceptors. For two *organic electron acceptors*

Table 2 Comparison between $\Delta E_{1/2}$ values calculated with the formula, $\Delta E_{1/2}$(calcd.), and the observed $\Delta E_{1/2}$ values from CV measurements

A	B	ΔI_1(gas-phase)/eV	$\Delta E_{1/2}$(calcd.)/V	$\Delta E_{1/2}$(obs.)/V
3	**1**	−0.60	−0.70	−0.53
3	**4**	−0.23	−0.79	−0.90
3	**5**	−0.20	−0.82	−0.95
3	**7**	−1.18	−1.31	−1.31
3	**8**	−1.40	−1.31	−1.32
3	**9**	−1.39	−1.53	−1.51

A and B with molecular volumes V_A and V_B (zero or small static dipole moment, relatively uniform charge distribution in the reduced species), one then obtains [46]

$$\Delta E_A = e \cdot \Delta E_{1/2} + C_1\left(\frac{1}{\sqrt[3]{V_A}} - \frac{1}{\sqrt[3]{V_B}}\right)$$

where $\Delta E_A = E_A(A) - E_A(B)$ is the difference in the adiabatic gas-phase electron affinities, $\Delta E_{1/2}$ is the difference in the reduction potential in solution (e.g. measured by CV measurements) and $C_1 = 12.29$ eV · Å.

3 Guanidinate-Substituted Diboranes: Synthesis and Reactivity

Bicyclic guanidines such as hppH (1,3,4,6,7,8-hexahydro-2*H*-pyrimido[1,2-*a*] pyrimidine; see Scheme 14) were shown to be strong organic Brønsted bases [31] and therefore are used as (auxiliary) bases in a number of organic synthesis protocols. As already mentioned in the Introduction, bicyclic guanidinates such as hpp, tbo and tbn (the deprotonated versions of the three guanidines shown in Scheme 14) were intensively used as bridging ligands [25–29]. Especially, Cotton et al. used these ligands for the synthesis of dinuclear complexes with multiple bonding between two highly oxidised transition metals [25–28]. Recently our group showed that bicyclic guanidinates could also be used for the synthesis of new diborane compounds. Since hppH is a stronger Lewis base than NMe_3, it could replace NMe_3 from the borane adduct $H_3B \cdot NMe_3$. The borane adducts of the three bicyclic guanidines shown in Scheme 14 were then used as starting reagents for the development of this chemistry (see Fig. 9).

3.1 Dehydrogenation Reactions of Borane-Guanidine and Gallane-Guanidine Adducts

In the solid state, all characterised guanidine-borane and guanidine-gallane adducts show intramolecular and/or intermolecular $H(\delta+)\cdots H(\delta-)$ interactions between

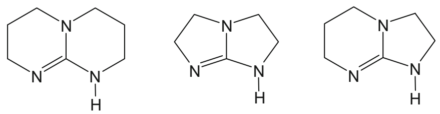

Scheme 14 The bicyclic guanidines which are of relevance for the discussion. hppH = 1,3,4,6,7,8-hexahydro-2*H*-pyrimido[1,2-*a*]pyrimidine, Htbo = 1,4,6-triazabicyclo[3.3.0] oct-4-ene and Htbn = 1,5,7-triazabicyclo[4.3.0]non-6-ene

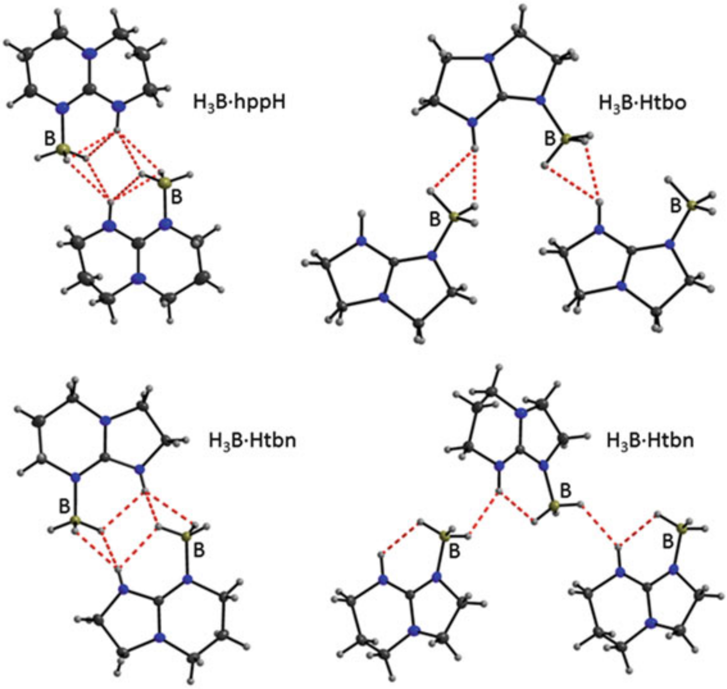

Fig. 9 Sections of the solid state structures of the guanidine-borane adducts $H_3B \cdot$hppH, $H_3B \cdot$Htbo and $H_3B \cdot$Htbn (two isomers) showing the intramolecular and/or intermolecular H(δ+)···H(δ−) interactions between the negatively polarised hydrogen atoms attached to the group 13 element and the positively polarised hydrogen atom attached to nitrogen. Vibrational ellipsoids drawn at the 50% probability level

the negatively polarised hydrogen atoms attached to the group 13 element and the positively polarised hydrogen atom attached to nitrogen (see Fig. 9). The intramolecular interactions are likely to be preserved in solution. For all adducts, dihydrogen elimination is observed upon heating in solution, and in all cases, the products are diboranes with two bridging guanidinate substituents ($[H_2B(hpp)]_2$, $[H_2B(tbn)]_2$ (two isomers) and $[H_2B(tbo)]_2$). In the case of $[H_2B(hpp)]_2$, the product

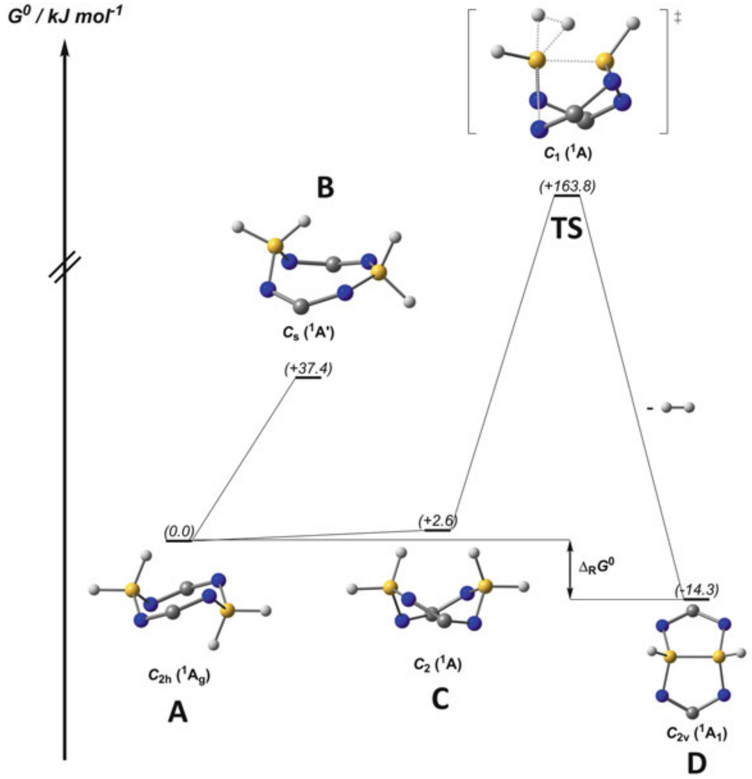

Fig. 10 Result of the calculations on the mechanism of the B–B dehydrocoupling reaction of $[H_2B(hpp)]_2$ to give $[HB(hpp)]_2$ (D). Only the N–C–N unit of the bicyclic guanidinate substituents are shown for sake of clarity

exhibits a "chair-type" conformation with the BH_2 groups on opposite sides of the two hpp substituents. For $[H_2B(tbn)]_2$ and $[H_2B(tbo)]_2$, "boat-type" conformations were observed. The observed conformations are in agreement with the results of quantum chemical calculations. The energy difference between chair and boat form is 3 kJ mol^{-1} for $[H_2B(hpp)]_2$, but -9 and -22 kJ mol^{-1} for $[H_2B(tbn)]_2$ and $[H_2B(tbo)]_2$, respectively. Despite of the advantageous conformation, B–B dehydrocoupling is not possible for $[H_2B(tbn)]_2$ and $[H_2B(tbo)]_2$. The smaller ring sizes of the guanidinate bridges favour a larger separation of the B atoms, leading both to a reduced B–B bond energy and a higher activation barrier for dehydrocoupling.

Further dihydrogen elimination with the formation of a boron–boron bond is only possible for $[H_2B(hpp)]_2$. This reaction, which leads to the diborane $[HB(hpp)]_2$, requires the use of a catalyst (see Sect. 3.2). Figure 10 illustrates the results of quantum chemical calculations (B3LYP) on the mechanism for an uncatalysed B–B dehydrocoupling reaction starting with $[H_2B(hpp)]_2$. For clarity only the N–C–

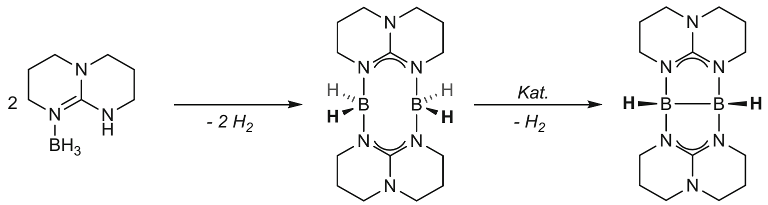

Scheme 15 Synthesis of $[HB(hpp)]_2$ by B–N and B–B dehydrocoupling reactions

N unit of each guanidinate is reproduced. The first step is the change from a chair-type (A) to a boat-type (B) conformation. From this conformation, the thermal dehydrogenation takes place, leading to the dehydrocoupling product D. However, it is subjected to a quite high thermal barrier of ca. 164 kJ mol^{-1}, indicating that a catalyst (e.g. $[RhCl(cod)]_2$) is needed (see the discussion in the next section). At the transition state (TS), one of the B–H bonds is cleaved, while the H–H bond starts to form (Scheme 15) [79].

Catalysis also showed to be useful to initiate dehydrocoupling reactions in the case of gallium chemistry [80]. However, the catalysts which were successfully tested for the analogue boron compounds failed. A suitable catalyst for Ga–N dehydrocoupling reactions turned out to be the Ir^{III} complex [(*p*-HPCP)IrH_2] (see Scheme 16, *p*-HPCP = η^3-1,3-(OP*t*Bu_2)$_2C_6H_3$), which was used by Goldberg et al. for fast ammine-borane dehydrogenation [81]. This complex does not catalyse dehydrogenation of the boron analogue. A Ga–Ga dehydrocoupling reaction was not observed, and therefore compound $[HGa(hpp)]_2$ or related compounds remain unknown. Figure 11 compares the possible reaction pathways for the uncatalysed reaction between $H_3Ga \cdot NMe_3$ and Htbu (B3LYP/TZVP calculations). In the experiments using Htbu, exclusively H_2Ga(tbn)(Htbn) was formed, in line with the relative stabilities predicted by the quantum chemical calculations.

3.2 (Catalytic) B–B Dehydrocoupling Reaction

A series of pre-catalysts was tested to optimise the yield and the kinetics for the B–B dehydrocoupling reaction leading to $[HB(hpp)]_2$ [79]. The kinetics was determined from the intensity of the signals in the ^{1}H NMR spectra (see Fig. 12). The reaction times for 80% conversion were generally estimated by curve fitting (see Fig. 13). Table 3 gives an overview of the results obtained with various pre-catalysts. It could be seen that especially late transition metal complexes are good pre-catalysts.

As an alternative to catalytic dehydrocoupling, a two-step process was tested which comprises hydride abstraction followed by deprotonation. It was indeed possible to synthesise the cation $[H_3B_2(hpp)_2]^+$ by hydride abstraction of $[H_2B(hpp)]_2$ with $B(C_6F_5)_3$. This cation was previously obtained by protonation of $[HB(hpp)]_2$ [82] and features two terminal B–H bonds and a B–H–B bridge. It could

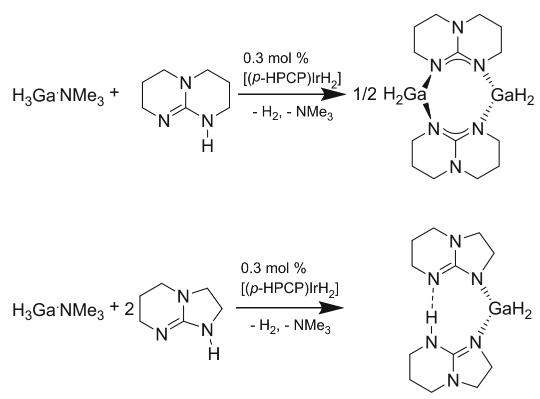

Scheme 16 Catalytic dehydrocoupling reactions of gallanes in diethyl ether/toluene at temperatures below −18°C

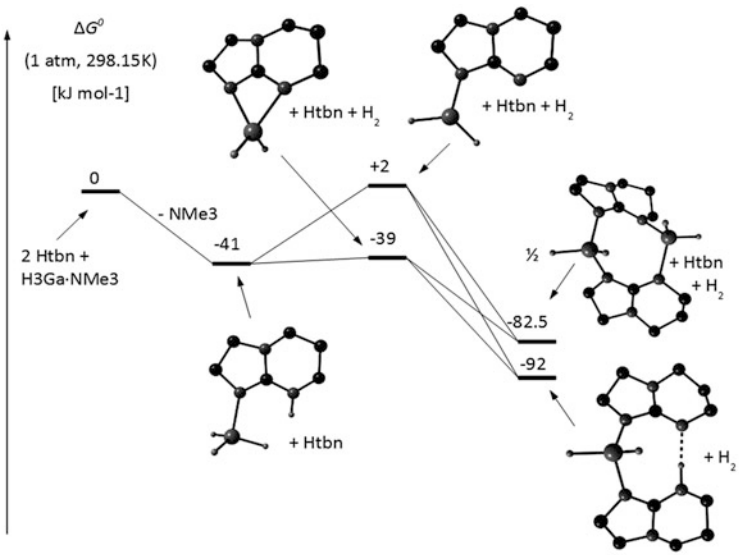

Fig. 11 Results of quantum chemical calculations (B3LYP/TZVP) on the pathway of the uncatalysed reaction between Htbn and $H_3Ga \cdot NMe_3$

subsequently be deprotonated quantitatively with KO*t*Bu to $[HB(hpp)]_2$ (see Scheme 17).

The catalytic dehydrocoupling reaction is clearly favourable for the synthesis of $[HB(hpp)]_2$. However, the two-step way is interesting for two reasons. First it shows the possibility of a reversible deprotonation of cationic boron hydrides. Then, the two-step process might be interesting for the synthesis of diboranes for which a

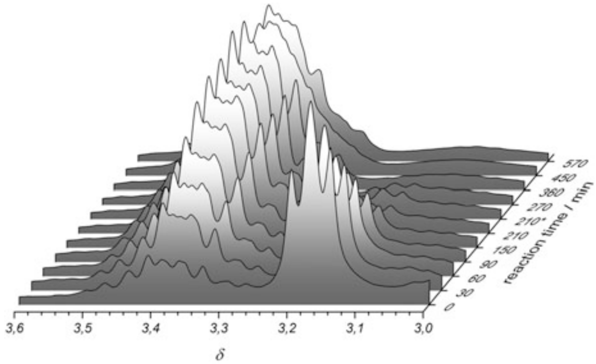

Fig. 12 ^{1}H NMR spectra in [D_8]-toluene of the reaction solution using [RhCl(cod){HB(hpp)}$_2$] as dehydrocoupling pre-catalyst. The intensity ratio between the signal pair of [H_2B(hpp)]$_2$/[HB(hpp)]$_2$ ($\delta = 3.05$–$3.25/\delta = 3.25$–3.55) reflects the progress of the conversion

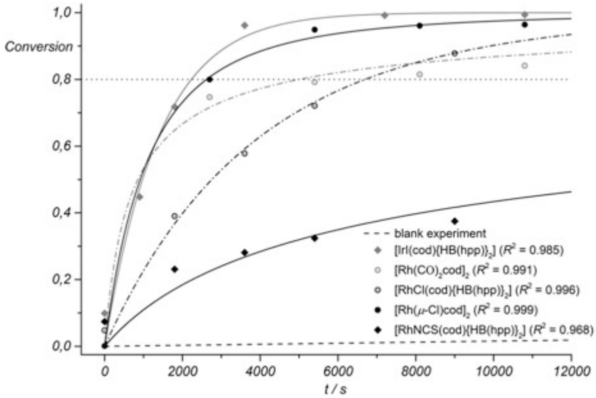

Fig. 13 Progress of the dehydrocoupling reaction as function of the reflux time using five different pre-catalysts. The blank experiment is shown by a *dashed line*. All NMR integrals were corrected by the integral ratio ($\delta = 3.05$–$3.25/\delta = 3.25$–3.55) of pure [H_2B(hpp)]$_2$. Due to broadening, partial signal overlap and integration accuracy of the ^{1}H NMR spectra conversions above 0.95 were not obtained for any pre-catalyst. However, ^{11}B{^{1}H} NMR spectra only show the resonance of [HB(hpp)]$_2$ for these solutions. The *solid lines* represent the data obtained from a least-square fit (values of R^2 given in *parentheses*) of the measured data to the general rate equation (see Wagner et al. [79] for more details)

catalytic dehydrocoupling reaction fails. This was tested for the two compounds [H_2B(tbo)]$_2$ and [H_2B(tbn)]$_2$, for which catalytic dehydrocoupling is not feasible [83]. However, the hydride abstraction with B(C_6F_5)$_3$ did not give [H_3B_2(tbo)$_2$]$^+$ or [H_3B_2(tbn)$_2$]$^+$, but instead the new compounds [H_2B_2(tbo)$_3$]$^+$ and [H_2B_2(tbn)$_3$]$^+$ respectively, incorporating three bridging guanidinate substituents. Obviously, the larger separation of the two boron atoms, which results from the small ring sizes of the guanidinates, disfavours the formation of a B–H–B bond [84].

Table 3 Results of the catalysed B–B dehydrocoupling reaction of $[H_2B(hpp)]_2$ to give $[HB(hpp)]_2$

Entry	Precatalyst (2 mol%)[a]	t_{conv}/min[b]
1	$[Rh(\mu\text{-}Cl)(cod)]_2$	44
2	$[Rh(\mu\text{-}Cl)(CO)_2]_2$	83
3	$[Rh(\mu\text{-}Cl)(coe)_2]_2$	[c]
4	$[RhCl(PPh_3)_3]$	[c]
5	$[RhH(CO)(PPh_3)_3]$	[c]
6	$[RhCl(cod)\{HB(hpp)\}_2]$	112
7	$[RhNCS(cod)\{HB(hpp)\}_2]$	3,558
8	$[Ir(\mu\text{-}Cl)(cod)]_2$	(40)
9	$[IrCl(cod)\{HB(hpp)\}_2]$	(30)
10	$[IrI(cod)\{HB(hpp)\}_2]$	37
11	$[(p\text{-HPCP})IrH_2]$	[c]
12	$[CoCl_2]$	>8,000
13	$[FeCl_2]$	[c]
14	$[CuCl]$	≈5,300
15	$[Cr(CO)_6]$	[c]

cod 1,5-cyclooctadiene, *coe* cyclooctene, *p-HPCP* κ^3-2,6-$C_6H_3(OP^tBu_2)_2$

[a]With respect to the transition metal. All reactions were carried out in refluxing toluene. For $[Cr(CO)_6]$, the mixture was irradiated for 10 min with a medium-pressure UV lamp before heating

[b]Reaction times required for 80% conversion (t_{conv}) determined by kinetic fits as shown in Fig. 12, values in parentheses are estimated purely from the experimental data; for [CuCl] and $[CoCl_2]$, the conversion times were calculated based on a fit of the ^{11}B NMR spectra and are only given for orientation

[c]No product formation observed

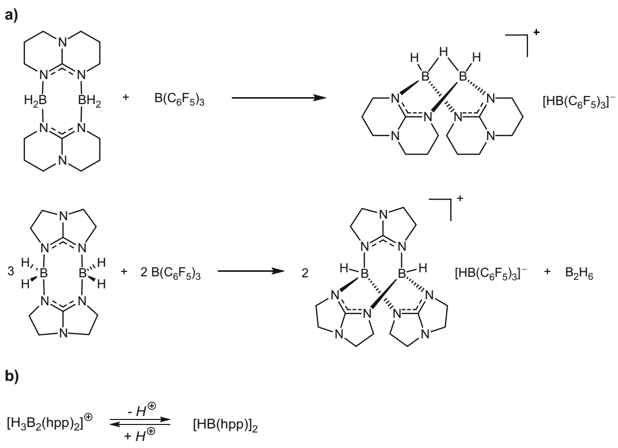

Scheme 17 (**a**) Hydride abstraction reaction with different outcome for guanidinate-substituted diboranes. (**b**) Reversible deprotonation of $[H_3B_2(hpp)]^+$

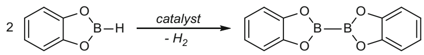

Scheme 18 B–B dehydrocoupling reaction of catecholborane according to Braunschweig et al. [85–87]

It should be emphasised that B–B dehydrocoupling reactions are extremely rare. A further example, studied by the group of Braunschweig, is provided in Scheme 18 [85–87]. Completely different catalysts (especially Rh, Pd or Pt supported on alumina as heterogeneous catalysts) were used for this reaction. In difference to $[H_2B(hpp)]_2$ and its dehydrogenation product $[HB(hpp)]_2$, catecholborane and bis (catecholato)diborane exhibit sp^2-hybridised boron atoms.

3.3 Coordination Chemistry with $[HB(hpp)]_2$

Coordination to metal complexes could activate the B–H or the B–B bond of $[HB(hpp)]_2$ and therefore provides the key for further transformations. To find out which metal is suitable for strong activation of the diborane, a series of transition metal complexes was synthesised and characterised and the bond properties studied in detail (see, e.g. Scheme 19) [88–90]. These studies showed that the complexes could be grouped into two categories. In one category, the B–B electrons participate significantly in the metal-diborane bonding (as in $[Rh(cod)\{HB(hpp)\}_2Cl]$, $[Ir(cod)\{HB(hpp)\}_2Cl]$ (see Fig. 14 left side) and $[ZnX_2\{HB(hpp)\}_2]$ (X = Cl, Br or Me)). Consequently the B–B bond is elongated upon coordination. In the other category, the bonding mainly involves the B–H electrons, and the B–B bond length decreases upon coordination (as in $[Cr\{HB(hpp)\}_2(CO)_4]$ (see Fig. 14 right side), $[Mo\{HB(hpp)\}_2(CO)_4]$ and $[W\{HB(hpp)\}_2(CO)_4]$). Table 4 includes some parameters which highlight the difference in the bonding mode. The wavenumber of the B–H stretching mode is higher than in free $[HB(hpp)]_2$ for complexes in which the B–B bond is elongated. By contrast, it is red-shifted in complexes in which the B–B bond length decreases. The direct bonding of the hydrogens in this category also manifests itself in a significant ^1H NMR chemical shift.

Figure 15 shows a simplified MO picture. In the case of the late transition metal fragments, the orbital which interacts with the HOMO-2 of the diborane is occupied. Bonding and antibonding contributions compensate each other, so that the bond between the orbital of next-higher energy and the HOMO of the diborane, which consist of the boron orbitals in the B–B bond, becomes decisive.

3.4 Hydride Substitution and Oxidative Insertion into the B–B Bond of $[HB(hpp)]_2$

Reaction between sulphur and $[HB(hpp)]_2$ leads to the oxidative insertion of a sulphur atom into the B–B bond and formation of a B–S–B bridge [91]. Figure 16

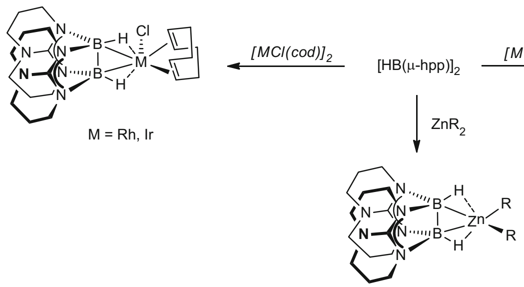

Scheme 19 Examples for the synthesis of transition metal complexes with $[HB(hpp)]_2$ as ligand

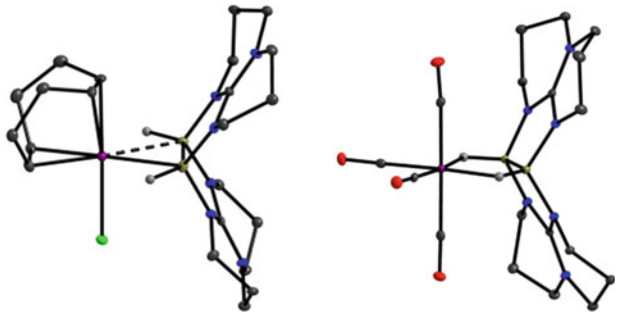

Fig. 14 Examples for two complexes with $[HB(hpp)]_2$ as a ligand, $[Ir(cod)\{HB(hpp)\}_2Cl]$ (*left*) and $[Cr\{HB(hpp)\}_2(CO)_4]$ (*right*). Vibrational ellipsoids drawn at the 50% probability level. Hydrogens attached to carbon omitted

reproduces the structure of the product $[HB(hpp)]_2S$. Oxygen and selenium atoms could also insert. The reaction between $[HB(hpp)]_2$ and disulfides was shown to lead to several products, which could be separated from each other (Scheme 20) [91]. The first step is likely to be oxidative addition and formation of the unstable intermediate $[(RS)HB(hpp)]_2$. This intermediate eliminates RSH, H_2 or RSH. Consequently, a mixture of $(RS)HB_2(hpp)_2$, $[(RS)B(hpp)]_2$ and $[HB(hpp)]_2S$ is obtained. All these products were isolated and completely characterised. Quantum chemical calculations were carried out which are in full agreement with the experimental results (see Fig. 17) [91]. All elimination reactions from the intermediate species are exotherm. The energetically preferred product is $[HB(hpp)]_2S$.

Interestingly, the experimental results indicate that the thermal barrier for reductive B–B coupling reactions starting from $[H(PhS)B(hpp)]_2$ is much lower than for the dehydrocoupling reaction starting with $[H_2B(hpp)]_2$. Quantitative conversion is achieved at room temperature in the absence of any catalyst. This result shows that the metal-free reductive B–B coupling of diboranes with bridging guanidinate substituents is not restricted to H_2 elimination.

Table 4 Selected experimental parameters for some transition metal complexes with $[HB(hpp)]_2$ ligand

	d(B–B)/Å	ν(B–H)/ cm^{-1}	$\delta(^{1}H\{^{11}B\})$/ ppm	$\delta(^{11}B)$/ ppm	^{1}J(B–H)/ Hz
$[HB(hpp)]_2$	1.772(3)	2,272 2,249	2.17	−1.14	–
$[Cr\{HB(hpp)\}_2(CO)_4]$	1.739(3)	2,010	−4.84	−8.76	55
$[Mo\{HB(hpp)\}_2(CO)_4]$	1.742(4)	2,018	−2.91	−7.65	64
$[W\{HB(hpp)\}_2(CO)_4]$	1.748(7)	2,041	−3.26	−7.73	63
$[Rh(cod)\{HB(hpp)\}_2Cl]$	1.811(6)	2,258	2.09	−7.59	54
$[Ir(cod)\{HB(hpp)\}_2Cl]$	1.835(8)	2,282	0.67	−4.69	90
$[ZnCl_2\{HB(hpp)\}_2]$	1.834(4) 1.841(4)	2,180 2,152	3.36	−8.61	70
$[ZnBr_2\{HB(hpp)\}_2]$	1.834(4) 1.851(6)	2,175	3.35	−7.93	72
$[ZnMe_2\{HB(hpp)\}_2]$	1.805(4)	2,219	3.32	−1.75	–

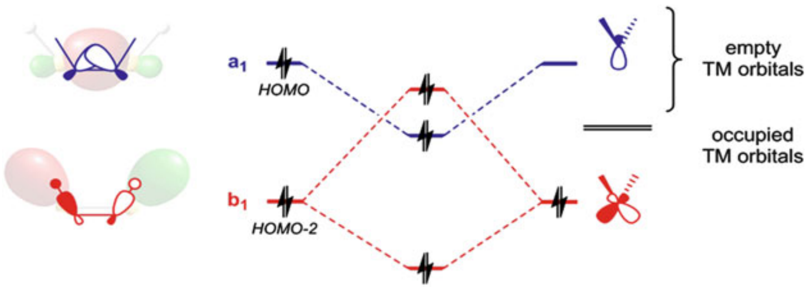

Fig. 15 Simplified MO scheme for the understanding of B–B bond activation by late transition metal fragments

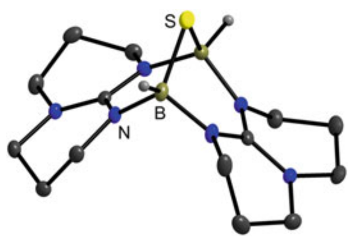

Fig. 16 Structure of the compound $[HB(hpp)]_2S$ which arises from oxidative insertion of sulphur into the B–B bond of $[HB(hpp)]_2$. Vibrational ellipsoids drawn at the 50% probability level. Hydrogens attached to carbon omitted

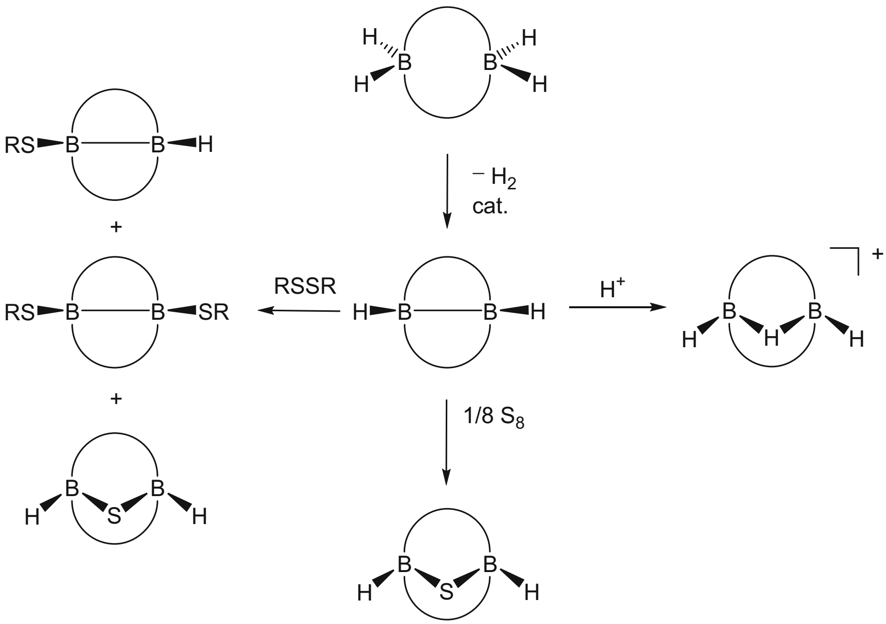

Scheme 20 Oxidative insertion of sulphur and a proton into the B–B bond and hydride substitution reactions of $[HB(hpp)]_2$

3.5 *Cationic Boron Hydrides*

In the previous sections, we have shown that bicyclic guanidinates could be used to form diboranes with a direct B–B bond via a dehydrocoupling reaction. The guanidinate substituents bring together the two boron atoms and facilitate the coupling reaction. The electronic properties of the guanidinate substituents are of particular importance in this section, which deals with the synthesis of unprecedented new cationic boron hydrides. Without the guanidinate substituents, some of the cationic structures presented below are probably not stable. The diborane $[HB(hpp)]_2$ is the starting agent for the synthesis of cationic boron hydrides. The simplest cation, namely, $[HB(hpp)_2(\mu\text{-}H)BH]^+$, is produced by oxidative insertion of a proton into the B–B bond (see Scheme 17b) [82]. Reaction of $[HB(hpp)]_2$ with R_2BX (X = NTf_2 or OTf, generated in situ from 9-BBN and HX [92]) yielded a cationic three-membered boron-ring compound (see Scheme 21) with a closed B–B–B 3-centre 2-electron bond [93].

Reaction between $B_2Cl_2(NMe_2)_2$ and hppH or Htbn afforded the first diboronium dications (see Scheme 22) [83, 94]. The B–B bond distances measure 174.6(2) pm in $[B_2(hpp)_2(NHMe_2)_2]^{2+}$ [94] and 180.1(5) pm in $[B_2(tbn)_2(NHMe_2)_2]^{2+}$ [83]. Reaction of $B_2Cl_2(NMe_2)_2$ with Li(hpp) led to the instable diamino compound $[B_2(NMe_2)_2(hpp)_2]$, which could be converted first to $[B_2(hpp)_2(NMe_2)(NHMe_2)]^+$ and then to $[B_2(hpp)_2(NHMe_2)_2]^{2+}$ by protonation

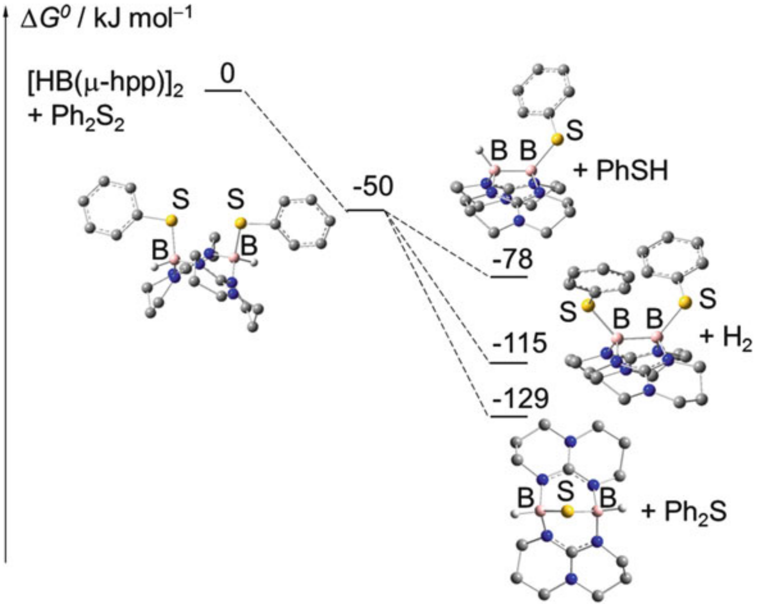

Fig. 17 Pathway for the reaction between $[HB(hpp)]_2$ and Ph_2S_2 (BP86/SV(P) calculations). The intermediate product $[H(PhS)B(hpp)]_2$ is not stable and eliminates PhSH, H_2 or Ph_2S, leading eventually to a product mixture from which all three products were experimentally isolated and characterised

Scheme 21 Reaction leading to a cationic three-membered boron-ring compound with a closed 3-centre 2-electron bond

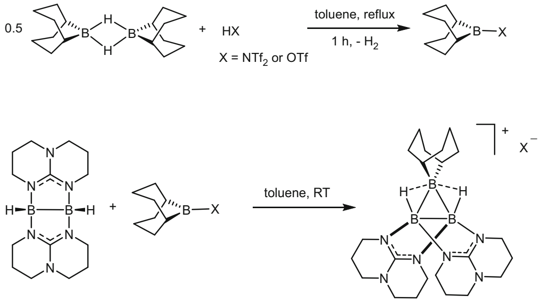

with HCl [95]. It proved so far impossible to remove the $NHMe_2$ groups [96]. Quantum chemical calculations suggest that elimination of both $NHMe_2$ moieties from $[B_2(hpp)_2(NHMe_2)_2]^{2+}$ is associated with a relatively low ΔG^0 value of 127 kJ mol^{-1} (at 298 K) and leads to $[B_2(hpp)_2]^{2+}$ with a planar B_2N_4 core [94].

Hydride abstraction from $[HB(hpp)]_2$ with $B(C_6F_5)_3$ gave the dicationic tetraborane $[H_2B_4(hpp)_4]^{2+}$ (see Scheme 23 and Fig. 18), featuring a 4-centre 4-electron bond [97]. The four boron atoms form a rhombus. Its short diagonal measures 1.703(4) Å, being significantly shorter than the other B–B bond distances (1.896(3) and 1.949(3) Å). To rationalise this bonding situation, one could divide

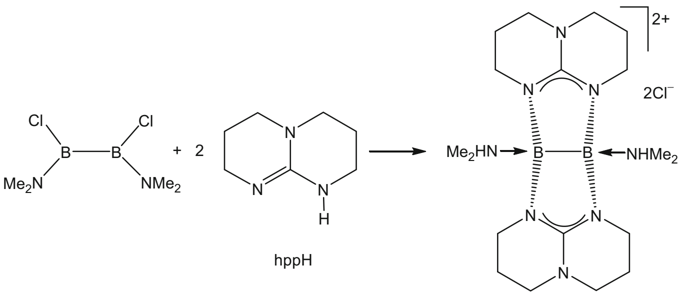

Scheme 22 Synthesis of the first diboronium dication

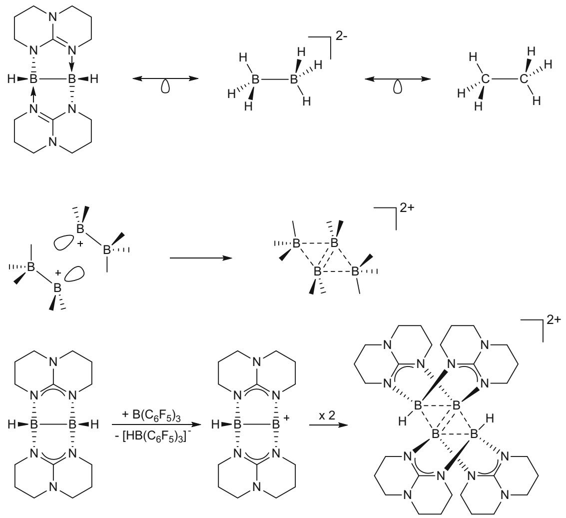

Scheme 23 Dimerisation of two $[HB(hpp)_2B]^+$ units and the course of the reaction between $[HB(hpp)]_2$ and $B(C_6F_5)_3$

the 4-centre 4-electron bond into two closed B–B–B 3-centre 2-electron bonds sharing two centres, as signified by the Lewis structure in Scheme 23.

Scheme 23 highlights the isolobal analogy between $[HB(hpp)]_2$ and ethane. Hydride abstraction leads to a compound which is isolobal to the ethyl cation. However, quantum chemical calculations predict a structure with a terminal B–H bond, which is more stable than a structure with a B–H–B bridge, in difference to the situation in $C_2H_5^+$. Moreover, the bridging guanidinate substituents force the boronium cation into a non-planar geometry.

The new cationic boron hydrides synthesised starting with $[HB(hpp)]_2$ differ in the $^1H\{^{11}B\}$ NMR chemical shift of the B–H protons (see Fig. 19). It seems possible to correlate the shift with the polarisation of the hydrogen atom.

In ongoing research, our group seeks to use the cationic boron hydrides as starting reagents for the synthesis of boron chain oligomers and polymers.

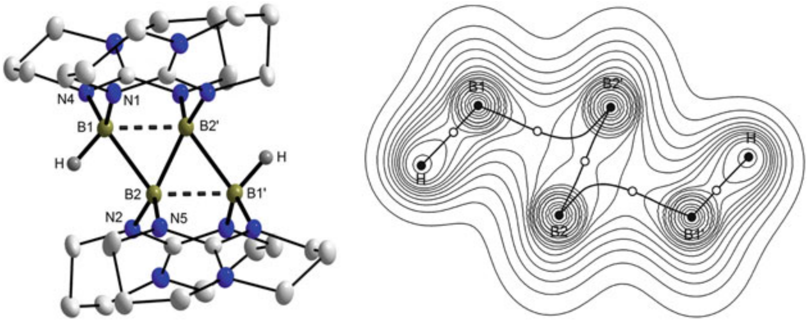

Fig. 18 Structure of $[H_2B_4(hpp)_4]^{2+}$ from X-ray diffraction and calculated charge density distribution

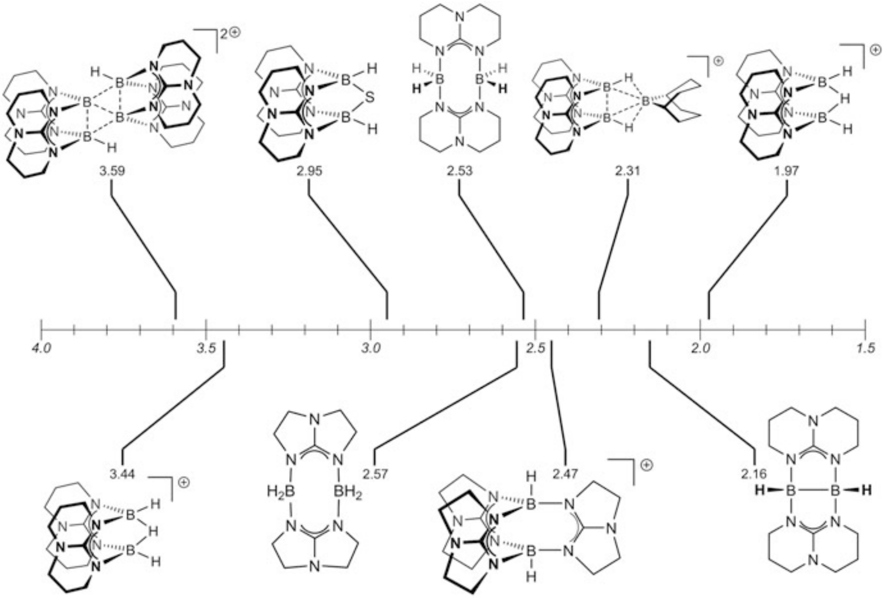

Fig. 19 Comparison of the $^{1}H\{^{11}B\}$ NMR chemical shifts (hydrogen atoms bound to boron) for several dinuclear boron compounds with guanidinate bridges. In the case of $[H_3B_2(hpp)_2]^+$, chemical shifts of 3.44 and 1.98 ppm were measured for the terminal and bridging H, respectively

If $[B_4(hpp)_4]^{2+}$ units (with 4-centre 4-electron bonding of the rhomboid B_4 core) are connected via 2-centre 2-electron B–B bonds, one should obtain a chain polymer which is structurally comparable to (semiconducting) β-SiB_3 [98] and expected to exhibit interesting electronic properties. Scheme 24 gives an overview of the three areas of research with the guanidinate-substituted diborane $[HB(hpp)]_2$.

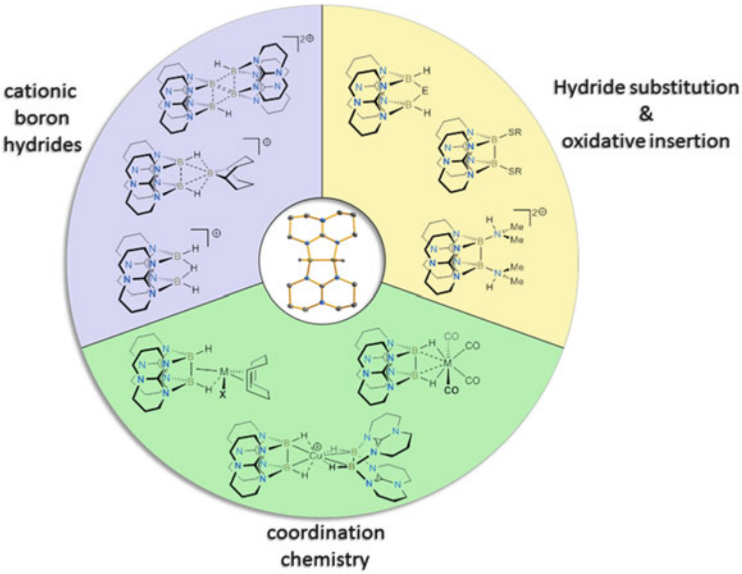

Scheme 24 Overview of the reactivity of the guanidinate-substituted diborane $[HB(hpp)]_2$

4 Conclusions

The substitution of molecular compounds by guanidino groups could bring about drastic changes in the electronic properties and reactivity. This is the case for guanidino-functionalised aromatic compounds (GFAs), which comprise a relatively new class of strong organic electron donors. These compounds could be used as reducing reagents, e.g. for the synthesis of polyanionic networks, for photochemical reductive C–C coupling reactions or as redox switch for the reversible formation of hydrogen-bonded aggregates. Organic electron donors could also be formed by connecting two guanidinyl groups. The resulting bisguanidines (commonly referred to as urea azines) could be oxidised in two separated one-electron steps. An analysis of the electron donor strength in GFAs, bisguanidines and other organic electron donors led to a relationship between the ionisation energy in the gas-phase and the redox potential in solution.

Bicyclic guanidinate ligands were employed for the synthesis of new sp^3–sp^3 hybridised diboranes, which show a rich chemistry. They could be used as ligands in coordination compounds, in which either the B–H or the B–B electrons contribute most to the metal-diborane bond. Oxidative insertion and hydride substitution reactions were also discussed. Finally, guanidinate-substituted cationic boron hydrides could be synthesised, in which several boron atoms are connected by multiple-centre bonding. Some of these compounds might be precursors for the synthesis of oligomeric or polymeric boron chain compounds.

References

1. Edelmann FT (2008) Advances in the coordination chemistry of amidinate and guanidinate ligands. Adv Organomet Chem 57:183–352
2. Edelmann FT (1994) *N*-silylated benzamidines: versatile building blocks in main group and coordination chemistry. Coord Chem Rev 137:403–481
3. Barker J, Kilner M (1994) The coordination chemistry of the amidine ligand. Coord Chem Rev 133:219–300
4. Bailey PJ, Price S (2001) The coordination chemistry of guanidines and guanidinates. Coord Chem Rev 214:91–141
5. Herres-Pawlis S (2009) Außergewöhnliche Donoren und synthetische Vielfalt: Guanidine. Nachr Chem 57:20–23
6. Coles MP (2006) Application of neutral amidines and guanidines in coordination chemistry. Dalton Trans 985–1001
7. Coles MP (2009) Bicyclic guanidines, guanidinates and guanidium salts: wide ranging applications from a simple family of molecules. Chem Commun 3659–3676
8. Himmel H-J (2011) Hydrogenation and dehydrogenation of dinuclear boron and gallium hydrides: quantum chemical calculations and experiments. In: Comba P (ed) Modeling of molecular properties. Wiley-VCH, Weinheim
9. Jones C (2010) Bulky guanidinates for the stabilization of low oxidation state metallacycles. Coord Chem Rev 254:1273–1289
10. Edelmann FT (2013) Recent progress in the chemistry of metal amidinates and guanidinates: syntheses, catalysis and materials. Adv Organomet Chem 61:55–374
11. Würtele C, Gaoutchenova E, Harms K, Holthausen MC, Sundermeyer J, Schindler S (2006) Crystallographic characterization of a synthetic 1:1 end-on copper dioxygen adduct complex. Angew Chem 118:3951–3954, Angew Chem Int Ed 45:3867–3869
12. Maiti D, Lee D-H, Gaoutchenova K, Würtele C, Holthausen MC, Sarjeant AAN, Sundermeyer J, Schindler S, Karlin KD (2007) Reactions of a copper (II) superoxo complex lead to C-H and O-H substrate oxygenation: modeling copper monooxygenase C-H hydroxynation. Angew Chem 120:88–91, Angew Chem Int Ed 47:82–85
13. Lanci MP, Smirnov VV, Cramer CJ, Gauchenova EV, Sundermeyer J, Roth JP (2007) Isotopic probing of molecular oxygen activation and copper(I) sites. J Am Chem Soc 129 (47):14697–14709
14. Maiti D, Lee D-H, Gaoutchenova K, Würtele C, Holthausen MC, Sarjeant AAN, Sundermeyer J, Schindler S, Karlin KD (2008) Coordination chemistry and reactivity of a cubric hyperoxide species featuring a proximal H-bonding substituent. Angew Chem 120:88–91, Angew Chem Int Ed 47:82–85
15. Peterson RL, Ginsbach JW, Cowley RE, Qayyum MF, Himes RA, Siegler MA, Moore CD, Hedman B, Hodgson KO, Fukuzumi S, Solomon EI, Karlin KD (2013) Stepwise protonation and electron transfer reduction of a primary copper-dioxygen adduct. J Am Chem Soc 135 (44):16454–16467
16. Saracini C, Liakos DG, Zapata Rivera JE, Neese F, Meyer GJ, Karlin KD (2014) Excitation wavelength dependent O_2 release from copper(II) superoxide compounds: laser flash-photolysis experiments and theoretical studies. J Am Chem Soc 136(4):1260–1263
17. Börner J, Flörke U, Huber K, Döring A, Kuckling D, Herres-Pawlis S (2009) New catalysts for the ring-opening polymerisation of D, L-lactide. Chem Eur J 15:2362–2376
18. Börner J, dos Santos Vieira I, Pawlis A, Doering A, Kuckling D, Herres-Pawlis S (2011) Mechanism of the living lactide polymerisation mediated by robust zinc guanidine complexes. Chem Eur J 17:4507–4512
19. Börner J, dos Santos Vieira I, Jones MD, Döring A, Kuckling D, Flörke U, Herres-Pawlis S (2011) Zinc complexes with guanidine-pyridine hybrid-ligands – guanidine effect and catalytic activity. Eur J Inorg Chem 4441–4456

20. dos Santos VI, Herres-Pawlis S (2012) Lactide polymerisation with complexes of neutral N-donors – new strategies for robust catalysts. Eur J Inorg Chem 5:765–774
21. dos Santos Vieira I, Herres-Pawlis S (2012) Novel guanidine-quinoline hybrid ligands and the application of their zinc complexes in lactide polymerisation. Z Naturforsch B 67:320–330
22. Maronna A, Hübner O, Enders M, Kaifer E, Himmel H-J (2013) Bisguanidines with biphenyl, binaphthyl and bipyridyl cores: proton sponge properties and coordination chemistry. Chem Eur J 19:8958–8977
23. Green SP, Jones C, Stasch A (2007) Stable magnesium(I) compounds with Mg-Mg bonds. Science 318:1754–1757
24. Westerhausen M (2008) Molecular magnesium(I) compounds: from curiosity to kudos. Angew Chem 120:2215–2217, Angew Chem Int Ed 47:2185–2187
25. Cotton FA, Matonic JH, Murillo CA (1997) A new type of divalent niobium compound: the first Nb-Nb triple bond in a tetragonal lantern environment. J Am Chem Soc 119 (33):7889–7890
26. Bear JL, Li Y, Han B, Kadish KM (1996) Synthesis, molecular structure and electrochemistry of a paramagnetic diruthenium(III) complex. Characterisation or $Ru_2(hpp)_4Cl_2$, where hpp is the 1,3,4,6,8-hexahydro 2*H*-pyrimido[1,2-α]pyrimidinate ion. Inorg Chem 35(5):1395–1398
27. Clérac R, Cotton FA, Daniels LM, Donahue JP, Murillo CA, Timmons DJ (2000) Completion of the series of $M_2(hpp)_4Cl_2$ compounds from W to Pt: the W, Pt and Os compounds. Inorg Chem 39:2581–2584
28. Cotton FA, Murillo CA, Wang X, Wilkinson CC (2003) Structural studies of nickel complexes and the unsymmetrical ligand *N*-phenyl-*N*-(2-pyridyl)formamidinate. Inorg Chim Acta 351:191–200
29. Day BM, Mansfield NE, Coles MP, Hitchcock PB (2011) Bicyclic guanidine compounds of magnesium and their activity as pre-catalysts in the Tishchenko reaction. Chem Commun 47:4995–4997
30. Schwesinger R (1990) Organophosphorus reagents: a practical approach in chemistry. Nachr Chem Tech Lab 38:1214–1226
31. Ishikawa T (ed) (2009) Superbases for organic synthesis: guanidines, amidines and phosphazenes and related organocatalysts. Wiley, Chichester
32. Alder RW, Bowman PS, Steele WRS, Winterman DR (1968) The remarkable basicity of 1,8-bis(dimethylamino)naphthalene. J Chem Soc Chem Commun 723–724
33. Maksić ZB, Kovačević B (2000) Absolute proton affinity of some polyguanides. J Org Chem 65:3303–3309
34. Raab V, Kipke J, Gschwind RM, Sundermeyer J (2002) A new, superbasic and kinetically active proton sponge. Chem Eur J 8:1682–1693
35. Coles MP, Aragón-Sáez PJ, Oakley SH, Hitchcock PB, Davidson MG, Maksić ZB, Vianello R, Leito I, Kaljurand I, Apperley DC (2009) Superbasicity of a bis-guanidino compound with a flexible linker: a theoretical and experimental study. J Am Chem Soc 131:16858–16868
36. Kovačević B, Maksić ZB (2002) Relationships between basicity, structure, chemical shift and the charge distribution in resonance stabilized imioamines. Chem Eur J 8:1694–1702
37. Raab V, Harms K, Sundermeyer J, Kovačević B, Maksić ZB (2003) 1,8-Bis (dimethylethyleneguanidino) naphthalene, DMEGN: tailoring the basicity of bisguanidine proton sponges by experiment and theory. J Org Chem 68:8790–8797
38. Singh A, Ganguly B (2008) Strategic design of small and versatile bicyclic organic superbases: a density functional study. New J Chem 32:210–213
39. Wild U, Hübner O, Maronna A, Enders M, Kaifer E, Wadepohl H, Himmel H-J (2008) The first metal complexes of the proton sponge 1,8-bis(*N*,*N*,*N′*,*N′*-tetramethylguanidino)naphthalene: synthesis and properties. Eur J Inorg Chem 4440–4447
40. Ishikawa T (2009) Superbases for organic synthesis. Wiley, Chichester
41. Broggi J, Terme T, Vanelle P (2014) Organic electron donors as powerful single electron reducing agents in organic synthesis. Angew Chem 126:392–423, Angew Chem Int Ed 53:384–413

42. Pruett RL, Barr JT, Rapp KE, Bahner CT, Gibson JD, Lafferty RH (1950) Reactions of polyfluoro olefins. II. Reactions with primary and secondary amines. J Am Chem Soc 72:3646–3650
43. Fox JR, Foxman BM, Guarrera D, Miller JS, Calabrese JC, Reis AH Jr (1996) Characterization of two novel TCNQ and TCNE 1:1 and 1:2 salts of the tetrakis (dimethylamino)ethylene dication $[\{(CH_3)_2N\}_2C\text{-}C\{N(CH_3)_2\}_2]^{2+}$. J Mater Chem 6:1627–1631
44. Burkholder C, Dolbier WR Jr, Médebielle M (1998) Nucleophilic trifluoromethylation using trifluoromethyl iodide. A new and simple alternative for the trifluoromethylation of aldehydes and ketones. J Org Chem 63:5385–5394
45. Bock H, Jaculi D (1984) Oxidation reactions with "naked" permanganate ions under aprotic conditions. Angew Chem 96:298–299, Angew Chem Int Ed 23:305–307
46. Eberle B, Hübner O, Ziesak A, Kaifer E, Himmel H-J (2015) What makes a strong organic electron donor (or acceptor)? Chem Eur J 21:8578–8590. doi:10.1002/chem.201406597
47. Wanzlick H-W, Schikora E (1960) Ein neuer Zugang zur Carben-Chemie. Angew Chem 72 (16):494
48. Wiberg N (1968) Photochemical cyclodehydrogenations in the indole series. Angew Chem 80:466–481, Angew Chem Int Ed 7:766–779
49. Taton TA, Chen PA (1996) A stable tetraazafulvalene. Angew Chem 108:1098–1100, Angew Chem Int Ed 35:1011–1013
50. Murphy JA, Zhou SZ, Thomson DW, Schoenebeck F, Mahesh M, Park SR, Tuttle T, Berlouis LEA (2007) The generation of aryl anions by double electron transfer to aryl iodides from a neutral ground state organic super-electron donor. Angew Chem 119:5270–5275, Angew Chem Int Ed 46:5178–5183
51. Doni E, Murphy JA (2014) Evolution of neutral organic super-electron-donors and their applications. Chem Commun 50:6073–6087
52. Peters A, Kaifer E, Himmel H-J (2008) 1,2,4,5-tetrakis(tetramethylguanidine) benzene: synthesis and properties of a new molecular electron donor. Eur J Org Chem 5907–5914
53. Himmel H-J (2013) Guanidinyl-functionalized aromatic compounds (GFAs) – charge and spin density studies as starting points for the development of a new class of redox-active ligands. Z Anorg Allg Chem 639:1940–1952
54. Peters A, Herrmann H, Magg M, Kaifer E, Himmel, H-J (2012) Tuning the properties of guanidino-functionalized aromatic electron donors by substitution: experiment and theory. Eur J Inorg Chem 1620–1631
55. Farwaha HS, Buchr G, Murphy JA (2013) A novel neutral organic electronic with record half-wave potential. Org Biomol Chem 11:8073–8081
56. Vitske V, König C, Kaifer E, Hübner O, Himmel H-J (2010) Syntheses of the first coordination compounds of the new strong molecular electron donor and double proton sponge 1,4,5,8-tetrakis(tetra-methylguanidino)naphthalene. Eur J Inorg Chem 115–126
57. Vitske V, Roquette P, Leingang S, Adam C, Kaifer E, Wadepohl H, Himmel H-J (2011) Donor-acceptor couples and late transition metal complexes of oxidation-labile 1,4,5,8-tetrakis (guanidino)naphthalene superbases. Eur J Inorg Chem 1593–1604
58. Maronna A, Bindewald E, Kaifer E, Wadepohl H, Himmel H-J (2011) Synthesis and characterization of novel guanidine ligands featuring a biphenyl or binaphthyl backbone. Eur J Inorg Chem 1302–1314
59. Stang S, Lebkücher A, Walter P, Kaifer E, Himmel H-J (2012) Redox-active guanidine ligands with pyridine and p-benzoquinone backbones. Eur J Inorg Chem 4833–4845
60. Bindewald E, Lorenz R, Hübner O, Brox D, Herten D-P, Kaifer E, Himmel H-J (2015) Tetraguanidino-functionalized phenazine and fluorene dyes: synthesis, optical properties and metal coordination. Dalton Trans 44:3467–3485
61. Vitske V, Herrmann H, Enders M, Kaifer E, Himmel H-J (2012) The wrapping up of an organic reducing reagent in a cationic boron complex and its use for the synthesis of polyhalide monoanionic networks. Chem Eur J 18:14108–14116

62. Herrmann H, Ziesak A, Wild U, Leingang S, Schrempp D, Wagner N, Beck J, Kaifer E, Wadepohl H, Himmel H-J (2014) Tetracyanoquinodimethane (TCNQ) reduction by complexed guanidinyl-functionalized aromatic compounds (GFAs). ChemPhysChem 15:351–365
63. Stang S, Kaifer E, Himmel H-J (2014) Metal-free C-C coupling reactions with tetraguanidino-functionalized pyridines and light. Chem Eur J 20:5288–5297
64. Emeljanenko D, Peters A, Vitske V, Kaifer E, Himmel H-J (2010) Guanidine-functionalized aromatic electron donors at work: competing hydrogen and electron transfer reactions in the course of the synthesis of gold acetylide complexes. Eur J Inorg Chem 4783–4789
65. Wild U, Neuhäuser C, Wiesner S, Kaifer E, Wadepohl H, Himmel H-J (2014) Redox-controlled hydrogen bonding: turning a superbase into a strong hydrogen-bond donor. Chem Eur J 20:5914–5925
66. Emeljanenko D, Peters A, Wagner N, Beck J, Kaifer E, Himmel H-J (2010) Successive ligand and metal oxidation: redox reactions involving binuclear Cu(I) complexes of chelating guanidine ligands. Eur J Inorg Chem 1839–1846
67. Trumm C, Hübner O, Walter P, Leingang S, Wild U, Kaifer E, Eberle B, Himmel H-J (2014) One-versus two-electron oxidation of complexed guanidino-functionalized aromatic compounds. Eur J Inorg Chem 6039–6050
68. Trumm C, Kaifer E, Hübner O, Himmel H-J (2010) Trapped in a complex: the 1,2,4,5-tetrakis (tetramethyl-guanidino)benzene radical cation (ttmgb$^{+\cdot}$) featuring a bisallylic structure. Eur J Inorg Chem 3102–3108
69. Peters A, Trumm C, Reinmuth M, Emeljanenko D, Kaifer E, Himmel H-J (2009) On the chemistry of the strong organic electron-donor 1,2,4,5-tetrakis(tetramethylguanidino)benzene: electron transfer in donor-acceptor couples and binuclear late transition metal complexes. Eur J Inorg Chem 3791–3800
70. Lebkücher A, Wagner C, Hübner O, Kaifer E, Himmel H-J (2014) Trinuclear complexes and coordination polymers of redox-active guanidino-functionalized aromatic compounds (GFA) with triphenylene core. Inorg Chem 53:9876–9896
71. Villiers C, Thuéry P, Ephritikhine M (2007) The first urea azine molecule and its coordination to uranium in the first actinide guanidine complexes. Chem Commun 2832–2834
72. Reinmuth M, Neuhäuser C, Walter P, Enders M, Kaifer E, Himmel H-J (2011) The flexible coordination modes of guanidine ligands in Zn Alkyl and halide complexes: chances for catalysis. Eur J Inorg Chem 83–90
73. Herrmann H, Reinmuth M, Wiesner S, Hübner O, Kaifer E, Wadepohl H, Himmel H-J (2015) Urea azines (bisguanidines): electronic structure, redox properties and coordination chemistry. Eur J Inorg Chem 2345–2361. doi:10.1002/ejic.201500228
74. Hünig S, Balli H, Conrad H, Schott A (1964) 2,2′-Azine aromatischer Heterocyclen und ihre höheren Oxydationsstufen. Liebigs Ann Chem 676:36–51
75. Hünig S, Balli H, Conrad H, Schott A (1964) Polarographie von 2,2′-Azinen aromatischer Heterocyclen. Liebigs Ann Chem 676:52–65
76. Appel R, Schöllhorn R (1964) Triphenylphosphineazine $Ph_3P=N—N=Ph_3$. Angew Chem 76:991–992, Angew Chem Int Ed 3:805-806
77. Holzmann N, Dange D, Jones C, Frenking G (2013) Dinitrogen as double Lewis acid: structure and bonding of triphenylphosphineazine $N_2(PPh_3)_2$. Angew Chem 125:3078–3082, Angew Chem Int Ed 52:3004–3008
78. Wilson DJD, Couchman SA, Dutton JL (2012) Are N-heterocyclic carbenes "better" ligands than phosphines in main group chemistry? A theoretical case study of ligand-stabilized E_2 molecules, L-E-E-L (L = NHC, phosphine; E = C, Si, Ge, Sn, Pb, N, P, as, Sb, Bi). Inorg Chem 51:7657–7668
79. Wagner A, Litters S, Elias J, Kaifer E, Himmel H-J (2014) Chemistry of guanidinate-stabilised diboranes: transition metal catalysed dehydrocoupling and hydride abstraction. Chem Eur J 20:12514–12527

80. Rudolf D, Storch G, Kaifer E, Himmel H-J (2012) Synthesis of molecular gallium hydrides by means of low-temperature catalytic dehydrogenation. Eur J Inorg Chem 2368–2372
81. Denney MC, Pons V, Hebden TJ, Heinekey DM, Goldberg KI (2006) Efficient catalysis of ammonia borane dehydrogenation. J Am Chem Soc 128:12048–12049
82. Ciobanu O, Kaifer E, Enders M, Himmel H-J (2009) Synthesis of a stable $B_2H_5^+$ analogue by protonation of a double base-stabilized diborane(4). Angew Chem 121:5646–5649, Angew Chem Int Ed 48:5538–5541
83. Schulenberg N, Jäkel M, Kaifer E, Himmel H-J (2009) The borane complexes Htbo BH_3 and Htbn·BH_3 (Htbo = 1,4,6-triazabicyclo[3.3.0]oct-4-ene, Htbn = 1,5,7-triazabicyclo[3.4.0]non-6-ene): synthesis and dehydrogenation to binuclear boron hydrides. Eur J Inorg Chem 4809–4819
84. Himmel H-J (2011) Hydrogenation and dehydrogenation of dinuclear boron and gallium hydrides. In: Comba P (ed) Modeling of molecular properties. Wiley-VCH, Weinheim
85. Braunschweig H, Guethlein F (2011) Transition-metal-catalyzed synthesis of diboranes(4). Angew Chem 123:12821–12824, Angew Chem Int Ed 50:12613 – 12616
86. Braunschweig H, Claes C, Guethlein F (2012) Dehydrocoupling of catecholborane catalyzed by group 4 compounds. J Organomet Chem 706–707:144–145
87. Braunschweig H, Guethlein F, Mailänder L, Marder TB (2013) Synthesis of catechol- pinacol-, and neopenthylglycolborane through the heterogeneous catalytic B-B hydrogenolysis of diboranes(4). Chem Eur J 19:14831–14835
88. Wagner A, Kaifer E, Himmel H-J (2013) Bonding in diborane-metal complexes: a quantum-chemical and experimental study of complexes featuring early and late transition metals. Chem Eur J 19:7395–7409
89. Wagner A, Kaifer E, Himmel H-J (2012) Diborane(4)-metal bonding: between hydrogen bridges and frustrated oxidative addition. Chem Commun 5277–5279
90. Schulenberg N, Litters S, Kaifer E, Himmel H-J (2011) Zinc halide and alkyl complexes of a neutral doubly base-stabilized diborane(4). Eur J Inorg Chem 2657–2661
91. Schulenberg N, Ciobanu O, Kaifer E, Wadepohl H, Himmel H-J (2010) The double-base stabilized diborane(4) $[HB(\mu\text{-hpp})]_2$ (hpp = 1,3,4,6,7,8-hexahydro-2*H*-pyrimido[e,2-a] pyrimidinate): synthesis via catalytic dehydrogenation and reactions with S_8 and disulfides. Eur J Inorg Chem 5201–5210
92. Prokofjevs A, Kampf JW, Vedejs E (2011) A boronium ion with exceptional electrophilicity. Angew Chem 123:2146–2149, Angew Chem Int Ed 50:2098–2101
93. Schulenberg N, Wadepohl H, Himmel H-J (2011) Synthesis and characterization of a doubly base-stabilized $B_3H_6^+$ analogue. Angew Chem 123:10628–10631, Angew Chem Int Ed 50:10444–10447
94. Dinda R, Ciobanu O, Wadepohl H, Hübner O, Acharyya R, Himmel H-J (2007) Synthesis and structural characterization of a stable dimeric boron(II) dication. Angew Chem 119:9270–9273, Angew Chem Int Ed 46:9110–9113
95. Ciobanu O, Emeljanenko D, Kaifer E, Mautz J, Himmel H-J (2008) First dinuclear B (II) monocations with bridging guanidinate ligands: synthesis and properties. Inorg Chem 47:4774–4778
96. Ciobanu O, Fuchs A, Reinmuth M, Lebkücher A, Kaifer E, Wadepohl H, Himmel H-J (2010) Reactions between boron and magnesium halides and the bicyclic guanidine hppH (1,3,4,6,7,8-hexahydro-2*H*-pyrimido[1,2-*a*]pyrimidine): guanidinates with new structural motifs. Z Anorg Allg Chem 636:543–550
97. Litters S, Kaifer E, Enders M, Himmel H-J (2013) A boron-boron coupling reaction between two ethyl cation analogues. Nat Chem 5:1029–1034
98. Balakrishnarajan MM, Hoffmann R (1986) Electron-deficient bonding in rhomboid rings. J Am Chem Soc 108:5732–5737

Index